Assessment of Inundation Risk from Sea Level Rise and Critical area for Barrier Construction: A GIS-Based Framework and Application on the Eastern Coastal Areas of Qatar

By

A.AZIZ ALI M AL-MANNAI

A thesis submitted for the degree of Doctor of Philosophy

University of East Anglia, Norwich

School of Environmental Sciences

May

2021

Abstract

Climate has changed throughout geological history as part of the natural process, which consequently altered the extent and the level of seas. However, the rate of these changes has accelerated from the second half of the last century. There is much scientific evidence that climate change has and will continue to accelerate the rate of sea level rise in the 21st century. This creates a significant risk for many countries in terms of flooding, coastal erosion and wetland inundation, which in turn will impact human communities (socially and economically) and ecosystems. It is therefore vital to have reliable strategies for modelling and reducing the impact of climate change.

This study provided a methodology based on geospatial technology to provide stakeholders with a decision-making tool for better understanding of uncertainties in climate change study and future flood defence planning. This study integrated the uncertainties from both DEM and RCPs to provide a better projection of flooding that results from sea level rise. The study also looked at the errors and the spatial autocorrelation aspect and provides evidence that the independency of the error did not improve the outcomes significantly.

Identifying the critical area in studying sea level rise inundation is crucially important for the decision makers to plan to and prevent future flooding by building barriers. This study developed a method to include the factors affecting the site selection by integrating the multi-criterial evaluation with GIS tool for site selection. In Qatar and many other countries, industrial activities, especially from the oil and gas industry, are concentrated in the coastal areas. The economic benefit of protecting the coastal areas from flooding is important for the wider economy of the country. Therefore, prioritising the areas based on the risk of flooding and identification of the critical areas to build barriers will help in making decisions on future investments by governments and companies operating in those areas.

Acknowledgement

After a long journey of learning and a truly life-changing experience acquired in the completion of this research, I thank the Almighty God for His abundant grace and blessings bestowed upon me.

First, I would like to thank those who contributed greatly to this research and helped me in this journey. To Dr. Iain Lake, my main supervisor. I am particularly grateful to him for his continuous guidance, support and encouragement throughout this research. Thanks also go to my second supervisor, Professor Andrew Lovett, for his valuable comments and feedback which have enhanced the quality of this research.

It is a great pleasure to thank the Qatar University, which offered me the opportunity to undertake a PhD degree. A special thanks to each of the government departments that provided me with data and information, especially the Ministry of Municipality and Environment, The Center for Geographic Information Systems and Civil Aviation Authority – Department of Meteorology.

My next words of thanks and appreciation go to my dear father, my first teacher, who died on 14th January 2019. Thanks to my beloved mother for her prayers, support and encouragement. Special thanks to my brothers - especially Eisa and Yousef - my sisters and my friends – especially Dr. Ibrahim Al-Kaabi – who supported me and encouraged me to complete this work.

Last but not least, I am very grateful to my wife for her patience and tolerance and her great care looking after my family. Special acknowledgement to my sons Ali, Mohammed and Fahad, and to my daughters AlJohara and AlJouri. Without their love, patience and help, I could not accomplish this research.

Table of Contents

List of Figures

List of Tables

List of Abbreviations

AHP	Analytic Hierarchy Process
AIM	Asia-Pacific Integrated Model
ANUDEM	Australian National University DEM
AR	Assessment Reports
AR5	Fifth Assessment Report
ASTER	Advanced Spaceborne Thermal Emission and Reflection Radiometer
CCI	Climate Change Impacts
CRS	Coordinate Reference System
CVI	Coastal Vulnerability Index
CZMS	Coastal Zone Management Subgroup
DEM	Digital Elevation Model
EDP	Error Density Map
ESI	Environmental Sensitivity Index
FBMB	Fundamental Bench Mark B
GCM	Global Circulation Models
GDP	Gross Domestic Product
GHG	Greenhouse Gas
GIS	Geographical Information Systems
GISP	Geographic Information Systems and Planning
GMSL	Global Mean Sea Level
GNSS	Global Navigation Satellite System
HOT	Highest Observed Tide
ICZMP	Integrated Coastal Zone Management Plan
IDW	Inverse Distance Weighted
IFSAR	Interferometric Synthetic Aperture Radar
IIASA	International Institute for Applied Systems Analysis

IPCC	Intergovernmental Panel on Climate Change
JGCRI	Joint Global Change Research Institute
LiDAR	Light Detection and Ranging
MCE	Multi-Criteria Evaluation
MCS	Monte Carlo Simulation
MDPS	Ministry of Development Planning and Statistics
MHHW	Mean Higher High Water
MHT	Mean High Tide
MME	Ministry of Municipality and Environment
MMUP	Ministry of Municipality and Urban Planning
MSL	Mean Sea Level
NIES	National Institute for Environmental Studies
OE Kriging	Ordinary Exponential Kriging
OS Kriging	Ordinary Spherical Kriging
PSE	Prediction Standard Error
QMD	Qatar Meteorology Department
RCP	Representative Concentration Pathways
RMSE	Root Mean Square Error
SLR	Sea Level Rise
SRTM	Shuttle Radar Topography Mission
TIN	Triangular Irregular Networks
TOPSIS	Technique for Order of Preference by Similarity to Ideal Solutions
UN	United Nations

Chapter 1: Introduction

1.1. Background

Sea levels have fluctuated throughout history as a result of climate changes and geological events. In the last deglaciation (20,000 - 8000 years ago), it is estimated that the rate of sea level rise (SLR) increased by 10 mm per year, with eustatic sea level reaching a total of 130 m during that period (Alley et al., 2005). Since 1850, the sea level has risen by about 19 cm worldwide (Stocker, 2014). Thus, SLR is not a new phenomenon. However, in the last century it has become the subject of increasing concern for scientists, policy makers and the wider public, particularly since the early 1990s when more precise and global data became available. This is because it is widely viewed as a consequence of human activities (Oppenheimer et al., 2019). Most current studies suggest that climate change has and will continue to accelerate the rate of SLR. The rate of rise projected for the 21st century is predicted to be faster than in the previous century. This in turn will increase the risk of floods, erosion, wetland inundation and all the associated material damages to human communities and the ecosystem (Stocker, 2014). Therefore, understanding the causes and consequences of climate change is a social challenge that is needed to help predict changes in impact, develop adaptation and mitigation measures and to assess climate change impacts on human health and the environment (Nicholls et al., 2007; Small and Nicholls, 2003). It is therefore vital to have a better understanding of the impact of climate change on SLR.

1.2. Sea level rise and climate change

This section will now consider how SLR is affected by climate change. The science of climate change has increased substantially since the creation in 1988 of the Intergovernmental Panel on Climate Change (IPCC), the international body tasked with evaluating climate change causes and consequences. The regular comprehensive assessment reports (AR) of the IPCC are prepared by gathering technical and socio-economic information regarding climate change, human mediated climate change, effects and consequences and measures that can be adapted for their mitigation.

The latest report presents a clear and up to date view of the state of art in climate change science in the Fifth Assessment Report (AR5) of the IPCC, published in 2014 (IPCC, 2018). A range has been given for future imminent global mean sea level (GMSL) rise by the year 2100 with a low level of 0.2 m and a high level of 2.0 m (Parris et al., 2012) and an intermediate range falling between 0.5 m and 1.2 m (Figure 1-1).

There are two main causes for SLR. One is the melting of glaciers and polar ice sheets; the other is the thermal expansion of oceans due to warming. These two causes have contributed to 75percent of SLR observed globally. Glacier mass loss and changes in land water storage appear to explain 90percent of the observed global mean SLR for 1971–2010 and 1993–2010 (Pachauri et al., 2014). Weissenberger and Chouinard (2015) contend that the two main causes mentioned above have an almost equal contribution to SLR. The best estimates of the likely changes in SLR moving forward are produced by the IPCC (Table 1-1).

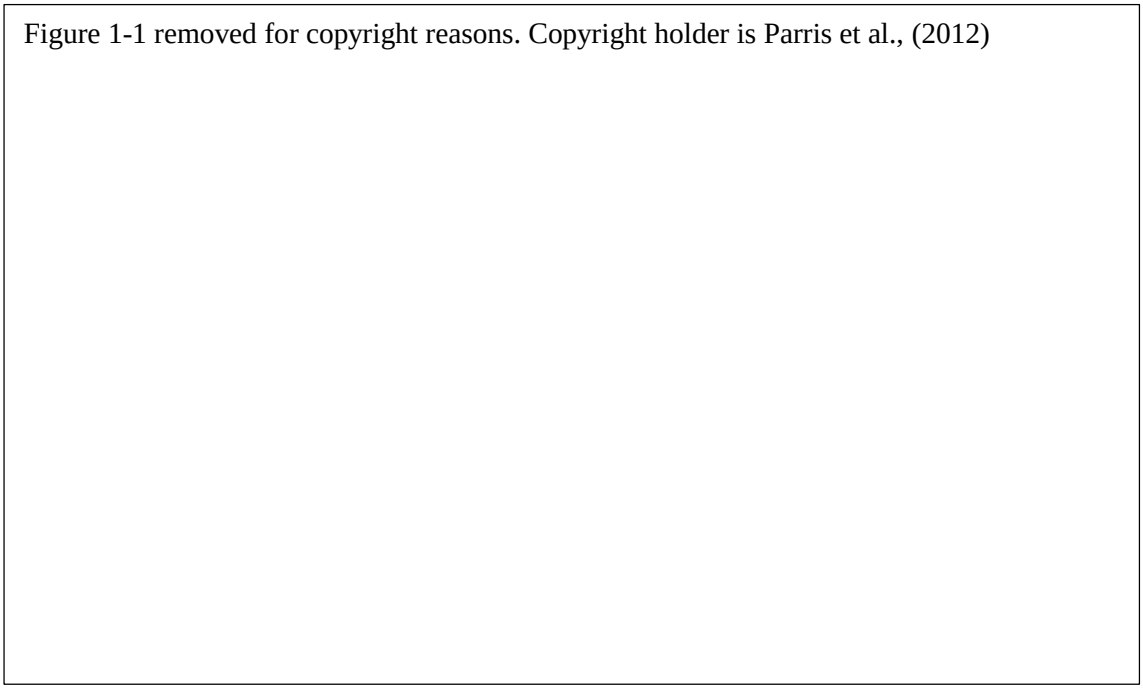

Figure 1- 1: The rate of GMSL rise scenarios (Parris et al., 2012)

Table 1- 1: The SLRs for different RCP scenario from Stocker (2014).

	RCP 2.6	**RCP 4.5**	**RCP 6.0**	**RCP 8.5**
Global mean sea level rise in 2100 (m)	0.44	0.53	0.55	0.74
Range of global sea level rise in 2100 (m)	0.28 to 0.61	0.36 to 0.71	0.38 to 0.73	0.52 to 0.98

For climate modelling a set of new methods were developed for long-term and short-term modelling, which are called representative concentration pathways (RCPs) (Van Vuuren et al., 2011), which are approved by the IPCC. Deriving the probable trajectories for the significant drivers of climate change by 2100 is the main objective of these RCPs. Representative concentration pathways are based on the concentrations of greenhouse gases (GHG), which are calculated as CO_2 equivalents in units of Watts per square metre. These will provide a framework to research and model the possible climate conditions in the future, along with their consequences. There are four main RCPs: RCP 2.6 is a stringent mitigation scenario that projects a peak in emissions between 2010 and 2020, after which there will be a significant decline; both RCP 4.5 and RCP 6.0 (intermediate scenarios) are projected to peak around 2040 and 2080, respectively, with a decline later; RCP 8.5 (scenario with very high emissions) predicts increasing GHG atmospheric concentrations over the current century (Church et al., 2013).

Climate change and SLR are important as millions of people living in coastal areas are exposed to SLR and AR5 is carrying out studies on SLR specifically (Nicholls & Cazenave, 2010). The average SLR was around 3.0 mm/year between 1993-2010 (Hay et al., 2015), and RCP 8.5 predicts it will increase in the coming 100 years. The SLR forecast until 2100, depending on different RCPs, is summarised in Figure 1.2 and Table 1.1. RCP 8.5 means the worst-case scenario with a consequent SLR between 0.52 and 0.98 m, with a 66 percent likelihood range (global average by 2100) predicted as “likely” by AR5 IPCC (Figure 1-2). This is relative to the sea level during the period 1986-2005 (Church et al., 2013).

Figure 1-2 removed for copyright reasons. Copyright holder is Church et al., (2013).

Figure 1- 2: Projections of global mean SLR over the 21st century (relative to 1986–2005) for a low emissions scenario (RCP 2.6), intermediate scenarios (RCP 4.5 and 6.0) and high emissions scenario (RCP 8.5). The assessed likely range is shown as a shaded band. Source: Church et al., (2013).

There is also the possibility of more extreme SLR, and the possibility of sections of Antarctic ice sheets melting and a subsequent higher SLR in the 21st century, which is not excluded in AR5 (Church et al., 2013). As DeConto and Pollard (2016) predicted, Antarctica has the potential to contribute more than one metre of SLR by 2100 and more than 13 m by 2500. Because of this uncertainty, high-end SLR scenarios must be considered when modelling its impacts. For example, the upper-limit SLR generated by Jevrejeva et al. (2014) (including estimates with low probability, that are seemingly not possible but cannot be ruled out as per paleoclimate observations) estimated higher SLR up to 1.80 m by 2100, with less than a 5 percent probability. This was based on the construction of a probability density function for global mean SLR.

Sea level rise will also vary by location and depends on several factors, like ocean currents, temperature and sea depth. Therefore, SLR is not universally uniform and it can vary from place to place due to climatic differences, especially in the equatorial Pacific Ocean, as shown in Figure 1-3. This is related to the movement of water in the oceans as per the changing wind patterns, which in turn are affected by the El Niño-Southern Oscillation phenomenon indicated by the

patterns of ocean thermal expansion at the regional level. Variations in SLR also occur over time, from short-lived phenomena like waves and storms, to changes lasting decades or even centuries (Figure 1-3).

Figure 1-3 removed for copyright reasons. Copyright holder is (Titus & Wang, 2008).

Figure 1- 3: Global Sea Level Trends. Source: Titus & Wang (2008) (using data from the Permanent Service for Mean Sea Level)

The regional patterns of SLR are particularly important as society and the environment are directly affected by the local sea-level changes. The variations in the rate of SLR regionally are significant, as shown by satellite altimeter data (Figure 1-4), with an increase in SLR of about five times the global average since 1993 in some regions (Aarup et al., 2010). However, the relatively short altimeter record and differences in climate, particularly in the equatorial Pacific Ocean, might be responsible for some of the extreme observations.

Figure 1- 4 removed for copyright reasons. Copyright holder is (CSIRO, 2014)

Figure 1-4: The spatial distribution of the rates of SLR, plotted about the global average rate of rise for the period January 1993 to December 2009, as measured from satellite altimeter data (CSIRO, 2014)

This variability in climate will continue in the 21st century with an impact on coastal communities by the long-term SLR, variations in sea level and also by extreme sea level alterations caused by storms and waves.

1.3. Uncertainty in SLR assessment

Estimations about the magnitude of SLR vary widely in various reports and documents (see Section 1.2). Although slowing of the amount of GHG is being reported from different regions in the world, SLR will continue even after the emissions of GHG stop rising due to inertia in the climate system (Levermann et al., 2013).

Predicting SLR for any specific location with a high degree of certainty can be a challenging task as changes in ocean currents, ocean density and sea level are all connected, and changes at one location can impact another (Yin et al., 2010). This is illustrated in the uncertainty calculations of SLR carried out by the IPCC. This implies that the sea level in the regions close to the mass of ice sheets lowers and rises in other areas (Kopp et al., 2010). More recent research in AR5 shows

that the West Antarctic ice sheet has been melting faster throughout the latest decade than had originally been expected. This implies a further SLR of several decimetres more. This was regarded as highly unlikely in the IPCC report but is now a clear possibility (Turner et al., 2017). There is a 17 per cent chance of the SLR being more than that predicted in IPCC´s RCP 8.5 (Wuebbles et al., 2017).

1.4. The implications of SLR and flooding on global coastal population

Coastal and low-elevation populations are at risk from SLR and other seaward hazards (e.g. changes in ocean currents, winds and storm intensity) induced by climate change. The densely populated low-lying areas where the population is continuously growing are becoming more vulnerable to the risks caused by climate change. The area that is less than 10 metres above sea level represents only two per cent of the Earth's land surface but is inhabited by 10 per cent of the world's population in general, which is also 13 per cent of the world's urban population (McGranahan et al., 2007). The coastal population is projected to be 1.8-5.2 billion people by 2080, based on expected migration (Nicholls et al., 2007). There is a wide conversion of natural coastal land into agriculture and aquaculture, as well as industrial and residential land by the growing populations (Valiela, 2009), which are becoming regions of highly economical productivity. Thus, it is not only coastal populations but also their socio-economic activities that are threatened by SLR. The impacts of SLR on coastal areas include land flooding and storm damage, erosion, saltwater intrusion, rising water tables and wetland loss (Nicholls & Tol, 2006). The inundation of low-lying coastal areas around the world is currently considered one of the most dramatic and immediate effects of SLR (FitzGerald et al., 2008). It is foreseen expected to reach 50 per cent of the total population living within a distance of 100 km of the shores in the next two decades (Small & Nicholls, 2003; Neumann et al, 2015). The projected population at risk by country by the year 2050 is given in Woosnam (2017), including 37.2 million people from India being exposed to the impacts of SLR by the year 2050. The coastal areas are also home to some of the world's most productive and complex systems and support a diversity of plant, fish and wildlife species. There are global and sub-global estimates of vulnerability of coastal populations and ecosystems to rapid SLR (Small and Nicholls 2003; Woodroffe et al., 2006; McGranahan et al., 2007; Nicholls et al.,

2007), due to irretrievable inundation of low-lying regions, intensified flooding events and heightened beach erosion and salination of coastal land. Millions of people might be displaced due to loss of property and infrastructure, and the coastal ecosystems might also be lost considerably by the end of the 21st century (Nicholls & Lowe, 2004).

An increase in storm intensities and coastal flooding are potential outcomes of SLR, which is gaining wider concern as it threatens the low-lying coastal areas with submergence and inundation, e.g. for coastal areas of Bangladesh (Broadus et al., 1986; Huq et al., 1995).

The protection costs that can be incurred by a one metre rise in sea level was estimated by the IPCC Coastal Zone Management Subgroup (CZMS) in 1990. The common methodology framed by the IPCC CZMS was used to complete the first analysis of global vulnerability in 1992, where the flood risk and accompanying costs were evaluated based on the assumption of one metre SLR globally from 1990 to 2020 (Hoozemans et al., 1992). This was updated soon after in its second edition (Hoozemans et al., 1993). The findings were publicised at the United Nations (UN) Conference on Environment and Development in Rio de Janeiro, Brazil, in 1992 (IPCC CZMS, 1992) and the World Coast Conference in Noordwijk, the Netherlands, in 1993 (WCC'93, 1994). The impact algorithms were subsequently improved, making the flood impact analysis more dynamic (Nicholls et al., 1999; Nicholls, 2000). This could combine a range of implications of SLR on rising coastal populations and their living standards. Thereafter, many studies were conducted on sector-wise impacts on climate related to socio-economic activities (Parry et al., 1999; Arnell et al., 2002; Parry et al., 2001) and are cited many times in the IPCC Third Assessment Report (McCarthy et al., 2001).

Coastal habitations and establishments are increasingly exposed to floods (Hanson et al., 2011; De Sherbinin et al., 2007) due to climate change, the increasing burden of populations and assets, as well as subsidence (Nicholls, 1995; The World Bank, 2010). Based on the evaluation of present flood losses, an estimation of future losses based on socio-economic impacts alone were shown to be US$ 6 billion per year, which may rise to US$ 52 billion by 2050. There is an urgent need to upgrade current coastal protection measures to prevent losses of more than US$ 1 trillion per annum due to climate change and subsidence. Although present investments maintain adaptations

to flood probability, the subsidence and SLR can cause losses up to US$ 60–63 billion per year by 2050. It is critical to prepare for more severe disasters in future as there is a probability that the magnitude of loss will increase by more than 50 per cent.

Climate change in ecosystems along the coast can result in SLR and more intense, frequent storms (Murdukhayeva et al., 2013). The low-lying areas in coastal parks can be inundated due to such phenomena. To assess this risk of coastal inundation, appropriate geospatial data, tools and models were chosen to conduct case studies.

Human action will be the driving factor for increased risks of coastal flooding, as depicted in Figure 1-5. Variability in mean SLR can affect the flood occurrence and flood risk that can impact climate change too. The assets that are exposed to specific floods and the extent of their damage impact the monetary loss ensuing from the flood. The socio-economic development, along with adaptation measures, are anthropogenic factors that can reduce flood risks. Human behaviour can change the patterns of global climate and occurrence of floods by affecting the emission of GHG. These interactions require comprehension to control human actions and mitigate the effects of SLR (IPCC, 2014).

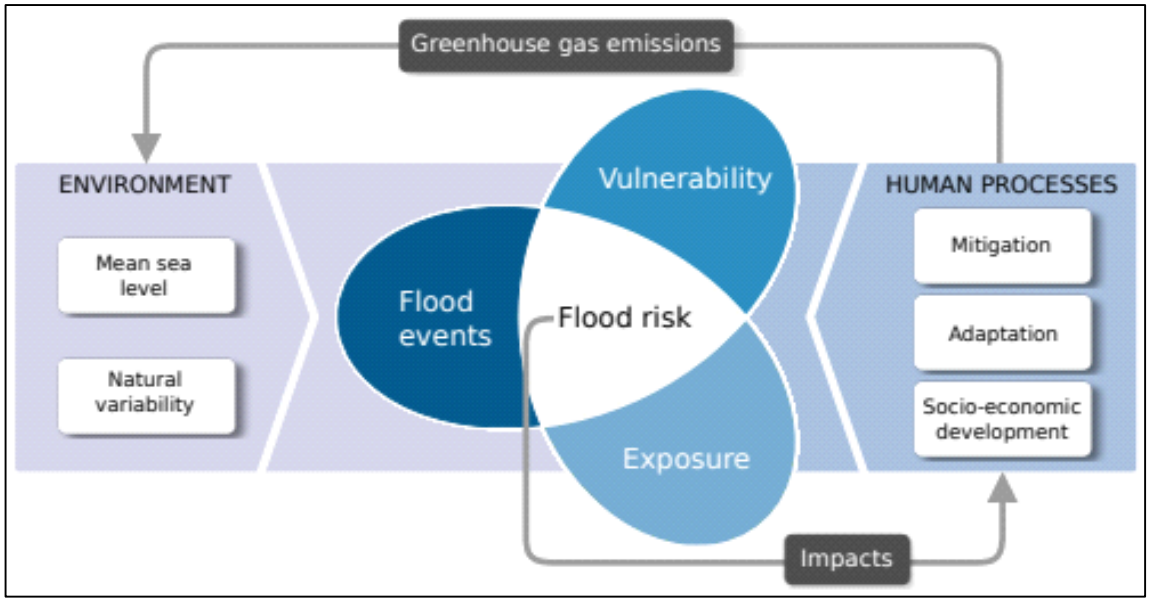

Figure 1- 5: Illustration of environmental and human processes relevant for the assessment of SLR impacts. Adapted from IPCC (2014).

Many of the major cities and ports in the world with thriving populations are concentrated along the coast (Nicholls et al., 2008). The population numbers are constantly increasing in the low-lying coastal areas (below 10 m), which will reach 879 million in 2030 from 625 million in 2000 (Neumann et al., 2015). Coastal zones can be hubs of economic activity and contain industries like tourism. They are further economically paramount in fuel-based economies like Qatar, and in developing countries the coastal regions play a significant role in the economy and commerce. An extreme coastal flooding event occurring with a 100-year return period can affect global coastal cities and their economies by around US$ 3 trillion. This may increase to US$ 35 trillion by 2070 (Hanson et al., 2011). Coastal disasters include waves, winds, tides and tsunamis, along with SLR-related cyclones and floods (IPCC, 2014).

1.5. Adaptation and mitigation measures to sea level rise impacts

The international community is yet to seriously consider the implications of SLR for infrastructure planning, economic development and population aspects (Dasgupta et al., 2007). There are three important concepts in relation to climate change impacts and the response of both natural and human systems:

i. vulnerability: the threats to a given system, and its susceptibility to the harmful effects of climate change;
ii. adaptation: a system's ability to adjust and reduce its vulnerability to climate change enhancing resilience to observed and predicted climate change impacts. The IPCC defined 'adaptation' as adjustment in natural or human systems to a new or changing environment;
iii. mitigation: the strategies and actions (i.e. policies) applied to reduce the emission and concentration of GHGs in the environment. 'Mitigation' is defined by the IPCC as technological change and substitution that reduce resource inputs and emissions per unit of output with respect to climate change (Cardona et al., 2012; Netz et al., 2007; Smith et al., 2001; Watson et al., 1996).

Adaptation measures include social and environmental process modifications, climate risk perception, actions to reduce climate risk and the exploration of new opportunities to cope with the modified environment. If mitigation measures are successful, the impacts are lessened and the need for adaptation also lessens. Thus, adaptation and mitigation are reciprocal. Adaptation measures are used to deal with the effects of climate change and SLR and to reduce the uncertainties associated with their impacts by incrementally planning ahead. They allow stakeholders and policy makers to consider a range of options for choosing the best approach, avoiding inappropriate decisions (i.e. too little, too much, too soon, or too late), which may inadvertently increase the socio-economic and environmental SLR impacts (Barnett & O'Neill, 2010).

Sea level rise has many adverse effects on the environment and coastal populations globally, which are increasing mainly due to climate change. The exposure to increased occurrences of floods and other SLR-related consequences are becoming more notable, severe and catastrophic. Floods are unstoppable natural disasters that cause extensive economic damage and loss of life. This puts an onus on the societies to develop adaptive measures, despite uncertainty in knowing how rapid and extensive the future SLR will be (Griggs et al., 2017).

Mitigation measures include alleviating the causes of climate change, such as emission of GHG, deforestation, urban heat islands, etc., and adaptation measures, including constructing seawalls, blue-green solutions or dykes (Nicholls, 2011). Developing adaptive measures to climate change is becoming paramount in tackling climate change worldwide.

Sea level rise progresses relatively slowly and is hardly noticeable (Moser, 2005). Thus, SLR appears to be another coastal development, along with the impacts of floods and storms, and it is hard to link them to the slow process of SLR (Spirandelli et al., 2016).

1.6. The use of geographic information science for SLR

The current phenomena of global climate change and increasing sea levels necessitates scientific information on likely impacts, to direct planning in coastal areas. These are subject to erosion, flooding and other coastal hazards, both currently and in the future, due to SLR. In this regard, spatial technology, such as geographic information systems (GIS), is an important tool to provide

stakeholders with relevant and timely information for use in a decision-supporting capacity. In this respect, GIS has proved that it has the potential to act as a first assessment of many SLR-induced effects, including inundation and flooding risk, shoreline recession and seawater intrusion risk, as well as socio-economic vulnerability (Snoussi et al., 2011). The outcome of GIS-based models identifies priority areas where natural and human systems are likely to be the most vulnerable. Geographic information systems also provide visualisations so that SLR and its associated impacts can be visualised for various stakeholders in the coastal environment and economy. These may enable planners and government authorities to make well-informed decisions, integrating this knowledge in coastal planning and development (Faour et al., 2013).

1.7. Aims and objectives

The aim of this study is to develop a methodology that can be used to examine the impact of SLR on flooding by taking into account the many uncertainties involved. This is then developed into a methodology for identifying appropriate sites to build a barrier to prevent future flooding. The specific objectives are:

1. To apply and evaluate various spatial interpolation methods and techniques to generate high-resolution digital elevation models (DEM) in complex urban areas.
2. To assess the SLR inundation in a coastal area.
3. To quantify the impact of uncertainty in the DEM and in SLR estimates upon flooding projections.
4. To evaluate the importance of taking spatial autocorrelation into account when modelling the impacts of uncertainty.
5. To explore methods to identify critical areas for barrier construction to prevent sea level inundation.

This study is based on the east coast of Qatar.

1.8. Thesis outline

This thesis comprises seven chapters. A brief description of each is provided below:

- **Chapter 1: Introduction**: Presents the background, aims and objectives of the research.
- **Chapter 2**: **Background to the Study Area and Previous Studies of Sea Level Rise in the Middle East:** Introduces the country of the study, Qatar, including information on climate, topography, changing sea levels and socio-economic characteristics. An overview of previous studies on climate change and SLR is presented with a focus on Qatar, the Gulf and the Middle East.
- **Chapter 3: Digital Elevation Model**: This chapter describes the collection of secondary elevation data points and the various interpolation methods used to build a DEM in a complex urban area.
- **Chapter 4: Assessing sea level rise and mapping inundation**: The purpose of this chapter is to develop a method to map inundated areas based on climate change scenarios.
- **Chapter 5: Assessing uncertainty in sea level rise and mapping inundation:** The main objectives of this chapter are to estimate the impact of uncertainties associated with DEM and SLR projections on the inundation mapping and to compare the impact of these two sources of uncertainties on the final flood probability map. The need to understand the impact of spatial autocorrelation on the final outcomes of inundation mapping is also addressed.
- **Chapter 6: Critical areas for barrier construction:** This chapter provides a new methodology for identifying and selecting areas to build barriers to prevent flooding from SLR.
- **Chapter 7: Conclusions:** Overall conclusions of this research are presented.

1.9. Gaps in the scientific literature that this study will address

1.9.1. Chapter 3

Although there are many papers in the literature on flooding, one of the key challenges is to estimate flooding in urban areas, taking account of the complexity of the urban form (Wang et al., 2018). Previous research into SLR is often limited by the coarse resolution of elevation data and this makes it difficult to model future SLR associated with climate change (Nicholls, 2004). Flood prediction in urban areas using DEMs is dependent upon the accuracy of the digital terrain data (Kim et al., 2020). A high-accuracy DEM is an important input in modelling future SLR (Gesch, 2018). Marginal differences in the DEM will give a different predicted area and it becomes important to apply accurate topographical data. For this chapter we used elevation datasets with high spatial resolution (10 m grid) and vertical accuracy of 10 cm. Yet for modelling flooding in urban areas this resolution was not thought to be high enough. There are few papers in the literature on the relative merits of interpolating regularly spaced data of an existing raster DEM to a finer resolution. In this chapter we apply and evaluate a number of different interpolation techniques (e.g. IDW, spline, kriging (with four different semi-variogram models) and TIN) to produce a grid with a spatial resolution of 5 m.

The DEMs that such techniques generate are often bare-earth models, where buildings and other urban features are removed. Yet flooding is influenced by many urban features and objects, like bridges over main roads, trees and buildings. The bare-earth DEM sets the topographical base for 2D surface modelling. Objects and features may be reincorporated into the bare-earth DEM using different methods to incorporate the detailed flow dynamics around buildings (Wang et al., 2018; Shen et al., 2018). Realistic urban flooding by DEM has limitations that can be challenging. Researchers have tried incorporating supplementary data like transportation and other related anthropogenic information (Duke et al., 2003; Duke et al., 2006). The ultimate goal is to develop a DEM which depicts the flow through complex urban features like roads, railroads, road or embankments/cuttings. Chapter 3 adds to this literature, generating urban DEMs exploring a range of techniques for incorporating features such as embankments and cuttings into the DEM and also interpolating into data “gaps” where buildings have been removed.

1.9.2. Chapter 4

A basic analysis of coastal flooding uses a “bathtub” method to demarcate the coastal areas below a set water height. Coastal flooding modelled using the bathtub approach is extensively used in SLR assessments (Van De Sande et al., 2012; Sahin, 2014; Poulter & Halpin, 2008; Gesch 2009, 2013; Leon et al., 2014; Schmid et al., 2014; West et al., 2018). However, this simplistic approach does not consider whether the flooded area is connected to the sea and the impacts of not making this assumption are also explored. This allows for a better represented model of surface flooding (Sahin, 2014).

To prevent inaccurate projections and misunderstanding of spatial processes, uncertainty is a key factor to consider (Couclelis, 2003; Tucci & Giordano, 2011). To model the uncertainty in GIS, Monte Carlo Simulation (MCS) and other approaches based on MCS have been extensively used in GIS-based flood modelling (Openshaw et al., 1991; Fisher,1991; Lanter & Veregin, 1992; Holmes et al., 2000). Although there is much research on DEM uncertainty, there is less research on how uncertainties in climate model projections may influence flooding extent (Collet et al., 2018). Notable exceptions exist (Amante, 2019), and the research that has been conducted has not led to guidance or methodologies that can be used by decision makers (Collet et al., 2018). Flooding projections that do not consider these uncertainties may result in incorrect assessments, which in turn may lead to poor coastal management (West et al., 2018). In Chapter 4 we demonstrate how to model flooding, incorporating both uncertainty in DEM and uncertainty in the climate model. It also demonstrates how uncertainty associated with RCPs predictions can be quantified and displayed to enable the reader to make an informed assessment on the potential impact of flooding or to compare different RCP scenarios (Stammer et al., 2013).

1.9.3. Chapter 5

Closer points are more related than farther ones and this is known as positive spatial autocorrelation. The existence of autocorrelation indicates that the objects are not independent. The theoretical advantages of taking spatial autocorrelation into account in error simulations were highlighted by Hunter and Goodchild (1997). However, from the review of literature there are few studies using spatial autocorrelation for assessment of DEM uncertainty. Notable examples include

Darnell et al. (2008). The relationship between flooding at hydrological stations and nine related factors was studied by the Poisson regression model (Fang et al., 2019). The accuracy of predictions increased when spatial autocorrelation was included in this regression model, which increased further when the autocorrelation of the rates of flooding events were incorporated. In Chapter 5, the impact of such refinements are highlighted, enabling the chapter to explore whether such refinements are important in a flooding context (also explored in Chapter 6).

1.9.4. Chapter 6

In the literature there are many studies using GIS to assess the impact of flooding. There are also several studies assessing the most suitable location for dam placement along river systems (Jozaghi et al., 2018; Al-Ruzouq et al., 2019; Adham et al., 2018). However, there are virtually no studies using GIS as a decision-making tool to assess the most suitable location for dams to prevent coastal inundation. This is the focus of Chapter 6. Including uncertainties in the site selection is a new approach, as previous researchers have tended to use one DEM (Maanan et al., 2018; Boateng et al., 2017; Li et al., 2017). This is in spite of the multiple use of MCS in GIS in flood modelling studies (Openshaw et al., 1991; Fisher,1991; Lanter & Veregin 1992; Holmes et al., 2000). In addition to the use of GIS as a decision-making tool for coastal dam location, the method developed also incorporates MCS to account for DEM uncertainties.

Chapter 2: Background to the Study Area and Previous Studies of Sea Level Rise in the Middle East

2.1. Background of the study area

Qatar is situated halfway along the western coast of the Arabian Gulf, located between the latitudes 24° 27´ and 26° 10´ north and the longitudes 50° 40´ and 51° 40´ east (Figure 2-1). The Qatar peninsula extends northwards, covering an area of approximately 11627 km^2 (MDPS, 2015). It includes several islands, reefs and shoals. The Qatari peninsula is about 185 km in length in the north – south direction, while the maximum width east-west is about 85 km. The territorial waters of Qatar extend approximately 95 nautical miles east and around 51 nautical miles north into the Arabian Gulf. The only land border (approximately 86 km) is shared with the Kingdom of Saudi Arabia.

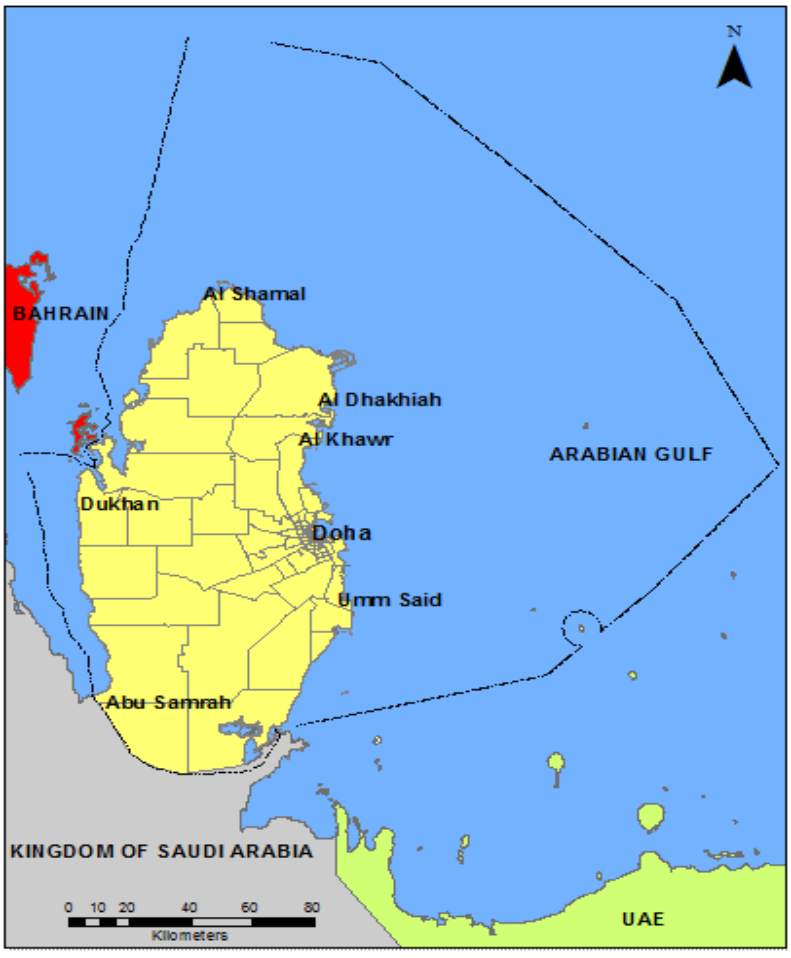

Figure 2-1: State of Qatar (Source: Qatar GISNet, Ministry of Municipality and Environment, MME)

The State of Qatar is divided into eight municipalities, namely Doha, Al Rayyan, Al Wakra, Umm Salal, Al Khor and Al Thakhira, Al Shamal, Al Daayen and Al Sheehaniya. Each municipality is further divided into zones for the convenience of planning. Doha is the capital of the country and the hub for most of the economic, social, cultural and diplomatic activities. Most of the government offices and important establishments are located there. Qatar also includes a range of islands, the largest being Halul, which is a hub for the oil and gas industry. Qatar is mainly arid (Norton et al., 2009), with large areas of urban development, the majority of which occurs on Qatar's east coast. The largest urban development is Metropolitan Doha, which comprises of five different municipalities: Doha, Al Rayyan, Al Daayen, Umm Salal and Al Wakra. Other key settlements in Qatar include Al Khor, Al Shamal and Industrial Cities (Mesaieed, Ras Laffan and Dukhan).

2.2. Climate of Qatar

2.2.1. Temperature and humidity

Qatar's climate is characterised by hot and humid summers and semi-dry short winters with little rainfall. The extremes of temperature in Qatar are experienced during June, July and August, with the lowest temperature experienced in December and January. Generally, the absolute maximum temperature is 47 °C and the absolute minimum temperature is 1 °C (Abulfatih et al., 2001). The winter months are more humid, whereas June is the driest month of the year.

Qatar experiences summer from May to September, with elevated temperatures, and lower temperatures during winter (from October to April) with semi-dry conditions. The maximum temperature during summer can go up to 50 °C. The monthly average temperature and relative humidity are shown in Figure 2-2. The relative humidity varies significantly from 20 per cent to 90 per cent. The natural evaporation rate is generally high, with about 2000 mm/year (Darwish, 2015).

Figure 2-2 removed for copyright reasons. Copyright holder is (MMUP, 2013)

Figure 2-2: Overview of daily, minimum and maximum temperature and relative humidity in Qatar (MMUP, 2013).

2.2.2. Rainfall

Rainfall is unpredictable, irregular and variable in terms of both time and space, with an average annual rate of only 73 mm. Rainfall is confined to the period between October and May. The amount and pattern of rainfall is one of the keys to understanding the dynamic processes of the different terrestrial ground features. The average annual maximum daily rainfall ranges from 24 mm in the south of Qatar to 29 mm in the north.

Like other Arabian Gulf countries, the precipitation in Qatar varies significantly from year to year in intensity and volume. Some years are nearly completely dry, and some years have more than 200 mm annual precipitation, as shown in Figure 2-3. The mean monthly rainfall during the period of 1972-2011 is shown in Figure 2-4.

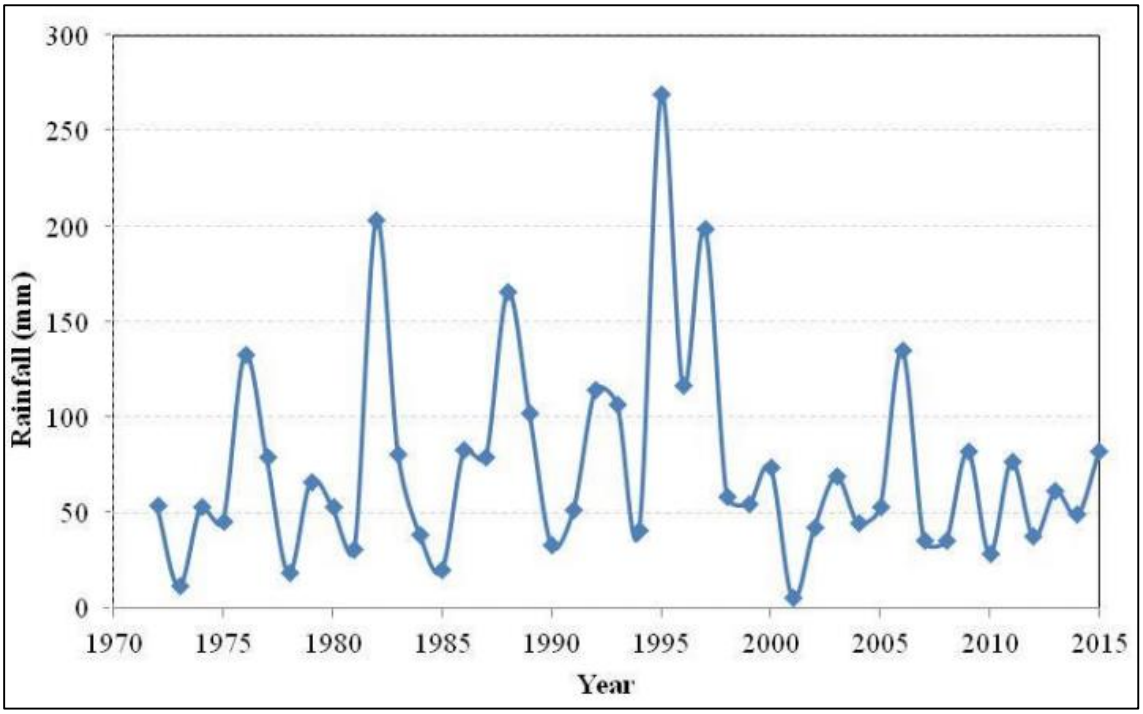

Figure 2-3: Overview of annual rainfall in Qatar (MME, 2017).

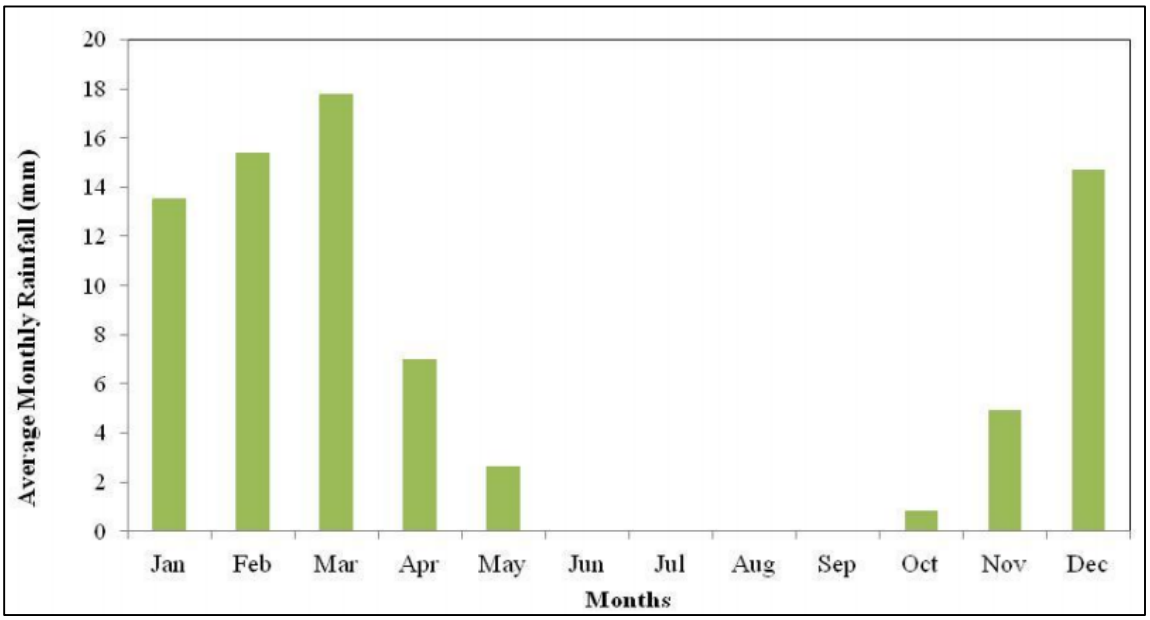

Figure 2-4: Mean monthly rainfall in Qatar (QMD, 2016).

2.3. Topography and geomorphology

The topography of Qatar is mainly flat to lightly undulating, with sand formations of calcareous rocks in the south-east (Norton et al., 2009). It consists mostly of barren plains with lowlands covered with sand. Surrounding an inlet of the Arabian Gulf there is an area of rolling sand dunes at the Khor al Adaid, to the south-east of the country. The land surface has a relief with maximum height of 103 metres above sea level (Qurayn Abu al Bawl), low to moderate relief (SEL, 1980;

Eccleston & Ḥarḥash, 1982) and the lowest part of the peninsula is at about 6 m below sea level (Yehia et al., 1982). The north-south axis is around 180 km long and the east-west axis is widest at its centre, which is 85 km (Batanouny, 1981).

Much of the Qatari peninsula is less than 40 m above sea level. The significant geological features are small mounts (jabals) in the south that are over 100 m above sea level and a rocky Miocene ridge spreading from Dukhan to the southern border on the west coast (Norton et al., 2009). In the west of the country there are several relatively low hills around and over Qatar's main oil field. The centre of the peninsula is relatively flat and covered with loose stones. There are small depressions in which there is a marginally different microclimate supporting some plant life, more evident in winter than in summer. Towards the south of the country are the sand dunes, which initially stand separately but merge and increase in size as they approach the border into Saudi Arabia.

A range of geological formations dating from the Palaeogene to Quaternary ages encompass the surface soils in Qatar (Winslow & El Hakim, 2009). The limestone spreads over the deeper geology of the Qatari landscape, which can be seen on the surface as karst-related processes, like regular depressions, sinkholes, caves and solution hollows. The karst features are attributed to the dissolution of the gypsum and anhydrite deposits of the Rus Formation. Another geological formation, the Dammam Formation, has carbon sequences which are supposed to be associated to a lesser extent with these karst features (Winslow & El Hakim, 2009).

Three quarters of the land surface is formed from the tertiary sedimentary sequences and one quarter is covered by quaternary deposits. The Aeolian sand deposits can be found in the south-east and south-west coastal parts of the peninsula. Qatar is a peninsula limestone peninsula with gentle relief, resulting from the modest tectonic sections of the Earth's surface. It is divided into two areas by the Qatar Dome – the eastern and western areas. Its landscape is controlled by karstic surface appearance, including widespread depressions up to 25 m deep (Ashghal, 2012). The coastline of Qatar is softly appearing and presents an isolating outline with different islands, reefs, caps and extensive areas of marshes (sabkhas). Sabkhas exist widely along the coastal outer parts or the borders of the country. They are close to the water table and covered with salt crust (Batanouny, 1981; Yehia et al., 1982). Rocky hill areas are also common along the coastal areas.

2.4. Soils

Almost half of the soils in Qatar are calcareous, while one third are characterised by the presence of gypsum. The soils in Qatar are also characterised by water deficiency and extremely poor levels of organic matter. They are very shallow in depth, ranging from 10 to 30 cm. Overall, the country is covered by calcareous sandy-loam to loam soils, whereas small-to-large patches of rocky limestone outcrops are found scattered over the south-western part of the country. There are some colluvium depressions (Rodah soils) scattered at some places in the northern part. These are the most fertile lands of the country, with soil depths ranging from 30 to 150 cm. Some of the coastal areas have sabkha deposits, a high-salinity depression soil intermixed with moderately deep to very deep sand to sandy loam soils (Scheibert et al., 2005; Ashghal, 2012).

2.5. Environment

Sabkhas are salty flat areas where the percentage of evaporation is high. This area covers seven per cent of Qatar land area and is classified into two different types: coastal sabkhas and internal sabkhas. Coastal sabkhas spread along the coast of Qatar. There are many changes happening to this type of sabkha, one of which happens on a daily basis when the seawater submerges the area during tidal movement (twice a day), and then it goes away leaving a residue of salt in the area.

2.6. Oceanography

2.6.1. Tides and currents

The currents around Qatar seldom exceed one knot yearly. There are many factors that have an indirect influence on these currents. The strong dominant Al Shamal winds in the winter can turn the waters and cause a small difference between bottom and surface water temperatures. Because of the high rate of evaporation and the high salinity in the summer, the salty Gulf water floods out through the Strait of Hormuz. In addition, the currents along the Qatar's coast flow anticlockwise. The range of tide around the Qatar peninsula is 1.6 m and the Salwa tidal amplitude is considered the smallest (United Nations, 1997).

2.6.2. Waves and water level

The height of waves around Qatar is 30 cm for waters near the shore (inshore); this can rise to 1.52 m. However, the waves in the waters that are far from the shore (offshore) are between 0.30 to 1.22 m. When the Al Shamal wind occurs, the height of the waves increases to reach 4.27 to 4.57 m (United Nations, 1997).

2.6.3. Salinity

There are three main factors that cause the increase in seawater salinity. These are low rainfall, high evaporation rates of water in summer and the small amount of freshwater inputs from land. The salinity in the surface water of Qatar is between 39 ppt and 41 ppt. However, the salinity in the bottom waters far from the shore and near the boundaries is around 1 to 2 ppt lower than the surface. The higher salinity in Qatar is found on the south-east coast, especially in Khor Udaid. Gulf Salwa is considered to be the place with the highest salinity, which is around 55 ppt (United Nations, 1997).

2.7. Changing sea levels in Qatar

There are two main stations that can provide historical data on SLR in Qatar. The first one is the Mina Sulman station in Bahrain, as shown in Figure 2-5. Recordings from this station showed that the sea level rose by 3.28 mm/year from 1982 to 2003 and 2.97 mm/year from 1993 to 2008. There is a gap of data from 1998 to 2003. This increased the uncertainty of the trend estimation (ICZMP-CCSLR, 2014).

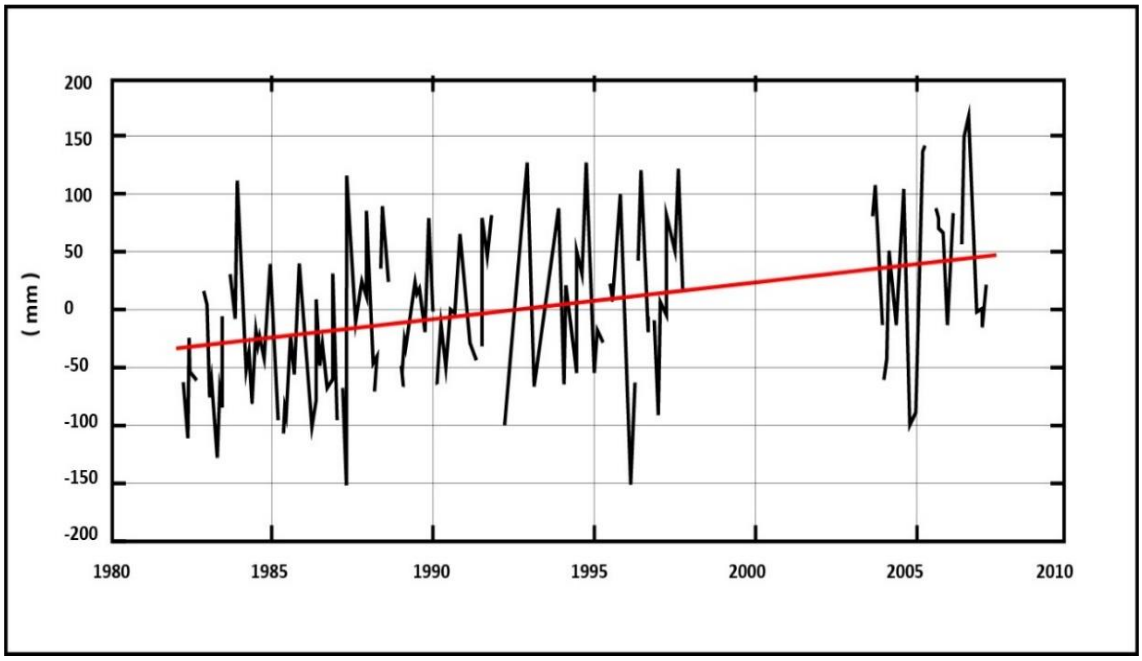

Figure 2-5: The trend in mean SLR during time series 1980-2010 from the Mina Sulman station from PSLMSL data set. (ICZMP-CCSLR, 2014).

The second station is located at Doha port. Estimated sea level changes from 1976 to 2013 using recordings from this station are shown in Figure 2-6. It shows that the sea level rose by 1.47 mm/year. However, this figure was revised to an estimated 2.8 mm/year from 1993 to 2013 (ICZMP-CCSR, 2014).

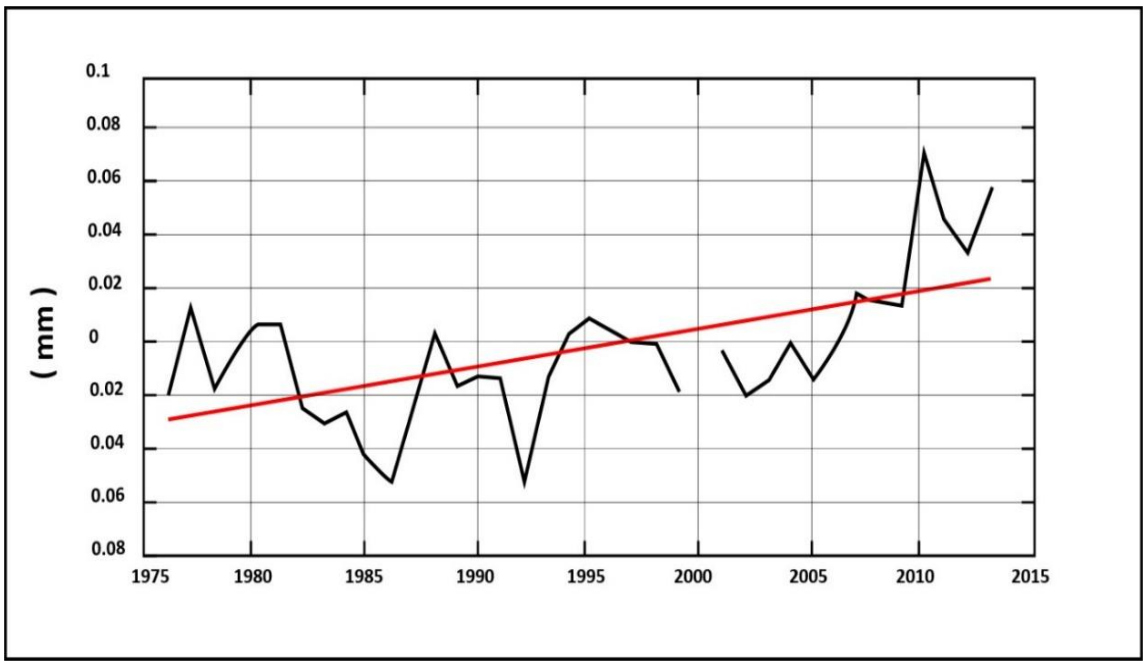

Figure 2-6: The linear trend in mean sea level for Doha station (ICZMP-CCSLR, 2014).

Sea level rise around Qatar does not different from regional and global trends (Table 2-1).

Table 2-1: Summary of local, regional and GMSL increase (ICZMP-CCSLR, 2014).

Scale	Data set	SLR increase (mm/year)	Period
Local (Qatar)	Main Sulman station (PSMSL data set)	3.28 ± 1.1 2.97 ± 2.55	1983-2007 1993-2007
	Doha Station	1.47 ± 0.69 2.8 ± 1.58	1976 – 2013 1993 - 2013
Regional	4 stations (PSMSL) (Ayhan & Alothman, 2009)	1.96 ± 0.21 2.7 ± 0.21	Longer than 19 years
	Church & White (2011) database	1.9 ± 0.44	1950 - 2009
	TOPEX and Jason Altimeter (Cazenave at al., 2012)	1.0 – 3.0	1993 - 2009
Global	Global data from Church & White (2011)	1.7 ± 0.2 1.9 ± 0.4	1900 – 2009 Since 1961
	TOPEX and Jason Altimeter (Cazenave at al., 2012)	3.4 ± 0.4	1993 - 2009
	IPCC ARC (2013)	1.7 ± 0.20	1901 - 2010
	IPCC ARC (2013)	3.2 ± 0.40	1993 - 2010

Sea level rise is expected to accelerate and continue in the future. This will have a significant impact on the coastal areas and increase the vulnerability and likelihood of flooding in these areas.

2.8. Socio-economic characteristics

The population of Qatar has exponentially increased from about 50,000 in 1960 to about 2.5 million in 2015 (The World Bank Databank, 2015; Ministry of Development Planning and Statistics, 2016; Trading Economics, 2016). According to the Planning and Statistics Authority (2019), the population in 2019 was approximately 2,753,045. Doha is the capital of the country and 39.8 per cent of the total population of Qatar lives there. The second city is Al Rayyan, with around 25.2 per cent of the population, and the third city is Al Wakra, with 12.4 per cent of the population (MDPS, 2016).

The population in Qatar increased from 369,000 to 522,000 during the period of 1986-1997, i.e. a rise of 41.6 per cent. This increase in population continued during the period of 1997-2004, from 522,000 to 744,000, a rise of 42.5 per cent, and during the period of 2004-2010 the population increased from 744,000 to 1,699,000, a rise of 128.4 per cent. There was also a 41.5 per cent

increase in population (1,699,000 to 2,405,000) in the five-year period from 2010 to 2015. This clearly shows that the population increased six and a half times during a period of 29 years from 1986 to 2015, which means that the average annual growth rate of the population stands at 6.7 per cent, mainly due to the rapid development in the country (Figure 2-7).

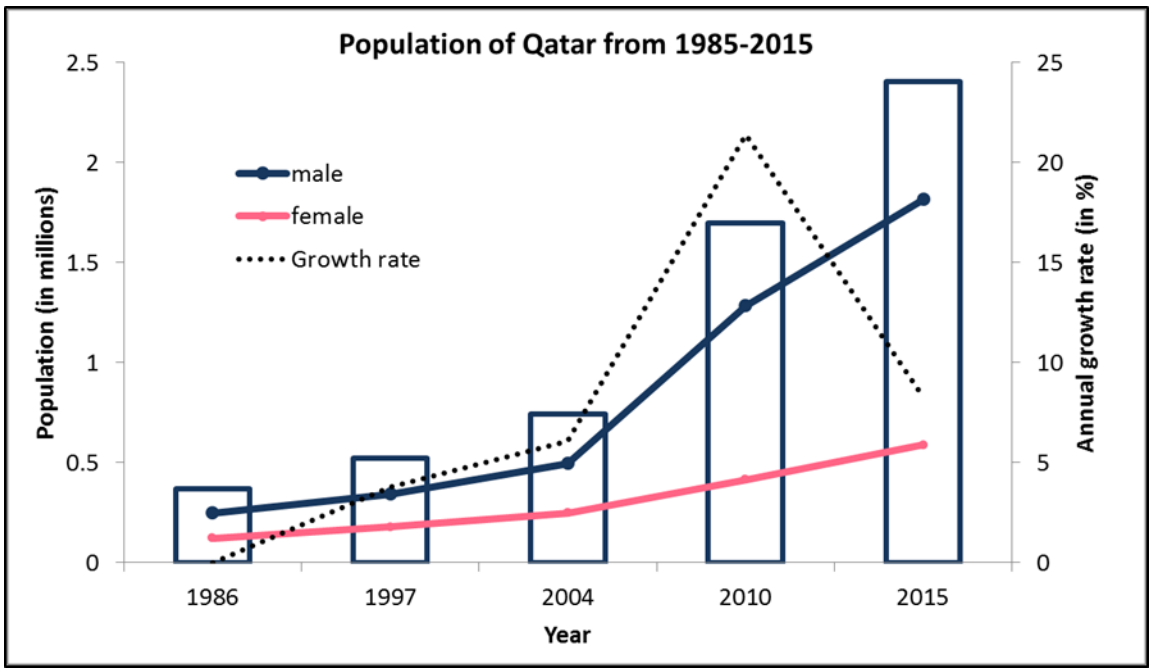

Figure 2-7: Qatar's population growth during the Census years (1986-2015); the overall annual growth rate (in %) is also shown with the male and female population. (Data source: Qatar GISnet).

The growth of the population has varied from zone to zone. The zones with industrial and commercial activities have shown the maximum growth. Many zones in Al Rayyan, Umm Slal, Al Khor and in the fringe areas of Doha municipality have populations that more than doubled during this period, while other zones in old Doha have registered a decrease. The decrease can mostly be attributed to the demolition of buildings in the old Doha area for new construction and displacement of activities, such as farms or cattle shades, etc., in the outer urban areas. However, the majority of zones in the country have recorded an increase in population during this period.

Since exploration started of Qatar's oil and gas resources, there has been an observable increase in the population in the country, mainly due to migrant workers. In the 1970s, Qatar's population was just over 111,000 and historical evidence suggests that, even during this time, the majority of the population were already "foreigners" (Babar, 2015). The staggering increase in

population between 2004 and 2010 can be expected as the country was experiencing modernisation during these times, with large investments in both infrastructure and human development.

The launch of Qatar National Vision 2030 in October of 2008 may also have played a great role in demographic explosion, as it gave frameworks on several aspects of Qatar's development, including human, social and economic development. This further encouraged more migration of skilled and unskilled workers in order to cater for the attainment of the country's vision. The population continued to rise until 2015, albeit at a slower rate compared to the last five years, because of the continuous recruitment of workers which can be attributed to the awarding of the Football World Cup to Qatar in late 2010 (De Bel-Air, 2015).

Figure 2-8 shows population growth that took place at zone level during 1986-2015, as per the censuses undertaken in 1986, 1997, 2004, 2010 and 2015. In 1986, a large number of the population was concentrated in a few areas in Doha, as well as in the nearby Al Rayaan area. Around 10,000–20,000 people were living in Al Khor, Umm Slal, west and east parts of Al Sheehaniya and Al Wakra municipality. An increase in population was observed in north-east Al Rayyan and Umm Slal in 1997, and some areas of northern Al Wakra. More apparent increases in population, however, were observed in north Al Khor (Ras Laffan area) and in industrial zones in Doha municipality. This observation can be attributed to the increasing population due to workers' recruitment.

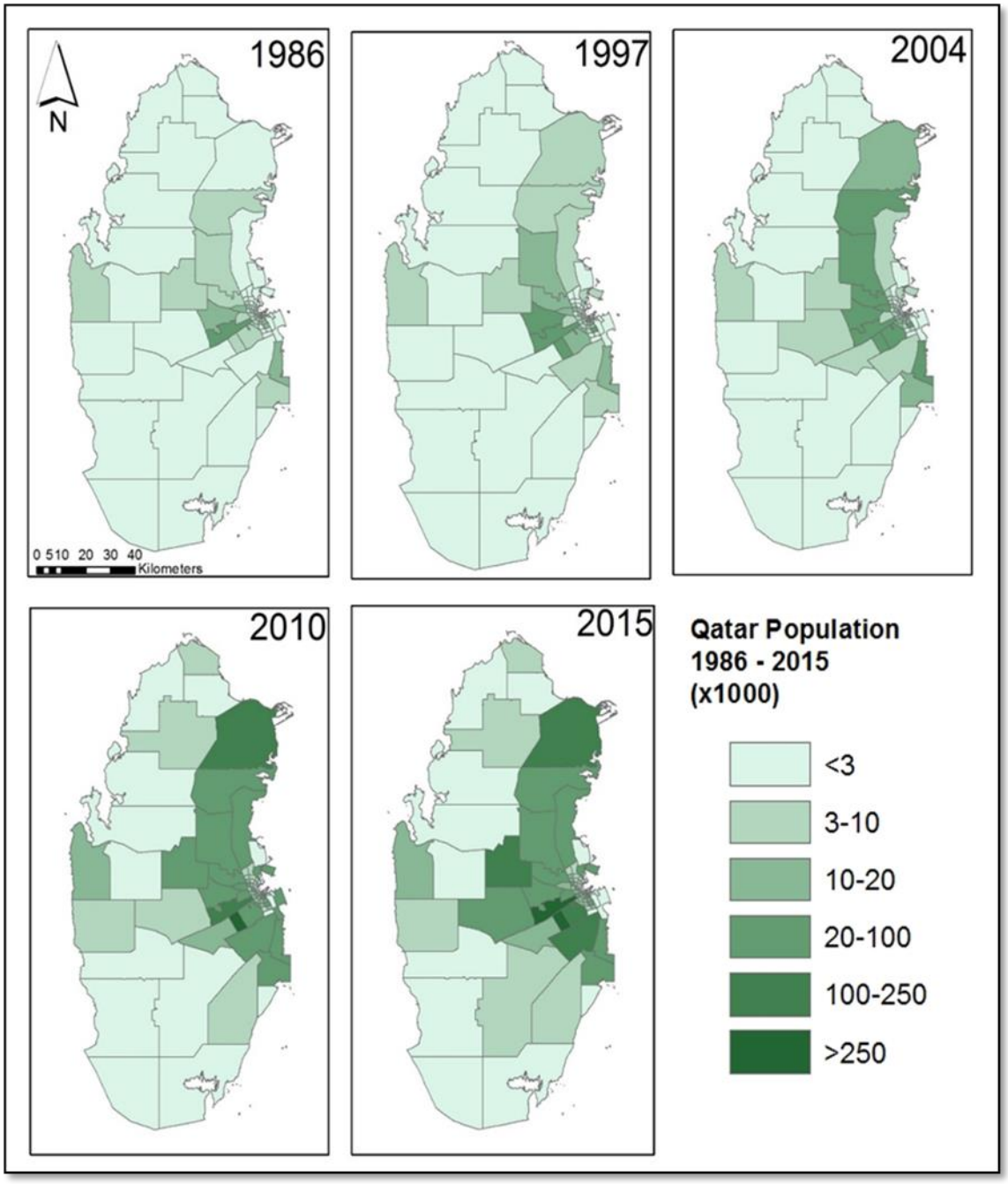

Figure 2-8: Population distribution per zonal area of Qatar from 1986 to 2015 using Natural Breaks (Jenks) classification (Data source: Qatar GISnet).

In 2004, the population became more intense in areas adjacent to the capital city of Doha, from the northern portion of Al Khor towards the south, including Umm Slal, Al Rayyan and northern portions of Al Wakra. The population also started to spread out of these areas in a western direction towards the areas of Al Sheehaniya. In 2010, municipalities that had high populations in 2004, i.e. Al Khor, Umm Slal and Al Rayyan, showed a decrease in population. The population distribution revealed a shift to north Al Khor (Ras Laffan), Al Wakra or west Al Sheehaniya (Dukhan), which

exhibited an increase in population or in some other parts of the country, e.g. Al Shamal, north Al Sheehaniya (Al-Ghuwariyah) and mid-Al Wakra area (Umm Saeeid), as shown by the more dispersed population during this time. There was little change in the distribution of population in 2015, except for the increase in population in eastern parts of Al Sheehaniya and northern Al Wakra.

There is a significant increase in population along the east coast of Qatar, from 1986 to 2015, where the oil industries are located, such as Ras Laffan and Umm Saeeid, and on the west coast at Dukhan. As such, these coastal regions stand vulnerable to SLR from a socio-economic aspect. However, the population inside Doha municipality was comparatively low, except in areas like the industrial area, Al Mansoura, in 2015. Most of the areas in Doha were intended for commercial purposes; moreover, companies prefer to house their employees in areas outside but adjacent to Doha, where housing costs are cheaper than in the capital.

2.9. Climate change and sea level rise in the study area

Qatar is the second largest producer of natural gas (Economides & Wood, 2009), making the country one of the world's richest. Historically, maritime trade was the main economic activity in Qatar (Carter, 2006), bringing urban settlements to the coastal areas. Therefore, most current residents of Qatar are living in the coastal areas. More than 90 per cent of the population lives in the capital Doha. Also, major industrial activities, including petrochemical companies, ports, desalination facilities and other supporting industries are concentrated in the eastern coastline north and south of Doha (Norton, 2009).

In the past two decades, the coastal areas in Qatar have grown fast due to the economic development in two key industries, oil and gas, and fisheries. The oil and gas industry, particularly, played an important role in the rapid development taking place in Qatar and most of the reserves in the sea or near the coastal area (Figure 2-9). Northfield, the biggest natural gas field in the world, is located in the sea with large production, refining and exportation activities on the north coast of Qatar.

Therefore, the coastal areas are crucial to support the oil and gas industry and among the high priorities to be protected from any future SLR. Any destruction of the oil and gas industry will have a significant economic impact in terms of the revenue for the government and the future for these areas.

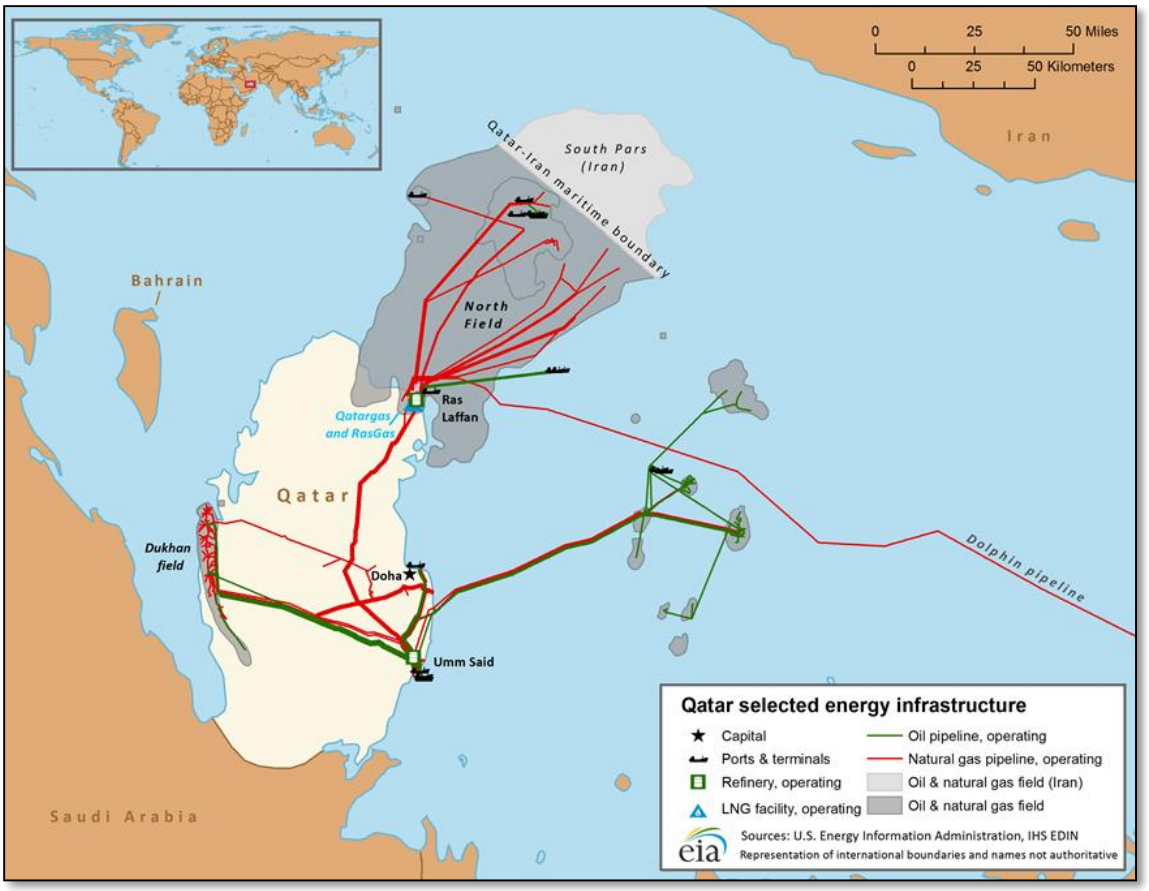

Figure 2-9: Qatar oil and gas infrastructure (source: http://www.eia.gov/).

Globally, research on climate change and SLR is extensive and widely reported. However, there is no published research work in this regard for Qatar. Despite the intrinsic value of current literature on climate change and related SLR at global levels a gap still exists, particularly in site-specific research that uncovers the vulnerabilities of the coastal region to potential SLR and ways to improve regional resilience.

The global climate change risk assessment studies for Qatar are limited. In one study (Maplecroft, 2009), Qatar is considered one of the three countries in the Arabian Gulf exhibiting "extreme" vulnerability to SLR, along with Kuwait and Bahrain. The study estimated that Qatar is susceptible to inland flooding at less than 5 m SLR, with 18.2 per cent of its land area and 13.7 per

cent of its population being adversely impacted. In another study by a World Bank group, it has been suggested that a 1 m SLR could impact two per cent of the population and GDP and one per cent of urban land.

Worldwide, coastal areas have held a significant economic, social and environmental value. According to the UN Atlas of the Oceans, 44 per cent of the world's population live within 150 km of the coastline (Syvitski et al., 2005). Of the world's ten most densely populated cities, nine are located on the coast. The coastal areas are also highly prone to disaster as they are exposed to a variety of natural hazards, both episodic and chronic. Episodic hazards include flooding due to heavy rain, cyclones, storm surges, earthquakes and tsunamis. Chronic hazards include coastal erosion and SLR (Bush et al., 2001).

Climate change, associated with SLR and its impact on the coastal zone, constitutes a current issue of global magnitude and concern. These are compounded by other factors, such as the increase in human population and other developmental activities of the modern era (industrial development, urbanisation and agricultural). These factors have exerted significant pressure on coastal areas. For example, Ciscar et al. (2011) have estimated the impact of climate change on agriculture in Europe. They produced estimates of crop yield reductions by ten per cent, river flooding causing economic damages of up to € 15 billion, sea flooding affecting up to 5.5 million people and a reduction of annual growth by 0.2-1 per cent.

2.9.1. Impacts of sea level rise in the Arab world

The regions of Arab countries are hyper-arid to arid with some scattered semi-arid zones. The climate remains extremely harsh for major parts of the year, with low precipitation and scarce water resources. Desertification, minimal biodiversity and excess of extreme weather conditions are common features of these hyper-arid regions. There are 22 countries in this Arab region, which include ten African countries and 12 west Asian countries. Significant numbers of the population live in economic centres located on the coastal zones of the Mediterranean Sea, the Red Sea, the Gulf and the Atlantic Sea. There has been a significant growth in both the population and tourism in these coastal areas (Massoud et al., 2003).

The Arab Forum for Environment and Development carried out a study in 2009 on the effects of climate change on the Arab region that provided detailed data on the impact of SLR in this region. Remote sensing techniques were used to demonstrate the impact of climate change on SLR scenarios that range from conservative (1 m) to extreme (5 m) until the year 2100. It was found that, in an event of less than 1 m SLR, about 41,500 km^2 of the Arab countries would be directly affected by the displacement of a fast-growing population of at least 37 million (~11 per cent). If the SLR is 2 m, 3 m and 4 m, then 60,000 km^2, 80,700 km^2 and 100,800 km^2, respectively, of the Arab coastal region will be seriously impacted. Up to 113,000 km^2 (0.8 per cent) of the coastal region would be inundated in the extreme event of a 5 m SLR (Tolba & Saab, 2009).

The study also found that Egypt, Saudi Arabia, Algeria and Morocco will be the most affected, while other countries such as Sudan, Syria, and Jordan will be less affected. In the extreme scenario of a 5 m SLR, Egypt will be the most impacted country with a displacement of at least 12 million Egyptians. This implies that Egyptians alone make up one third of the Arab population affected by SLR (Figure 2-10 and 2-11).

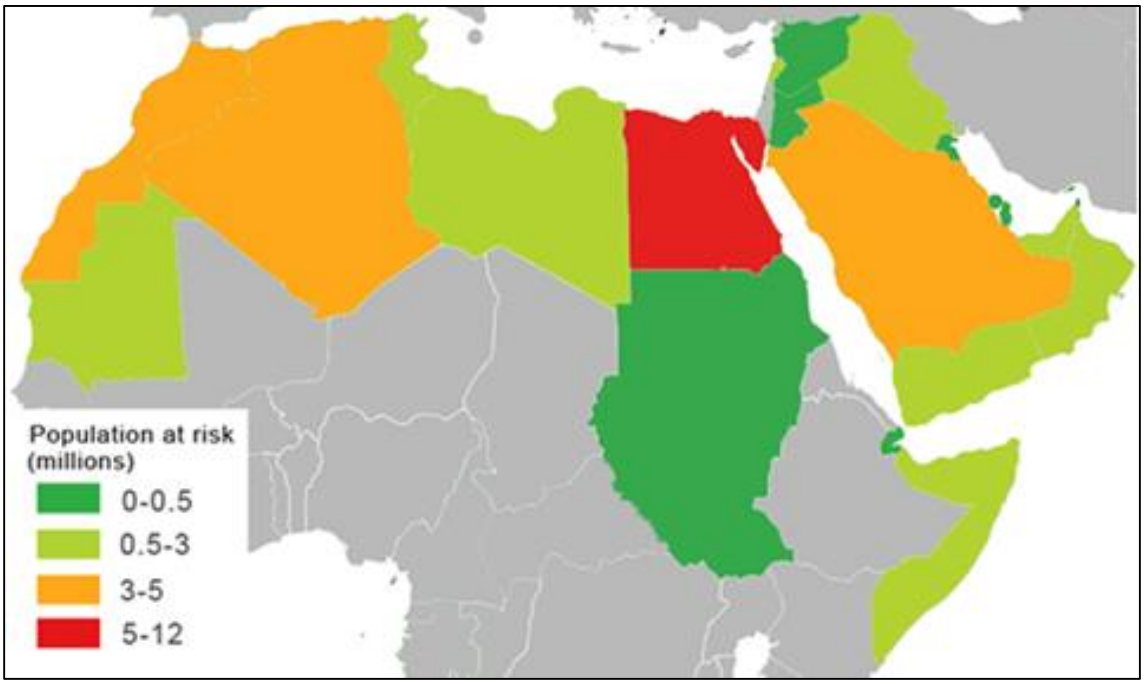

Figure 2-10: Extreme scenario (5 m SLR) impacts on the Arab world, by total population affected. ***Source: (Tolba & Saab, 2009).***

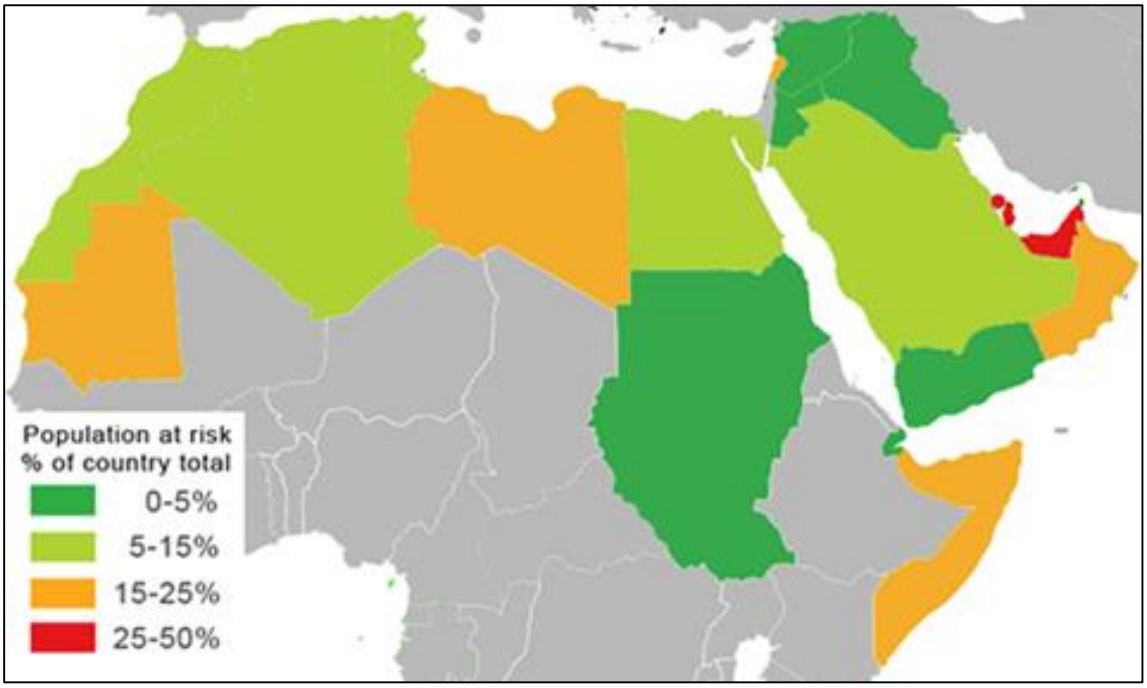

Figure 2-11: Extreme scenario (5 m SLR) impacts on the Arab world, by percentage of population affected. ***Source: (Tolba & Saab, 2009).***

In a similar, extreme 5 m SLR scenario, 50 per cent of the population in the United Arab Emirates (UAE), Qatar and Bahrain are estimated to be at risk. It is also indicated that Qatar, UAE, Kuwait and Tunisia are most vulnerable in terms of their land mass, since 1 m of SLR will affect one to three per cent of land in these countries. The extreme case of a 5 m SLR would reduce about 13.4 per cent and 6.9 per cent of land in Bahrain and Qatar, respectively, (Figure 2-12 and 2-13).

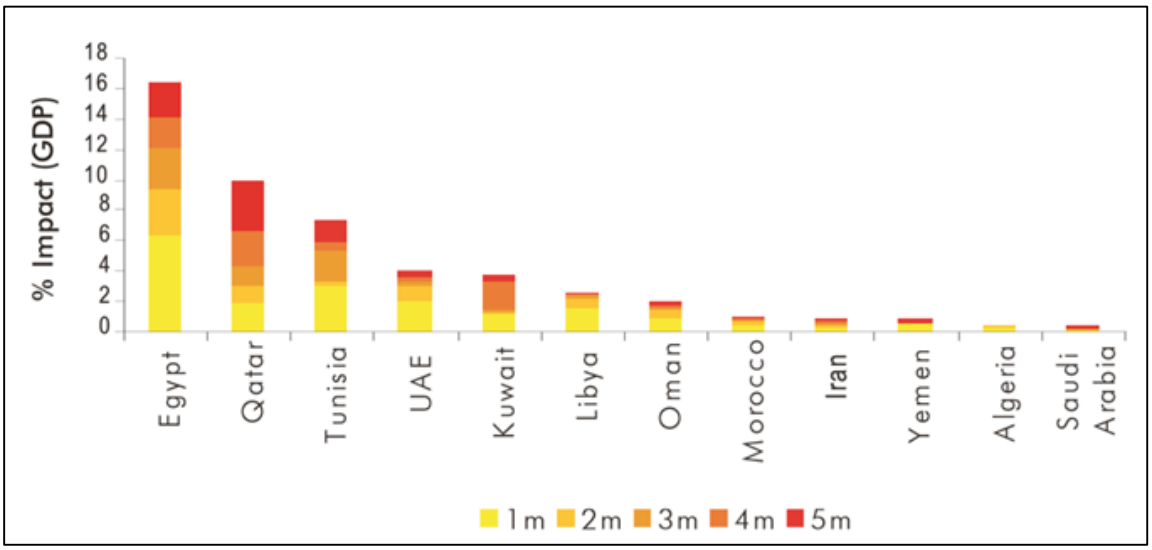

Figure 2-12: A comparison of percentage impact of SLR on gross domestic product (GDP) in the Arab Countries. ***Source: (Tolba & Saab, 2009).***

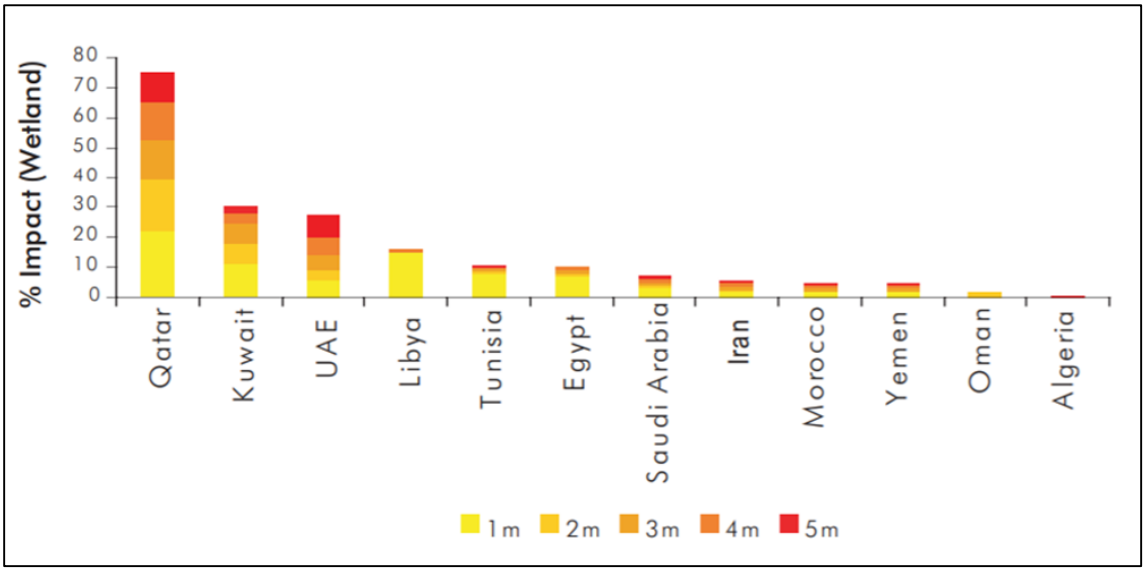

Figure 2-13: A comparison of percentage impact of SLR on land in the Arab Countries. ***Source: (Tolba & Saab, 2009).***

Although SLR may have less impact on the land area of the Middle East and North African regions than the developing world (0.25 per cent vs. 0.31 per cent with a 1 m SLR), it may have other severe impacts. For example, 3.2 per cent of its population (vs. 1.28 per cent worldwide), 1.49 per cent of its GDP (vs. 1.30 per cent worldwide), 1.94 per cent of its urban population (vs. 1.02 per cent worldwide) and 3.32 per cent of its wetlands (vs. 1.86 per cent worldwide) will be impacted (Dasgupta et al., 2007).

2.9.2. Sea level rise in the Arabian/Persian Gulf

The Arabian/Persian Gulf is a marginal and semi-enclosed sea which overlooks the Indian Ocean. It also lies in a semi-arid area of the Middle East, north to the Tropic of Cancer (Khan et al., 2002). It extends between the 24˚ and 30˚N latitudes and 48˚ and 57˚E longitudes and is located within the coordinates of eight countries: Iran, Iraq, Kuwait, Saudi Arabia, Bahrain, Qatar, the UAE and Oman (Figure 2-14).

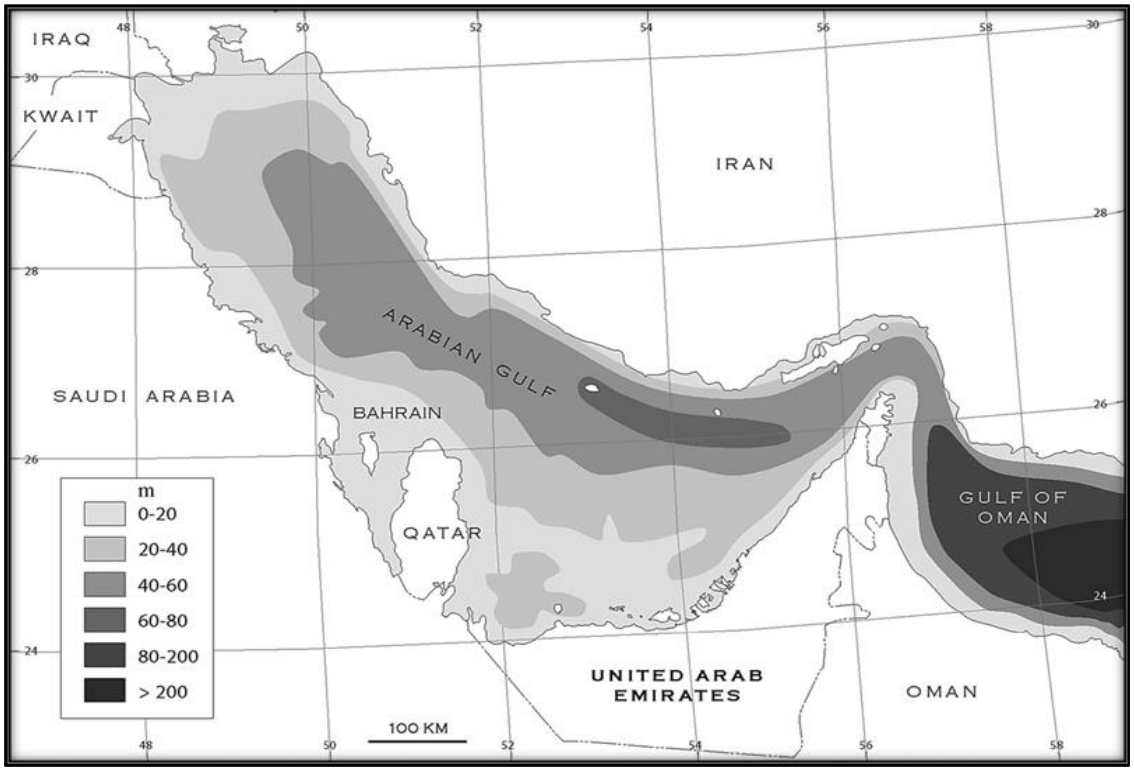

Figure 2-14: The mean depth of the Arabian/Persian Gulf (Source: Hamza & Munawar, 2009).

The Gulf extends over an area of about 239,000 km^2, with a length of 1000 km and a width that ranges from 75 to 350 km. The depth of the waters in the Gulf ranges from 20 to 100 m, increasing in the Strait of Hormuz to 130 m (Hamza & Munawar, 2009). According to the results obtained by the Sea Level Rise Explorer in 2015, the Arabian Gulf Coast is vulnerable to the consequences of SLR (Figure 2-15).

Figure 2-15: The Gulf countries, which will be affected by SLR (Source: Sea Level Rise Explorer, 2015).

In 2012, Ksiksi et al. focused on the city of Abu Dhabi and studied the effects of SLR on mangrove areas and land use. Five SLR scenarios were scrutinised (0.5, 1.5, 2, 2.5, 3 metres), leading to the conclusion that, in the event of the worst-case scenario (rise of 3 m), 40 per cent of urban areas and 82 per cent of mangrove forests would be affected. Ksiksi et al. (2012) used Shuttle Radar Topography Mission (SRTM) in order to create a DEM, and analysis was conducted in ArcGIS.

In the same year, the Environment Public Authority of Kuwait conducted a study in conjunction with the Convention on Climate Changes (2012). Chapter 3 of the report dealt with the vulnerability of the coasts of Kuwait to SLR. The study divided the Kuwaiti coast into three zones: northern, central and southern. The researchers used the global DEM by the United States Geological Survey and implemented four scenarios of SLR (0.5, 1, 1.5 and 2 m). They also created a database of 793 points along the coastal line and recorded all points in relation to the lines of latitude/longitude and vertical distance above the average sea level. However, the study relied on SLR scenarios during high tide and only focused on the risks to human beings, therefore ignoring risks to ecosystems, such as coral reefs, mangroves and other marine flora and fauna.

In 2014, Al-Buloshi et al. set out to study the effects of floods and SLR in six governorates of Oman using GIS. They adopted seven SLR scenarios (0.2, 0.5, 1, 2, 3, 4, 5 m) and concluded that, in the event of SLR, Al-Wusta and Al-Bathina are the most at risk, with an expected land loss of 900 km^2. This study relied on a coarse DEM of a horizontal spatial resolution of 40 metres.

Babu et al. (2011) focused on the impact of SLR on the Saudi Gulf coast and its effects on the ecosystem, population and social and economic infrastructure. To assess the climate change impacts (CCI) and adaptation, three scenarios of SLR (1, 2 and 3 m), as well as an environmental sensitivity index (ESI), were used to highlight vulnerable areas. Geographic information systems and remote sensing were used to gather data. The author concluded that a 3 m SLR will submerge 3600 km^2 of Saudi coastal land along the Gulf. What distinguishes this research from other studies is that it was developed from SRTM with 30 m resolution. However, control mechanisms and adaptations to these changes were not discussed by the author.

Al-Jeneid et al. (2007) assessed the vulnerability of environmental systems to SLR in Bahrain and attempted to measure their capacity for adaptation. They used GIS and remote sensing as tools and focused on two scenarios, digitising a topographic map with a contour interval of 5 m and ground truth data of more than 6,000 points. In the first place, the effects of 0.5 m, 1 m and 1.5 m SLR were studied, leading to conclusions that Bahrain could lose 17.5 per cent of its land to floods. In the second scenario, they analysed SLR risks of 2 m and 5 m and concluded that Bahrain would lose 47 per cent of its land. The success of this study lies in the use of a high-resolution (5 by 5 m) DEM, as well as proposing an action plan for national development policy makers to consider in order to secure the country's systems environment. However, the weakness of this paper lies in the fact that its focus did not consider other factors, such as tide and storms. This is important because surge heights will amplify surge magnitudes in funnel-shaped water bodies, such as the Arabian Gulf, resulting in higher water levels during storms (Reid & Bodine, 1968). Overall, this will exacerbate adverse impacts of SLR on coastal zones. These impacts are well known, and they include land inundation, coastal flooding, shoreline erosion and loss of wetlands (Solomon et al., 2007; Nicholls, 2007).

An additional problem in the Arabian Gulf is subsidence caused by the large-scale extractions of petroleum and natural gases (El-Raey, 2009). However, there is no long-term data or information about this phenomenon, which prevents any meaningful longitudinal analysis. This is particularly worrying in a region which Dasgupta et al. (2007) describe as highly vulnerable to the potential impacts of SLR. The same study identifies Qatar as a highly vulnerable country in the Arabian Gulf region, where around 2.8 per cent of its total terrestrial area will be impacted by the scenario of a 1 m SLR. Another study by Al Janeid et al. (2008) draws a very grim picture for the Kingdom of Bahrain, where 11 per cent and 14 per cent of its total lands will be impacted by a SLR of 50 cm and 1 m, respectively.

Chapter 3: Digital Elevation Model

3.1. Introduction

Digital elevation models are widely used in various studies and the accuracy of the DEM is an important factor to ensure the accuracy of results. A basic fact is that it is impossible to measure or simulate the Earth's surface with an accurate value. Different kinds of elevation sampling errors will occur during the process of DEM generation. In addition, the true surface is complex and irregular. Even if there were no DEM sampling errors, the limited elevation sampling points would still lead to an approximate simulation of the true surface. The accuracy of the terrain representation crucially depends on DEM spatial resolution applied (Guo-an et al., 2001). There are three main types of DEM errors: systematic, blunders or random (USGS, 1997). Systematic errors associated with the DEM generation process are due to a predetermined cause. The second type of error, blunders, are vertical errors associated with the data collection process. The third type is a random error, caused by random factors, and is usually difficult to remove (Burrough, 1986).

For analyses using DEMs the vertical accuracy is a key consideration. This incorporates the three errors from the paragraph above. Vertical accuracy is linked to horizontal resolution (i.e. the size of each grid cell). In a DEM, elevations are a mean over the cell. Therefore, cell size will influence how accurately each cell represents the elevation within. For example, a DEM created at a horizontal resolution of a 10 cm by 10 cm grid will provide a much more accurate representation of the land surface than a 1 km by 1 km grid. The uncertainty of a DEM can be assessed by using root mean square error (RMSE) as a general indicator of DEM accuracy (Stefanescu et al., 2012).

Modelling the impact of climate change on SLR is a challenge in many locations because predicted SLR is smaller than the vertical error of many global elevation datasets. Sea level rise predictions by 2081 range from 28 cm to 98 cm (Pachauri et al., 2014), while the vertical resolution of most DEMs is more than a few metres. For example, the ASTER DEM RMSE vertical accuracy ranges between 2 m and 9 m (Satgé et al., 2015). Therefore, in many locations only a broad assessment can be done to investigate the impact of climate change on SLR (Poulter & Halpin, 2008).

Digital elevation models are usually produced by interpolating samples of elevation data points to predict the elevations at all positions inside the DEM area (Li et al., 2004). However, the resulting DEM will contain errors. There are several factors which contribute to error accumulation in DEMs. One of the most important sources of error is the accuracy of elevation data. For example, ground-based or airborne automatic laser scanners can produce high-resolution elevation datasets (vertical accuracy of 0.5 mm) for a small area (Darboux & Huang, 2003). In contrast, traditional topographic surveys or the use of stereoscopic air-photos or high-resolution satellite imagery can produce relatively lower resolutions (ranging from centimetres to metres in accuracy) for a larger geographic area. There are other factors that affect the quality of DEM, such as data density and landform (Chaplot et al., 2006), spatial distribution of elevation and morphology of the area and the interpolation method used to generate DEM (Wilson & Gallant, 2000). Fisher and Tate (2006) reviewed the causes and consequences of error in DEMs and identified three components of the error budget in the process of DEM creation:

1. Error occurs in measured or interpolated elevation values.
2. Uncertainty related to the resolution of the DEM.
3. Error introduced by the specific technique of interpolation.

The accuracy of the interpolation method and its outcomes are affected by many factors. These vary in each case study. For example, Chaplot et al., (2006) compared the accuracy of DEM generated in areas of France and Laos through kriging, Inverse Distance Weighted (IDW), Multi-quadratic Radial Basis Function and spline. They found that all methods generated DEMs with similar accuracy when the density of elevation points were high. However, when the density of points was low, Kriging and IDW performed better than other methods. Arun (2013) evaluated IDW, Ordinary kriging, ANUDEM, Nearest Neighbour and spline based on their accuracy and sensitivity to topography variations and concluded that, in most cases, Ordinary kriging performed better than the other methods. In terms of accuracy, the effect of topography variation on the performance of interpolation methods was studied by Binh and Thuy (2008). They suggested that spline interpolation methods generate more accurate DEM for mountainous areas, while IDW and Ordinary kriging with exponential models of semi-variogram are most suitable in hilly and flat areas.

This chapter focuses on the generation of DEMs for urban and industrial areas of Qatar using an initial elevation dataset with a high vertical accuracy (10 cm RMSE), with points spaced every 10 m. This allows a detailed assessment of the impacts of climate change on SLR to be produced. However, this data is not ideal for an assessment of SLR for several reasons. Firstly, these data points did not cover all the areas of interest in this study, and especially near the coast (Figure 3-1); there were data gaps where buildings and other man-made features were. Therefore, an interpolation of the elevation dataset was necessary to create a DEM covering the entire study area. In addition, the elevation data had points every 10 m, which was felt to be too coarse for an assessment of flooding in an urban area. Hence, the data needed to be interpolated to a higher resolution of 5 m. Finally, the elevation dataset incorporated many breaklines and methods to incorporate these into the DEM needed to be developed. Given these challenges this chapter explores how urban DEMs can be generated in Qatar, exploring a range of techniques for incorporating features such as embankments and cuttings into the DEM, interpolating into data "gaps" where buildings have been removed and producing a finer DEM for SLR assessment.

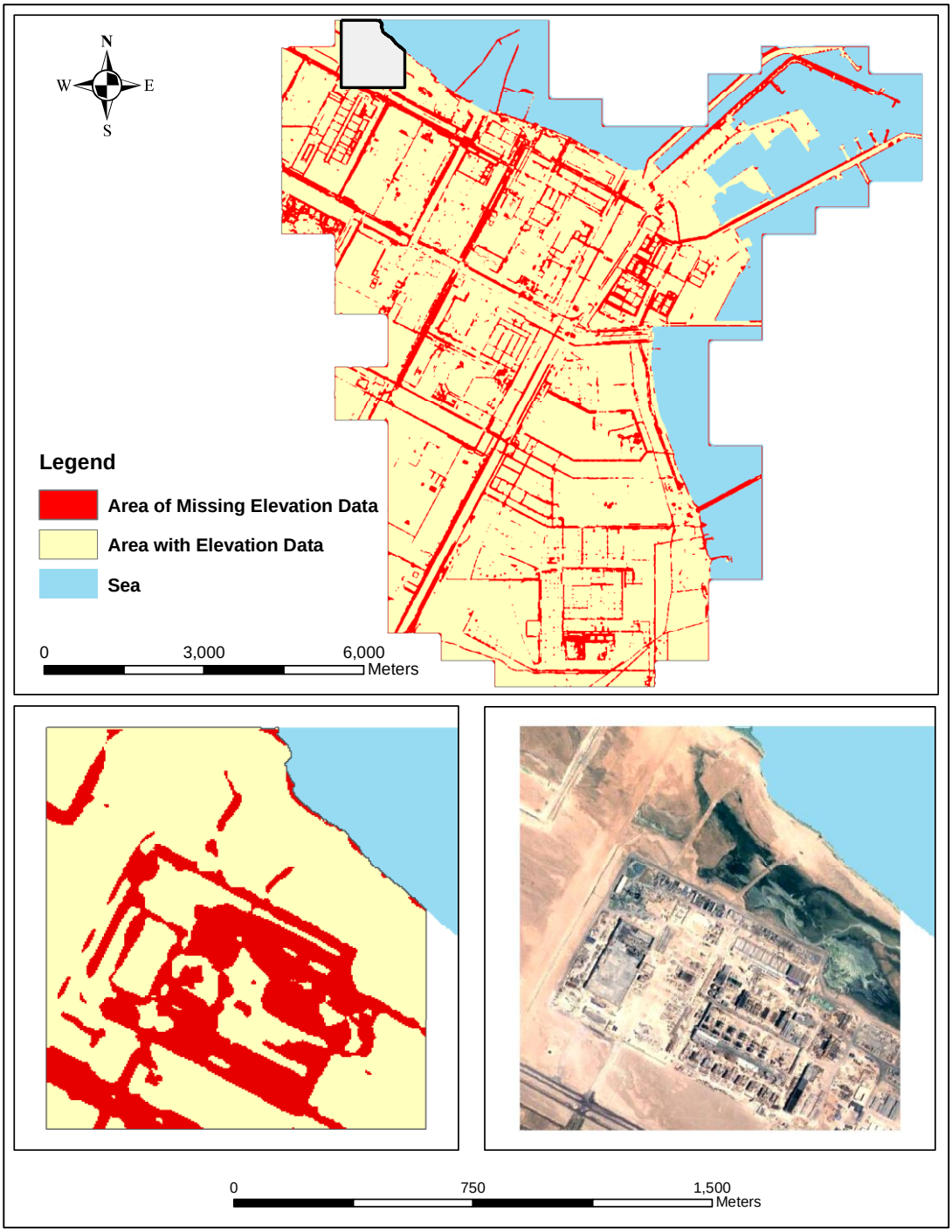

Figure 3- 1: Map showing the areas with no elevation points in Al Thakhira area

3.2. Methods

3.2.1. Elevation data collection

Elevation data points were obtained from the Centre for Geographic Information Systems and Planning (DEM-GISP) of the Ministry of the Municipality, Qatar. The DEM was delivered as part of the Qatar National Aerial Mapping 2008 project by COWI and Pace Imaging, a Middle East joint venture. It was generated using a Vexcel UltraCam-X for the capturing of 1:4,000 aerial photography for the production of an orthophoto with 10 cm spatial resolution (COWI, 2008). The DEM was created based on photogrammetric techniques in three dimensions (3D) using stereo imagery for inhabited and industrial areas covering approximately 650 km^2.

The resulting DEM comprises a mass of grid spaced points, at intervals of 10 m on the ground, and 90 per cent are stated to have vertical accuracy of 0.1 m RMSE. The data was collected using the Qatar national grid coordinate reference system (CRS), which is based on the QND95 geographic 2D CRS (Pallathu, 2015). This dataset did not cover the whole of Qatar, and its spatial extent is limited to urban areas, economically important areas and areas with the potential for future urban development projects. The distribution of these elevation points within Qatar is shown in (Figure 3-2).

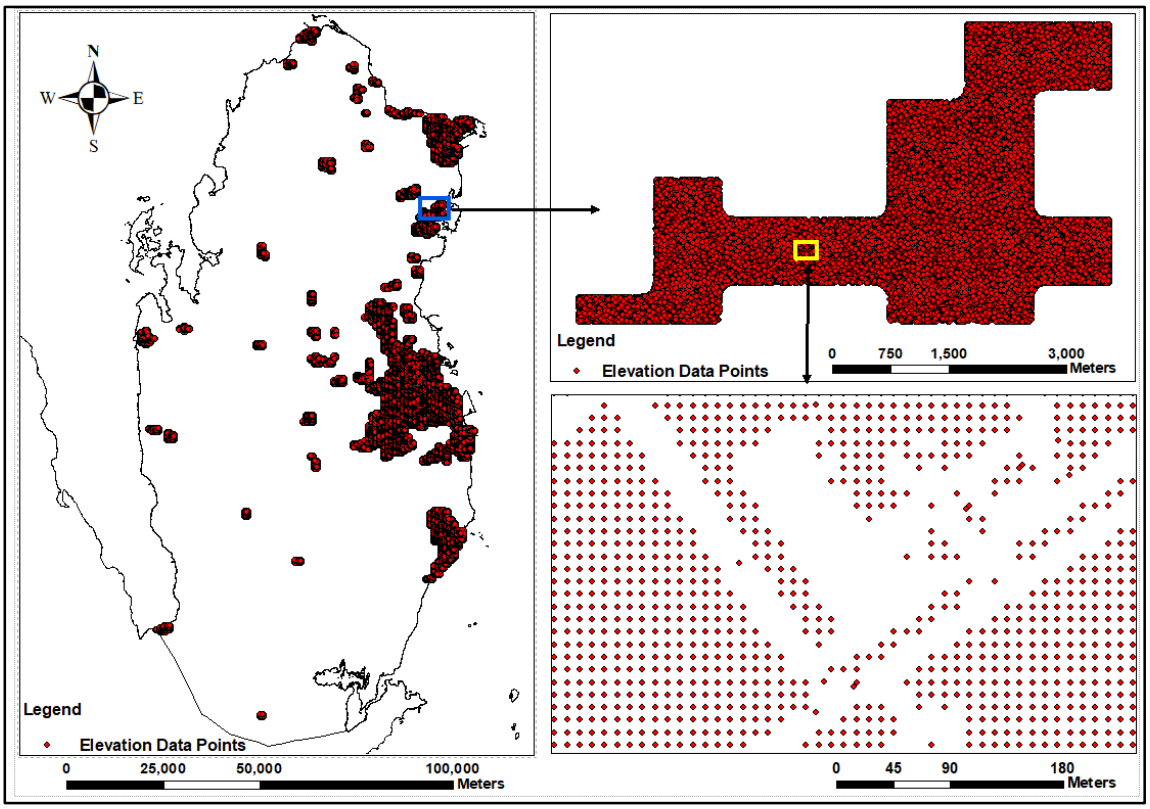

Figure 3-2: Distribution of elevation data points with 10 m horizontal resolution and 10 cm vertical accuracy

The entire country is covered by another DEM-GISP generated from 1:30,000 aerial photography, with points approximately 100 m apart and a vertical accuracy of 1 m (Pallathu, 2015). However, it was not suitable for this study to assess the changes in the sea level because the stated vertical accuracy of this data was not considered good enough to assess sub-metre changes in sea level.

The DEM was generated using automated methods, but manual intervention was required. This was necessary to remove elevations associated with buildings and other man-made features. Therefore, the elevation data points do not cover streets and spaces where buildings exist. An example of these gaps is presented in Figure 3-7, indicating that, in addition to avoiding roads, there are other areas where elevation points are not present. This is the case for areas with rapid changes of elevation and sand dunes. In some cases, the reason for the gaps is unknown.

3.2.2. Defining the study area

Elevation data was not available for the whole of Qatar (Figure 3-2). Therefore, five study areas where clusters of elevation data points were available were selected (Figure 3-3). These areas are Doha, Mesaieed, Al Khor-1, Al Khor-2 and Al Thakhira. Nearly 90 per cent of the population lives in these five locations in Qatar (Planning and Statistics Authority, 2015). Besides, these areas have potential for future developments. The Doha area (465 km^2) is the capital city of Qatar, where all government departments are based. Doha is considered as the centre of economic activities in Qatar, with 74 per cent of the population living there. While Mesaieed, Al Khor and Al Thakhira are less populated than Doha, they are economically important for Qatar; they are hubs for the petrochemical, chemical fertiliser, oil refining and natural gas industries. These areas were defined geographically by manually selecting five clusters of points.

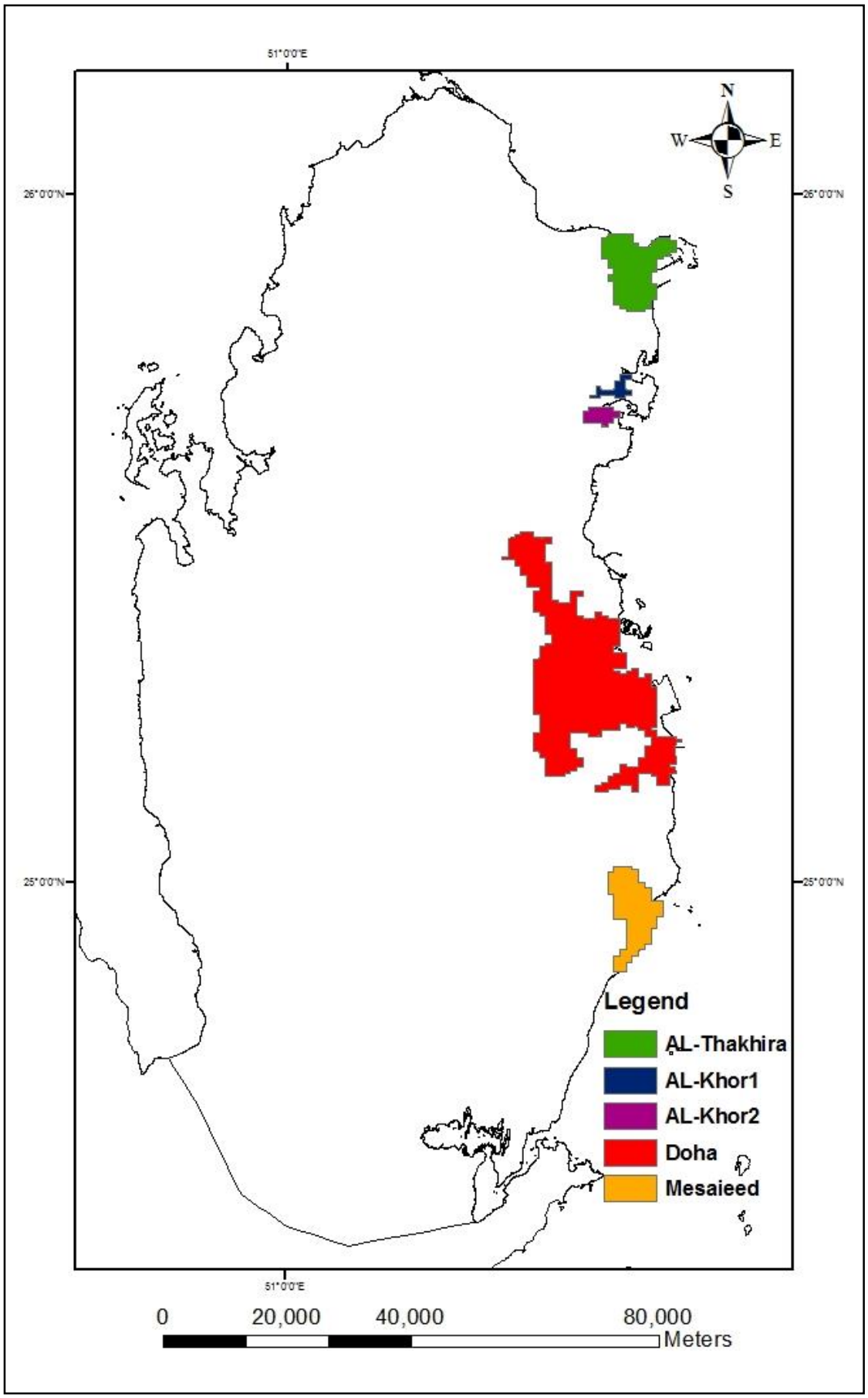

Figure 3-3: The selected study areas where a large number of elevation points were available and also economically important for Qatar.

The DEM points were scattered in these five locations with no administrative or geographic boundaries to define the study sites. To define the boundary of each site as a single polygon, the following method was used. The boundary needed to include all points and avoid gaps within the study boundary. These could occur where there were large spaces within the study area with no DEM points (e.g. large buildings). It was also decided that the polygon should not extend more than 10 m beyond the outer points of the study area. The boundaries were created in two steps:

1. A buffer zone of 100 m around all the points was created to cover a much wider area, to ensure that any gaps within the study area were closed.
2. The 100 m buffer line was buffered inwards by 90 m to produce a 10 m buffer zone from the outside points.

This process is illustrated in (Figure 3-4). The beige colour represents the area of clustered points and the final study area. The light green represents the buffer zone, which ensures that the boundaries do not contain gaps, or that the interpolation is not done to more than 10 m (cell width) from the mass of points. The sizes of the five study areas are presented in (Table 3-1).

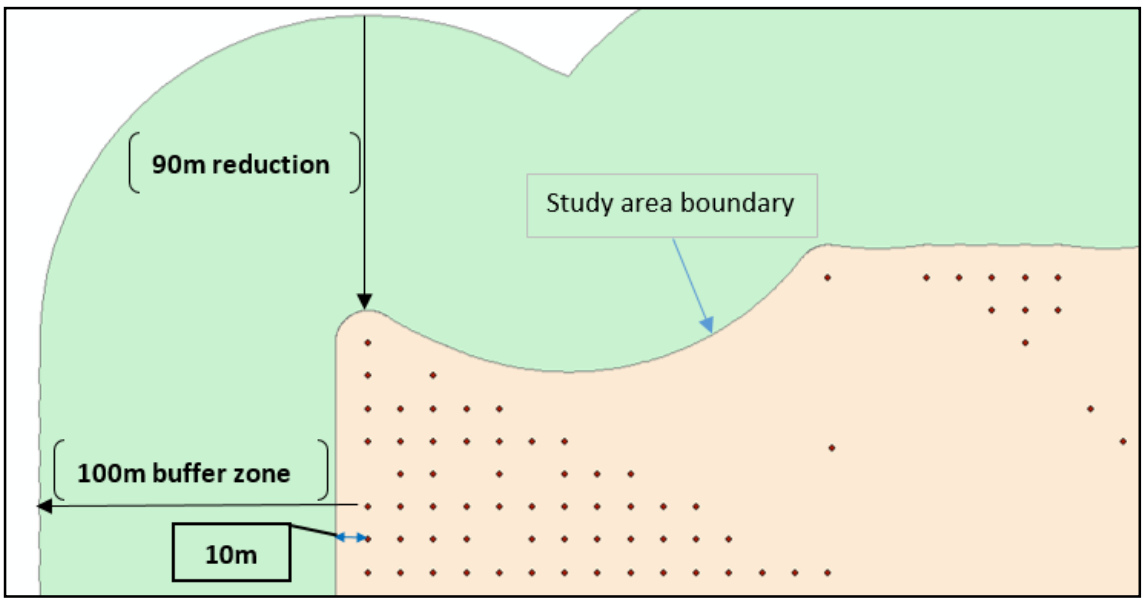

Figure 3-4: Defining study area by creating buffer zones to include all elevation points

Table 3-1: Name, area and number of elevation points for the five selected study areas

Area Number	Name of the study areas	Area (km^2)	Total number of elevation points
1	Al Thakhira	93.78	736,234
2	Al Khor-1	11.42	89,567
3	Al Khor-2	13.62	102,111
4	Doha	465.04	3,352,917
5	Mesaieed	88.24	603,810

3.2.3. Accuracy assessment

In addition to the stated accuracy of this data, the stated accuracy was further validated by visiting a number of sites in the study area. A field survey was arranged in January 2016. The researcher, along with a technician from the Centre for Geographic Information Systems and Planning, assessed the accuracy of elevation data points from DEM-GISP using a Leica Viva GNSS GS08 plus receiver (Figure 3-5) with a stated ±10 mm vertical accuracy (Leica Geosystems AG - Part of Hexagon, 2019).

Figure 3-5: Leica Viva GNSS GS08 plus receiver used in field validation

The accuracy of the Leica Viva GNSS GS08 is dependent upon many factors, such as the number of satellites and constellation geometry. The accuracy, which is measured as RMSE, is estimated: 5 mm (horizontal), 10 mm (vertical) and compliant to ISO17123-8 standard (Leica, 2012).

In total, 43 random points were chosen from the original dataset in the five studied areas. These points were visited and the elevation recorded. Ten points were excluded from the analysis because there was evidence that the elevation had changed significantly due to land flattening for urban and industrial development since the original survey (Figure 3-6). The result of the survey (Table 3-2) shows the 33 points surveyed to have errors of less than a metre, with an average error of 33 cm. There were 78.8 per cent of the points with errors of less than half a metre and 51.5 per cent had less than 25 cm error.

In most cases, the elevation of these points has a lower elevation value reading from the survey compared to what was recorded in the DEM. This ranged from a few centimetres to just below a metre. There are a few cases where the elevation was higher, but this was likely due to artificial increases in the elevation for the purpose of development. For example, the maximum differences were in Doha (just below one metre), likely because the area was elevated prior to new urban developments.

This relatively small validation suggests that the stated accuracy in the DEM data may be an overestimate. However, it is important to recognise other reasons why the two datasets may differ (Figure 3-7). The first reason is that the GISP DEM data was collected in 2009. Much of the study area consists of a sand substrate, hence natural processes may have altered the elevation since 2009. Also, man-made development not spotted by the researcher may have occurred. It is also possible that the location of the two elevation points was not identical. Secondly, the high accuracy of the Leica Viva GNSS GS08 device also contributed to error because it has an extremely low level of vertical error (5 mm to 20 mm) while the DEM data had a much higher vertical error (10 cm). Based on the validation, it was decided to proceed with the DEM as a suitable source for assessing SLR.

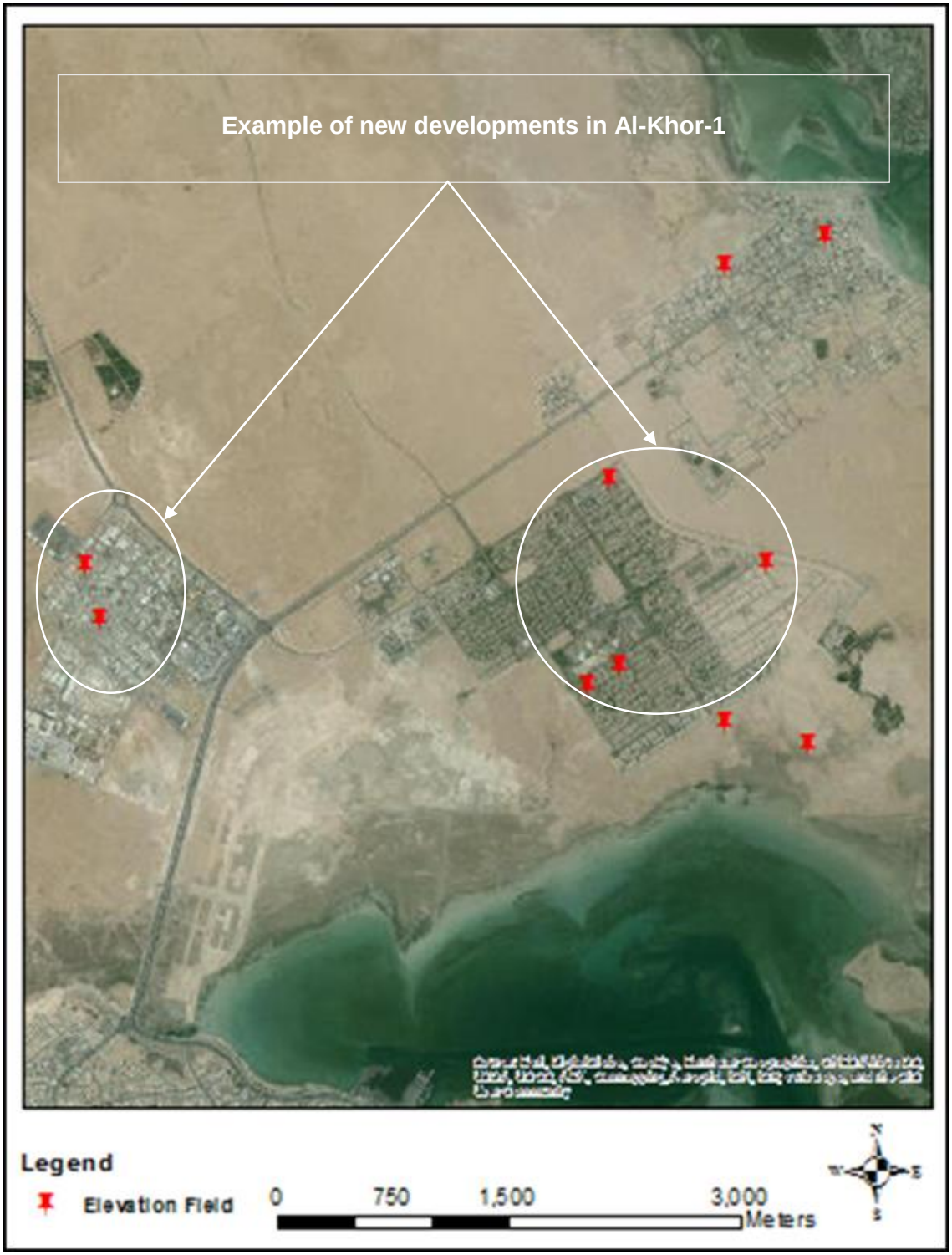

Figure 3-6: Satellite imagery showing the new development in Al Khor-1, causing changes in elevation values between 2009 and 2016

Table 3-2: Field measurement of elevation using Leica to calculate the error of DEM-GISP

Study areas	SN	Location	Surface type	Elevation Leica Viva GNSS GS08 (m)	Elevation DEM-GISP (m)	Error (±m)	RMSE (m)
Al Thakhira	1	51°31'47.772"E 25°50'47.502"N	Dolomite and limestone	5.03	5.28	0.24	0.45
	2	51°31'39.378"E 25°50'30.11"N	Dolomite and limestone	4.89	5.28	0.39	
	3	51°32'1.157"E 25°50'30.063"N	Settlements	4.68	5.18	0.51	
	4	51°32'36.795"E 25°50'53.635"N	Silt Flats Sabkha	4.53	5.11	0.58	
Al Khor-1	5	51°32'43.39"E 25°44'11.549"N	Settlements	6.83	7.02	0.19	0.28
	6	51°32'20.08"E 25°44'5.518"N	Settlements	7.22	6.86	0.36	
	7	51°32'38.869"E 25°42'24.832"N	Dolomite and limestone	6.43	6.75	0.32	
	8	51°32'19.089"E 25°42'29.906"N	Dolomite and limestone	6.75	6.51	0.24	
Al khor-2	9	51°31'19.11"E 25°41'6.222"N	Settlements	2.21	2.28	0.07	0.44
	10	51°31'20.929"E 25°40'57.816"N	Settlements	4.60	4.22	0.38	
	11	51°31'17.653"E 25°40'42.856"N	Settlements	3.26	3.08	0.18	
	12	51°31'0.797"E 25°40'43.553"N	Settlements	3.00	3.17	0.17	
	13	51°30'1.194"E 25°40'56.261"N	Settlements	9.27	8.69	0.58	
	14	51°29'15.707"E 25°41'6.851"N	Settlements	5.39	5.43	0.04	
	15	51°29'28.61"E 25°40'30.465"N	Settlements	5.50	5.94	0.44	
	16	51°29'55.843"E 25°40'10.242"N	Settlements	4.56	5.45	0.89	
Doha	17	51°26'43.151"E 25°24'16.701"N	Dolomite and limestone	19.68	19.46	0.21	0.63
	18	51°28'5.35"E 25°20'9.15"N	Settlements	9.36	9.46	0.10	
	19	51°31'13.025"E 25°21'19.95"N	Settlements	2.53	2.17	0.36	
	20	51°31'17.009"E 25°19'26.791"N	Settlements	2.29	1.32	0.96	
	21	51°25'56.32"E 25°19'17.317"N	Settlements	17.27	18.02	0.74	
	22	51°26'59.439"E 25°13'55.36"N	Settlements	18.14	17.19	0.95	
	23	51°26'37.243"E 25°10'50.486"N	Settlements	27.71	28.17	0.46	

Study areas	SN	Location	Surface type	Elevation Leica Viva GNSS GS08 (m)	Elevation DEM-GISP (m)	Error (±m)	RMSE (m)
Mesaieed	24	51°31'46.873"E 25°1'8.747"N	Silt Flats Sabkha	1.10	1.20	0.10	0.21
	25	51°31'16.224"E 25°0'17.276"N	Dolomite and limestone	4.98	5.11	0.13	
	26	51°31'54.023"E 24°59'54.918"N	Dolomite and limestone	8.56	8.75	0.19	
	27	51°31'20.338"E 24°59'23.73"N	Dolomite and limestone	6.71	6.67	0.04	
	28	51°32'25.601"E 24°59'41.883"N	Dolomite and limestone	9.57	9.70	0.14	
	29	51°31'32.016"E 24°52'59.68"N	Sand Dunes	1.25	1.14	0.11	
	30	51°32'36.651"E 24°54'0.764"N	Sand Dunes	1.10	1.14	0.04	
	31	51°32'38.328"E 24°55'4.735"N	Sand Dunes	1.19	1.40	0.22	
	32	51°33'42.825"E 24°58'29.149"N	Silt Flats Sabkha	2.92	3.38	0.46	
	33	51°31'33.38"E 24°58'19.89"N	Silt Flats Sabkha	0.37	0.63	0.26	
RMSE (m) for all areas							0.42

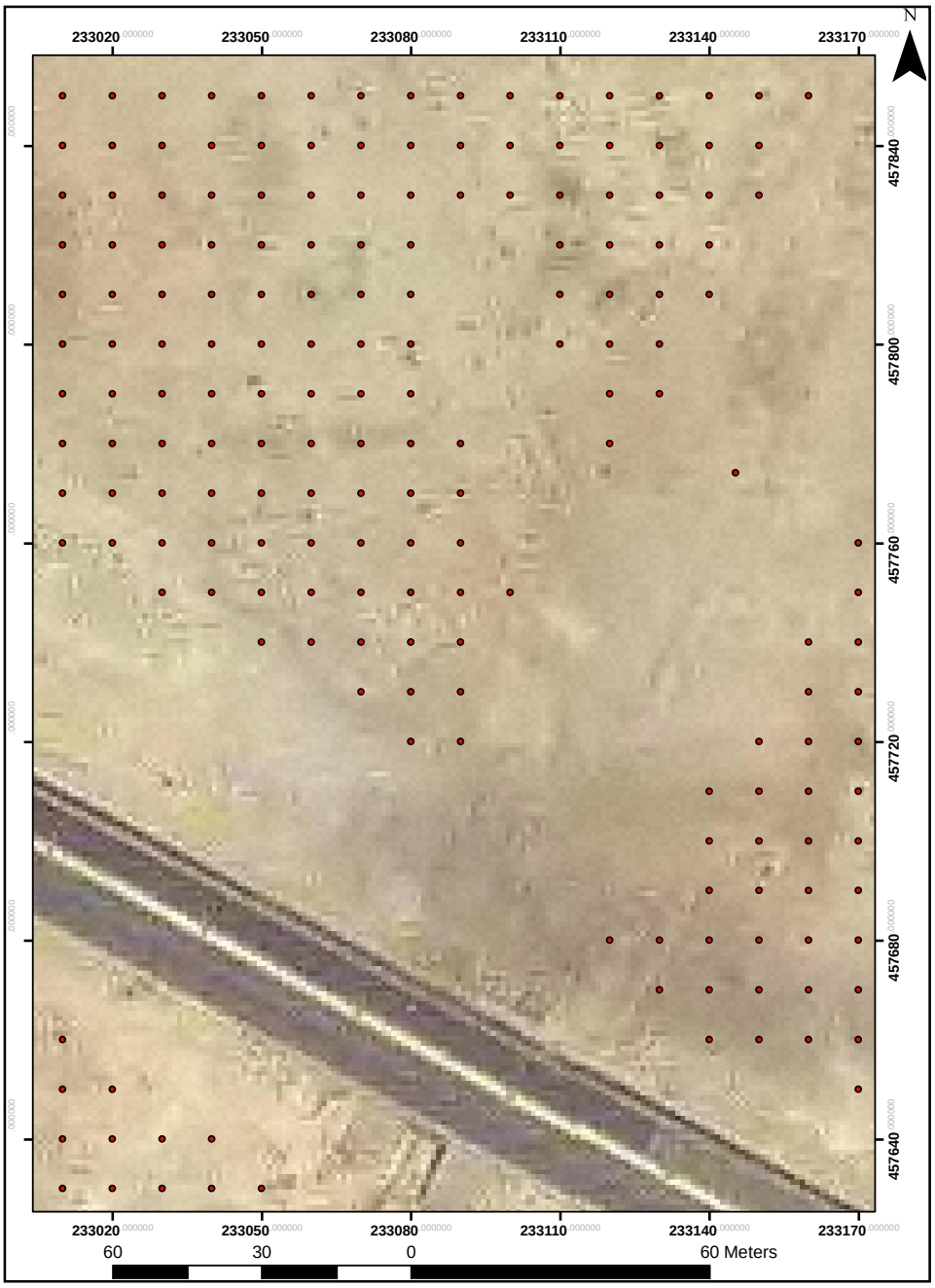

Figure 3-7: Google Earth image with an overlay of the 10 m DEM points

Digital elevation models are sampled arrays of elevation values representing ground positions at regularly spaced intervals. Digital elevation model is the terminology used to describe terrain elevation datasets in a digital raster form. The DEM is an important input to evaluate coastal vulnerability to flooding as the result of SLR. In this chapter, three different data interpolation methods were selected to create the DEM, namely IDW, Kriging and TIN. Spline was discounted at this point due to the exceptionally large computational requirements and, hence, time required, but is explored later in the chapter. Each of these interpolation methods will now be described.

3.2.4. Inverse distance weighting

Inverse distance weighting explicitly conveys the assumption that things that are close to one another are more alike than those that are further apart. To predict a value for any unmeasured location, IDW will use the measured values surrounding the prediction location. Those measured values closest to the prediction location will have more influence on the predicted value than those further away (Burrough & McDonnell, 1998). Thus, IDW assumes that each measured point has a local influence that diminishes with distance. It weights the points closer to the prediction location more than those further away, hence the name. Inverse distance weighting is proportional to the inverse of the distance (between the data point and the prediction location) raised to the power value. Consequently, as the distance increases, the weights decrease rapidly. The rate at which the weights decrease is dependent on the value of power function (p) (Equation 3-1).

$$w(i) = \frac{1}{Distance\text{^}p} \qquad (Eqution\ 3-1)$$

where w(i) is the inverse distance-weight and p is the power function.

If p = 0, there is no decrease with distance, and because each weight is the same, the prediction will be the mean of all the data values in the search neighbourhood. As p increases, the weights for distance points decrease rapidly. If the p-value is high, only the immediate surrounding points will influence the prediction (Burrough & McDonnell, 1998).

A power function of two is used as a default value in IDW analysis. However, in this study three power functions were tested, p = 1.5, 2.0 and 2.5, to identify the most appropriate power value and best outcomes. Small non-integer changes in p were used to avoid large differences between interpolations. The effect of changing p-value was investigated by examining the cross-validation statistics in order to identify the best power function.

Inverse distance weighting techniques have lots of advantages and disadvantages compared to other types of interpolation methods (Mitas and Mitasova, 2005; Yao et al. 2013)

Advantages:

1. It provides explicit control over the influence of distance (an advantage not offered by kriging).
2. The user can create a smoother surface by decreasing the power, increasing the number of sample points used or increasing the search radius.
3. The user has control over the mathematical form of the weighting function.

Disadvantages:

1. Decisions must be made about the power factor as well as the distance over which the points have an influence on the interpolated value.
2. Inverse distance weighting does not automatically provide an estimate of error associated with the interpolation.
3. The interpolated surfaces average out irregularities, and factors such as sharp changes in slopes are not considered unless these sites have a high point density.
4. Inverse distance weighting cannot make estimates above the maximum or below the minimum values of sample points. Thus, peaks and valleys, for example, will be flattened out if their high and low points are not part of the sample (Dumitru et al., 2013).

3.2.5. Kriging

This method is similar to IDW in that it weights the surrounding measured values to derive a prediction for an unmeasured location. The general formula for both interpolators is formed as a weighted sum of the data. In IDW, the weight depends solely on the distance to the prediction location. However, with kriging, the weights are based, not only on the distance between the measured points and the prediction location, but also on the overall spatial arrangement of the measured points (Equation 3-2). The kriging interpolation formula is as below:

$$\hat{Z}(s_0) = \sum_{i=1}^{N} \lambda_i Z(s_i)$$

(Equation 3-2) [from *Oliver & Webster (1990)*]

$\hat{Z}(s_o)$ = predicted value
$Z(s_i)$ = the measured value at the location i
λ_i = an unknown weight for the measured value at the location i
s_o= the prediction location
N = the number of measured values

The semi-variogram functions assume that things nearby tend to be more similar than things that are further apart. Both semi-variogram and covariance measure the strength of statistical correlation as a function of distance (Burrough & McDonnell, 1998). Semi-variogram models for all pairs of points are separated by distance *h*. The formula involves calculating half the difference squared between the values of the paired locations. To plot all pairs quickly becomes unmanageable. Instead of plotting each pair, the pairs are grouped into lag bins – for example, computing the average semi-variance for all pairs of points that are greater than 40 metres but less than 50 metres apart. The empirical semi-variogram present a graph with values on the y-axis and distance (or lag) on the x-axis (Figure 3-8).

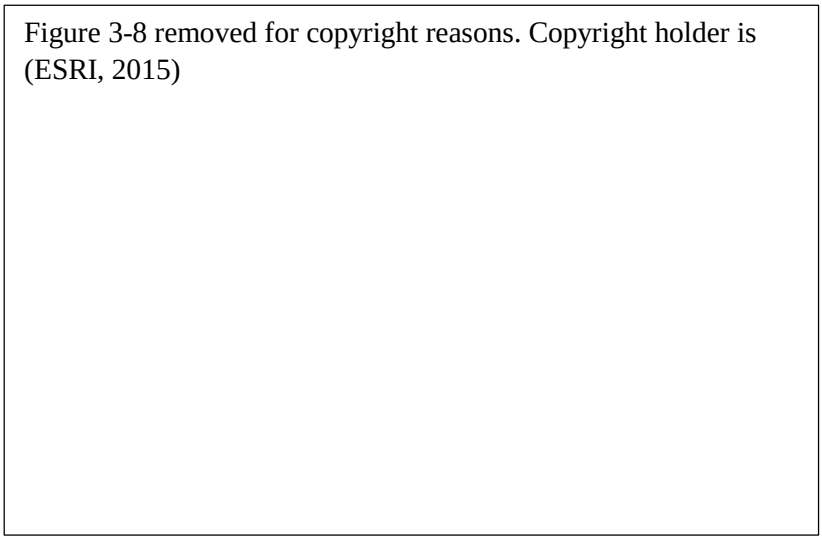

Figure 3-8: An example explaining the semi-variogram model (source, ESRI, 2015)

In this study, five different types of kriging were performed, based on semi-variogram models fitted to the dataset, namely Ordinary Spherical, ordinary exponential, Ordinary Gaussian and Ordinary Linear, in order to find the best prediction model with minimum statistical errors.

1. **Spherical Model**: Based on this model, spatial autocorrelation between points decreases where distance increases, until some level beyond which correlation becomes zero (Figure 3-9). The spherical model is one of the most used models.

Figure 3-9 removed for copyright reasons. Copyright holder is (ESRI, 2015)

Figure 3-9: Spherical semi-variogram (source, ESRI, 2015)

2. **Exponential Model:** Based on this model the spatial autocorrelation decreases exponentially with increasing distance and becomes zero at an infinite distance (Figure 3-10). The exponential model is one of the most used models.

Figure 3-10 removed for copyright reasons. Copyright holder is (ESRI, 2015)

Figure 3-10: Exponential semi-variogram (source, ESRI, 2015)

3. **Gaussian Model:** This model has an S-shaped semi-variogram model, which means that the points are correlated in a small distance. The S-shaped semi-variogram concaves upward to a point the curve begins to flatten (Figure 3-11).

Figure 3-11removed for copyright reasons. Copyright holder is (ESRI, 2015)

Figure 3-11: Gaussian model (source, ESRI, 2015)

4. **Linear Model:** Based on this model, the autocorrelation between points is decreased when distance increases in a linear function (Figure 3-12).

Figure 3-12 removed for copyright reasons. Copyright holder is (ESRI, 2015)

Figure 3-12: Linear model (source, ESRI, 2015)

There are many advantages for using the kriging method: (Mitas and Mitasova, 2005; Yao et al. 2013)

1. It produces better estimates than other methods because it considers the spatial dependence between points.
2. It is less susceptible to investigator's decisions (e.g. number of sample points to use) as it identifies the optimal interpolation weights and search radius.
3. It gives an indication of the reliability of the estimates (Dumitru et al., 2013).
4. It provides high statistical quality of predictions (e.g. unbiasedness).
5. It has the ability to predict the spatial distribution of uncertainty.

3.2.6. Triangulated irregular network

The triangulated irregular network (TIN) is based on vector data and is constructed by triangulating a set of vertices (points). The vertices are connected with a series of edges to form a network of triangles. There are different methods of interpolation to form these triangles, such as Delaunay triangulation or distance ordering (Burrough & McDonnell, 1998). ArcGIS supports the Delaunay triangulation method. Delaunay triangulation draws a circle through three nodes of a triangle and has the advantage of reducing imprecision and being independent of the order in which the points are processed.

The advantages and disadvantages of TIN methods include:

Advantages:

1. Better surface description at various levels of resolution.
2. Size of the triangles can be adjusted to fit the terrain surface (small triangles for complex reliefs, big triangles for simple reliefs), thus reducing unnecessary data storage and enhancing storage capacity.
3. Avoids redundancies of the regular grid.
4. Provides an efficient means for computing derived data such as slopes.
5. Allows extra information to be gathered in areas of complex relief without the need to gather huge amounts of redundant data from areas of simple relief (Burrough & McDonnell, 2015).

Disadvantages:

1. May require network visual inspection and manual control.
2. When the closest three points used to make a triangle are a sample from the same contour, the triangle has a zero slope and therefore becomes flat. This constitutes an error in the surface which requires adding supplementary points for correction, even though errors will remain (Fowler & Little, 1979).
3. The triangular digitisation may hinder some spatial analysis, such as surface geometry and topology (Burrough & McDonnell, 2015).

3.2.7. Spline

The spline method estimates surface elevation using a mathematical model that minimises all surface curvature to create a smooth surface which passes through the input points (ESRI, 2017). There are two types of spline: regularised and tension. Regularised spline interpolation uses first derivative (slope), second derivative (rate of change in slope) and third derivative (rate of change in the second derivative), while the tension spline uses only first and second derivative, which creates a smoother surface but increases the processing time (Equation 3-3).

$$S(\mathbf{x}) = T(\mathbf{x}) + \sum_{j=1}^{N} \lambda_j R(\mathbf{x}, \mathbf{x}^{[j]}) \qquad \text{(Equation 3-3)}$$

The index *j* denotes the measured points, the unknown coefficients and *R (x,x[j])* the basic functions. For the related cases, *T(x)* = a1 = constant (Mitas and Mitasova, 2005).

Advantages (Mitas and Mitasova, 2005; Yao et al. 2013)

1. It captures trends in data.
2. It performs better where sample values may not include the extreme elevation values.
3. It can create a smooth distribution of values.

Disadvantages

1. It does not give explicit control over the influence of distance.
2. It does not perform well when the points are too closely clustered, and their values are extremely different.

3.2.8. Uncertainty assessment using root mean square error

Upon completion of an interpolation, it is important to validate the data interpolation to assess its accuracy. One way of achieving this is by calculating a RMSE (Simpson & Wu, 2014). The RMSE is calculated as the average of the squares of the "errors" (Equation 3-4), that is the difference between the value of validation dataset and the elevation value in the DEM generated by interpolation method. The RMSE has been frequently used to assess model performance of many

environmental and climate research studies (Chai & Draxler, 2014). The formula for RMSE is presented below.

$$RMSE = \sqrt{\frac{\sum_{i=1}^{n}(X_{obs,i} - X_{model,i})^2}{n}} \qquad \text{(Equation 3-4)}$$

where X_{obs} stands for the observed values and X_{model} stands for the modelled values at time/place *i*. In this study it was not clear what percentage of the data points should be used for validation and what percentage should be used to generate the DEMs. To estimate this, we looked at the proportion of missing elevation points in each study area. Originally, the elevation points were supposed to be spaced at 10 m intervals, but in some cases this target was not achieved because of buildings, streets, sand dunes and other man-made features which were removed. Thus, in each study area there is a proportion of missing points. The percentage of missing data was calculated (Equation 3-5) by dividing the difference between numbers of data points, based on 10 m intervals and available data points, by number of data points based on 10 m interval and is explained in the equation below:

$$\%\ \text{of missing point} = \frac{\text{Total no.of available points} - \text{Area (m2)}\ /100(\text{m2})]}{\text{Area (m2)}\ /100\text{m2}]} X\ 100 \ldots. \text{(Equation 3-5)}$$

The results in Table 3-3 show that the proportion of missing elevation data points varied between 21 per cent in Al Khor-1 to 31 per cent in Mesaieed. From this table, the first scenario was to generate DEM using 80 per cent of elevation data and validate it with the other 20 per cent. A second scenario was tested to only use half the points for validation, i.e. 10 per cent, and generate the DEM with the other 90 per cent.

Table 3-3: Propotion of data points missing in each study area.

Name of the study areas	Area (m^2)	Complete number of elevation points	Total number of available elevation points	Number of missing elevation points	Proportion of elevation points missing (%)
Al Thakhira	94,000,000	940,000	736,234	203,766	22
Al Khor-1	11,420,000	137,000	89,567	28,774	20
Al Khor-2	13,620,000	136,000	102,111	33,889	25
Doha	465,040,000	4,650,000	3,352,917	1,297,083	28
Mesaieed	88,240,000	880,000	603,810	276,190	31

The results are shown in Table 3-4 for the three interpolation models. As there were small differences between the values of RMSE when 10 or 20 per cent was used, 10 per cent of the data was used as a validation set to assess the accuracy of the three interpolation methods for all five locations.

Table 3-4: The RMSE (m) values calculated using 10 and 20 per cent for all three interpolation methods in the Al Thakhira area

Location Name	Method	ID	Cell size	Power	Points	RMSE 10% (m)	RMSE 20% (m)	Difference RMSE10% RMSE 20%
AL-Thakhiar	IDW	1	5	1.5	6	0.114	0.114	0.0000
		2	5	1.5	8	0.1139	0.1195	-0.0056
		3	5	1.5	12	0.1275	0.1284	-0.0009
		4	5	2	6	0.1111	0.1107	0.0004
		5	5	2	8	0.1139	0.1146	-0.0007
		6	5	2	12	0.1199	0.1204	-0.0005
		7	5	2.5	6	0.1095	0.1086	0.0009
		8	5	2.5	8	0.1112	0.1113	-0.0001
		9	5	2.5	12	0.1149	0.115	-0.0001
	Kriging ordinary Spherical	1	5		6	0.2141	0.2134	0.0007
		2	5		8	0.2224	0.2205	0.0019
		3	5		12	0.2319	0.2285	0.0034
	Kriging ordinary circular	4	5		6	0.2191	0.2188	0.0003
		5	5		8	0.2283	0.2268	0.0015
		6	5		12	0.2393	0.2361	0.0032
	Kriging ordinary Exponential	7	5		6	0.1609	0.1487	0.0122
		8	5		8	0.1621	0.1489	0.0132
		9	5		12	0.1625	0.1491	0.0134
	Kriging ordinary Gaussian	10	5		6	0.2559	0.2585	-0.0026
		11	5		8	0.2748	0.2761	-0.0013
		12	5		12	0.3036	0.3028	0.0008
	Kriging ordinary Linear	13	5		6	0.1337	0.1331	0.0006
		14	5		8	0.1433	0.1448	-0.0015
		15	5		12	0.1615	0.163	-0.0015
	TIN	1	5			0.26013	0.26045	-0.00032

Using 90 per cent of the elevation data points (training set), 25 DEMs were generated by three interpolation techniques for each study area (130 DEMs in total), and the RMSE calculated using the other 10 per cent of the elevation data (validation set). The results in

show the accuracy of data interpolations for all five locations. Inverse distance weighting showed a better performance than other methods (RMSE highlighted in orange), especially in areas with less urbanisation, such as Alkhor-1 and 2. The best results (RMSE 0.09 m to 0.168 m) were achieved when the power was 2.5 and number of points six. Kriging, in particular ordinary exponential kriging (OE kriging), was the next best interpolator. This type of kriging showed better results (highlighted in green) with an average RMSE of 0.171 m for all five areas in comparison to other types of kriging. The TIN method was the least accurate, with and without using break lines. Breaklines were used to examine whether the accuracy of the DEM generated by TIN could be improved, but the result showed that there was not a large improvement (Table 3-5).Therefore, the decision was made not to investigate TIN techniques further.

Table 3-5: The RMSE (m) values calculated using 10 per cent for all five locations using three interpolation methods (Orange: IDW better results than other methods; Green: Kriging better results than other methods)

Method	ID	Cell size	Power	Points	RMSE 10% Al Thakhira	RMSE 10% Al Khor-1	RMSE 10% Al Khor-2	RMSE 10% Doha	RMSE 10% Mesaieed	Average RMSE
IDW	1	5	1.5	6	0.1138	0.1417	0.1026	0.1818	0.1785	0.1437
	2	5	1.5	8	0.1139	0.1539	0.1055	0.1933	0.1849	0.1503
	3	5	1.5	12	0.1269	0.1728	0.1147	0.2115	0.1957	0.1643
	4	5	2	6	0.1104	0.1239	0.1005	0.1654	0.1730	0.1346
	5	5	2	8	0.1138	0.1322	0.1018	0.1726	0.1776	0.1396
	6	5	2	12	0.1196	0.1448	0.1082	0.1840	0.1848	0.1483
	7	5	2.5	6	0.1089	0.0961	0.0997	0.1554	0.1684	0.1257
	8	5	2.5	8	0.1111	0.0971	0.1000	0.1596	0.1726	0.1281
	9	5	2.5	12	0.1148	0.1023	0.1042	0.1659	0.1771	0.1329
Kriging ordinary spherical	1	5		6	0.2138	0.2048	0.0945	0.2489	0.3143	0.2152
	2	5		8	0.2221	0.2184	0.0938	0.2610	0.3305	0.2251
	3	5		12	0.2315	0.2355	0.0949	0.2769	0.3544	0.2387
Kriging ordinary circular	4	5		6	0.2187	0.2013	0.1054	0.2581	0.3192	0.2206
	5	5		8	0.2279	0.2141	0.1080	0.2728	0.3363	0.2318
	6	5		12	0.2388	0.2296	0.1144	0.2933	0.3621	0.2477
Kriging ordinary exponential	7	5		6	0.1600	0.0922	0.0946	0.2295	0.2797	0.1712
	8	5		8	0.1611	0.0922	0.0938	0.2518	0.2900	0.1778
	9	5		12	0.1615	0.0917	0.0949	0.2742	0.3022	0.1849
Kriging ordinary Gaussian	10	5		6	0.2558	0.2264	0.1978	0.2746	0.3736	0.2657
	11	5		8	0.2747	0.2498	0.2148	0.2951	0.4060	0.2881
	12	5		12	0.3036	0.2325	0.2406	0.3272	0.4617	0.3131
Kriging ordinary linear	13	5		6	0.1332	0.2217	0.1129	0.3678	0.2099	0.2091
	14	5		8	0.1425	0.2416	0.1188	0.3883	0.2230	0.2228
	15	5		12	0.1612	0.2704	0.1307	0.3914	0.2448	0.2397
TIN	1	5			0.2601	0.1740	0.1507	0.7901	0.7822	0.4314
TIN with break line	2	5			0.3565	0.2691	0.2084	0.8874	0.7101	0.4863

When we looked at the error for individual data points, it appeared that very few points contribute to a large proportion of errors. Therefore, to assess the spatial variation of RMSE, an error density map (EDP) was produced. The EDP was created by calculating error between elevation values from the validation set and the DEM, estimated by IDW interpolation methods. The error was squared and then square-rooted to produce only positive values. Inverse distance weighting techniques were used to map the spatial distribution of error in all five locations. These maps were important to understand the extent of inaccuracy in the interpolation techniques in the studied areas. The results (Figure 3-13 to Figure 3-17) showed that the relatively high density of errors were limited to very small areas and did not cover a large part of the study area. When we looked at some of the high-density areas, they appeared to be those with gaps in the data points, those near gaps or those where changed elevation points had irregular intervals due to topography constraints, such as sand dunes and hills.

In Al Thakhira, most of the area has an error of less than 10 cm (yellow area), while the high error (red area) was restricted in small areas and ranged from 10 cm to 2.3 m. In Al Khor 1 and 2, most of the areas had less than 10 cm error. Even the highest errors (red) were less than 60 cm. In Doha, there were less areas with high errors (red), but it had a more scattered high error class, with values ranging from 10 cm to 3.4 m. Similarly, in Mesaieed, a large part of the study area had an error of less than 10 cm and fewer areas with high error (red) ranging in value from 10 cm to 1.3 m.

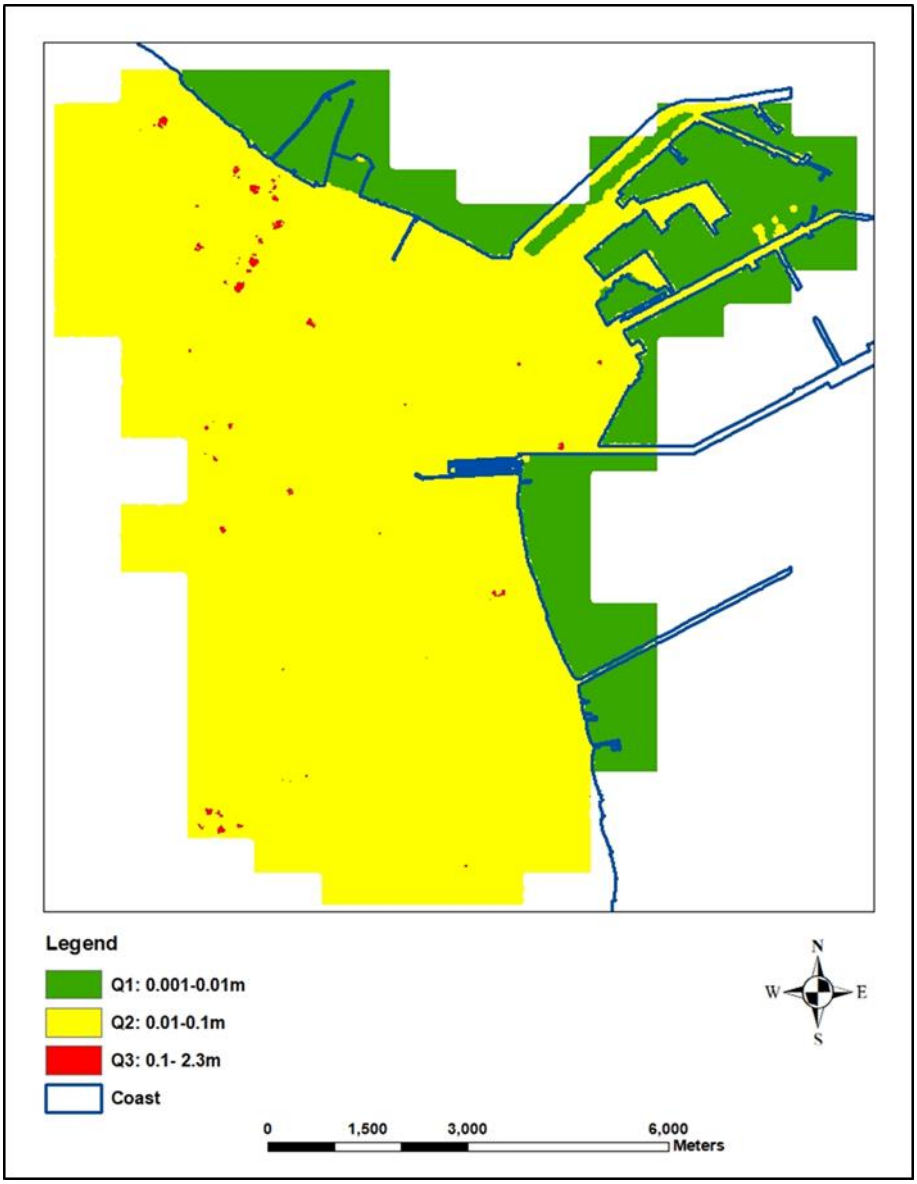

Figure 3-13: Error density map of Al Thakhira.

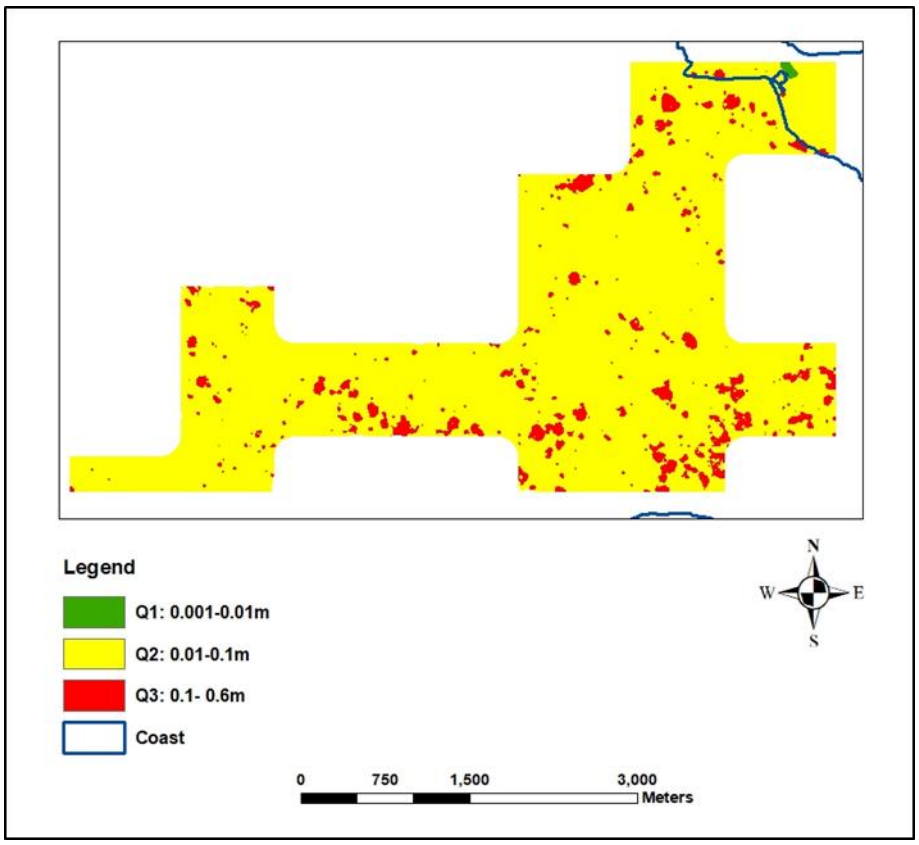

Figure 3-14: Error density map of Al Khor-1.

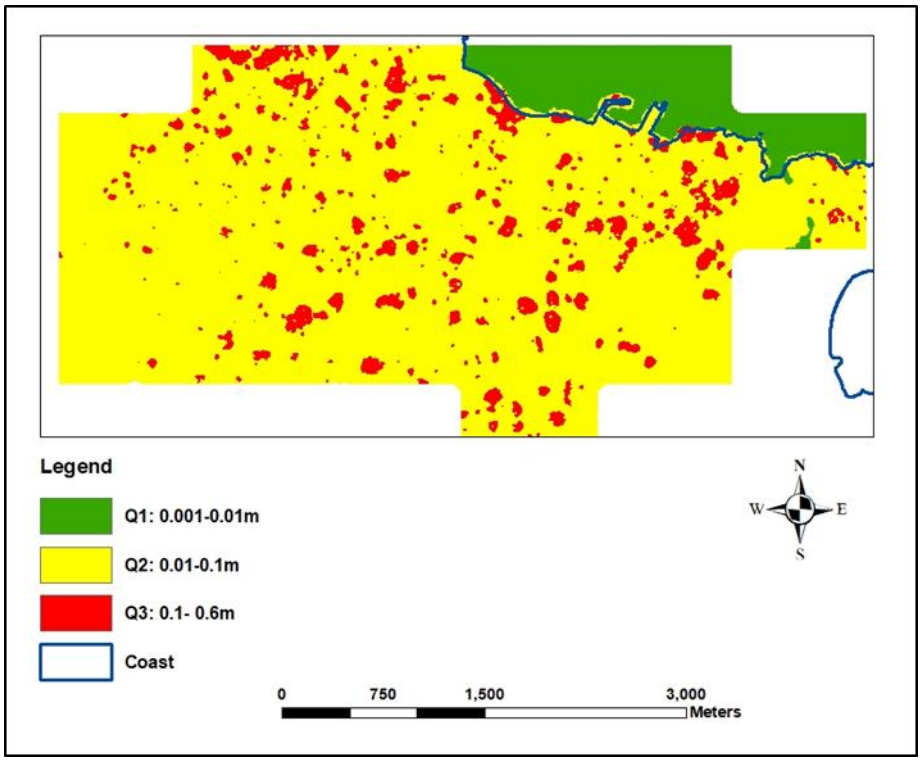

Figure 3-15: Error density map of Al Khor-2.

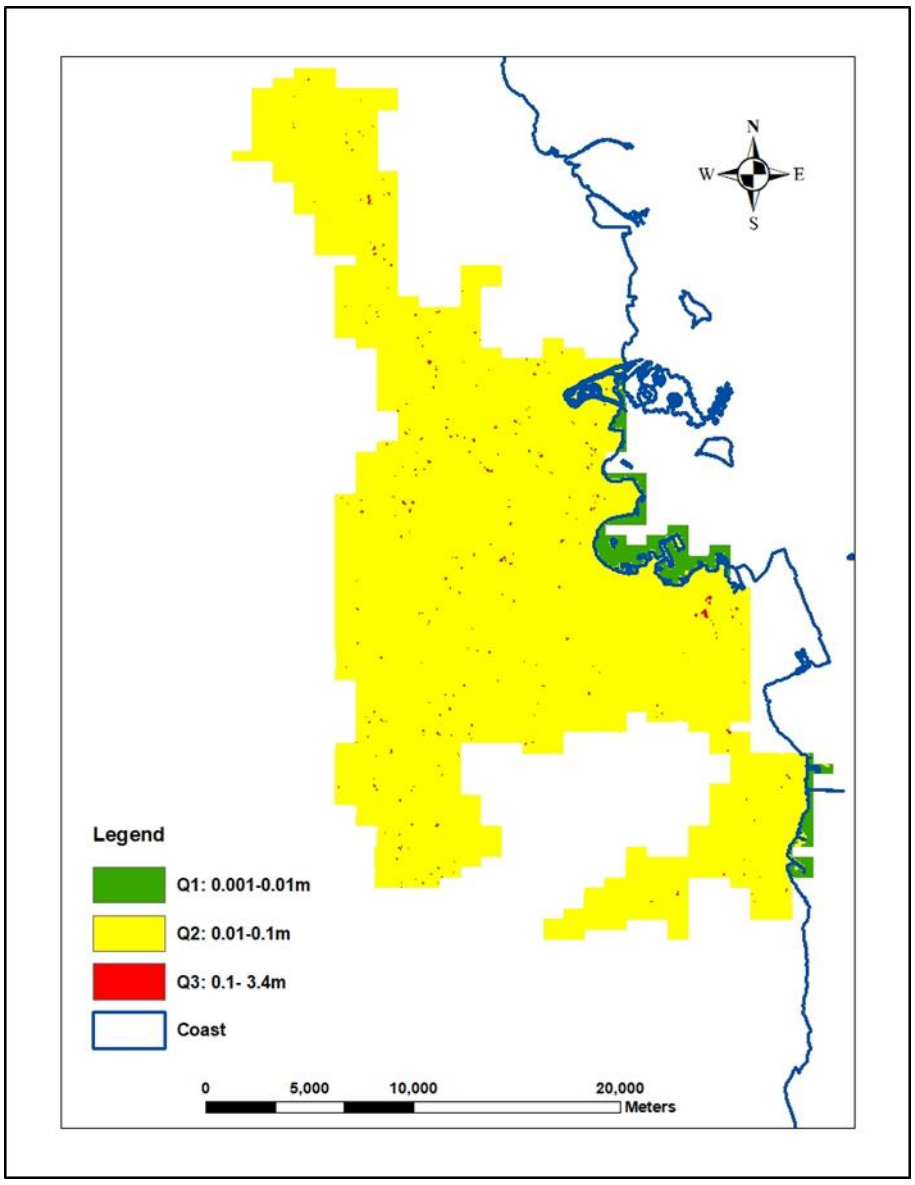

Figure 3-16: Error density map of Doha.

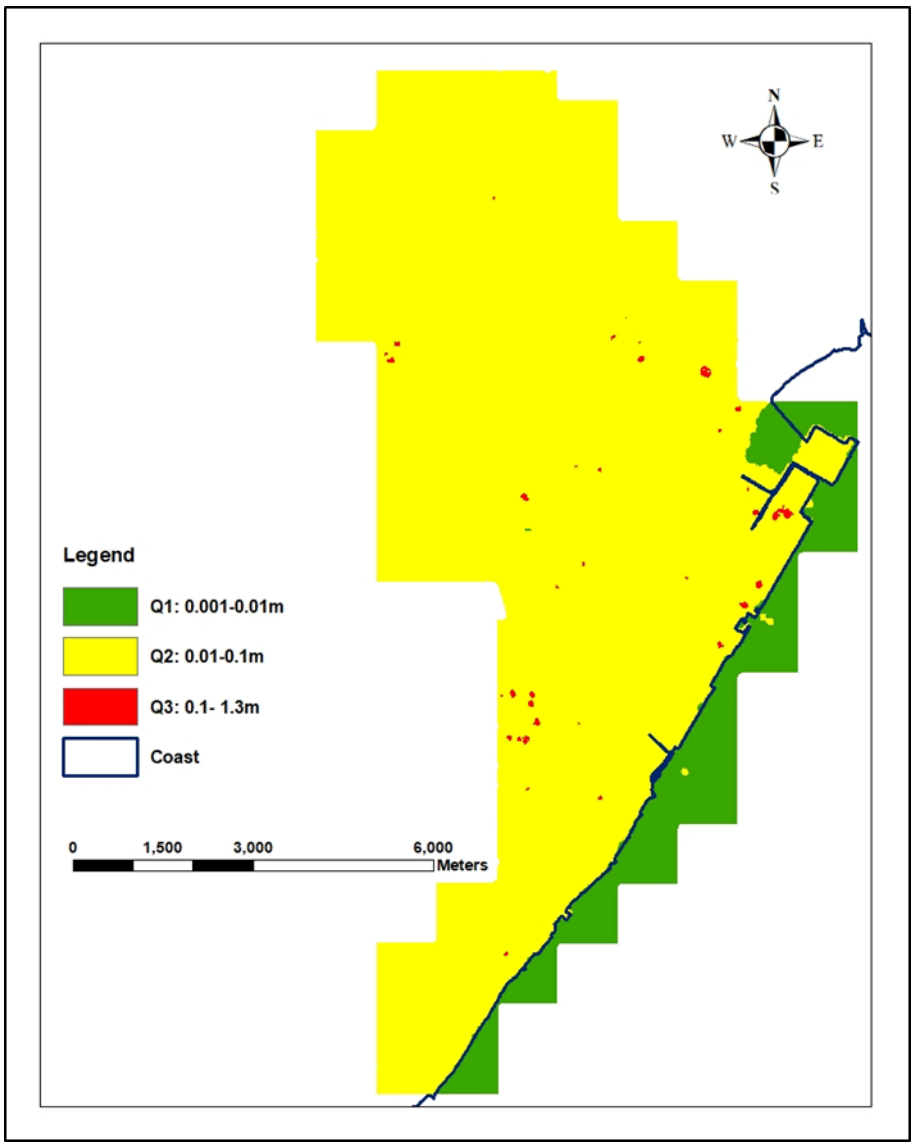

Figure 3-17: Error density map of Mesaieed.

Overall, the results also showed that IDW consistently created outputs with the lowest errors, especially with high power and low point number setting. This consistency was not observed for the kriging types. Ordinary exponential kriging in general performed better, but only Al Thakhira and Al Khor-1 produced the most accurate DEM in comparison to other kriging types. Ordinary spherical kriging was better in Al Khor-2 and Doha and ordinary linear kriging was better in Mesaieed.

The accuracy of IDW data interpolation was varied between all five locations. For example, IDW created DEM for Alkhor-1 with the least RMSE (0.096 m), while in Mesaieed the RMSE is the highest (0.168 m). There is no clear reason why this occurred. The two possible factors

affecting the accuracy of IDW outputs are slope and degree of spatial autocorrelation between elevation points. These will be considered.

The IDW output is highly affected by the nature of the terrain, especially slopes. Arun (2013) found that the RMSE of IDW is lower (RMSE = 0.93 m) in gentle slope areas compared to steep slope areas (RMSE = 1.45 m) or a combination of gentle and steep slopes (RMSE = 1.73 m). Qatar in general has a very flat terrain with little variation in topography. Figures 3-18 to 3-21 show the slope maps for all five areas.

Table 3-6 displays the average slope and RMSE for each study area. Inverse distance weighting generated the most accurate DEM for Alkhor-1 but was least accurate for Mesaieed. The average slope in Mesaieed was 0.91 degree, with slopes of 30 degree in some areas. In Doha, the slopes were generally gentler at 0.81 degree.

Hence, the relationship between slopes and RMSE was unable to explain the variation in IDW performance in these five studied areas. For example, Al Thakhira has the lowest average slope (0.62 degree), but the RMSE value is the third highest (0.109 m).

Table 3-6: The mean slope for the five study areas and IDW accuracy (RMSE)

Area Number	Name of the study areas	Mean Slope (degree)	RMSE (m)
1	Al Thakhira	0.62	0.109
2	AL khor-1	0.88	0.096
3	AL khor-2	0.77	0.100
4	Doha	0.81	0.155
5	Mesaieed	0.91	0.168

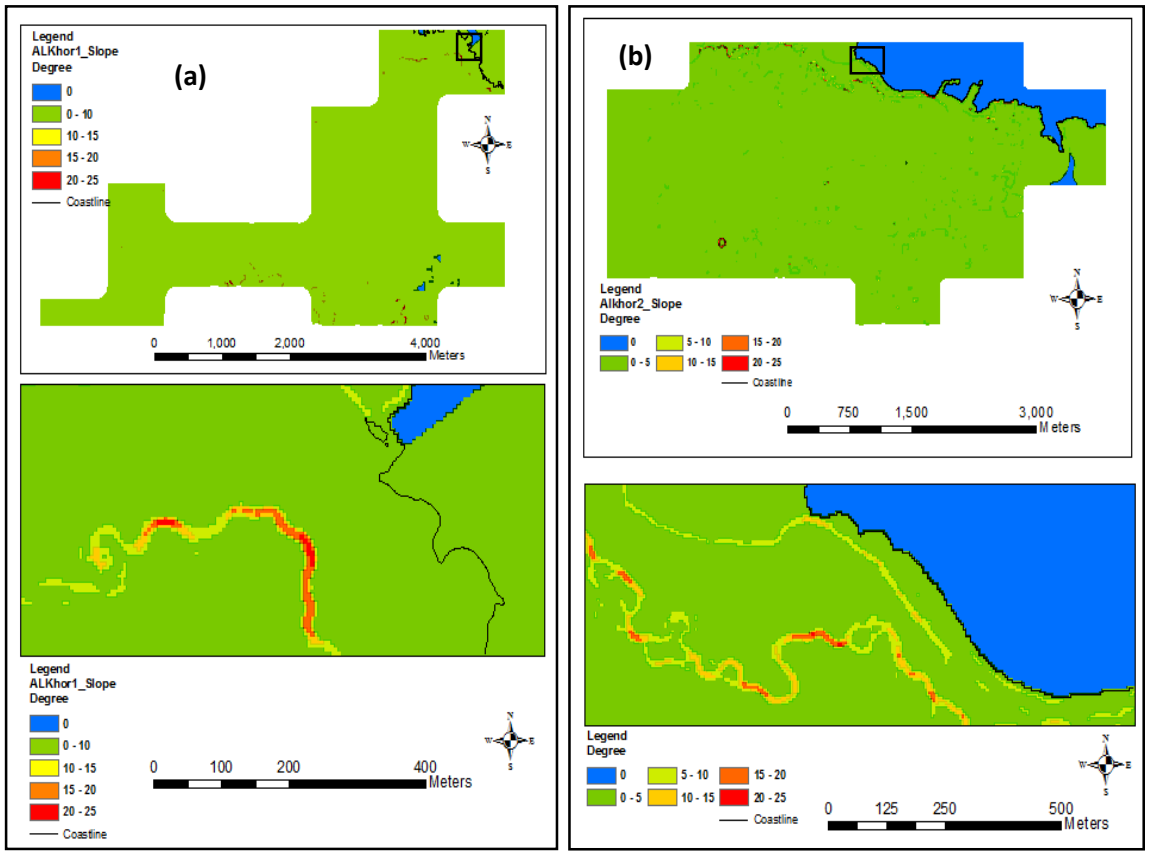

Figure 3-18: Slope map for Al Khor-1 (a) and Al Khor-2 (b)

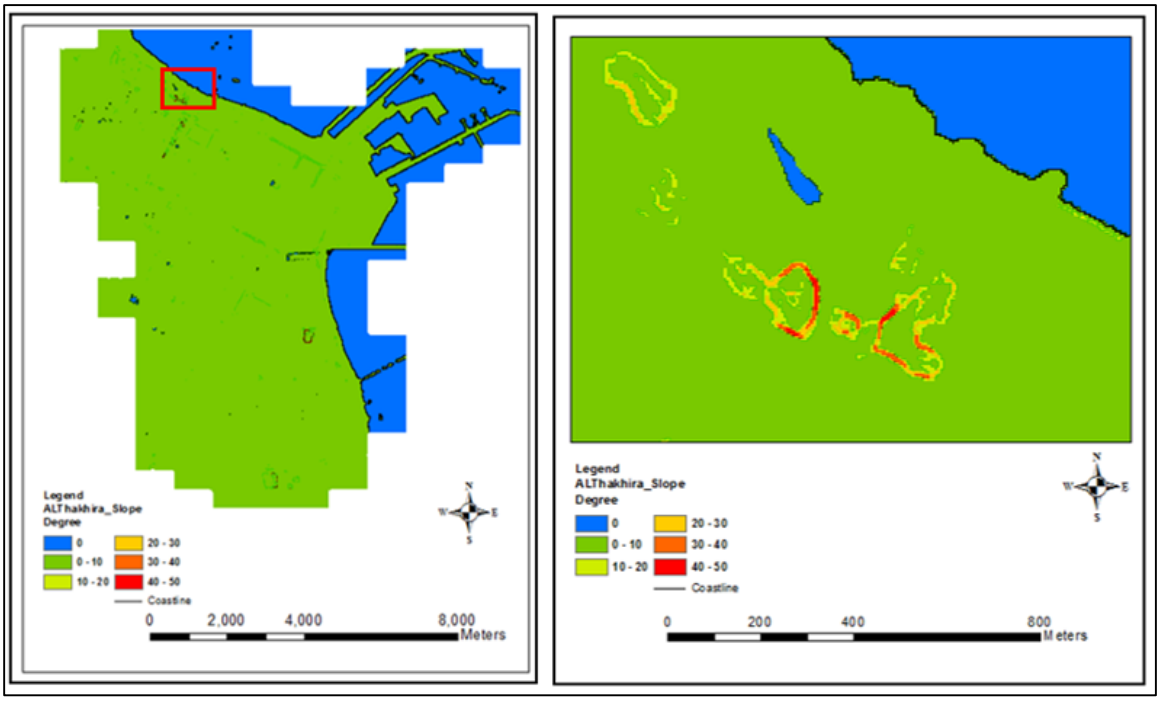

Figure 3-19: Slope of Al Thakhira

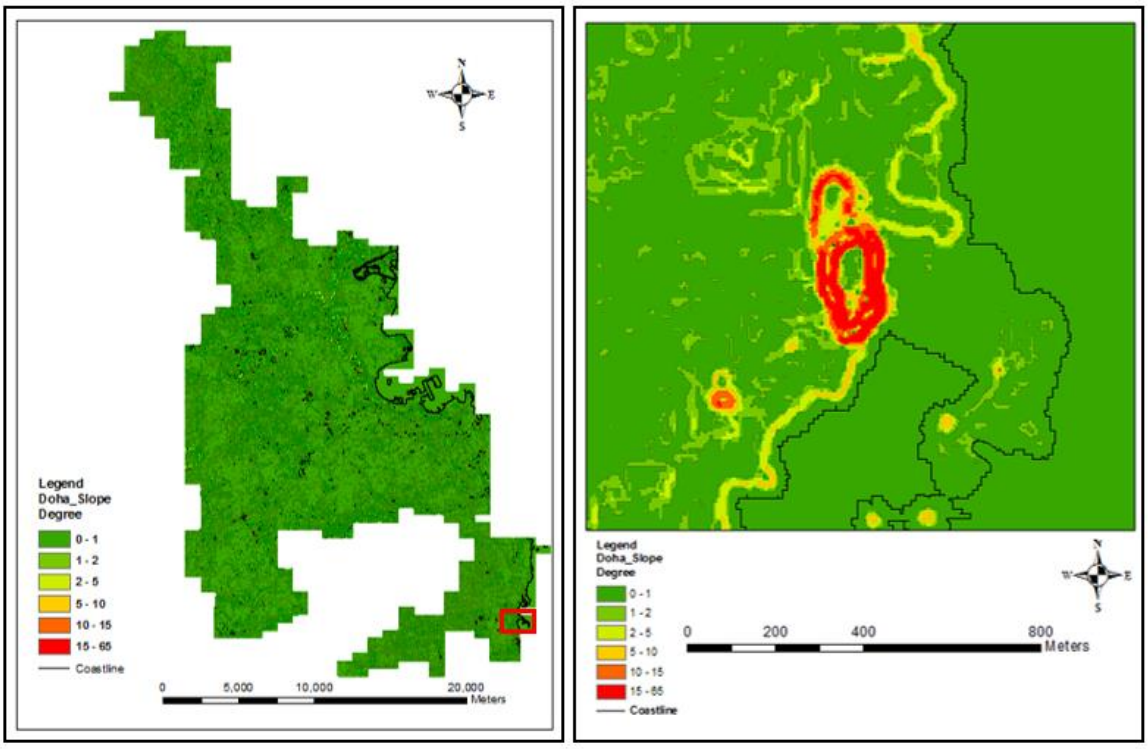

Figure 3-20: Slope of Doha

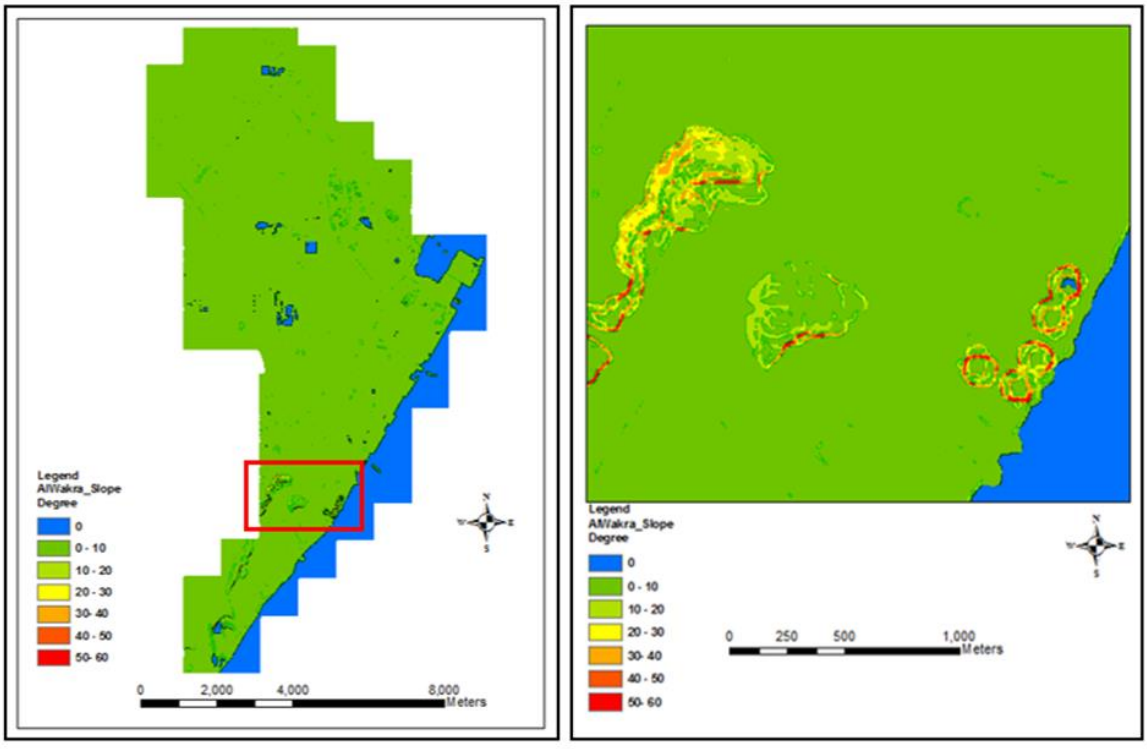

Figure 3-21: Slope of Mesaieed

3.2.9. Factors affecting digital elevation model, uncertainty spatial autocorrelation

The degree of spatial autocorrelation in each study area was investigated, as the correlation of elevation data with itself may influence the errors in generated DEMs (Xuejun & Lu, 2008). The spatial autocorrelation (Global Moran's I) tool in ArcGIS was used to measure spatial autocorrelation based on the locations and the values of elevation data points simultaneously for all the five studied areas. ArcGIS tool uses the Equation 3-6 to calculate Global Moran's I Index (Getis, 2007):

$$I = \frac{n}{S_0} \frac{\sum_i \sum_j w_{ij}(x_i - \bar{x})(x_j - \bar{x})}{\sum_i (x_i - \bar{x})^2} \qquad \text{(Equation 3-6)}$$

$\bar{x}$ is the mean of the x elevation, w_{ij} are the elements of the weight matrix and S_0 is the sum of the elements of the weight matrix: $S_0 = \sum_i \sum_j w_{ij}$.

The tool calculates the Moran's I Index value as clustered, dispersed or random. The Global Moran's I tool calculates a z-score and p-value. Values range from -1 (negative spatial autocorrelation) to +1 (positive spatial autocorrelation), and zero values indicate a random spatial pattern.

Moran's I was calculated for the five study areas in ArcGIS and the results (Table 3-7) show evidence that the degree of spatial autocorrelation between elevation data points may affect the performance of IDW and the best kriging method with exponential model. The accuracy of IDW and OE kriging tends to increase when the Moran's I index increased, except in Doha which is highly urbanised.

Table 3-7: Relationship between Moran's I Index and RMSE from IDW interpolation

Study area	Moran I	IDW -RMSE (m)	OE Kriging -RMSE (m)
Al Thakhira	+0.66	0.109	0.160
Alkhor-1	+0.82	0.096	0.0922
Alkhor-2	+0.78	0.100	0.0946
Doha	+0.95	0.155	0.229
Mesaieed	+0.55	0.168	0.280

The performance of OE kriging in the five study areas was assessed further by producing a prediction standard error (PSE) map. Prediction standard error is a cross-validation technique to estimate uncertainty in the data by removing one of the input data points from the dataset in turn, before using the remaining datasets to predict back to that location. By comparing true value against predicted value of that point, an error is produced.

The PSE map for each study area was produced using ArcGIS – Geostatistical Analyst. The result clearly showed that most of the errors occurred in areas where there are streets or buildings. This is likely because there were fewer data points available (more data points were missing) for the interpolation in these locations (Figures 3-22 to 3-26).

The average standard error calculated by PSE for the five locations (Table 3-8) demonstrate a similar pattern to the RMSE calculations (Table 3-5).

Table 3-8: Average standard error of OE kriging with proportion of missing elevation points in five study areas.

Area Number	Name of the Study Areas	Average Standard Error (m)
1	Al Thakhira	0.422238
2	AL khor-1	0.230774
3	AL khor-2	0.209793
4	Doha	2.190073
5	Mesaieed	1.514485

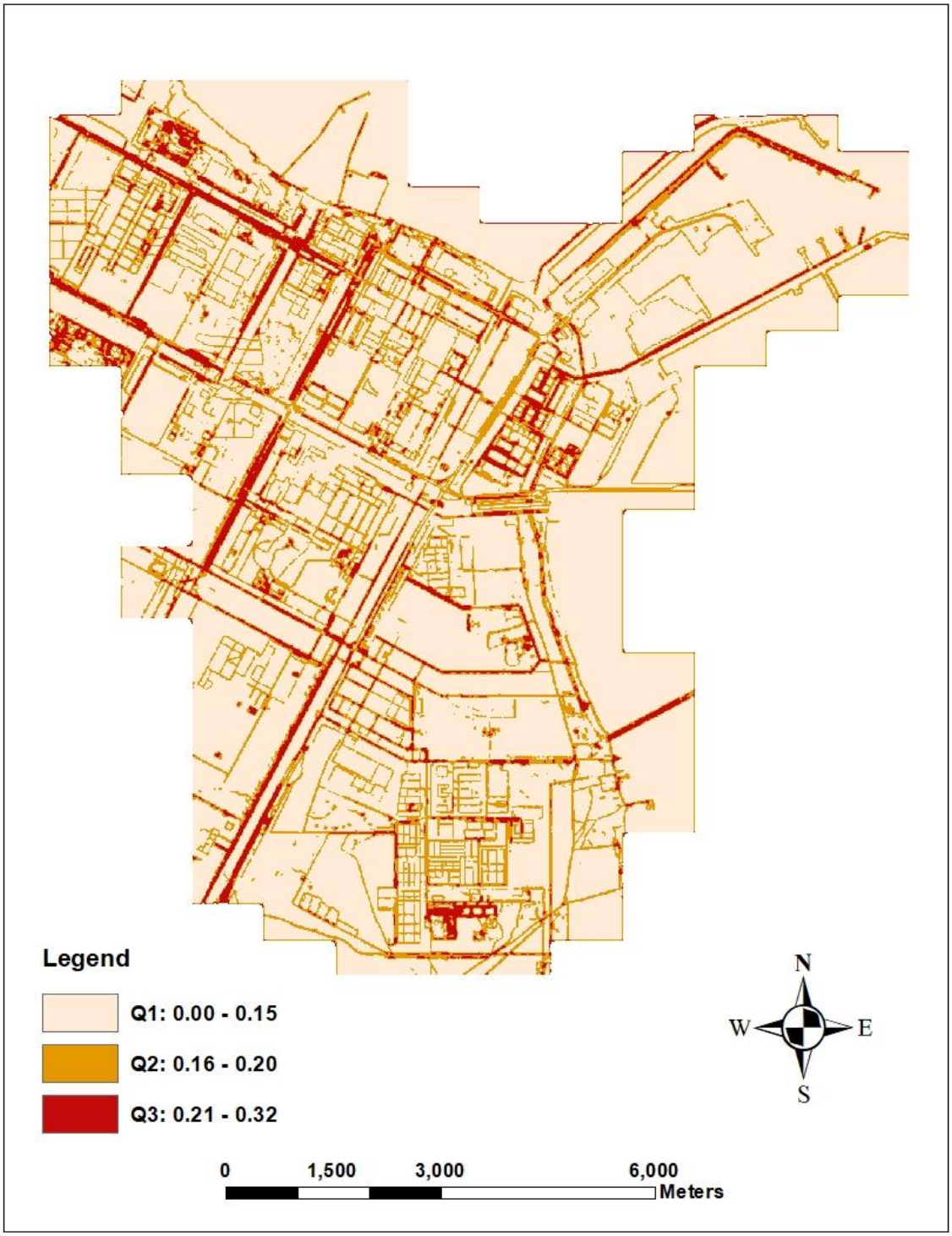

Figure 3-22: Prediction standrad error map for Al Thakhira area.

Figure 3-23: Prediction standard error map for Al Khor-1.

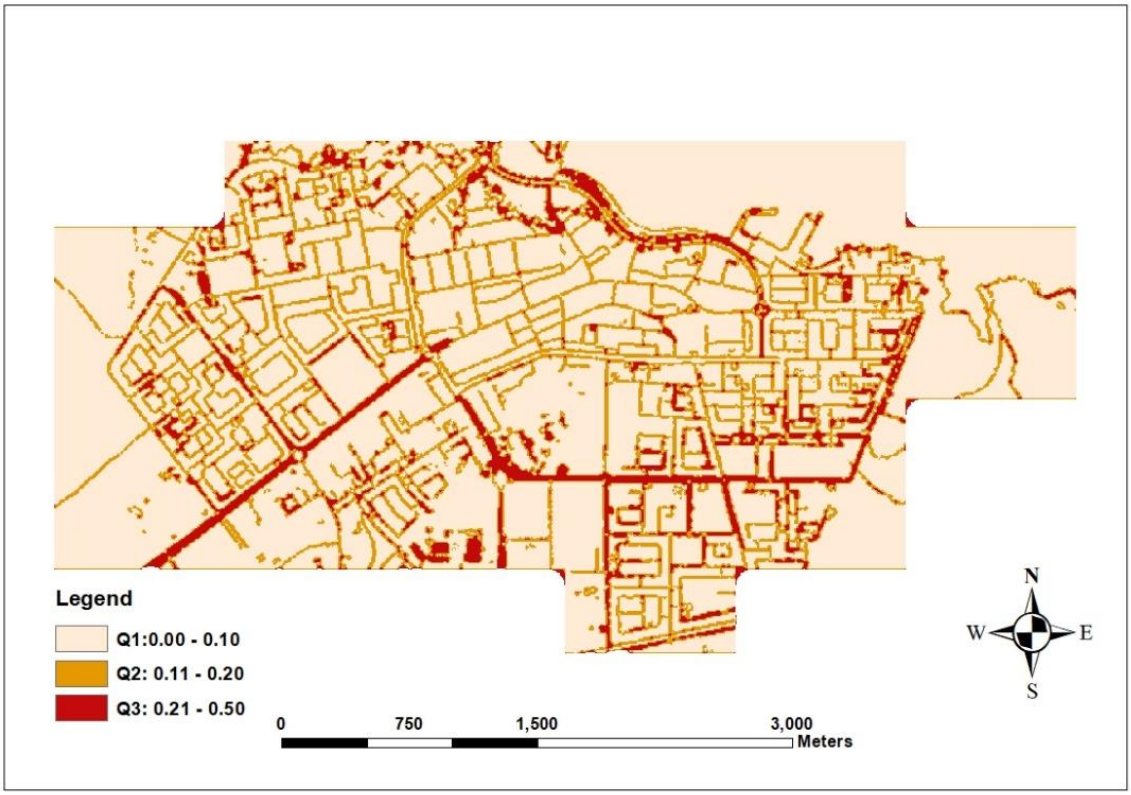

Figure 3-24: Prediction standard error map for Al Khor-2.

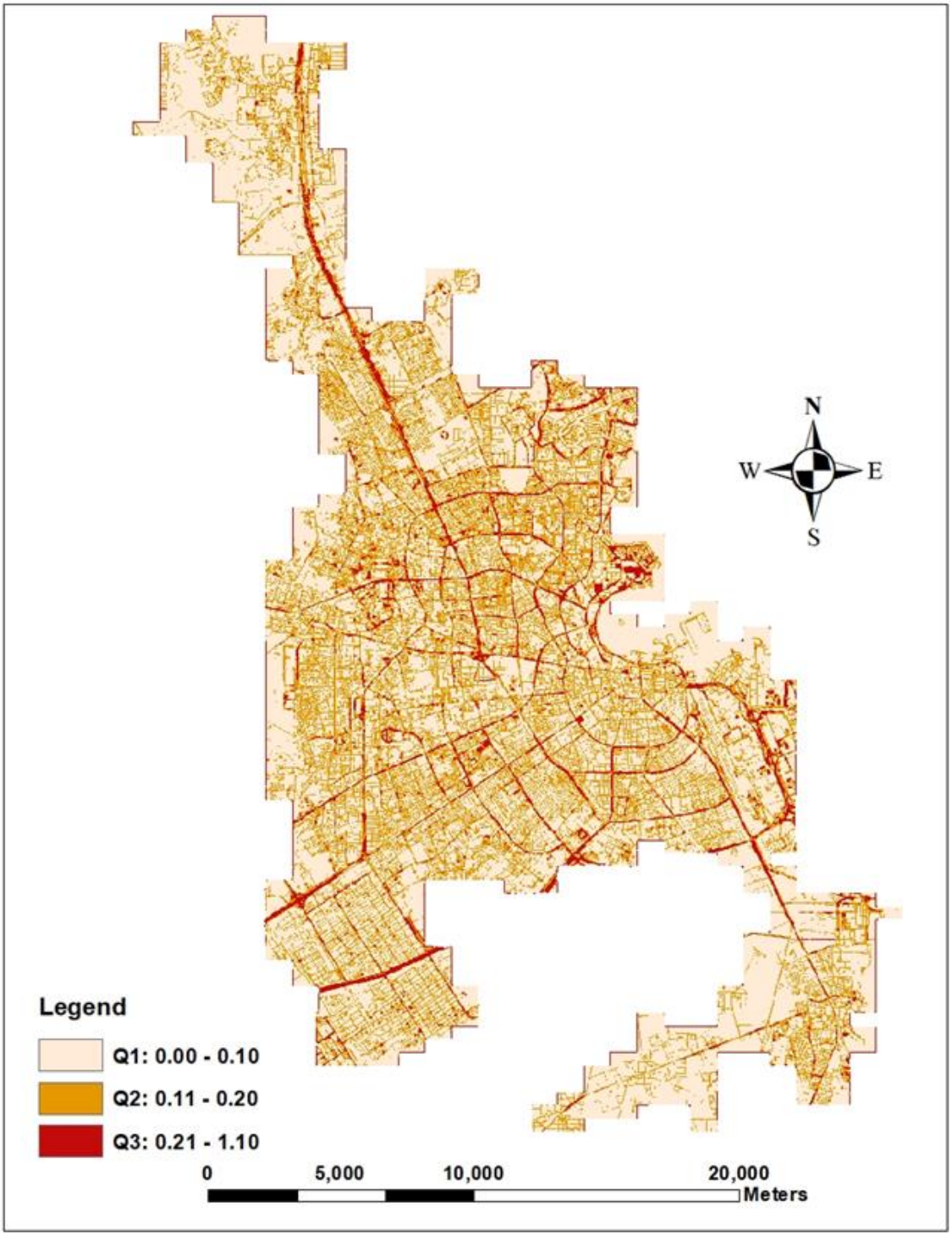

Figure 3-25: Prediction standard error map for Doha area.

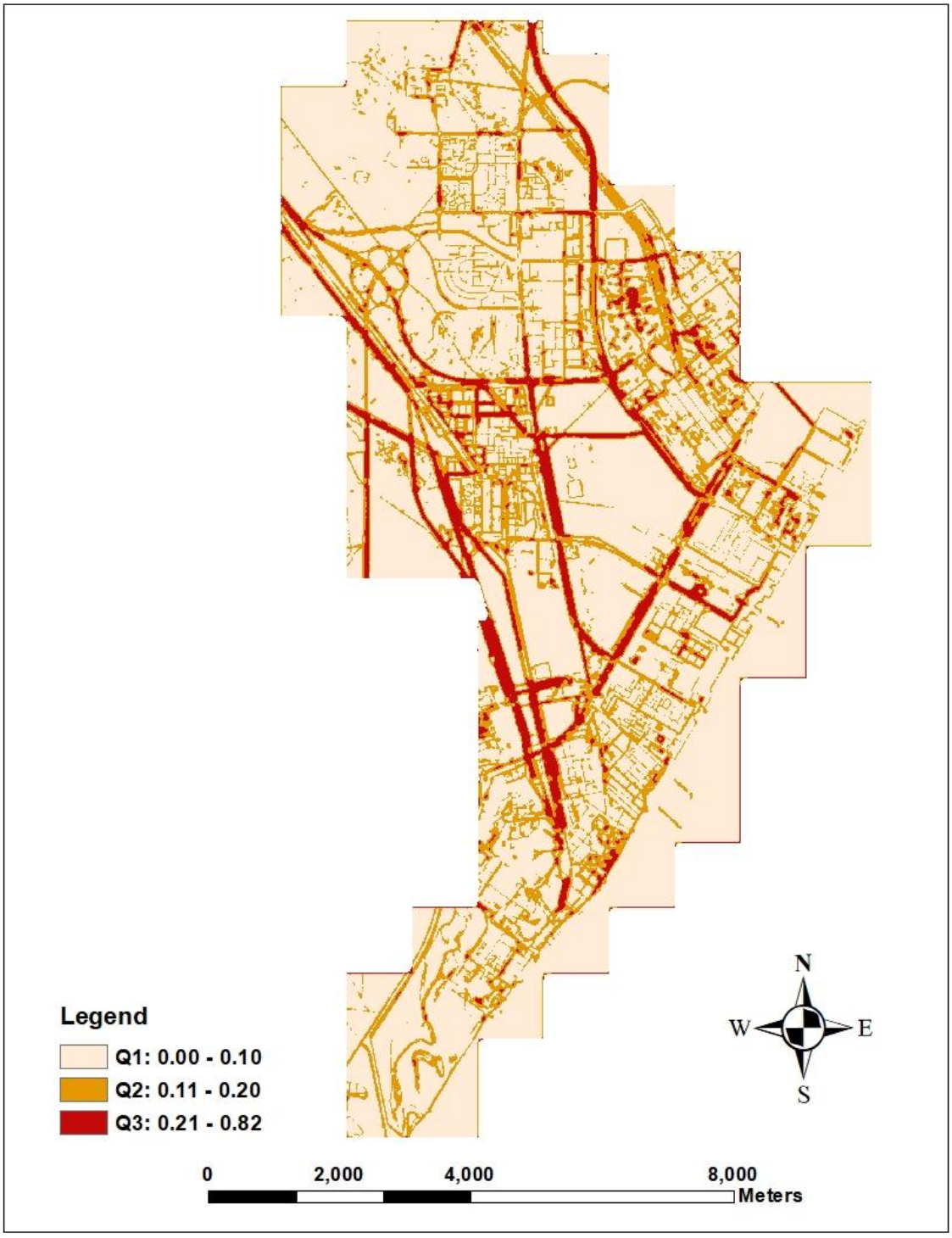

Figure 3-26: Prediction standard error map for Mesaieed.

3.2.10. Further comparison of inverse distance weighting and kriging

Inverse distance weighting and kriging were compared further as these two methods showed a consistently low RMSE. The next step compared the spatial accuracy of both methods for one study area.

The two methods with the least RMSE (Table 3-9) were used to generate a DEM at the five locations using all the data points. The RMSE is also presented. The purpose of this analysis was to determine the areas where both methods of prediction are similar and where their predicted DEM differs. This is important to quantify the amount of uncertainties between these two methods. For this purpose, the DEM outputs were converted into a raster map (grid) and then a difference map between the IDW and best kriging techniques.

The visual result did not show any major difference between the two techniques. The accuracy in generating DEM through both kriging and IDW methods was similar in areas where elevation data points were available. However, differences appeared in areas where there were missing points. This was greater along the coastline. Figures 3-27, 3-28, 3-29, 3-30 and 3-31 show the difference between DEM-IDW and DEM-kriging (ordinary spherical). The green colour indicates similar predictions by both methods; brown coloured areas indicate areas where OS kriging overestimated the DEM value compared to IDW. The blue colour indicates areas where IDW overestimated the DEM compared to kriging (ordinary spherical).

Table 3-9: Comparison between RMSE (m) from IDW and best kriging technique for the five study areas (From Table 3-5)

Study area	RMSE Best Kriging type	RMSE IDW	Difference in RMSE
Al Thakhira	0.13315	0.0002	0.13295
Al Khor-1	0.09171	0.000117	0.091593
Al Khor-2	0.09378	0.000011	0.093769
Doha	0.22947	0.000634	0.228836
Mesaieed	0.20989	0.000135	0.209755

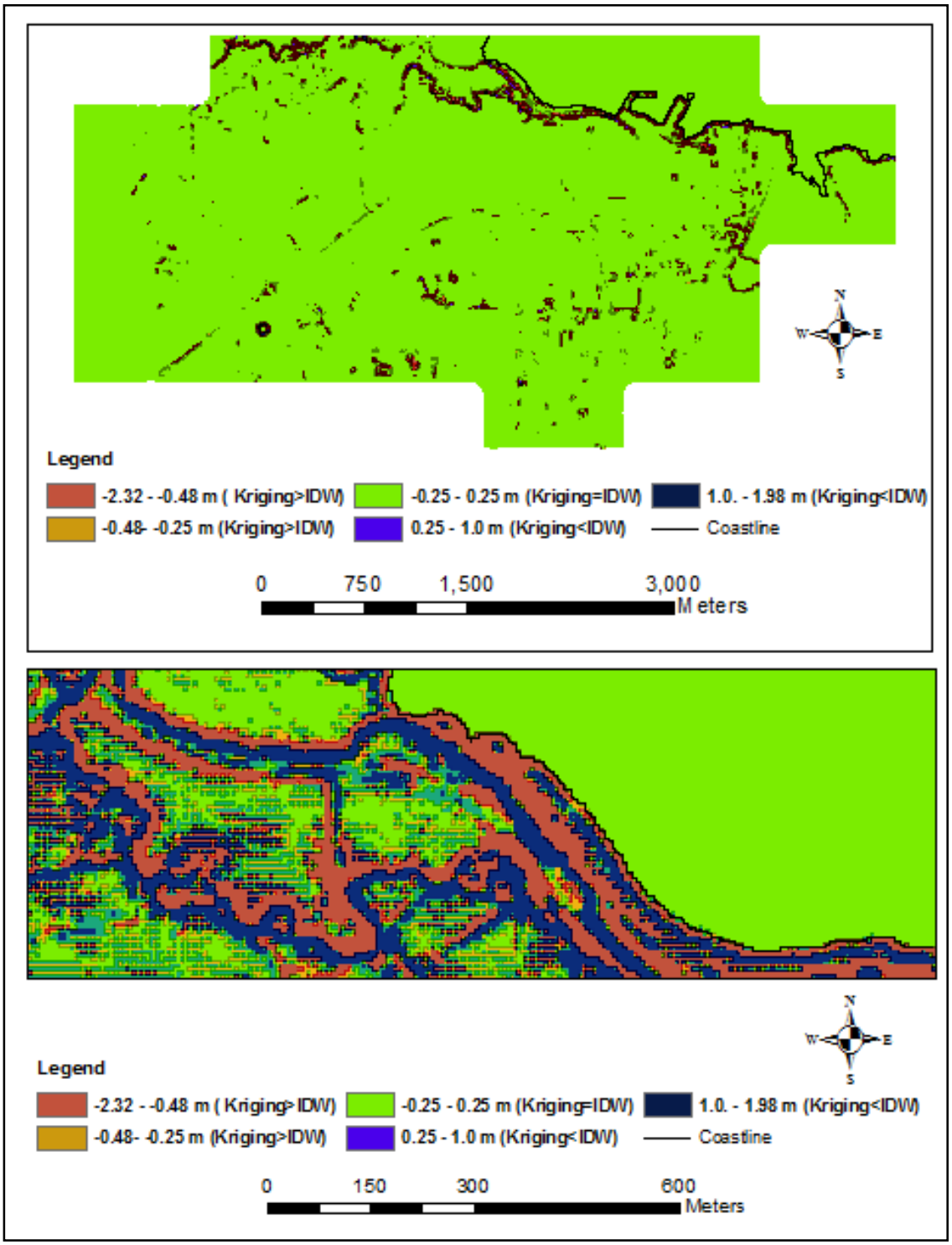

Figure 3-27: Difference map between DEM-IDW and DEM-kriging (ordinary spherical) showing similarity and differences in predicting DEM value.

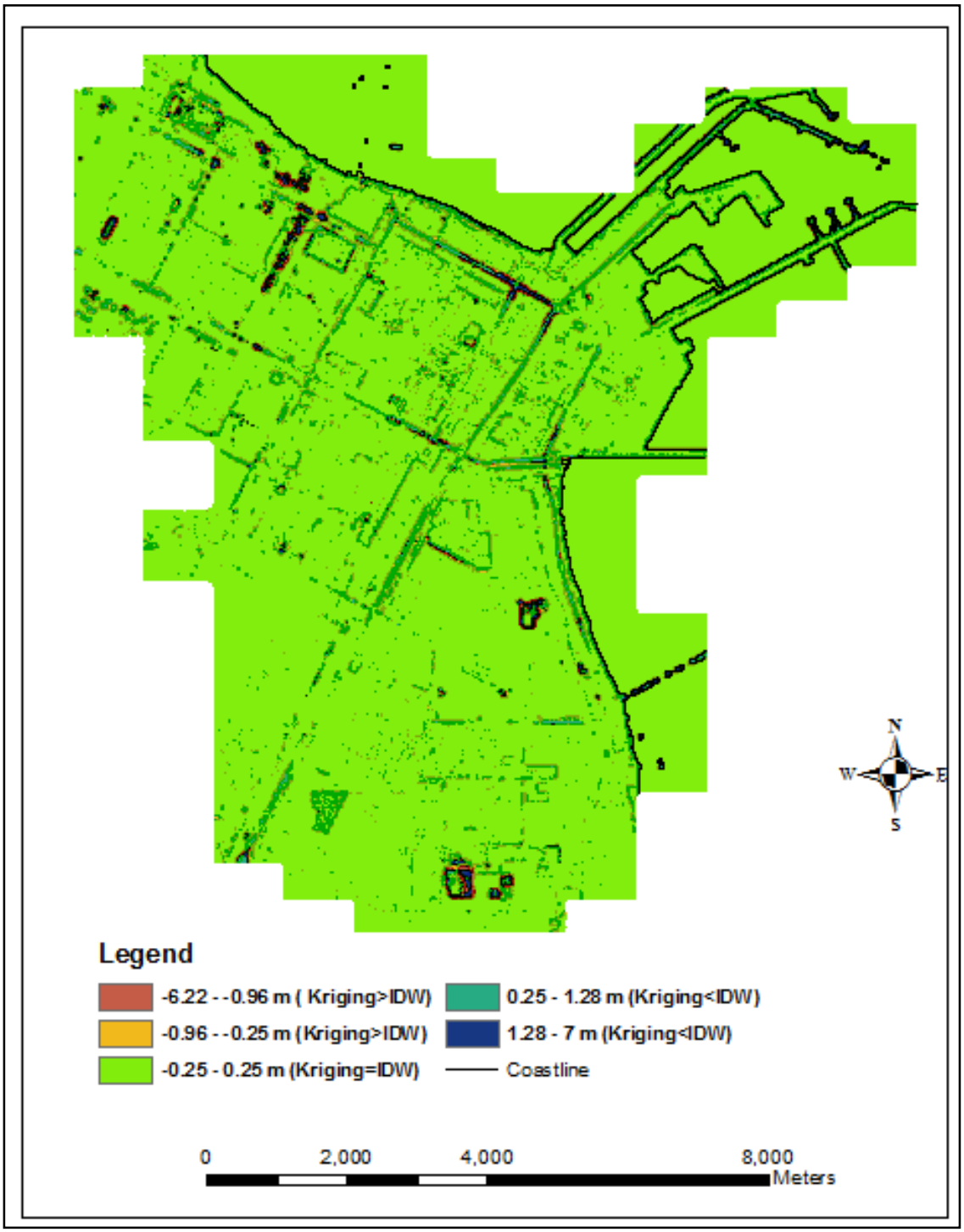

Figure 3-28: Difference map between DEM-IDW and DEM ordinary linear kriging showing similarity and differences in predicting DEM value for Al Thakhira.

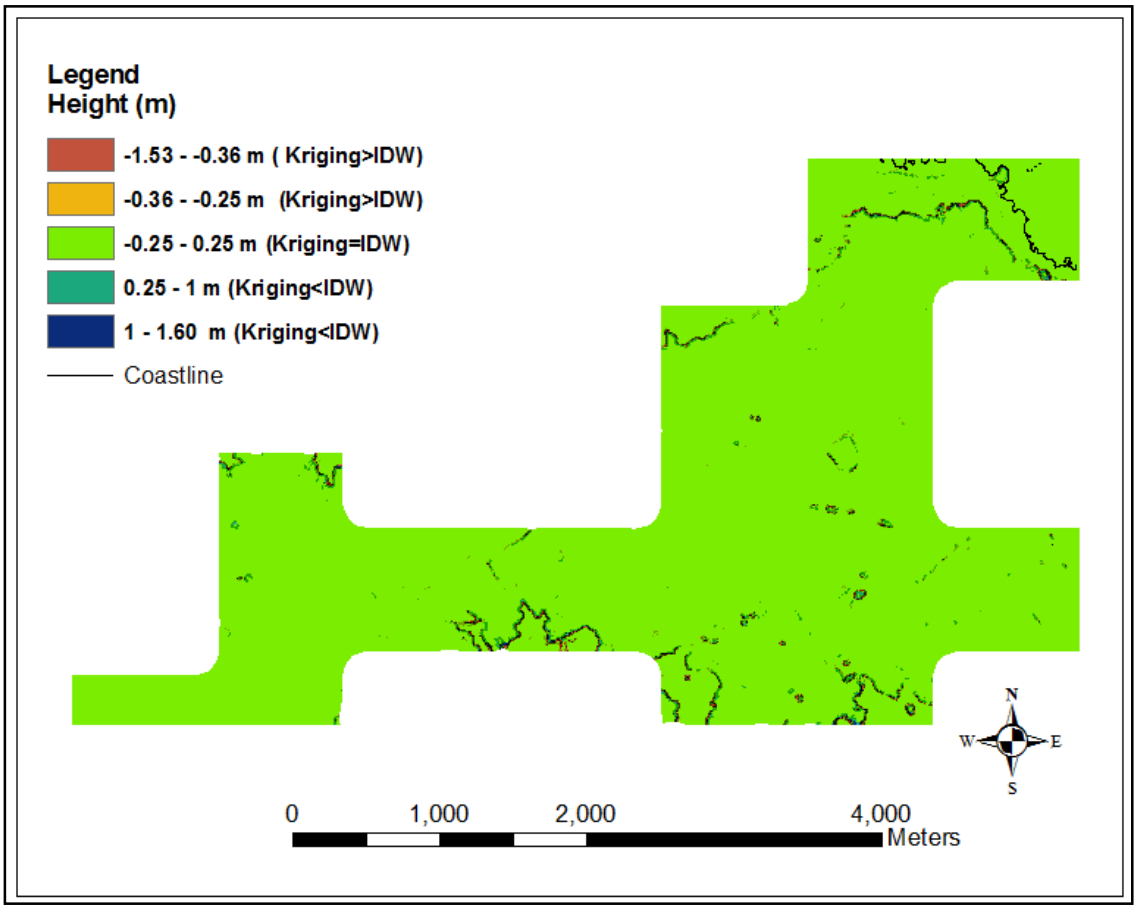

Figure 3-29: Difference map between DEM-IDW and DEM-kriging (OE) showing similarity and differences in predicting DEM value for Al Khor-1.

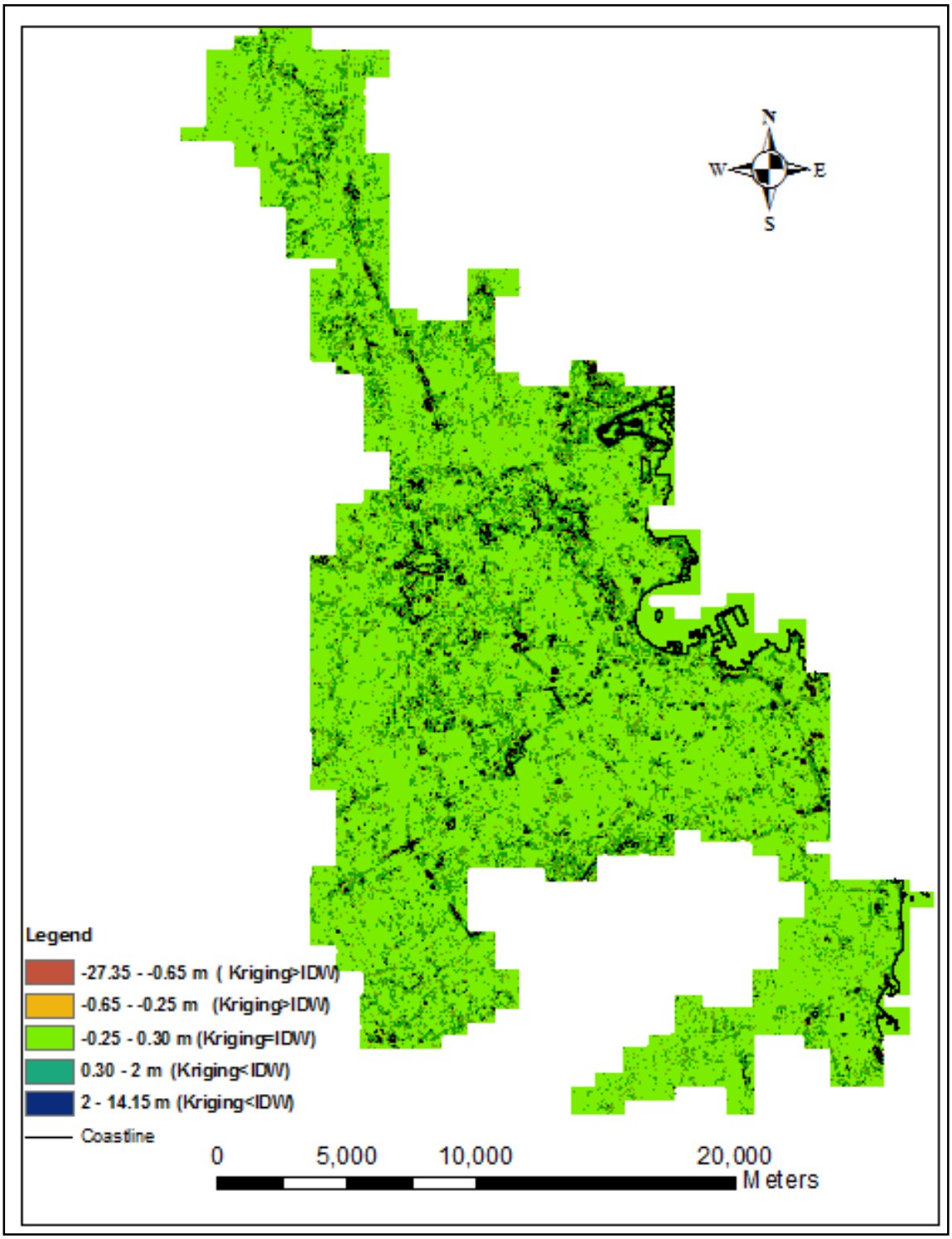

Figure 3-30: Difference map between DEM-IDW and DEM kriging (ordinary spherical) showing similarity and differences in predicting DEM value for Doha.

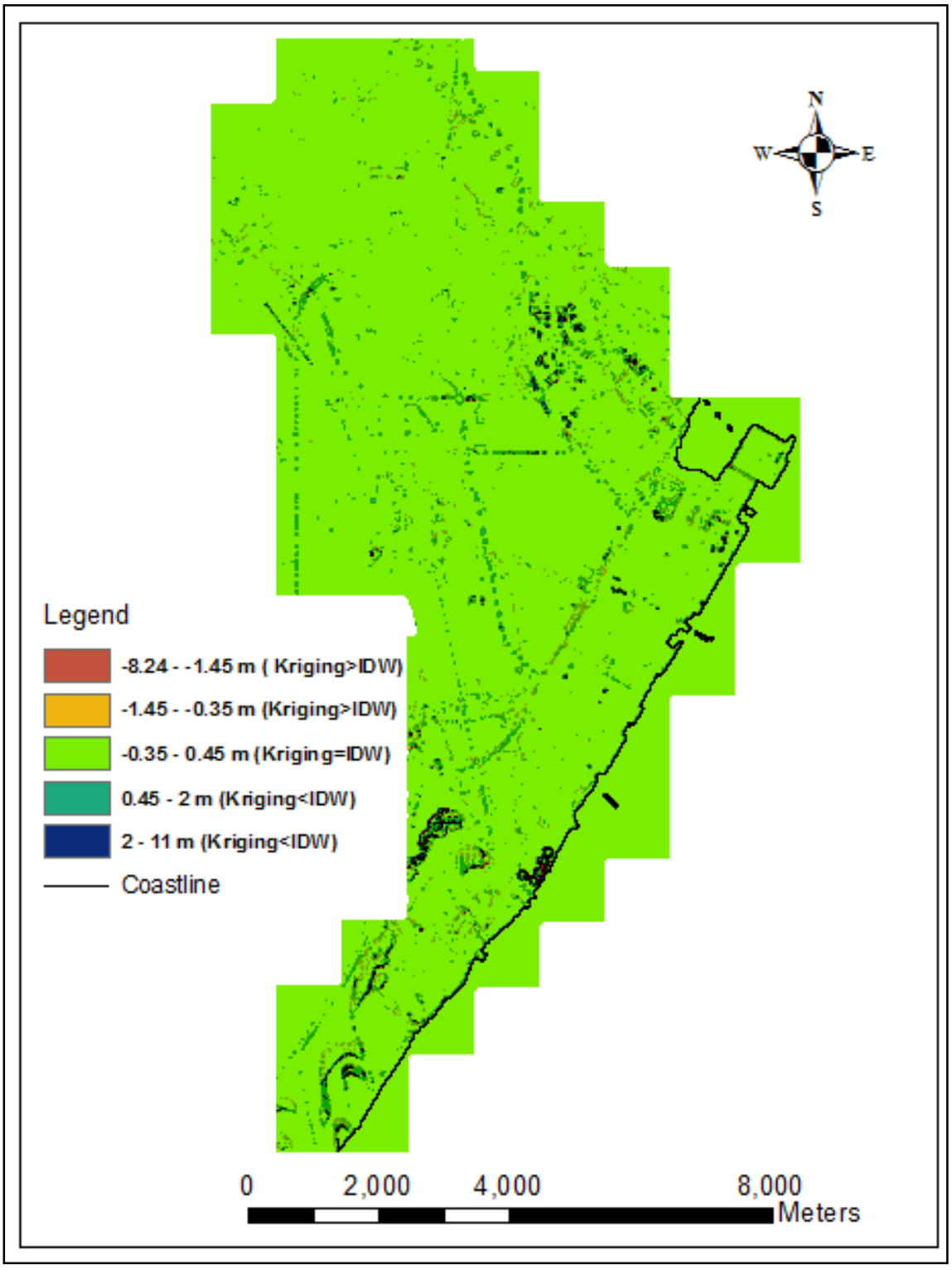

Figure 3-31: Difference map between DEM-IDW and DEM kriging (ordinary linear) showing similarity and differences in predicting DEM value for Mesaieed.

3.2.11. Incorporating breaklines into digital elevation models

In the elevation data for Qatar, breaklines are present. These provide additional information on the land surface and the next step in the DEM generation is to consider their incorporation and whether this improves accuracy. Breaklines generally outline sudden and sharp changes in surface elevation and there are two main types.

Soft breaklines provide information about the surface without implying a change in the surface behaviour across the line. They are often used to incorporate height values as a linear feature in TIN. Soft breaklines also help maintain linear features and edges in TIN surface modelling (ESRI, 2016). Hard breaklines represent sharp interruptions in surface elevation. Hard breaklines are mainly used to define linear features such as streams, ridges, shorelines, building footprints, dams and other locations of abrupt surface change.

Breaklines can be used as a barrier in data interpolation methods, such as IDW and spline, to limit the search for the input sample points for interpolation in areas where there are changes in the surface behaviour. Using breaklines as a barrier will help to improve the accuracy of the DEM (Linyu et al, 2012) as they provide more information about the feaures in the study area.

The next step in developing the DEM methodology is to test various options to incorporate break lines. These are illustrated in Figure 3-32 and use the breaklines as barriers as well as the elevation data contained on them to increase the number of sample points for the interpolation.. These use additional data and techniques to improve the quality of interpolation and include the use of breaklines as barriers and also the use of elevation information driven from breaklines

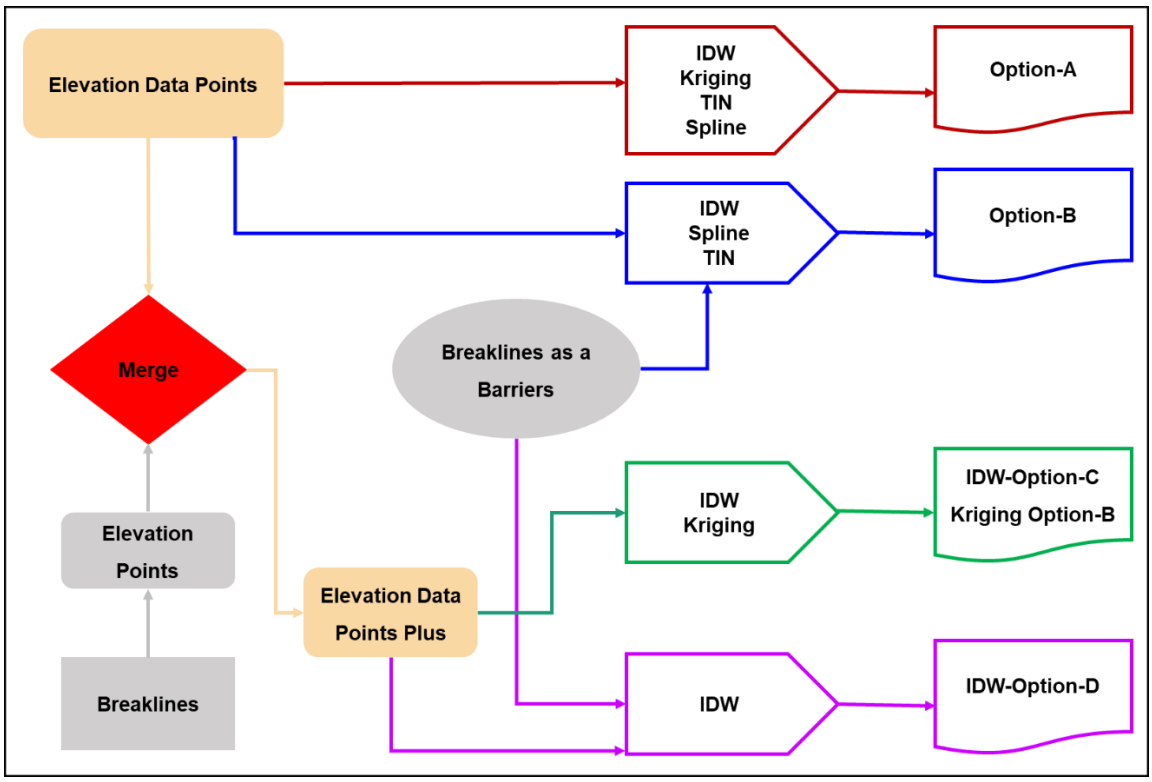

Figure 3-32: Diagram illustrating options considered to improve the DEM generated by using elevation data point and break lines.

Option A: Breaklines are not incorporated and the interpolation uses 90 per cent of elevation data to generate DEM and 10 per cent of the data for validation.

Option B: As Option A but includes breaklines as barriers. Within some interpolations (IDW for example), breaklines restrict the interpolation algorithm where there are sharp changes in elevation values to create a linear discontinuity in the surface. As the breaklines create discontinuity in the DEM, results indicated that some pixels had no elevation value. To add value to cells with no elevation values, the raster calculator was used in ArcGIS to remove and replace no data values within a raster using statistical information from the surrounding data values. A conditional statement and focal statistics function (expression below) was used to replace cells with no value within DEM (in raster format) with a value statistically derived from neighbouring cell values (three cells by three cells).

The expression used in the raster calculator (ArcGIS) is as below:

Con (IsNull(Raster File), FocalStatistics(Raster File, NbrRectangle(3,3, "CELL"), "MEAN"), Raster File).

Option C: This was as specified in Option A, except that the points generated from breaklines were also incorporated. Break line data files contain a huge amount of information about the elevation in the study areas. If the elevation data from breaklines is transformed into data points and merged with the original elevation data, this may increase DEM accuracy.

To generate these points, a tool developed by Nir Fulman, a research assistant at Tel Aviv University, was used. The tool is called *Points Along Line.* It takes an input layer of polylines and creates points along the lines at a given distance between points. This tool was used to generate data points, for every 10 m, along the break lines. Using an *Intersect* operator elevation, data was then applied to these points from the line. Finally, this new data set was merged with the original elevation data points. Then, 90 per cent of the elevation data points were used to generate DEM using IDW, and the other ten per cent to calculate the RMSE necessary to validate the DEM generated.

Option D: This is the same as Option C, but here breaklines were included as a barrier to restrict the data interpolation in areas where there were sharp changes in the elevation.

3.2.12. Incorporating break lines: Results

For IDW, the results showed a notable increase in the value of RMSE for Option C and D (Table 3-10). This suggests that, by including the elevation data points from break lines, sharp elevation changes were included in the data set which reduced accuracy. It is also worth noting that, for IDW, incorporating breaklines (A vs C) increased the RMSE. In contrast, procedures including breaklines as a barrier (Option B) produced some improvements in RMSE compared to Option A.

Table 3-10: Comparisons of DEM generated by IDW, spline, kriging and TIN and improved using breaklines data.

Study areas		IDW				Spline		Kriging		TIN	
		A	B	C	D	A	B	A	B	A	B
Al Thakhira	RMSE (m)	0.11	-	0.59	-	0.1	0.08	0.16	0.55	0.26	0.36
	Median	0.02	-	0.04	-	0.01	0.01	0.03	0.07	0.04	0.04
	Q25%	0	-	0	-	0	0	0	0.01	0	0
	Q50%	0.02	-	0.04	-	0.01	0.01	0.03	0.07	0.04	0.04
	Q75%	0.05	-	0.16	-	0.03	0.03	0.07	0.27	0.13	0.13
	Min	0	-	0	-	0	0	0	0	0	0
	Max	6.66	-	9.3	-	6.5	5.26	6.16	10.1	9.6	13.6
Al Khor-1	RMSE (m)	0.1	0.09	0.35	0.37	0.09	0.07	0.09	0.34	0.17	0.27
	Median	0.03	0.03	0.05	0.05	0.02	0.02	0.03	0.04	0.06	0.07
	Q25%	0.01	0.01	0.02	0.02	0.01	0.01	0.01	0.02	0.03	0.03
	Q50%	0.03	0.03	0.05	0.05	0.02	0.02	0.03	0.04	0.06	0.07
	Q75%	0.07	0.07	0.13	0.11	0.05	0.04	0.05	0.11	0.13	0.15
	Min	0	0	0	0	0	0	0	0	0	0
	Max	2.8	1.03	4.83	5.39	3.13	1.42	2.97	5.83	3.4	5.27
Al Khor-2	RMSE (m)	0.1	0.08	0.37	0.36	0.09	0.08	0.09	0.35	0.15	0.21
	Median	0.02	0.02	0.04	0.03	0.02	0.03	0.02	0.03	0.04	0.04
	Q25%	0.01	0.01	0.01	0.01	0	0.01	0.01	0.01	0.01	0.01
	Q50%	0.02	0.02	0.04	0.03	0.02	0.03	0.02	0.03	0.04	0.04
	Q75%	0.06	0.06	0.13	0.11	0.04	0.06	0.05	0.12	0.09	0.11
	Min	0	0	0	0	0	0	0	0	0	0
	Max	3.31	1.46	4.49	6.9	3.2	3.42	3.19	5.3	3.31	3.26
Doha	RMSE (m)	0.16	-	0.27	-	0.17	0.15	0.23	0.29	0.79	0.89
	Median	0.04	-	0.07	-	0.05	0.04	0.06	0.08	0.28	0.3
	Q25%	0.01	-	0.03	-	0.02	0.01	0.02	0.03	0.11	0.11
	Q50%	0.04	-	0.07	-	0.05	0.04	0.06	0.08	0.28	0.3
	Q75%	0.09	-	0.14	-	0.08	0.08	0.13	0.18	0.59	0.64
	Min	0	-	0	-	0	0	0	0	0	0
	Max	10.96	-	10.6	-	12.8	10	11.1	9.24	16.8	22.4

Study areas		IDW				Spline		Kriging		TIN	
		A	B	C	D	A	B	A	B	A	B
Mesaieed	RMSE (m)	0.17	-	0.72	-	0.13	0.1	0.28	0.69	0.78	0.71
	Median	0.03	-	0.06	-	0.02	0.02	0.05	0.07	0.35	0.08
	Q25%	0.01	-	0.01	-	0	0	0.01	0.02	0.1	0.02
	Q50%	0.03	-	0.06	-	0.02	0.02	0.05	0.07	0.35	0.08
	Q75%	0.07	-	0.23	-	0.06	0.05	0.12	0.27	0.73	0.21
	Min	0	-	0	-	0	0	0	0	0	0
	Max	9.03	-	20.1	-	6.91	5.92	11.1	18.7	19.1	20.7
Average RMSE (m)		0.12	0.13	0.08	0.46	0.15	0.10	0.11	0.17	0.44	0.43
Average Median		0.02	0.03	0.03	0.05	0.07	0.02	0.02	0.04	0.06	0.16

In terms of spline, two options were compared using original 90 per cent elevation points without breaklines as a barrier (Option A) and with barriers (Option B). The results indicate that Option B created DEM with the highest accuracy (Table 3-10). This option left many pixels without any value (areas overlapped with break lines). Conditional statement and focal statistics functions were used to fill these gaps. All statistical parameters indicated that this option (Option B, spline with breaklines as a barrier) is the best technique to create DEM for all the study areas.

For kriging, the break line data set was converted to data points and then merged with 90 per cent of the original data (Option B) to create a DEM. The DEM with barrier (Option B) was compared with Option A, which used only 90 per cent of the original data points. The results show no improvement in the accuracy of the DEM with barrier; it worsened in some cases (Table 3-10).

For TIN, using breaklines as a barrier (Option B) was also compared to the original option (Option A). The results show no improvement in the performance of TIN using breaklines (Table 3-10).

3.3. Final digital elevation model selection

The generation of a DEM with greater accuracy than the predicted SLR is crucial for estimating the impact of SLR. The State of Qatar is one of very few countries that provide a remarkably high spatial resolution of elevation data sets (10 m grid) for most economically and socially active parts of the country, with a vertical accuracy of 10 cm. This provides a good opportunity to generate high-resolution DEM in order to study the impact of climate change on SLR in Qatar.

Three interpolation techniques were investigated to generate a DEM with a horizontal resolution of 5 m, namely IDW, kriging (with four different semi-variogram models) and TIN. In total, 130 DEMs were generated for the five locations to assess the fitness and performance of each interpolation technique using RMSE.

In most cases, the IDW interpolation technique performed better than the other two techniques. Inverse distance weighting performed well in some areas, such as Al Khor-1, but not in Mesaieed. Slopes and autocorrelation were investigated as two factors behind these differences. Slope did not

explain the IDW variation in all the locations, but there were some indications that as spatial autocorrelation increased the IDW accuracy also improved.

Kriging techniques performed slightly poorer than IDW, especially in Doha, Al Thakhira and Mesaieed. Kriging (OE) performed better than other types. Kriging performed better in areas with higher spatial autocorrelation, except in Doha. The data gaps in the Doha area are particularly high because it is highly urbanised, which probably affected the performance of kriging. A similar situation was observed in the Mesaieed area. In order to understand the error and uncertainty in kriging, PSE maps were produced and they confirmed that the areas with a large proportion of missing elevation points, such as Doha and Mesaieed, had high error and uncertainty. Triangulated irregular network techniques were poorer than the other two techniques.

Overall, the difference between kriging and IDW was not considerable, but with IDW there were slightly better results. The average difference between RMSE from the best kriging technique and IDW was 5 cm (Table 3-10), with Mesaieed showing the largest difference between IDW and kriging. Inverse distance weighting consistently showed better predictions compared to kriging and TIN.

In this chapter then used breaklines to see if improvements to the DEM could be produced. Several methods of incorporation were trialled, using the breaklines as both data points and as barriers. Using breaklines as a barrier was only applicable to IDW and spline methods. In most cases the spline technique with breaklines as a barrier provided a slightly better DEM than IDW without break lines. Producing an IDW with breaklines was not always possible to do with data processing limitations, but where possible the results were slightly worse than the spline technique with break lines. Adding break line elevations as points produced DEMs with poorer RMSE. Therefore, the spline method incorporating breaklines as barriers was selected as optimal to create the DEM for studying the SLR in Qatar.

The final maps for each study area are shown in Figures 3-33 to 3-37. These will be used in the next chapter to model the impact climate change has on SLR in Qatar.

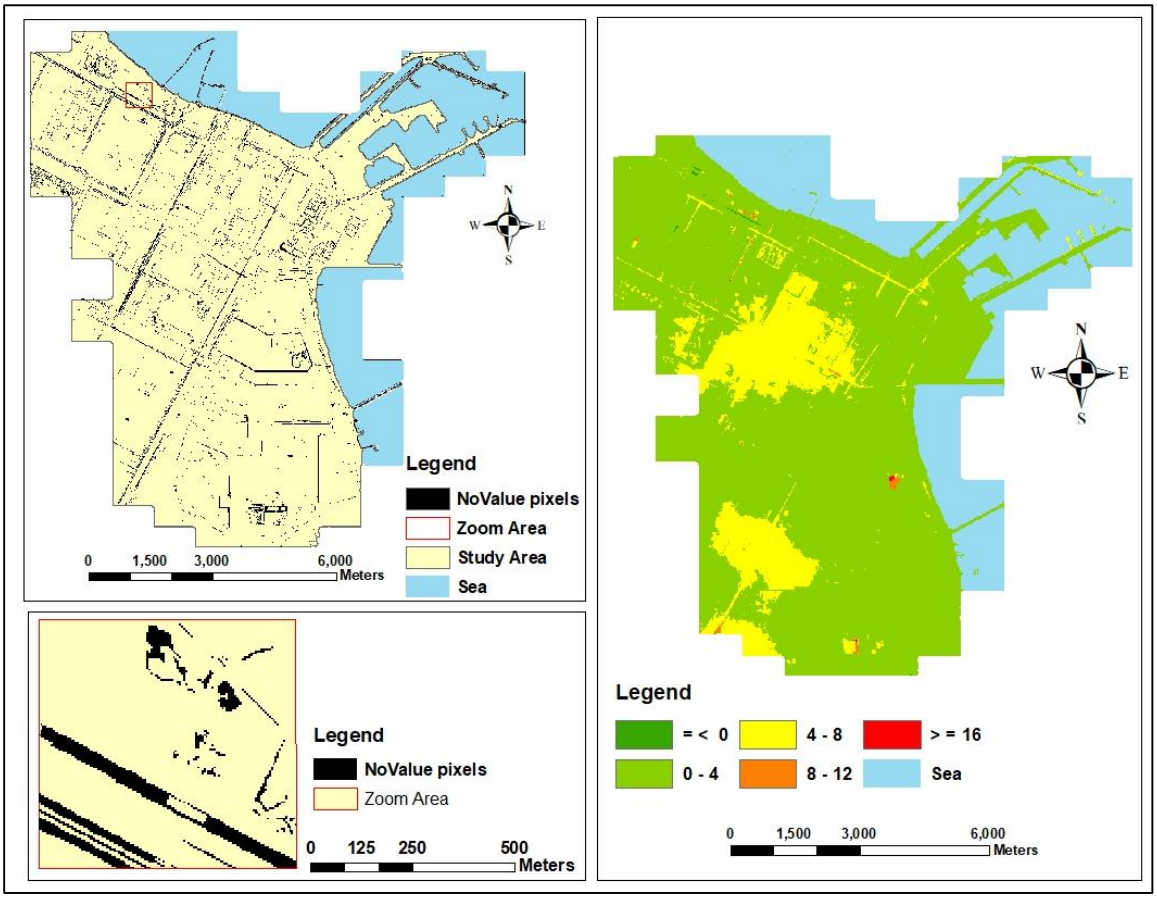

Figure 3-33: Final DEM map for Al Thakhira area using spline method and breaklines as a barrier and raster calculator to estimate the value of no value pixels.

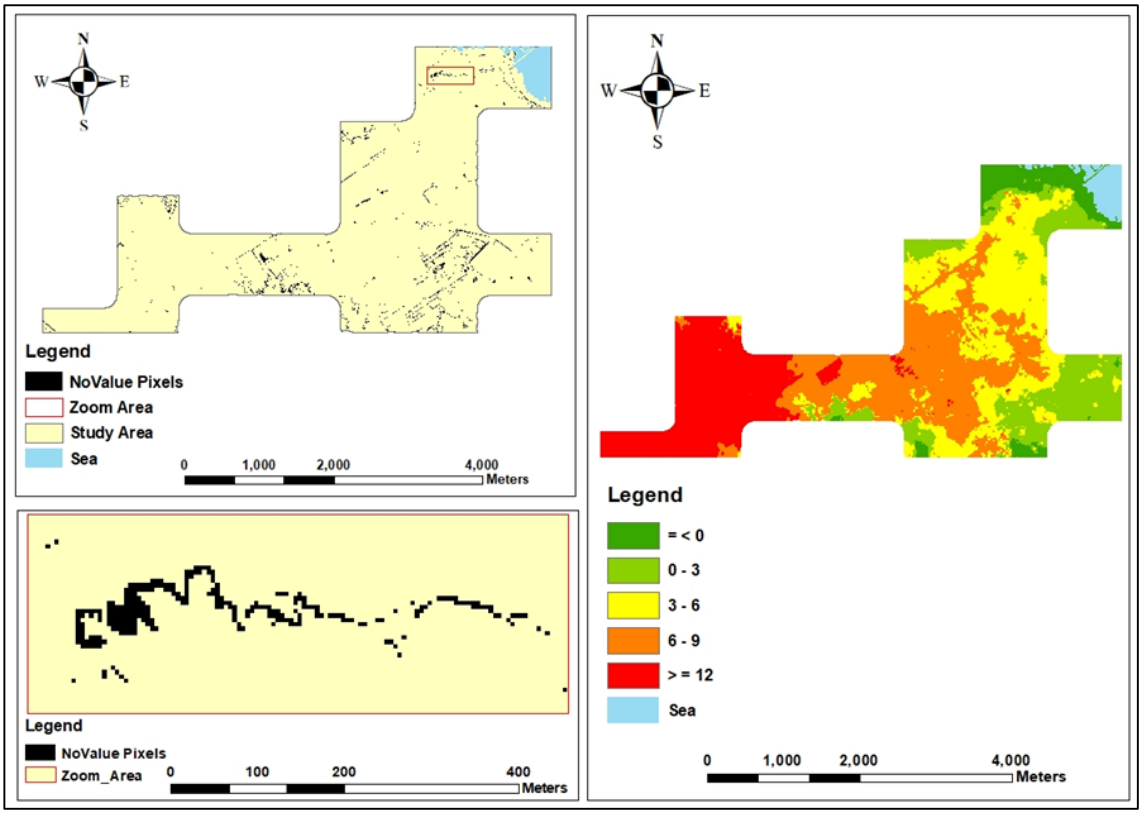

Figure 3-34: Final DEM map for Al Khor-1 area using spline method and breaklines as a barrier and raster calculator to estimate the value of no value pixels.

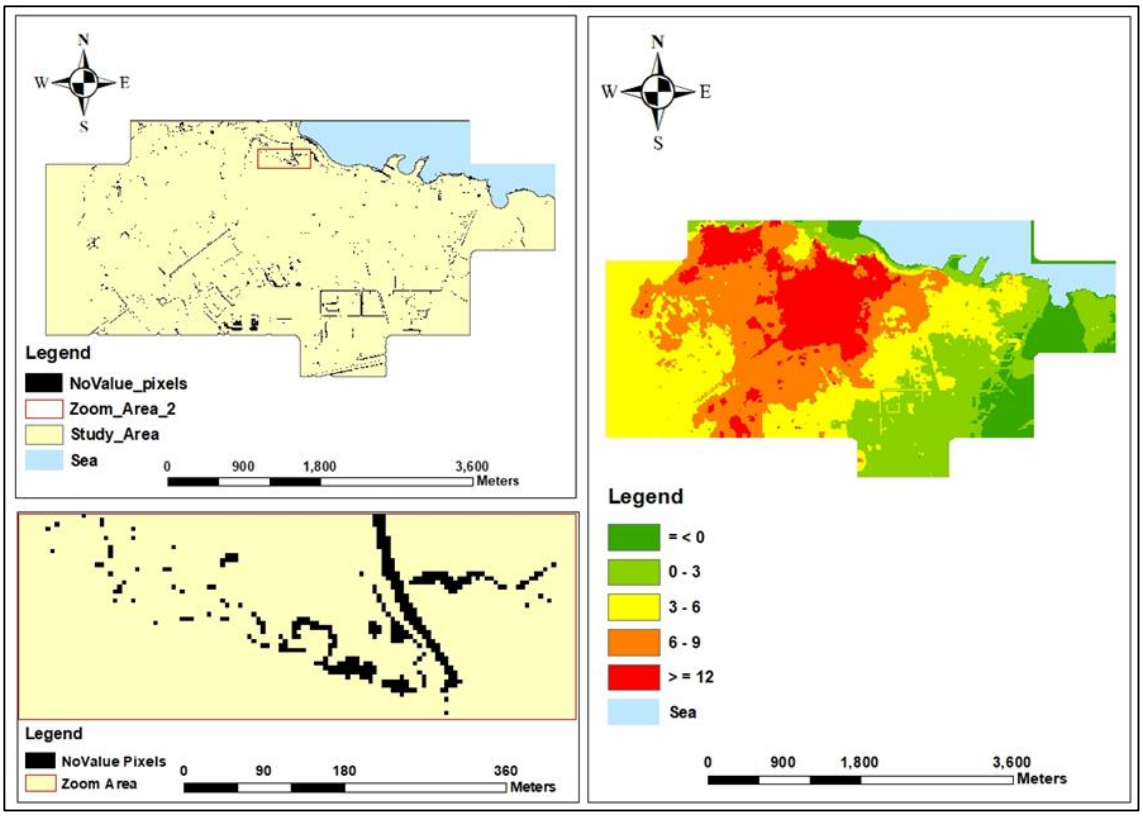

Figure 3-35: Final DEM map for Al Khor-2 area using spline method and breaklines as a barrier and raster calculator to estimate the value of no value pixels.

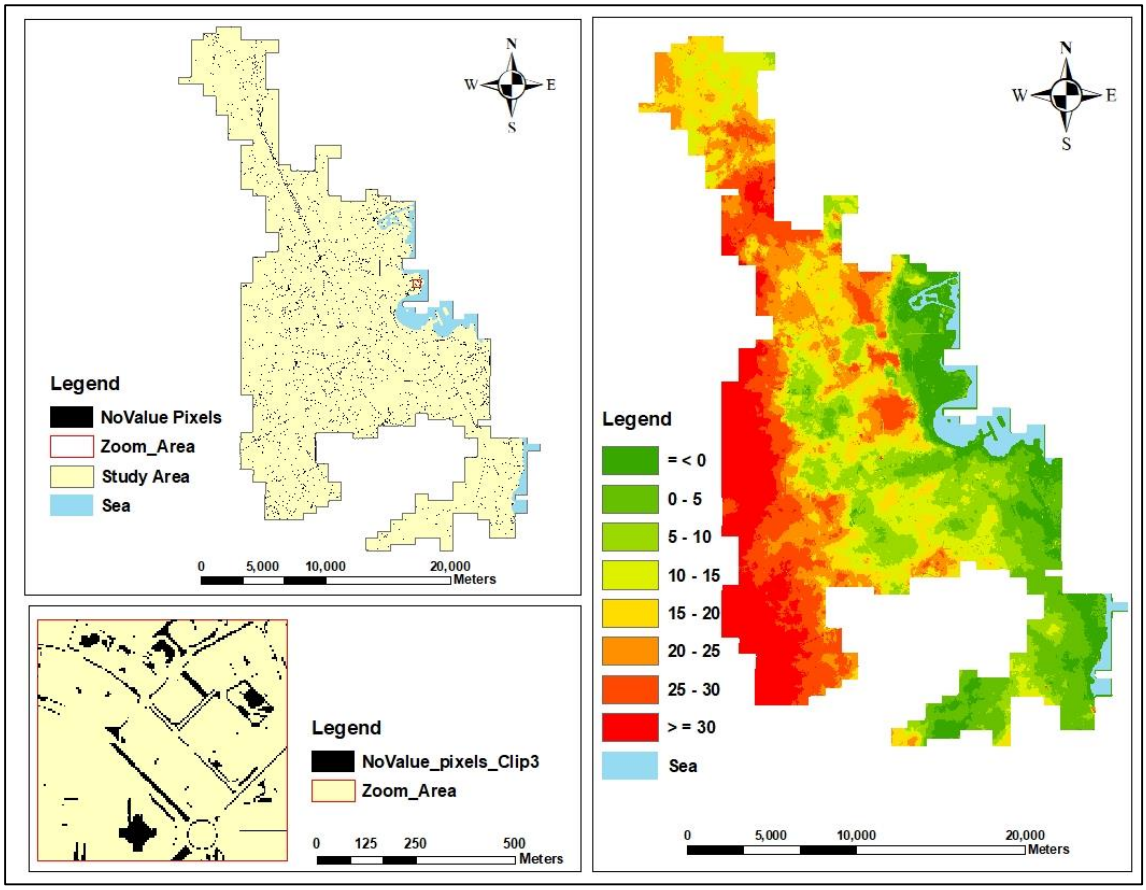

Figure 3-36: Final DEM map for Doha area using spline method and brea klines as a barrier and raster calculator to estimate the value of no value pixels.

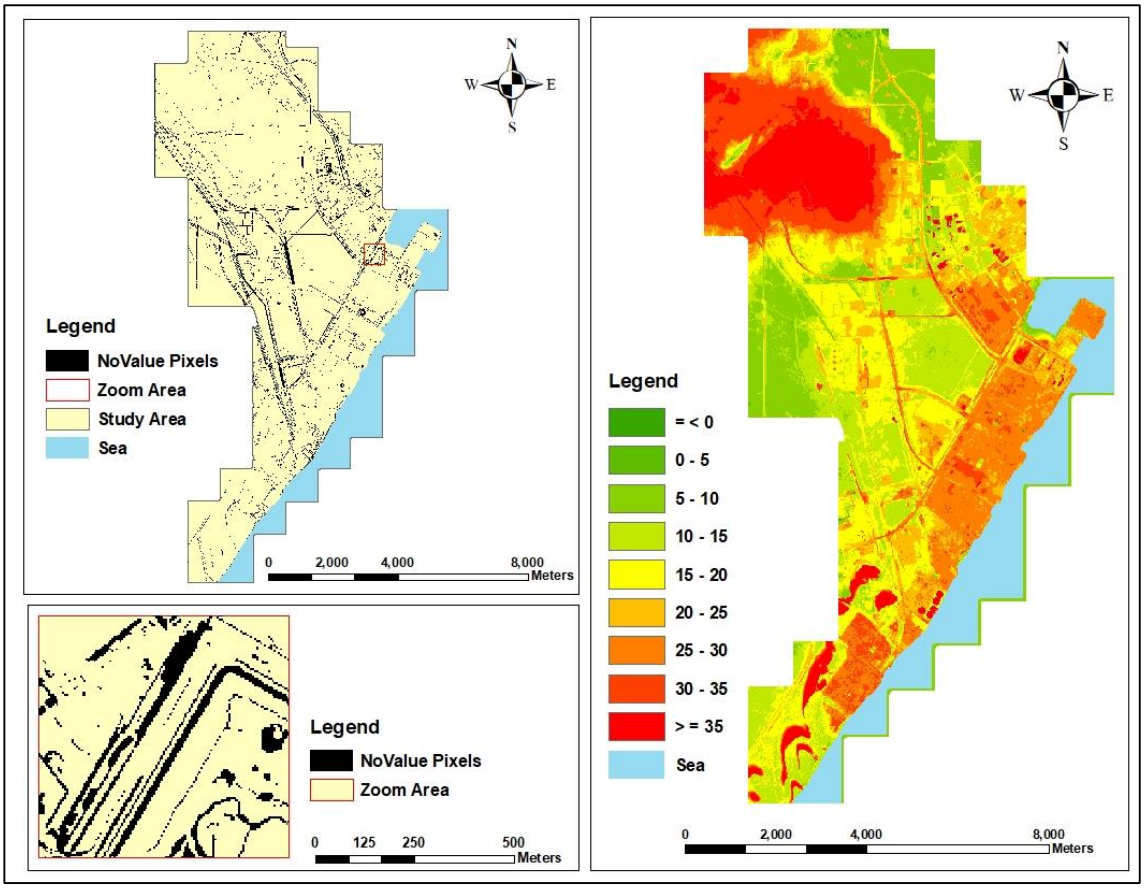

Figure 3-37: Final DEM map for Mesaieed area using spline method and breaklines as a barrier and raster calculator to estimate the value of no value pixels.

Chapter 4: Assessing Sea Level Rise and Mapping Inundation

4.1. Introduction

Climate projection explores how the climate will change in the future under various scenarios of GHG emissions. In contrast to a prediction, a projection specifically allows for changes in the set of boundary conditions, such as an increase in GHG, which may influence future climate. As a result, what emerges are conditional expectations (if x happens, then that is what is expected). For very long-term projections, scenarios are constructed around what could happen given various assumptions and judgements. The IPCC published a series of AR that summarised information on climate projections based on the IPCC emission scenarios. The latest report is the fifth Assessment Report (AR5) published in 2013. This report provides a clear and up-to-date overview of the current state of scientific knowledge relevant to climate change (Stocker et al., 2013).

In order to determine the impact of climate change on the environment in the short and long term, it is important to evaluate the concentrations of expected GHG and other pollutants in the atmosphere. The concentration of these adversely affects the climate, depending on their emissions from various sources, natural as well as man-made.

Emissions scenarios describe future releases of GHG, aerosols and other pollutants into the atmosphere. Along with information on land use and land cover, the scenarios also provide inputs to climate models. They are based on assumptions about driving forces, such as patterns of economic and population growth, technology development and other factors. Levels of future emissions are highly uncertain and scenarios only provide alternative images of the future. They provide a tool with which to analyse how driving forces may influence future emission outcomes and assess the associated uncertainties. They assist in climate change analysis, including climate modelling and impact assessment, adaptation and mitigation. The possibility that any single emission path will occur as described in scenarios is highly uncertain (IPCC, 2000).

4.2. The representative concentration pathways

The RCPs are based on selected scenarios from four models working on integrated assessment modelling, climate modelling and modelling and analysis of impacts (Eyring et al., 2010). The RCPs are consistent sets of projections of only the components of radiative forcing (the change in the balance between incoming and outgoing radiation to the atmosphere caused primarily by changes in atmospheric composition), that are meant to serve as input for climate modelling. Conceptually, the process begins with pathways of radiative forcing, not detailed socio-economic narratives or scenarios. Central to the process is the concept that any single radiative forcing pathway can result from a diverse range of socio-economic and technological development scenarios. Four RCPs were selected, defined and named according to their total radiative forcing in 2100, as shown in Table 4-1 (IPCC, 2007). Climate modellers use global circulation models (GCM) to conduct new climate model experiments using the time series of emissions and concentrations associated with the four RCPs, as part of the preparatory phase for the development of the scenarios in the IPCC's AR5 **(**Figure 4-1).

Table 4-1: Overview of RCPs.

Scenario	**Radiative forcing**
RCP 8.5	Rising radiative forcing pathway leading to 8.5 W/m² in 2100
RCP 6.0	Stabilisation without overshoot pathway to 6 W/m² at stabilisation after 2100
RCP 4.5	Stabilisation without overshoot pathway to 4.5 W/m² at stabilisation after 2100
RCP 2.6	Peak in radiative forcing at ~ 3 W/m² before 2100 returning to 2.6 W/m² by 2100

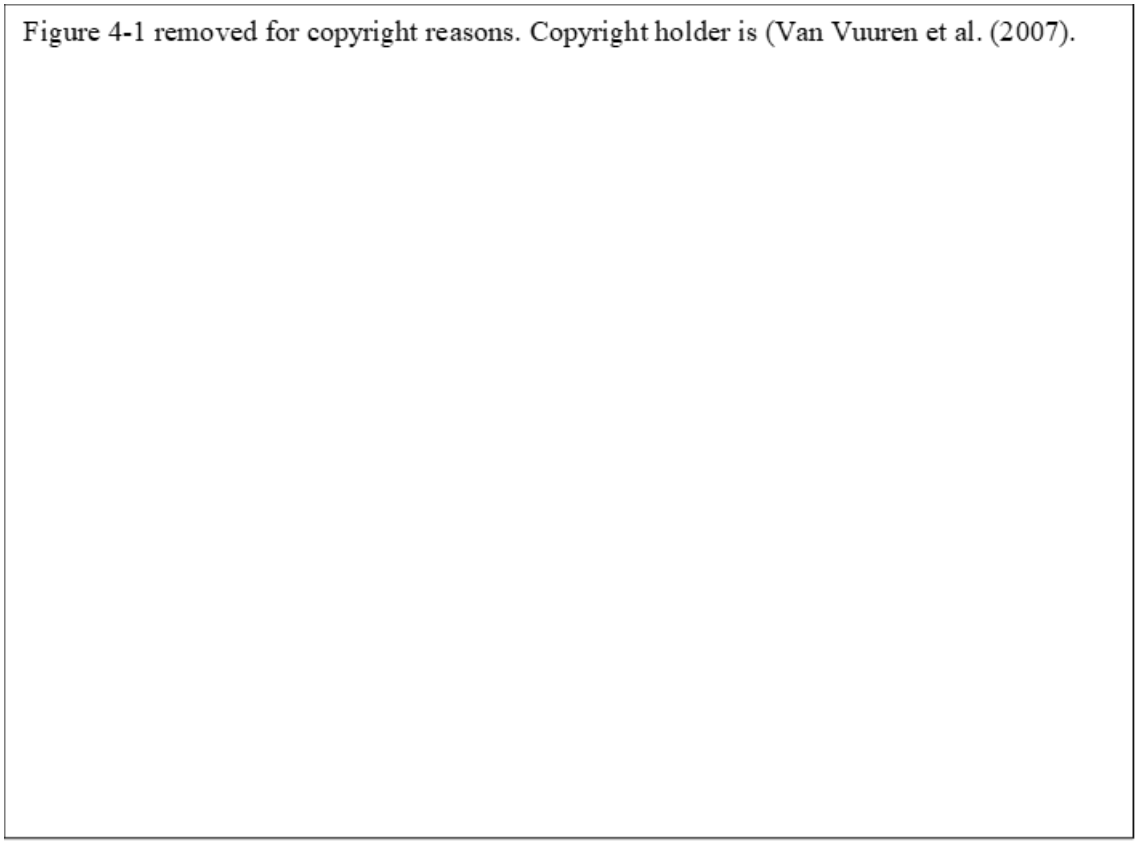

Figure 4-1: All forcing agents' atmospheric CO_2-equivalent concentrations (in parts-per-million-by-volume (ppmv)) according to four RCPs. Source: Van Vuuren et al. (2007).

- ***RCP 8.5:*** This was developed by the MESSAGE modelling team and the integrated assessment framework at the International Institute for Applied Systems Analysis (IIASA), Austria. The RCP 8.5 is characterised by increasing GHG emissions over time. It is representative of scenarios in the literature leading to high GHG concentration levels. The underlying scenario drivers and resulting development path are based on the A2r scenario detailed in Riahi et al. (2007).
- ***RCP 6.0:*** This was developed by the Asia-Pacific Integrated Model (AIM) modelling team at the National Institute for Environmental Studies (NIES), Japan. It is a stabilisation scenario where total radiative forcing is stabilised after 2100 without overshoot by employing a range of technologies and strategies for reducing GHG emissions. The details of the scenario are described in Fujino et al. (2006) and Hijioka et al. (2008).

- ***RCP 4.5:*** This was developed by the MiniCAM modelling team at the Pacific Northwest National Laboratory's Joint Global Change Research Institute (JGCRI). It is a stabilisation scenario where total radiative forcing is stabilised before 2100, through the use of diverse technologies and strategies for reducing GHG emissions. The scenario drivers and technology options are detailed in Clarke et al. (2007). Additional details on the simulation of land use and terrestrial carbon emissions are also given by Wise et al. (2009).
- ***RCP 2.6:*** This was developed by the IMAGE modelling team of the Netherlands Environmental Assessment Agency. The emission pathway is representative of scenarios in the literature leading to low GHG concentration levels. It is a so-called "peak" scenario: its radiative forcing level first reaches a value around 3.1 W/m^2 mid-century then decreases to 2.6 W/m^2 by 2100. In order to reach such radiative forcing levels, GHG emissions (and indirectly emissions of air pollutants) are reduced substantially over time. The RCP is based on the publication by Van Vuuren et al. (2007). Table 4-2 shows the AR5 global warming increase (°C) projections for each RCP.

Table 4-2: AR5 global warming increase (°C) projections. Source: IPCC (2014).

Scenario	2046-2065	2081-2100
	Temperature (°C) - Mean and *likely* range	**Temperature (°C) Mean and *likely* range**
RCP 2.6	1.0 (0.4 to 1.6)	1.0 (0.3 to 1.7)
RCP 4.5	1.4 (0.9 to 2.0)	1.8 (1.1 to 2.6)
RCP 6.0	1.3 (0.8 to 1.8)	2.2 (1.4 to 3.1)
RCP 8.5	2.0 (1.4 to 2.6)	3.7 (2.6 to 4.8)

4.3. Expected global sea level rise

Global sea levels are projected to continue to rise as the world warms, consequently affecting the mean SLR at local levels. The 2014 AR5 has projected that the rate of GMSL rise during the 21st century will exceed the rate observed during 1971– 2010 due to increases in ocean warming and loss of mass from glaciers and ice sheets. Projections of SLR are larger than in the 2007 fourth Assessment Report of IPCC, primarily because of improved modelling of land-ice contributions. Table 4-3 shows the AR5 GMSL (m) increase projections for each RCP for the period 2100 relative to 1986-2005.

Table 4-3: AR5 GMSL (m) increase projections in 2100 relative to 1986-2005 baseline.

	Sea level rise (m) RCP 4.5	Sea level rise (m) RCP 8.5
Maximum	0.71	0.98
Mean	0.53	0.74
Minimum	0.36	0.52

4.4. Mapping sea level rise – Literature review

In the past two decades there have been various studies to map the impact of climate change on the SLR. These studies used various methods in order to reduce uncertainties and improve the accuracy of the inundation mapping outcomes needed for planning and policy making processes. Thumerer et al. (2000) studied the impact of climate change on the east coast of England. Flood risks were modelled from sea level inundation based on sea defences, land elevations and subsidence rates. However, their results showed that there are significant uncertainties associated with modelling future SLR. They also highlighted the advantages of GIS as a tool for flood risk assessment.

Alsahli and AlHasem (2016) used remotely sensed data and GIS to assess the coastal vulnerability of Kuwaiti coasts to SLR in four scenarios, with physical (elevation, slope, geomorphology) and socio-economic (population, land use, cultural heritage and transportation) parameters as measures of impact. They used three steps. Firstly, they classified the DEM layer into zero and one values representing areas below and above the projected sea level, respectively. Secondly, the areas below the projected SLR were assessed to see if they were connected to the sea or not. Finally, they calculated areas of all pixels with an elevation value below the projected SLR and connected to the sea.

Al-Buloshi et al. (2014) used a simpler approach to assess the impacts of SLR and coastal flooding in Oman. The study took account of tides when considering areas at risk of inundation. To model the areas that will be affected by sea level inundation, the elevation of the tidal datum Mean Higher High Water (MHHW) level was used as the base sea level (Marcy et al., 2011). This is defined as the mean height of the highest tide measured at the tidal station. The SLR was added on top of this level and the authors suggest this should be the method used when modelling future SLR associated with climate change.

Single-value surface models, or bathtub models, have been widely used in the last two decades to map sea level inundation as they only use elevation maps and changes in sea level as their main inputs. Schmid et al. (2014) report many studies that use this method to map SLR inundation (Murdukhayeva et al., 2013; Poulter & Halpin, 2008; Strauss et al., 2012; Titus & Richman, 2001; Weiss & Overpeck, 2003). This method does not consider any changes in the land surface, erosion or ocean dynamics. Like a bathtub, the model simply projects the water level rise above fixed and known surfaces such as the MHHW line. The output of this model provides the potential extent of flooding due to SLR caused by climate change. While this method has limitations for detailed and site-specific modelling, it is useful for mapping and visualising the potential extent of future SLR on a large scale.

Webster et al. (2004) suggested that the bathtub method can be improved by considering only areas with a direct connection to the sea. Areas with low altitude behind higher altitude areas would not be flooded unless there was a channel allowing water to enter.

Poulter and Halpin (2008) used lidar DEMs with 6 and 15 m spatial resolution and three methods to evaluate the extent and timing of coastal flooding from the sea level. Firstly, they used a simple 'bathtub' method. They mapped flooded areas where the elevation value of a pixel was less than the projected sea level. This method did not consider the hydrologic connectivity of the pixel. They reported that this method had been used in previous research by Moorhead and Brinson (1995) and Titus and Richman (2001). Chust et al. (2010) reasoned that areas that were not open to direct sea inundation should also be included to locate potentially vulnerable areas.

In their second and third methods, Poulter and Halpin (2008) considered two hydrologic connectivity definitions. Both consider that the cell could be flooded if it were below sea level and if it were connected to flooded cells or open water. Two different methods were used to determine connectivity to flooded cells or open water. The second method used was the 'four-side rule', where a pixel was connected in any basic direction (north, east, south and west) to a flooded cell pixel, while in their third method they used the 'eight-side rule', where a pixel was considered to be flooded if the elevation value was less than the SLR and connected to flooded pixels in any direction (cardinal and diagonal).

Their results showed that the connected approach (second and third methods) estimated lower inundation areas than the bathtub method (no connectivity). Furthermore, areas flooded under the four-side rule (second method) were lower than the third method (eight-side rule), because the eight-side rule increased the number of connections compared to the four-side rule. This approach, proposed by Poulter and Halpin (2008), would be more practical for larger areas (Cooper et al., 2013).

Kane et al. (2015) also used a method similar to the eight-side rule to model the SLR vulnerability and salty inundation or groundwater inundation of three coastal areas in the USA. They calculated the final SLR vulnerability by ranking each cell based on other parameters, such as type and time of inundation, habitat, type of soil, erosion and infrastructure.

The disadvantage of the four-side connectivity rule is that it underestimates potential flooding impacts, while the eight-side connectivity rule overestimates them (Poulter & Halpin, 2008). The four-side rule works better for larger areas while the eight-side connectivity rule is better when an overestimated approach is acceptable.

Other authors have used visual approaches to select areas open to the sea or open water bodies. For example, Webster et al. (2006) found infrastructure in the DEM which can prevent flooding by cutting off the area from the sea. The DEM was changed accordingly. Webster et al. (2004) went a step further by consulting with engineers to determine and identify areas which should be included in the manual selection of flood-prone areas.

Based on the reviewed literature, there exist various ways of mapping SLR inundation. For this study, the methods used by Poulter and Halpin (2008) (hydrodynamic modelling with four-side and eight-side rules) are used to identify grid cells as vulnerable to inundation for all the five study areas in Qatar. Both methods will be tested, because the eight-side rule overestimates the flooded area but also increases the processing time. The four-side rule, on the contrary, underestimates the inundation area compared to the eight-side rule, and the processing time is lower. It is more practical for a larger area (Cooper et al., 2013).

The reason for not selecting a more dynamic model is the data and time available for this research. With little variation in the type of soil and insignificant annual rainfall, the coastal area in Qatar does not offer a considerable magnitude of tidal activity. Therefore, for modelling the

SLR inundation in Qatar, the DEM created in the previous chapter will be used. Four climate change scenarios (RCP 2.6, RCP 4.5, RCP 6.0 and RCP 8.5) above MHHW will be assessed for all five areas in this study.

4.5. Methodology for mapping inundation

The purpose of this section is to develop a method for mapping inundated areas based on climate change scenarios for the five study areas in Qatar. The method consists of six components to produce inundation maps for each scenario:

1- Selection of DEM

2- Determining the current coastline

3- Identifying tidal levels in the study area

4- Quantifying SLR as the result of climate change

5- Methods to map the spatial extent of inundated areas

6- Sea level rising mapping

In contrast to many other studies it was decided that the pits in the DEM would not be filled within the study area. Pits are small depressions in the DEM that can occur during DEM production (Burrough & McDonnell, 1998). However, within the coastal Qatar landscape depressions in the land surface are common and hence it was decided that removing them would not represent the situation in the study area. In addition, such depressions can have a large impact upon hydrological connectivity, but these tools are not used to a great extent in this chapter.

4.5.1. Selection of digital elevation model

The DEM was created in the previous chapter using the spline technique with breaklines as a barrier. This provided the most accurate DEM for all studied areas compared to other interpolation techniques (see Chapter 3).

4.5.2. Coastal line

Sea level changes need to be mapped in relation to the current coastline. The current coastline was determined in all the studied areas based on the DEM presented in the previous chapter. The reason is because the coastline is dynamic; existing maps of the coastline did not agree with the DEM. The current Qatar coastline, provided by the Qatar GIS Centre, represents the Mean Water Height.

However, it did not match the 0 m coastal line generated from the DEM. For example, in some coastal areas in Doha, these differences were more than 2 km horizontally.

To generate a coastline for the study area, the DEM was reclassified into two classes: above and below zero metres. Zero was assigned to areas below zero metres and no data for areas above zero-metre altitude. This raster file represented the coastline in 2009 (when the elevation points were generated). It was converted into a polygon in order for it to be used for mapping inundated areas. The elevation points used to generate the DEM for each study area records 0 metres as 8.0036 metres below the Fundamental Benchmark B (FBMB) located at the north end of the runway at the old Doha International Airport. This elevation is based on the Qatar Vertical Datum, which was defined in 1970 until 1972 as the mean sea level. Therefore, the coastline produced will represent the mean sea level on the DEM.

4.5.3. Tidal level

As well as looking at the effect of SLR above the mean sea level, we will also consider the effect of tidal extremes in the inundation mapping as more areas will be flooded during unusual high tides. For each area, we identified the mean sea level (MSL) (the average between maximum and minimum sea level), MHHW and highest observed tide (HOT) for all the five study areas from 2003 to 2015 (Table 4-4). The NOAA (2020) defined MHHW as "the average of the higher high-water height of each tidal day observed over the National Tidal Datum Epoch. For stations with shorter series, comparison of simultaneous observations with a control tide station is made in order to derive the equivalent datum of the National Tidal Datum Epoch" (NOAA, 2020, p.95). While the HOT is the "average of all the high-water heights observed over the National Tidal Datum Epoch" (NOAA, 2020, p.94).

This information was obtained from the Department of Land and Survey and the Ministry of Municipality and Environment in Qatar. The tide heights in this table are measured from the Qatar Vertical Datum. As this is the same datum as used to measure the DEM, the heights will correspond to heights on the DEM. Each study area has a gauging station, except for Al Khor-1 and 2. The value of tide for these two study areas was interpolated from a station located in Doha (49.63 km from Al Khor-1 and 43.15 km from Al Khor-2) and a station located in Al Thakhira (20.76 km

from Al Khor-1 and 27.03 km from Al Khor-2). A simple linear interpolation was used to model the relationship between the distance and tidal gauge, then a linear formula was used to determine the value of the tide in both Al Khor-1 and 2.

Table 4-4: Highest observed tide, MSL tide and MHHW tide for all the five study areas from 2003 to 2015 (from nearest tidal station measured from the Qatar Vertical Datum).

Study Areas	Tide		
	Highest Observed Tide (m)	Mean Sea Level (m)	Mean Higher High Water (m)
Al Thakhira	1.32	0.00	0.64
Al Khor_1	1.34	0.01	0.66
Al Khor_2	1.35	0.01	0.66
Doha	1.40	0.02	0.70
Mesaieed	1.56	0.03	0.81

4.5.4. Sea level rise as the result of climate change

To examine SLR, two scenarios were selected: RCP 4.5 and RCP 8.5. RCP 4.5 was selected because it is a stabilisation scenario where the total radiative forcing is stabilised before 2100 by employing a range of technologies and strategies to reduce GHG emissions. RCP 8.5 is characterised by increasing GHG emissions over time to represent a higher GHG concentration level. For both scenarios, to represent the uncertainty with each projection, the maximum, average and minimum SLR were selected in order to investigate the impact in each case (Table 4-4).

4.5.5. Mapping spatial extent of inundated areas

The next step in the methodology is to bring all these data sets to model the SLR in each study area for both RCP scenarios. To determine flooded areas, three methods were used to determine areas under inundation: bathtub, four-side connectivity rule and eight-side connectivity rule. In this section, each of these was evaluated. The aim was to select the most appropriate method to produce the final inundation map for all areas. To do this, we examined changes under maximum RCP 4.5 with the HOT using the three methods. Once a final method has been selected, a range of tides and RCPs will be considered in the next section.

4.5.6. Bathtub method

To map inundated areas using the bathtub method in ArcGIS, the reclassification function of the raster calculator function was used. Areas in the DEM with values lower than the projected SLR were labelled as inundated areas and the rest of the terrain labelled as non-inundated areas. These areas were converted into polygons and their areas calculated.

$$\text{Inundated Area} = \text{DEM} <= X$$

where X = RCP SLR

4.5.7. Hydrological connectivity methods (four and eight side)

Among the flooded areas identified by the bathtub method, the next step was to select those connected to the sea by using both the four-side and eight-side rule.

To implement these rules, the assumption was made that when converted to a polygon, all cells connected using the four-side rule will form a continuous polygon, and that cells connected using the eight-side rule will not form continuous pixels, but the separate pixels will touch each other (Figure 4-2).

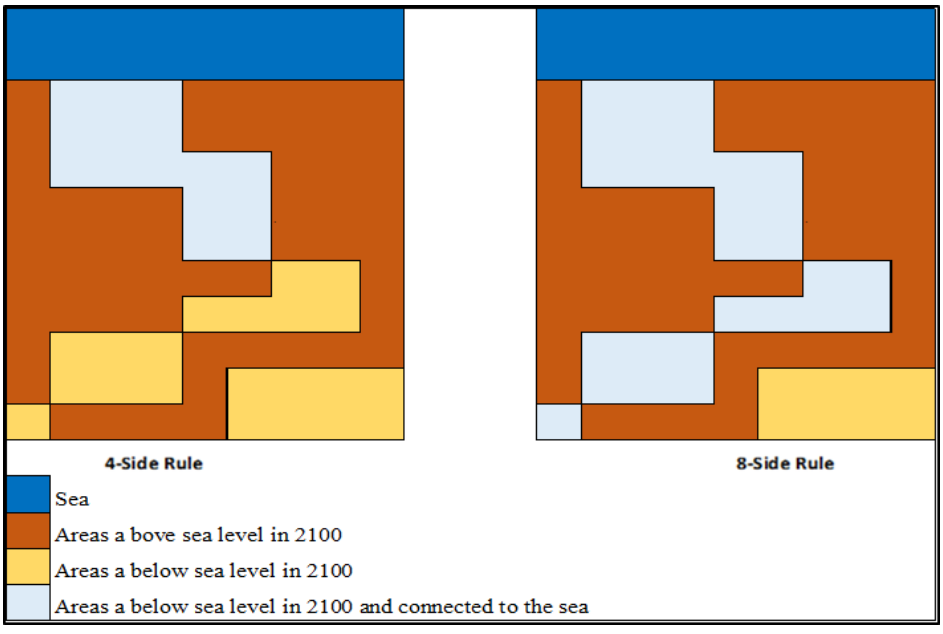

Figure 4-2: The difference between the coverage of inundated areas based on four-side and eight-side rule hydrologic connectivity to the sea.

To identify areas at risk of flooding based on the four-sided rule, the inundated polygons were identified which have a direct contact with the coastline (selection by location command in ArcGIS). These selected locations were identified, and their areas calculated. To identify additional

areas using the eight-sided rule, the additional inundated areas were selected which were connected to the identified inundated areas through the four-sided rule. This was performed multiple times until no more inundated areas were identified. Both methods are illustrated in Figure 4-2.

Table 4-5 shows, as expected, that the bathtub method produces a much larger inundated area than the four-side and eight-side rule hydrological connectivity methods. This indicates that many areas below the flood line are not connected to the sea and hence would not be flooded. The results also indicate that there are few differences between four and eight-side rules, although, as expected, the eight-sided rule does produce slightly more flooded areas. The exception to this is Mesaieed, where the eight-sided rule produced much larger flooded areas than the four-sided rule (Table 4-5).

As a result, the eight-side rule was selected because it has the potential to overestimate connectivity and hence flooding, compared to the four-sided rule, by allowing flow to occur across cell corners. It hence represents a worst-case scenario.

Table 4-5: Total area (km^2) inundated in each study area based on maximum RCP 4.5 scenarios at maximum tide using the bathtub, four-side and eight-side connectivity rule.

Study areas	Area (km^2)	Methods	Inundated Area (km^2) RCP 4.5 Maximum
Al Thakhira	93.78	Bathtub	30.19
		Four-side rule	19.54
		Eight-side rule	19.55
Al Khor-1	11.42	Bathtub	0.38
		Four-side rule	0.37
		Eight-side rule	0.37
Al Khor-2	13.62	Bathtub	1.65
		Four-side rule	0.65
		Eight-side rule	0.65
Doha	465.04	Bathtub	7.53
		Four-side rule	3.99
		Eight-side rule	4.00
Mesaieed	88.24	Bathtub	38.70
		Four-side rule	4.48
		Eight-side rule	10.29

4.6. Results

The final step was to include the tidal information in the inundation mapping. The total SLR (RCP +Tide) was calculated for both RCP 4.5 and RCP 8.5 scenarios (Maximum, Average and Minimum RCP scenario) and three tidal states (HOT, MSL and MHHW).

4.6.1. Al Thakhira

The total SLR (SLR from RCP scenario and tidal effect) were calculated (Table 4-6). As expected, the HOT effect (1.32 m) is greater than the MHHW (0.64 m) and the MSL (0.00 m). The sea level is expected to rise between 1.68 m and 2.03 m in the HOT event under RCP 4.5 by 2100. Under RCP 8.5, sea level is expected to rise between 1.84 m and 2.30 m. These SLRs and areas inundated are mapped as in Figure 4-3, Figure 4-4 and Table 4-7.

Table 4-6: Total SLR as the result of RCP scenarios and tidal events in the Al Thakhira area.

Tide	Scenario 2100 - RCP 4.5			Scenario 2100 - RCP 8.5		
	Maximum (0.71) m	Average (0.53) m	Minimum (0.36) m	Maximum (0.98) m	Average (0.74) m	Minimum (0.52) m
Highest Observed Tide (1.32) m	2.03	1.85	1.68	2.30	2.06	1.84
Mean Higher High Water (0.64) m	1.35	1.17	1.00	1.62	1.38	1.16
Mean Sea Level (0.00) m	0.71	0.53	0.36	0.98	0.74	0.52

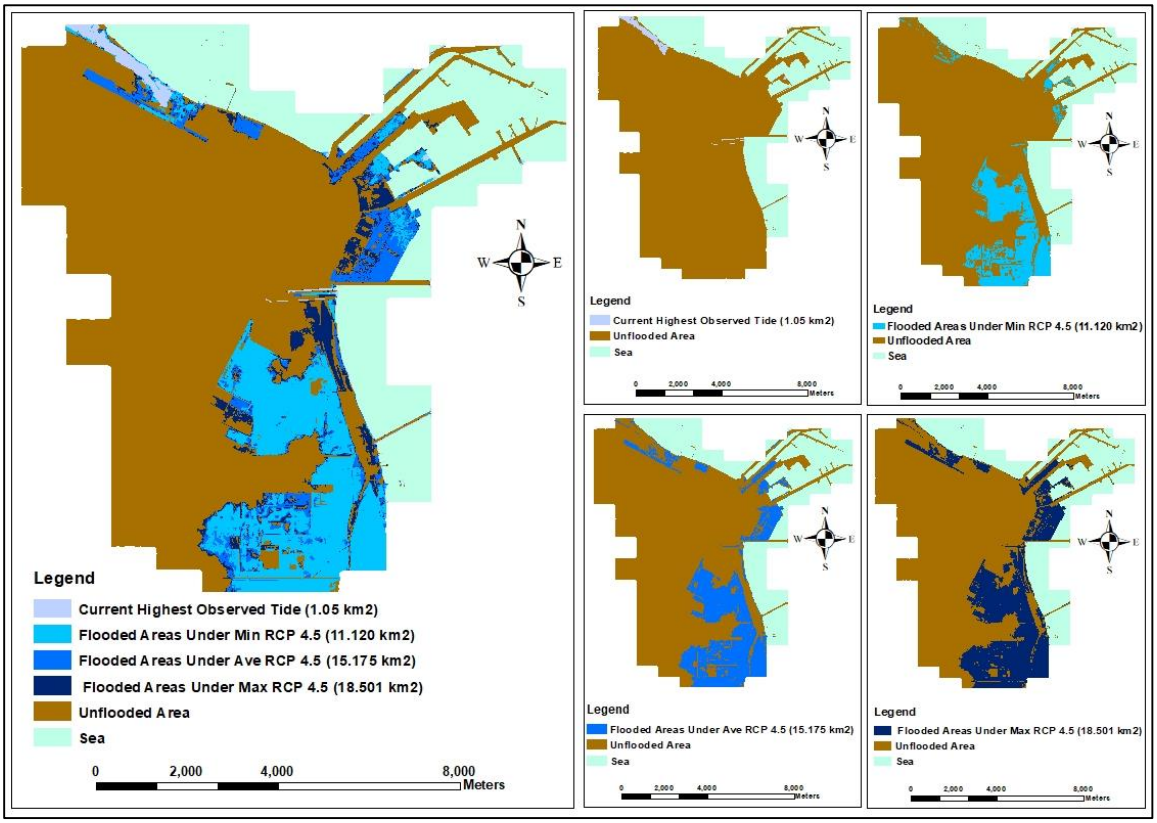

Figure 4-3: Mapping inundated area in Al Thakhira for RCP 4.5 scenarios and current flooding due to HOT.

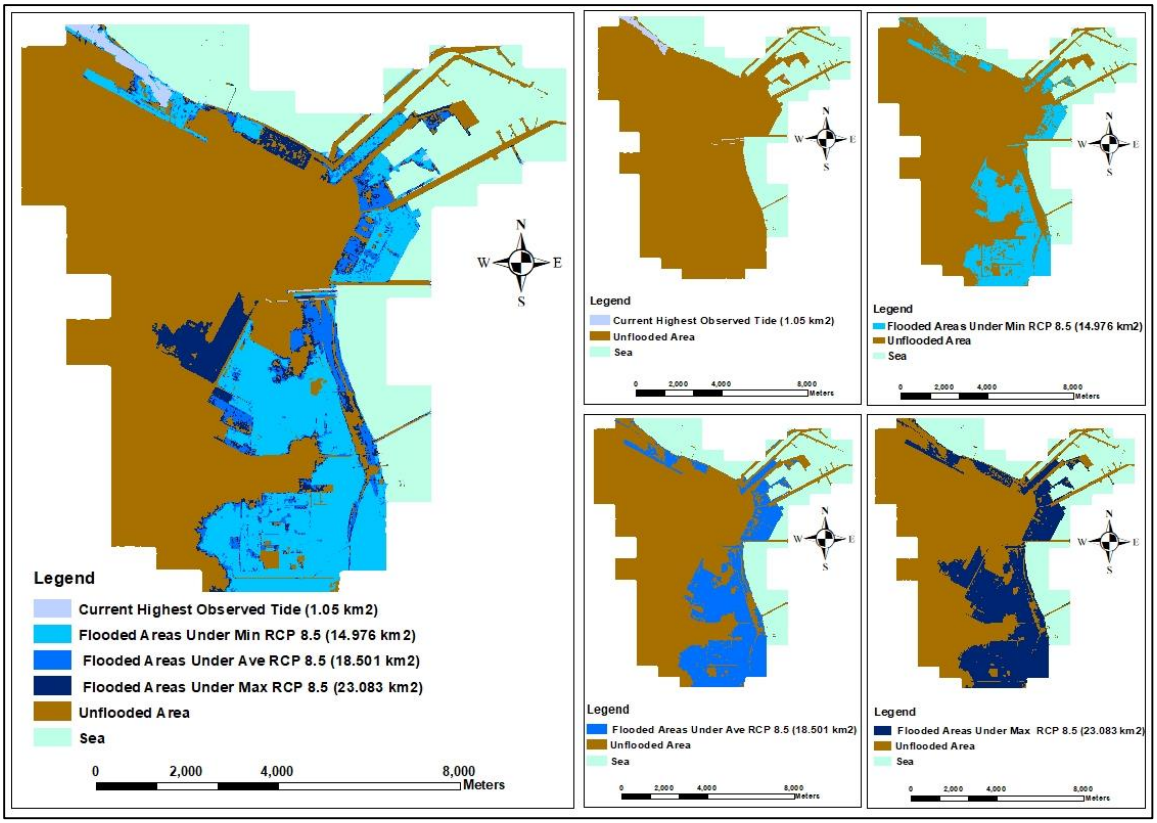

Figure 4-4: Mapping inundated area in Al Thakhira for RCP 8.5 scenarios and current flooding due to HOT.

The results indicate that for both RCPs in Al Thakhira the inundated areas will increase as the SLR increases. The SLR (in metres) for the three scenarios following the three tidal events were plotted against the flooded areas (in km^2). This allows us to show the flooded area as a function of SLR, which is mainly dictated by the elevation of the area (Figure 4-5). This figure indicates that the increase in flooded areas occurs notably after a SLR of 2.28 m. A map showing why this occurs is presented by Figure 4-6.

Table 4-7: Inundated area (km^2) in Al Thakhira based on combined RCP scenarios and tidal conditions as a total SLR.

Scenarios (RCP plus tide)		Total sea level (m) (RCP and Tide)	Flooded area (km^2)
RCP 4.5 Minimum (0.36) m	Mean Sea Level (0.00) m	0.36	0.05
RCP 8.5 Minimum (0.52) m	Mean Sea Level (0.00) m	0.52	0.08
RCP 4.5 Average (0.53) m	Mean Sea Level (0.00) m	0.53	0.095
RCP 4.5 Maximum (0.71) m	Mean Sea Level (0.00) m	0.71	0.424
RCP 8.5 Average (0.74) m	Mean Sea Level (0.00) m	0.74	0.467
RCP 4.5 Minimum (0.36) m	Mean Higher High Water (0.64) m	0.98	0.575
RCP 8.5 Maximum (0.98) m	Mean Sea Level (0.00) m	1.00	0.696
RCP 8.5 Minimum (0.52) m	Mean Higher High Water (0.64) m	1.16	0.71
RCP 4.5 Average (0.53) m	Mean Higher High Water (0.64) m	1.17	0.716
RCP 4.5 Maximum (0.71) m	Mean Higher High Water (0.64) m	1.35	0.894
RCP 8.5 Average (0.74) m	Mean Higher High Water (0.64) m	1.38	0.928
RCP 8.5 Maximum (0.98) m	Mean Higher High Water (0.64) m	1.62	2.459
RCP 4.5 Minimum (0.36) m	Highest Observed Tide (1.32) m	1.68	11.12
RCP 8.5 Minimum (0.52) m	Highest Observed Tide (1.32) m	1.84	14.976
RCP 4.5 Average (0.53) m	Highest Observed Tide (1.32) m	1.85	15.175
RCP 4.5 Maximum (0.71) m	Highest Observed Tide (1.32) m	2.03	18.501
RCP 8.5 Average (0.74) m	Highest Observed Tide (1.32) m	2.06	18.87
RCP 8.5 Maximum (0.98) m	Highest Observed Tide (1.32) m	2.30	23.083

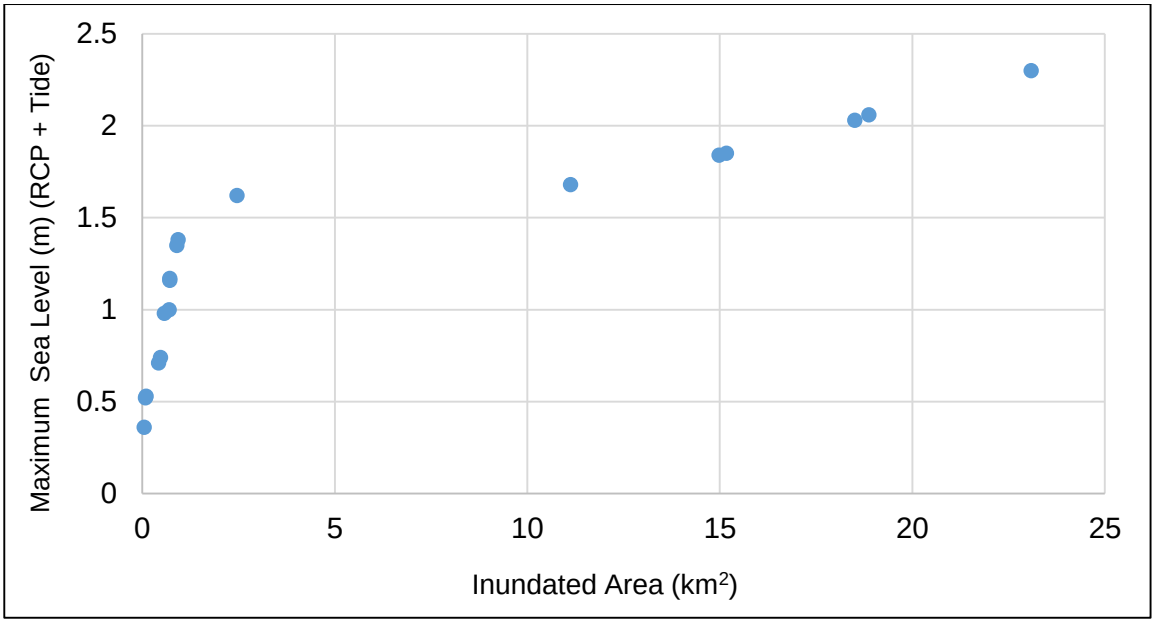

Figure 4-5: Relationship between the maximum sea level as the result of RCP (4.5 and 8.5) scenarios and tidal condition and the flooded area in Al Thakhira.

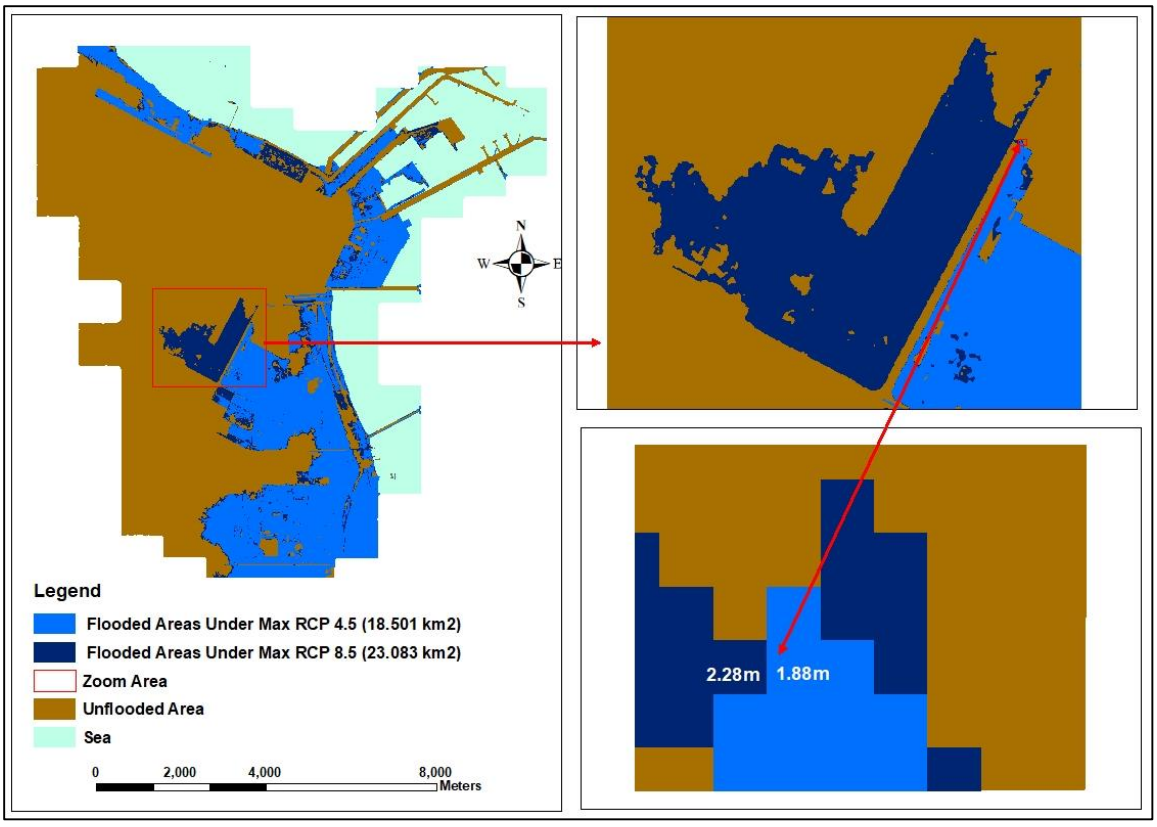

Figure 4-6: The elevation in Al Thakhira illustrates the difference between the flooded area under different RCP scenarios (numbers in lower panel represent DEM elevation).

The effect of climate change with the HOT represents the worst-case scenario, as the SLR will be at the highest level and flooding will cover larger areas. The large area of flooding is mainly due to the low elevations in Al Thakhira, and the HOT increases the area's risk of flooding as a result of climate change (Figure 4-7).

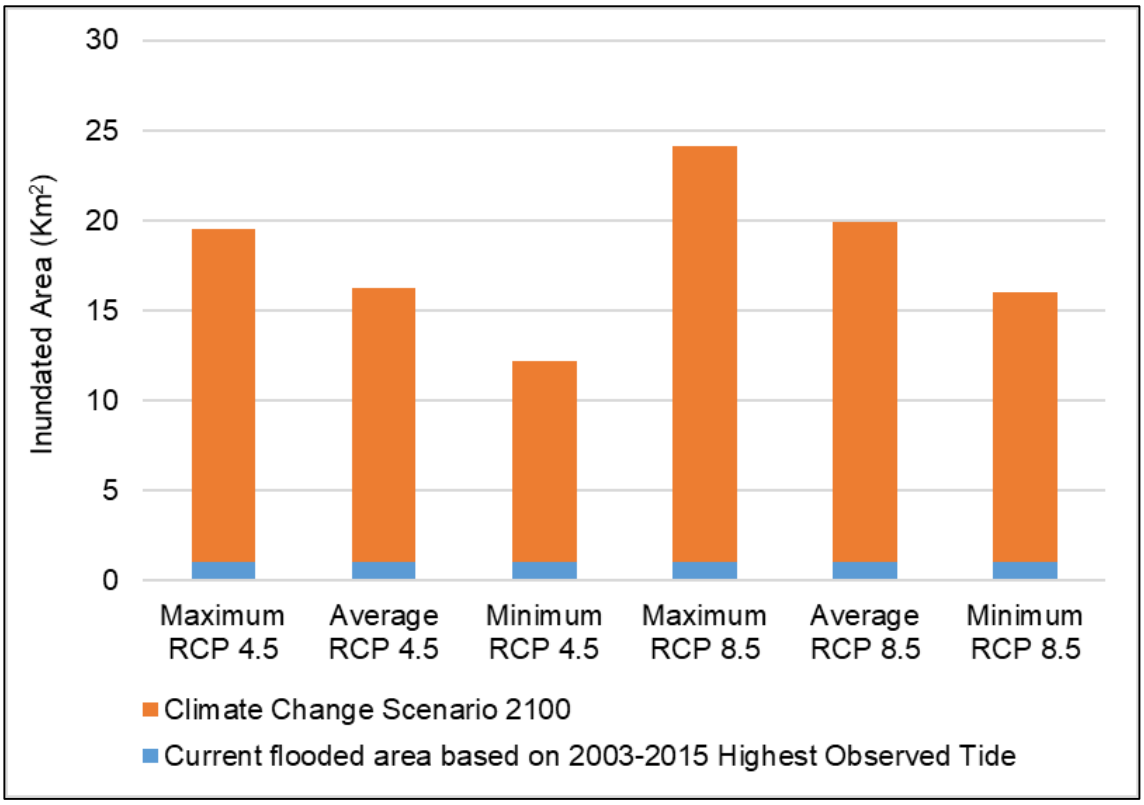

Figure 4-7: The effect of climate change and HOT on inundated areas in Al Thakhira.

4.6.2. Al Khor 1 and 2

The effect of SLR in both Al Khor 1 and 2 was not large, as the elevation in both areas is higher and the connectivity with the sea is less when compared to Al Thakhira. The total SLR (Table 4-8) was just above 2 m maximum, and the areas expected to be flooded were less than 1 km^2 (Table 4-9).

Table 4-8: Total SLR as a result of RCP scenarios and tidal events in Al Khor 1 and 2.

Tide	Scenario 2100 - RCP 4.5			Scenario 2100 - RCP 8.5		
	Maximum (0.71) m	Average (0.53) m	Minimum (0.36) m	Maximum (0.98) m	Average (0.74) m	Minimum (0.52) m
	Al khor_1			Al khor_1		
Highest Observed Tide (1.34) m	2.05	1.87	1.70	2.32	2.08	1.86
Mean Higher High Water (0.66) m	1.37	1.19	1.02	1.64	1.40	1.18
Mean Sea Level (0.01) m	0.72	0.54	0.37	0.99	0.75	0.53
	Al khor_2			Al khor_2		
Highest Observed Tide (1.35) m	2.06	1.88	1.71	2.33	2.09	1.87
Mean Higher High Water (0.66) m	1.37	1.19	1.02	1.64	1.40	1.18
Mean Sea Level (0.01) m	0.72	0.54	0.37	0.99	0.75	0.53

Table 4-9: Inundated areas in Al Khor 1 and 2.

Tide	Current flooded area based on 2003-2015 tidal events	Scenario 2100 - RCP 4.5			Scenario 2100 - RCP 8.5		
		Maximum (0.71) m	Average (0.53) m	Minimum (0.36) m	Maximum (0.98) m	Average (0.74) m	Minimum (0.52) m
		Al khor_1			Al khor_1		
Highest Observed Tide (1.34) m	0.169	0.207	0.084	0.057	0.266	0.215	0.083
Mean Higher High Water (0.66) m	0.146	0.024	0.020	0.016	0.068	0.027	0.020
Mean Sea Level (0.01) m	0.000	0.152	0.127	0.095	0.162	0.154	0.126
		Al khor_2			Al khor_2		
Highest Observed Tide (1.35) m	0.446	0.218	0.138	0.099	0.363	0.229	0.135
Mean Higher High Water (0.66) m	0.116	0.332	0.314	0.263	0.418	0.335	0.313
Mean Sea Level (0.01) m	0.000	0.146	0.084	0.046	0.312	0.162	0.083

In Al Khor-1, the inundated area will be 0.266 km^2 above the HOT (maximum RCP 8.5), with one third of this area currently flooded under the HOT. Also, in Al Khor-2, the maximum inundated area will be 0.363 km^2 above the HOT. The inundated areas in both Al Khor 1 and 2 are not large (Figure 4-8, Figure 4-9, Figure 4-10 and Figure 4-11).

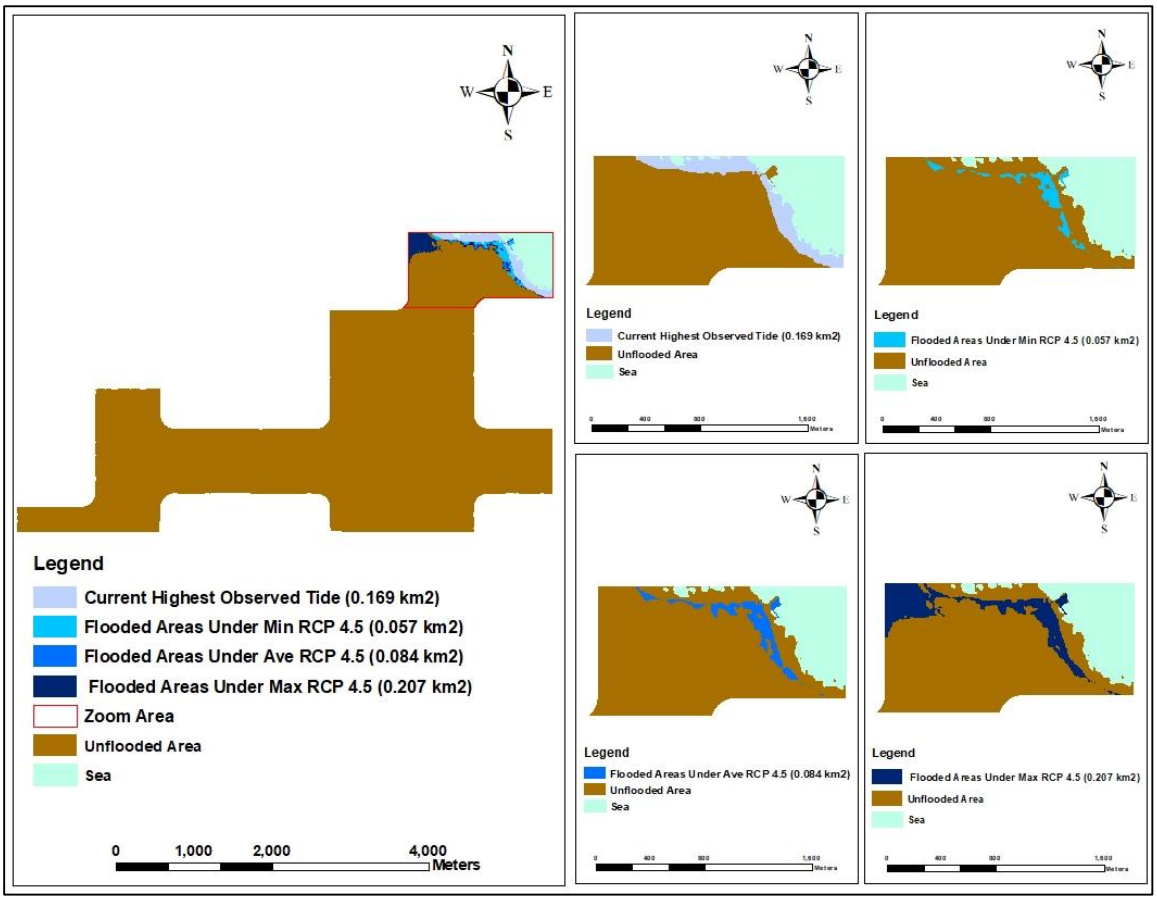

Figure 4-8: Mapping inundated area in Al Khor-1 for RCP 4.5 scenarios and current flooding due to HOT.

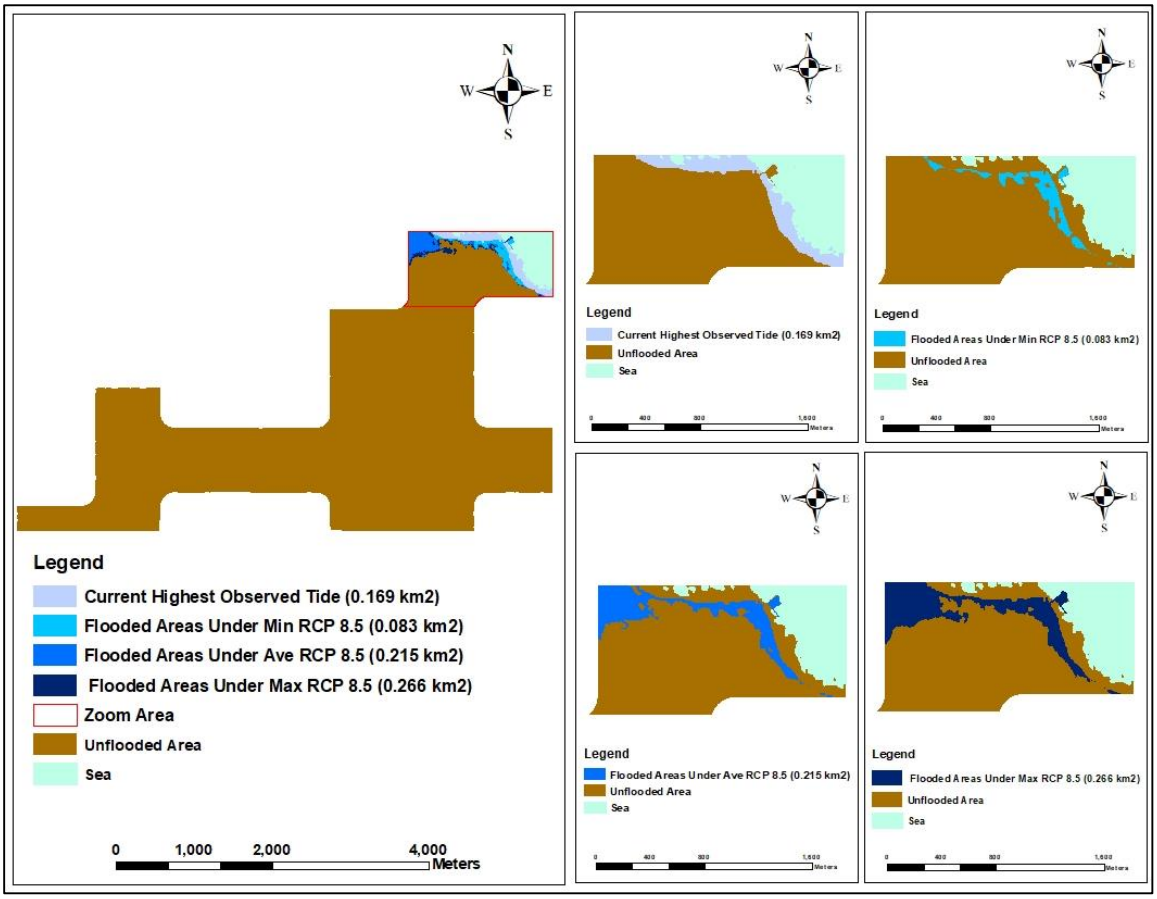

Figure 4-9: Mapping inundated area in Al Khor-1 for RCP 8.5 scenarios and current flooding due to HOT.

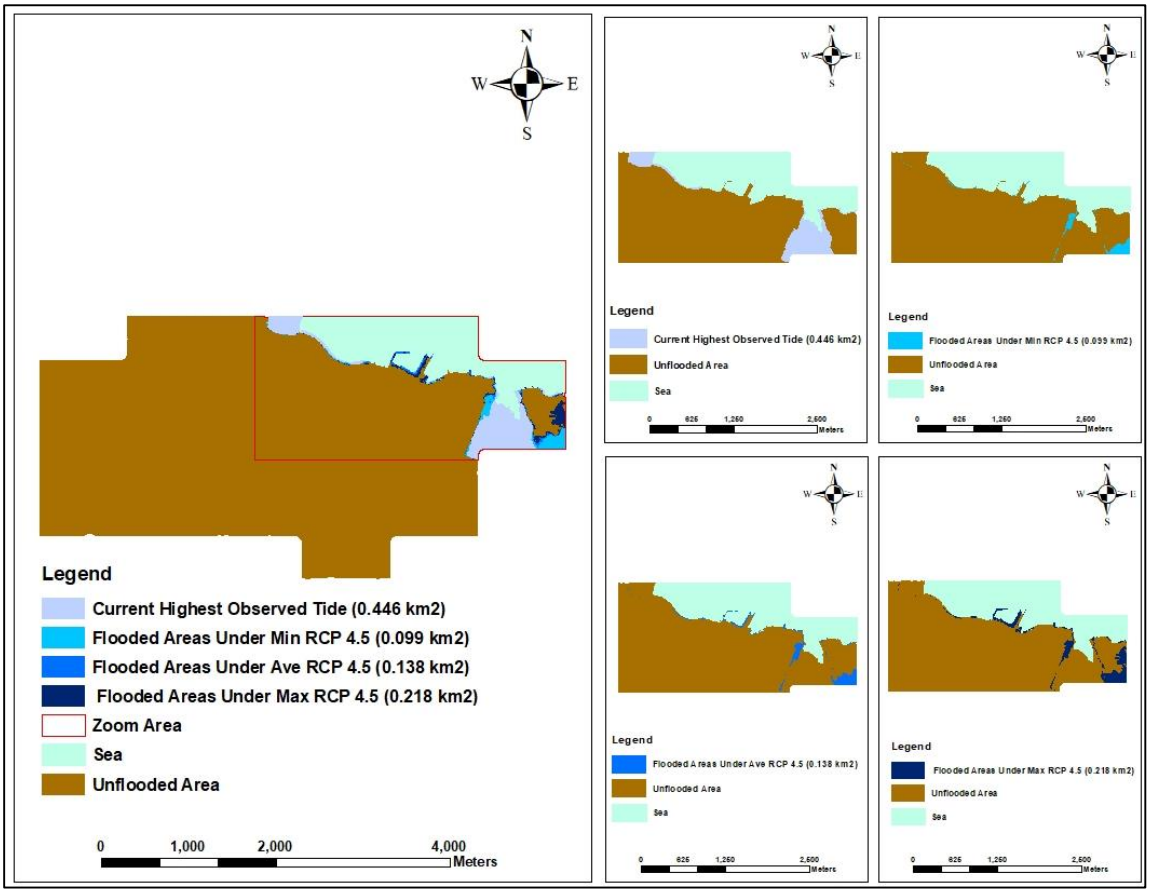

Figure 4-10: Mapping inundated area in Al Khor-2 for RCP 4.5 scenarios and current flooding due to HOT.

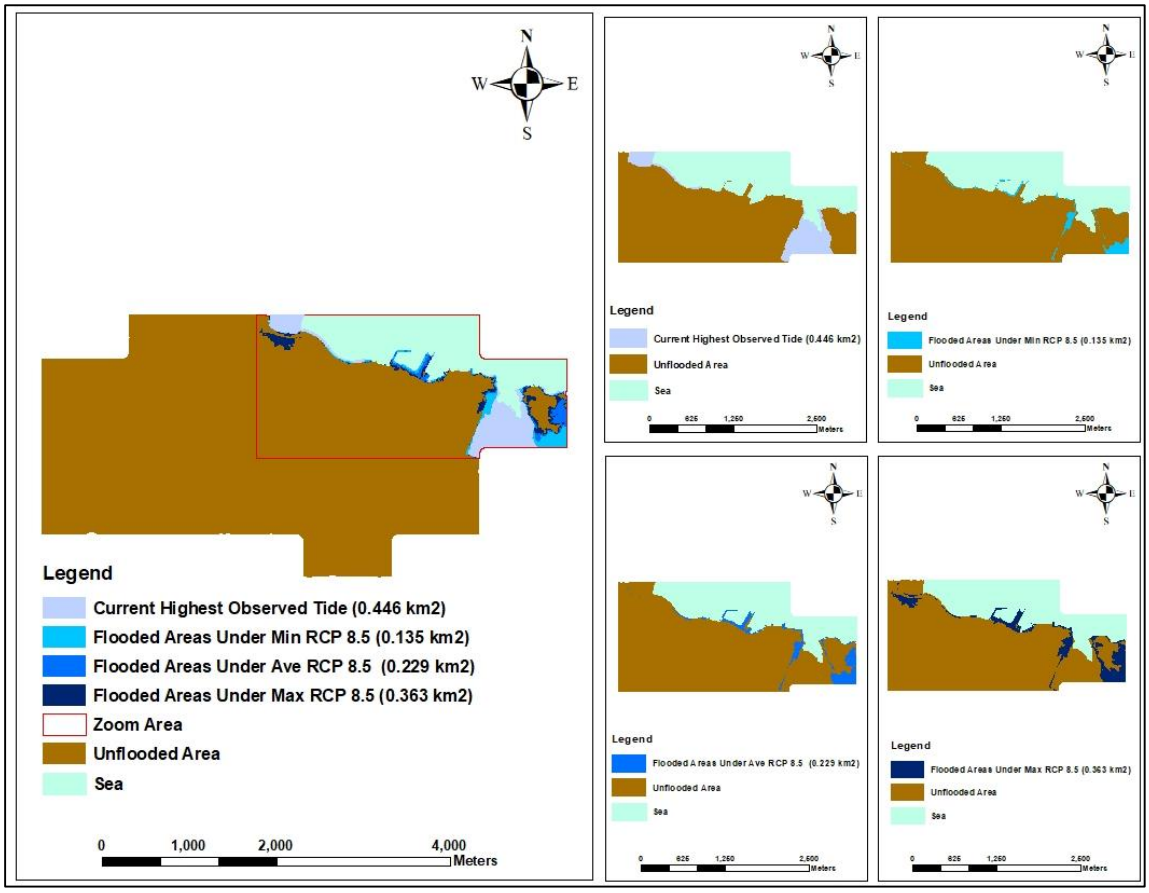

Figure 4-11: Mapping inundated area in Al Khor-2 for RCP 8.5 scenarios and current flooding due to HOT.

The flooded areas in both Al Khor 1 and 2 will increase relatively slowly with the SLR, but do not appear to have any large jumps in flooded areas as the sea level increases (Figure 4-12 and Figure 4-13).

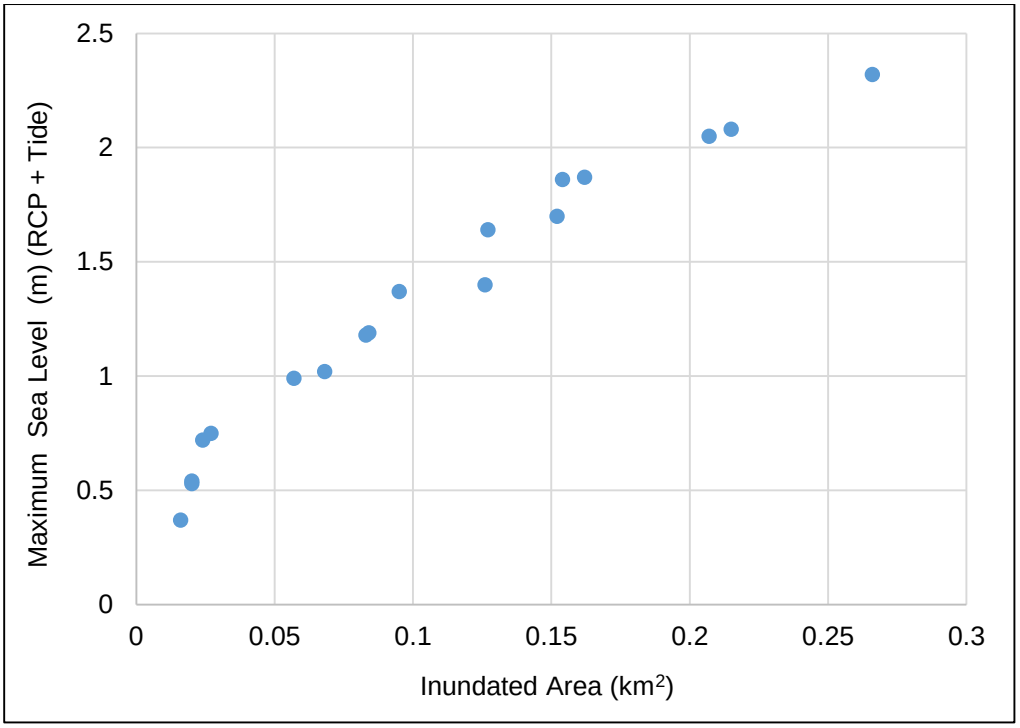

Figure 4-12: Relationship between the maximum sea level as the result of RCP (4.5 and 8.5) scenarios and tidal condition and the flooded area in Al Khor-1.

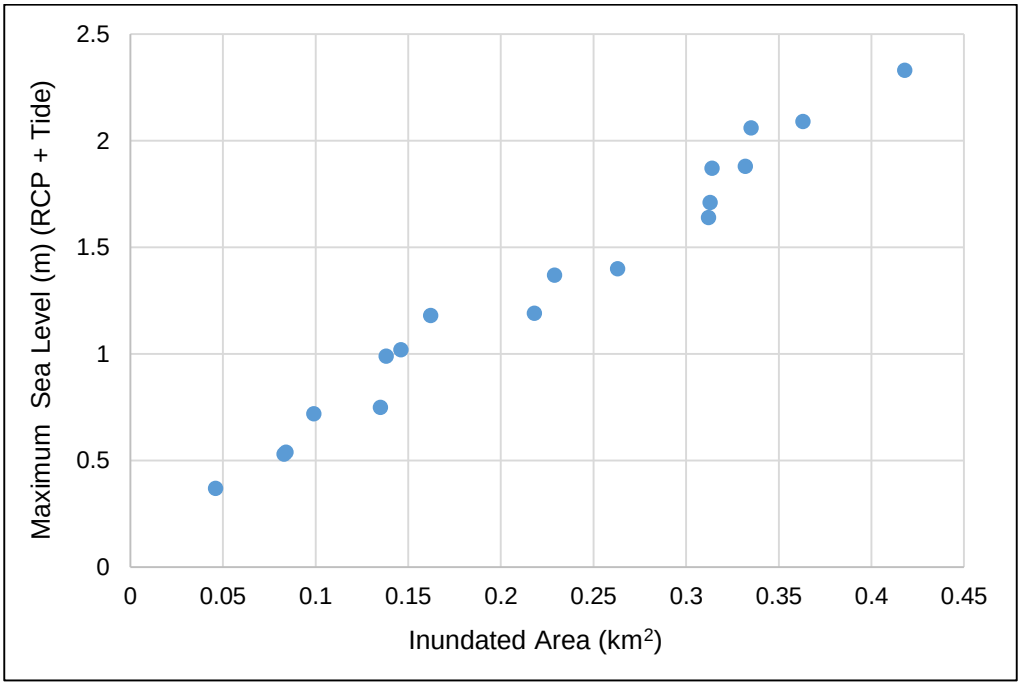

Figure 4-13: Relationship between the maximum sea level as the result of RCP (4.5 and 8.5) scenarios and tidal condition and the flooded area in Al Khor-2.

Areas currently under flooding as the result of HOT represent a large proportion of the flooded areas under most RCP scenarios (Figure 4-14 and Figure 4-15).

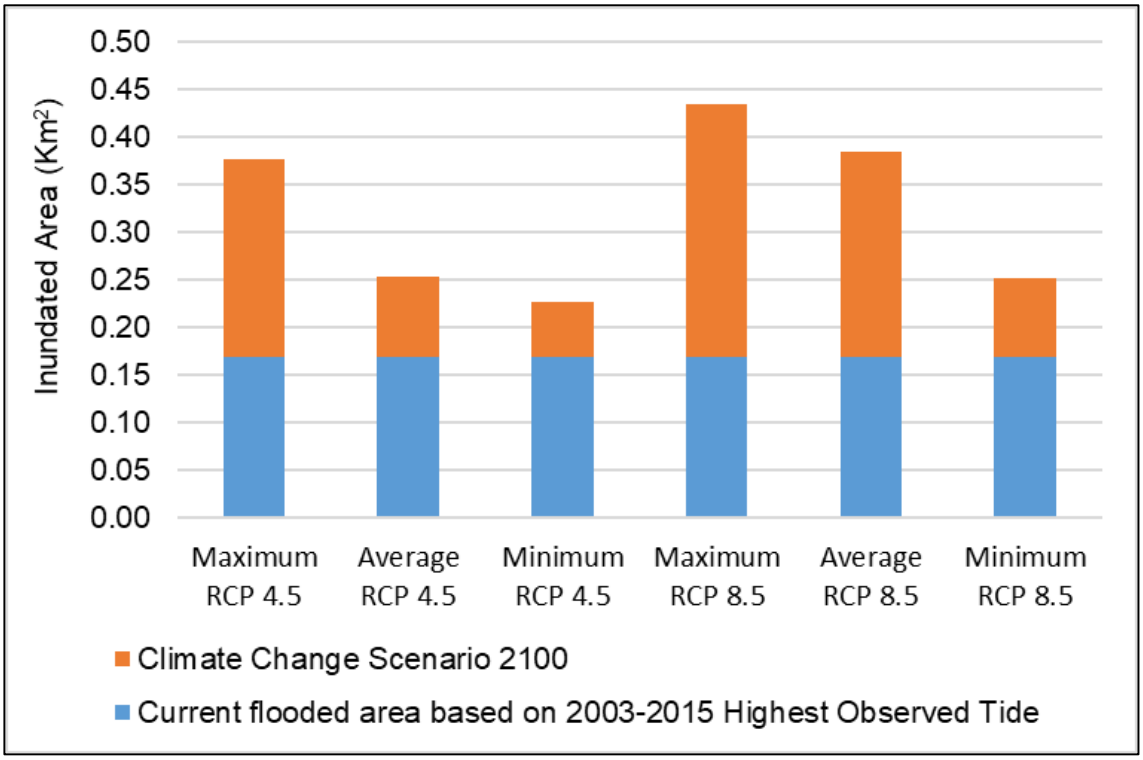

Figure 4-14: Proportion of current flooding under HOT to RCP scenarios in Al Khor-1.

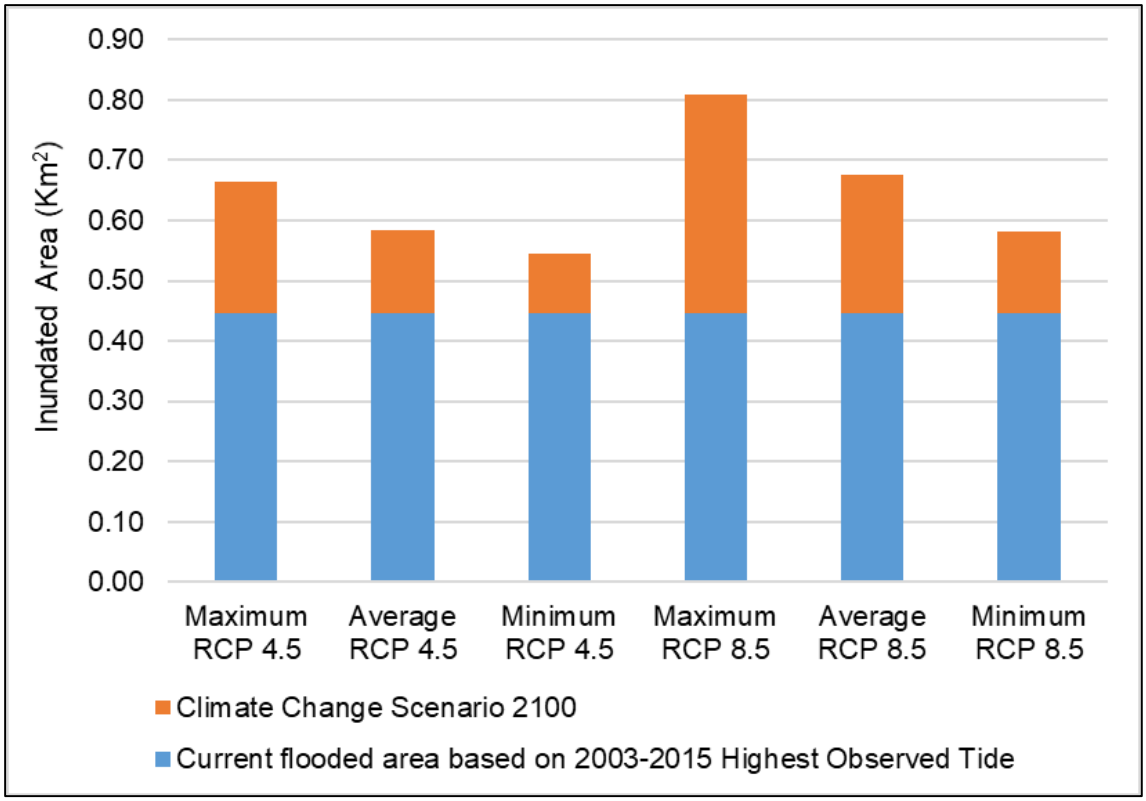

Figure 4-15: Proportion of current flooding under HOT to RCP scenarios in Al Khor-2.

4.6.3. Doha

The total SLR as a result of climate change and tidal events ranged from 2.38 m above the HOT (Maximum RCP 8.5 with HOT) to 0.38 m (Minimum RCP 4.5 and MSL) (Table 4-10). Sea level rise will only create flooding in less than two per cent of the area (7.55 km^2) under maximum RCP 8.5 and HOT (Table 4-11).

Table 4-10: Total SLR as the result of RCP scenarios and tidal events in Doha.

Tide	Scenario 2100 - RCP 4.5			Scenario 2100 - RCP 8.5		
	Maximum (0.71) m	Average (0.53) m	Minimum (0.36) m	Maximum (0.98) m	Average (0.74) m	Minimum (0.52) m
Highest Observed Tide (1.40) m	2.11	1.93	1.76	2.38	2.14	1.92
Mean Higher High Water (0.70) m	1.41	1.23	1.06	1.68	1.44	1.22
Mean Sea Level (0.02) m	0.73	0.55	0.38	1.00	0.76	0.54

Table 4-11: Inundated areas in Doha.

Tide	Current flooded area based on 2003-2015 tidal events	Scenario 2100 - RCP 4.5			Scenario 2100 - RCP 8.5		
		Maximum (0.71) m	Average (0.53) m	Minimum (0.36) m	Maximum (0.98) m	Average (0.74) m	Minimum (0.52) m
Highest Observed Tide (1.40) m	1.051	2.952	1.692	0.873	6.508	3.118	1.619
Mean Higher High Water (0.71) m	0.310	0.755	0.478	0.278	1.386	0.815	0.459
Mean Sea Level (0.02) m	0.000	0.325	0.247	0.177	0.533	0.343	0.244

The relationship between SLR and flooded areas shows a significant increase when the SLR is above 2 m (Figure 4-16).

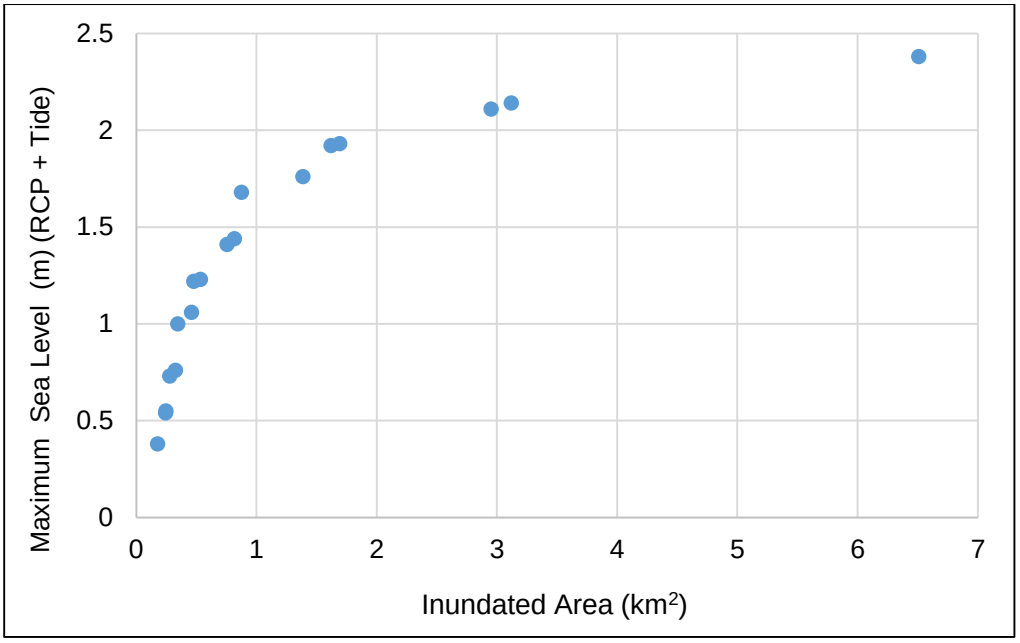

Figure 4-16: Relationship between the maximum sea level as the result of RCP (4.5 and 8.5) scenarios and tidal condition and the flooded area in Doha.

Most of the flooded areas are located north-east and south-east of Doha (Figure 4-17 and Figure 4-18). The current flooding due to the HOT will be less dramatic as it will not be more than 2 m. However, with SLR caused by climate change, flooding will increase notably (Figure 4-19).

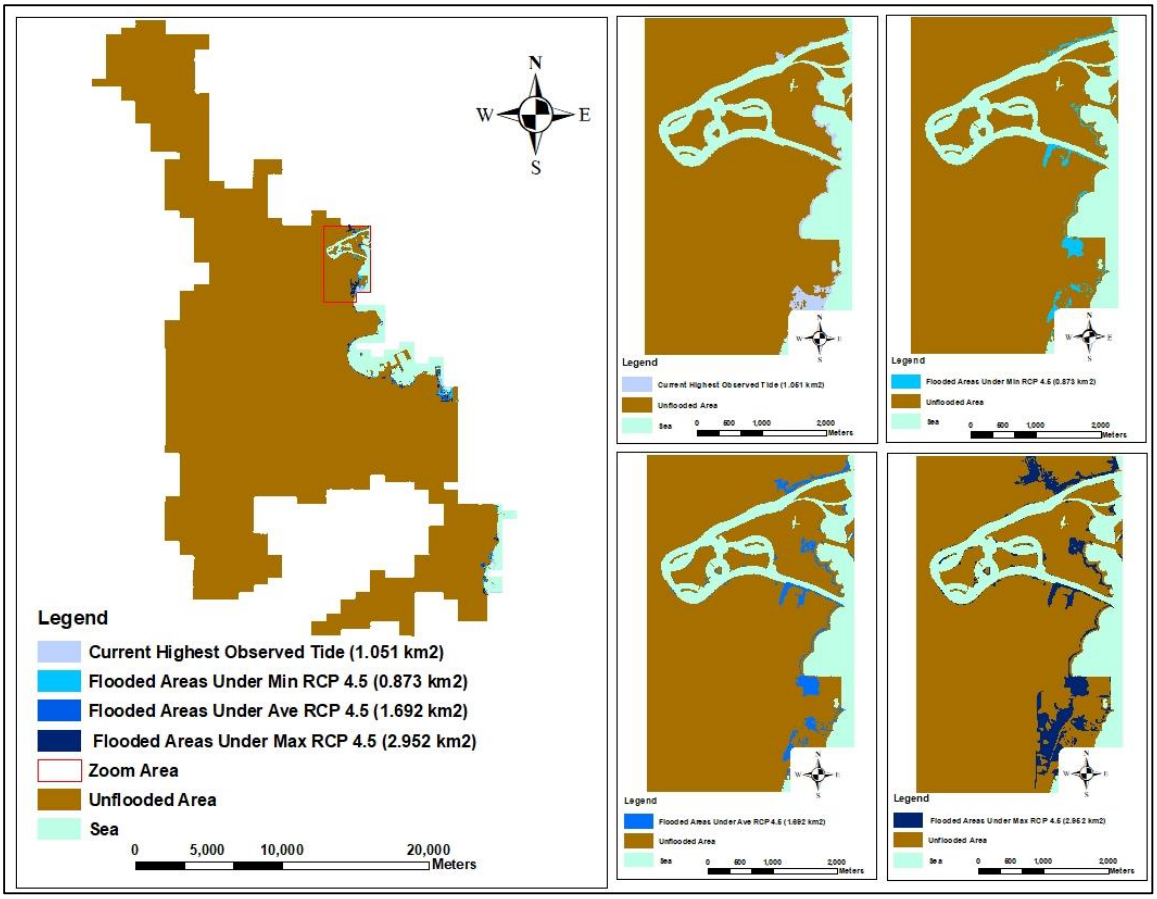

Figure 4-17: Mapping inundated area in Doha for RCP 4.5 scenarios and current flooding due to HOT.

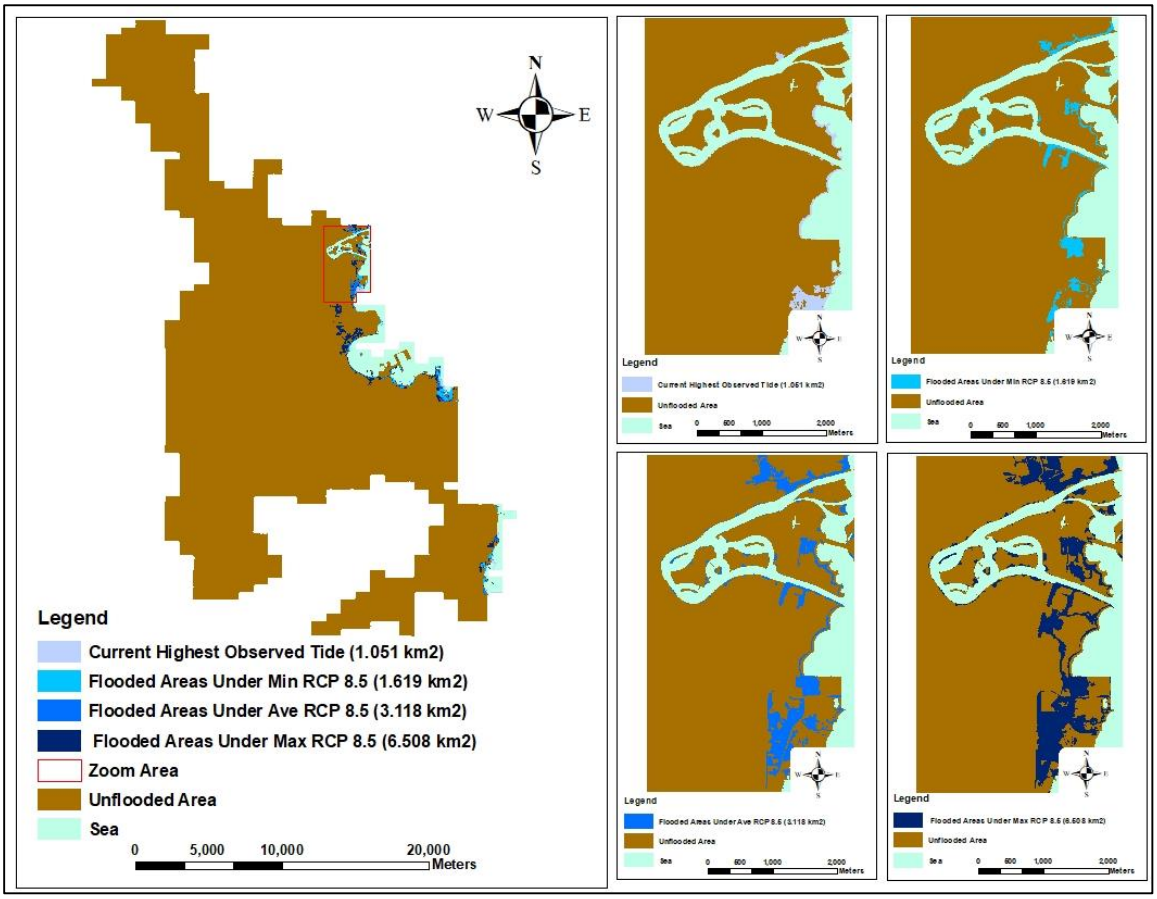

Figure 4-18: Mapping inundated area in Doha for RCP 8.5 scenarios and current flooding due to HOT.

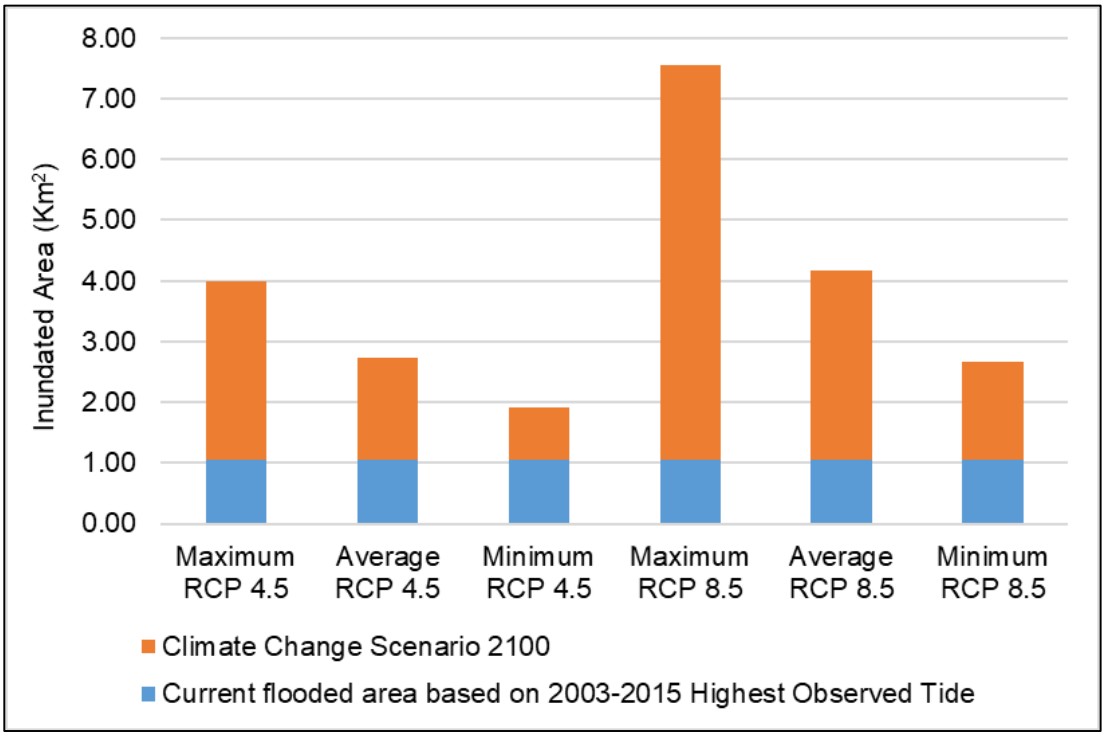

Figure 4-19: Proportion of current flooding under HOT to RCP scenarios in Doha.

4.6.4. Mesaieed

The level of the sea will rise by a similar height to other study areas, ranging from 0.39 m to 2.54 m (Table 4-12). The extent of the flooded area increased proportionally to the sea level. However, the rate increased slowly when the sea level remained under 2 m flooding, less than 4 km^2. After this point, the flooded area increased at a larger rate to more than 14 km^2 at a SLR of around 2.5 m (Table 4-13 and Figure 4-20).

Table 4-12: Total SLR as the result of RCP scenarios and tidal events in Mesaieed.

Tide	Scenario 2100 - RCP 4.5			Scenario 2100 - RCP 8.5		
	Maximum (0.71) m	Average (0.53) m	Minimum (0.36) m	Maximum (0.98) m	Average (0.74) m	Minimum (0.52) m
Highest Observed Tide (1.56) m	2.27	2.09	1.92	2.54	2.3	2.08
Mean Higher High Water (0.81) m	1.52	1.34	1.17	1.79	1.55	1.33
Mean Sea Level (0.03) m	0.74	0.56	0.39	1.01	0.77	0.55

Table 4-13: Inundated areas in Mesaieed.

Tide	Current flooded area based on 2003-2015 tidal events	Scenario 2100 - RCP 4.5			Scenario 2100 - RCP 8.5		
		Maximum (0.71) m	Average (0.53) m	Minimum (0.36) m	Maximum (0.98) m	Average (0.74) m	Minimum (0.52) m
Highest Observed Tide (1.56) m	2.857	7.435	6.492	0.570	14.261	7.579	6.475
Mean Higher High Water (0.81) m	0.379	2.457	2.221	1.176	2.723	2.474	2.192
Mean Sea Level (0.03) m	0.000	0.308	0.201	0.141	0.685	0.318	0.195

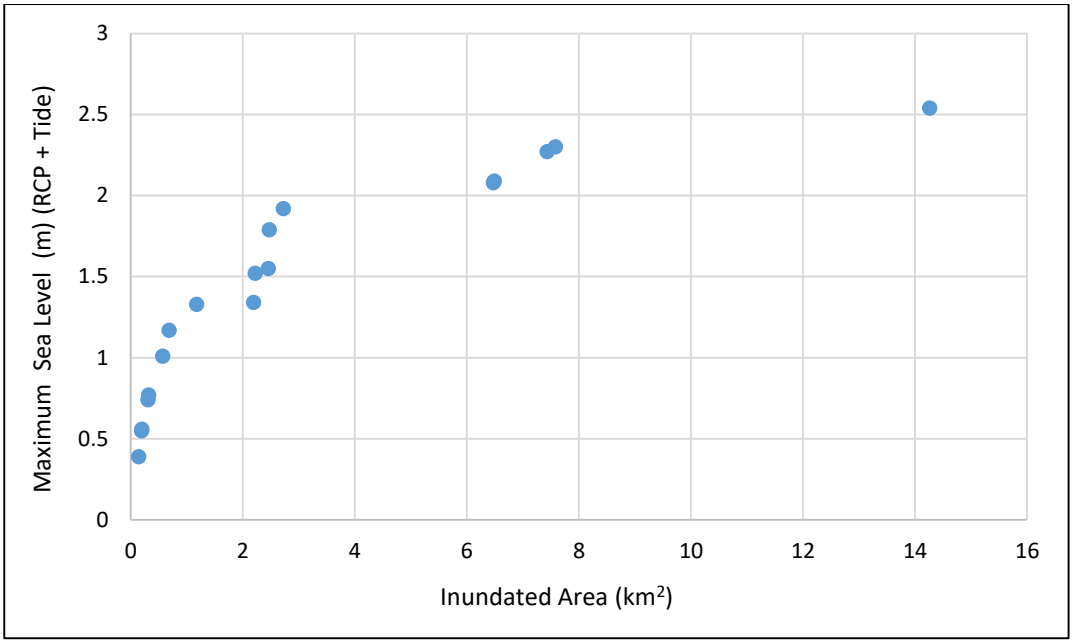

Figure 4-20: Relationship between the maximum sea level as the result of RCP (4.5 and 8.5) scenarios and tidal condition and the flooded area in Mesaieed.

The current flooding under the HOT was above 2.86 km^2. This will increase with the effect of climate change when the sea level reaches above 2 m (Figure 4-21). Most parts of the north-east will be flooded (Figure 4-22 and Figure 4-23).

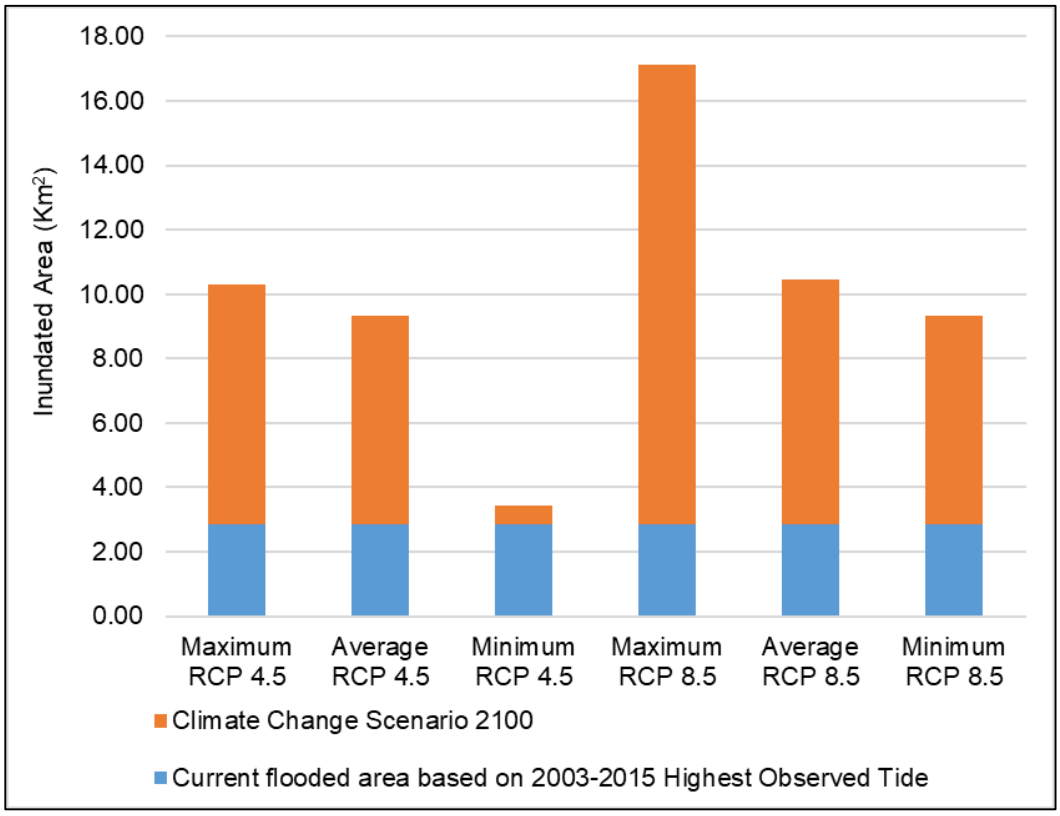

Figure 4-21: Proportion of current flooding under HOT to RCP scenarios in Mesaieed.

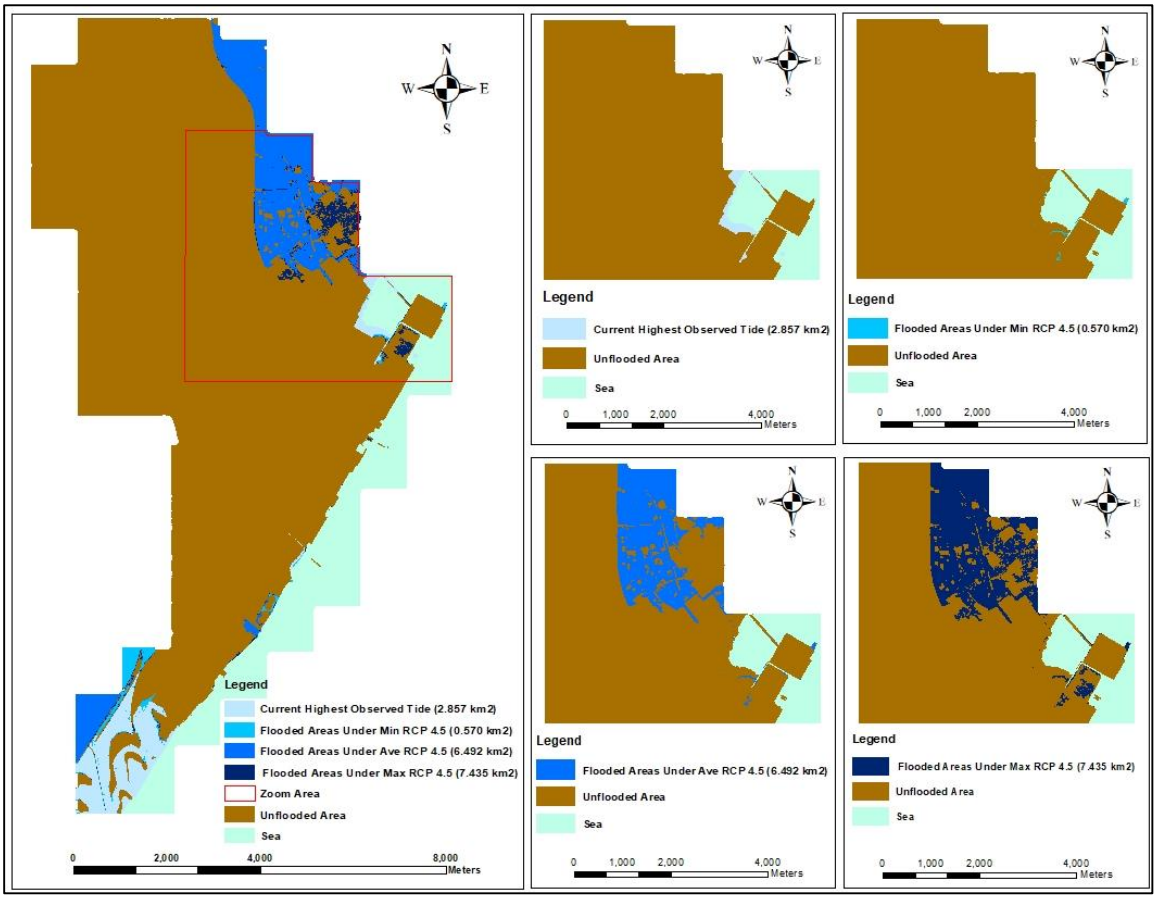

Figure 4-22: Mapping inundated area in Mesaieed for RCP 4.5 scenarios and current flooding due to HOT.

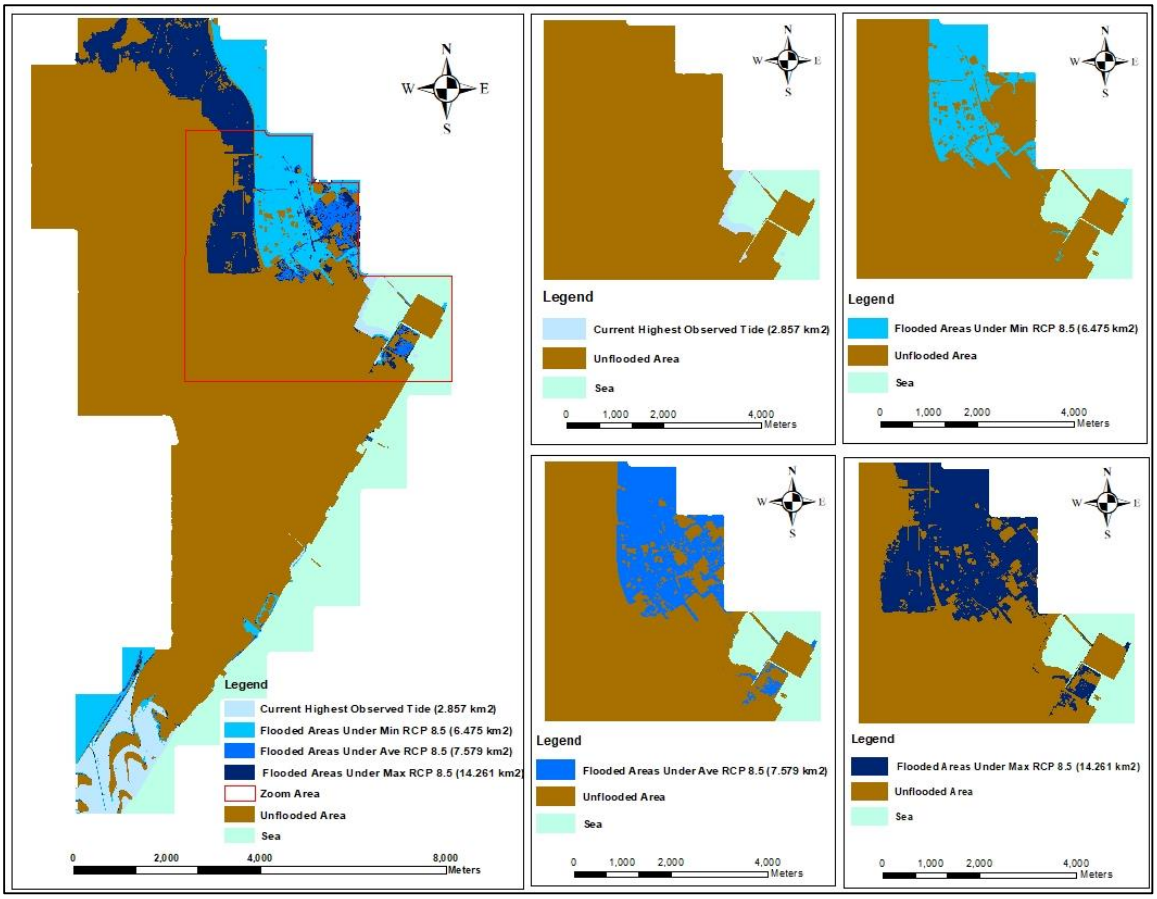

Figure 4-23: Mapping inundated area in Mesaieed for RCP 8.5 scenarios and current flooding due to HOT.

4.7. Discussion

Previous research into SLR is often limited by the coarse resolution of elevation data. This makes it difficult to model future SLR associated with climate change (Nicholls, 2004). In this study, a high-resolution DEM was used to map flood inundation from SLR simulations. A high-accuracy DEM is an important input in modelling future SLR (Gesch, 2018). The elevation data plays an important role in determining the extent of the area that will be under water as the result of SLR. The chapter also showed that the simple method for doing this is a bathtub method, which simply reclassifies all cells below an elevation threshold as at risk of flooding. However, this method does not consider hydrologic connectivity (i.e. connectivity to the sea) and the flow direction or slope (McGrath et al., 2018). As a result, this method overestimates inundated areas (Webster et al., 2004).

The two approaches that consider hydrologic connectivity (four-side and eight-side) helped to overcome the inaccuracy in the bathtub simulation by only considering the areas that connected to

the sea. In this study the difference between the flooded areas based on the four-side and the eight-side rule was not vastly different in all the study areas, apart from Mesaieed. In this case the flooded area under the eight-side approach was larger than the four-side. This similarity between the two approaches is contrary to the results from Poulter and Halpin (2008), where the eight-side approach produced generally higher inundated areas in comparison to the four-side approach. The reason might be because the topography of Qatar is very flat. There are, therefore, very subtle changes in elevation. Consequently, changes in hydrologic connectivity between the four and eight-side approach are low. The eight-side approach considers wider possibilities for the hydrologic connectivity and, therefore, was used in this study to improve the bathtub simulation.

Another factor in mapping inundation is how high the sea level will be in the future. The uncertainty in this prediction will impact the extent of inundation. The two scenarios, RCP 4.5 and RCP 8.5, provided a different magnitude of SLRs. However, these projections need to be adapted to local conditions by including other factors that can influence the level of sea, such as HOT and MHHW. There are wide variations in these from one region to another (Stammer et al., 2013). Another source of uncertainty is within the RCP variation (minimum, average and maximum). However, these variations were found to be less than the variability between RCPs. For example, in Al Thakhira the difference between RCP 4.5 and 8.5 was greater than the difference observed within RCP, that is between the minimum, average and maximum scenarios. The internal uncertainties do not change through time, but the uncertainties between the RCPs will increase (at different rates) with time (Troup & Fannon, 2016). In this chapter, we also demonstrate how uncertainty associated with RCP predictions can be quantified and displayed to enable the reader to make an informed assessment on the potential impact of flooding or to compare different RCP scenarios (Stammer et al., 2013).

There were several limitations of this study. In general, it was limited by time and resources for undertaking a full uncertainty comparison between different RCPs. Only two RCPs were selected, therefore, and minimum, average and maximum values explored within.

There were other limitations:

1- The study could have looked at other timescales as opposed to simply looking at 2100. For example, Antunes et al. (2019) looked at SLRs for the Atlantic Coast of Portugal's mainland for 2025, 2050, and 2100 with different sea level scenarios.

2- The maximum SLR was calculated based on the RCP scenario and the maximum tide from a limited range of dates. However, the impact of climate change on SLR flooding is likely to be greater if potential storm surges were included in the simulation (Antunes et al., 2019).

3- Coastal erosion, especially under rising sea levels, will change the current DEM and this was not considered in this study. This could affect the area under the risk of flooding and its hydrologic connectivity. Coastal erosion affects the future DEM, and a study by Coveney and Fotheringham (2011) estimated that saltmarsh could lose between seven per cent of its current area (under low SLR scenario) to 30 per cent (under high SLR). This changes the DEM and possibly the inundation patterns.

4- The approach taken in this study did not consider the drainage systems (e.g. draining pipes under roads) in place within the study area and other infrastructures, such as current and planned barriers, that effect the hydrologic connectivity. These will affect the inundation mapping as the result of SLR. However, including future drainage infrastructures such as canals, ditches and culverts remains a challenge in future flood mapping (Gesch, 2013).

5- Uncertainties associated with all parameters need to be quantified so that the simulation can recognise the source and magnitude of those uncertainties. In the following chapter, the uncertainties will be studied in detail to provide a better estimation of flood mapping.

Chapter 5: Assessing Uncertainty in Sea Level Rise

5.1. Introduction

The previous chapter highlighted the potential importance of uncertainty in affecting the SLR scenarios. The purpose of this chapter is to assess the potential impact of this uncertainty with the SLR scenarios produced in the previous chapter. Before doing this, it is important to define uncertainty and other terms that may be used in the uncertainty assessment. Booker and Ross (2011) defines these terms as follows:

- ***Certainty***: "a state, such that evidence to the contrary is below a threshold of disputation".
- ***Precision***: "refers to abilities in making good predictions, being exact, being correct, maintaining control, operating within specifications, and representing the physical world". The precision cannot be mixed with accuracy, as accuracy measures the difference between the actual (true) value and predicted value.
- ***Uncertainty***: "what is not known precisely" and manifests itself in numerous ways, most of which are undetected or considered too difficult to assess.
- ***Uncertainty Quantification:*** "refers to an analysis and assessment process or evaluation based upon models, data, expertise, etc".
- ***Confidence***: "is the state of feeling sure". Confidence has "an inverse relationship to uncertainty, which is assessed and/or quantified".

Assessing uncertainty provides decision makers with a more complete picture about the future SLR in Qatar. These uncertainties are inherent in the SLR study for a number of reasons. The two that we will focus on in this study are: the accuracy of the DEM and the accuracy of the SLR (RCP) scenarios.

The accuracy of the DEM has a significant influence on the quality of the inundation mapping and the quality of the results produced. Therefore, it is important to understand the magnitude and spatial distribution of uncertainty, especially when dealing with decisions related to SLR and climate change (Coveney & Fotheringham, 2011). There are a number of sources of error and

uncertainties within a DEM which are documented in the literature (Burrough, 1986; Heuvelink, 1998; Pike, 2002; Wise, 1998). According to existing literature, errors and uncertainties within a DEM originate from three major sources:

- Errors in the elevation data because of its age and sampling density or spatial distribution of the elevation points. For example, in some areas, the elevation might change due to natural factors, such as erosion, or man-made factors, such as urbanisation. These changes depend on the geomorphology (e.g. in desert, the impact of erosion is much greater than in the Rocky Mountains). Sampling density also reduces error. Östman (1987), for example, reported that an increase in the sampling density reduced the RMSE of a manually constructed DEM.
- Methods used to obtain the elevation maps, such as using field surveying, photogrammetry, surface sensing technologies (such as Light Detection and Ranging (LiDAR)), Interferometric Synthetic Aperture Radar (IFSAR) or sonar (for bathymetric data) and digitising from existing maps. An example of this is when the elevation data was validated (Table 3-1); there was an average error of 33 cm, 78.8 per cent of the points had errors less than half a metre and 51.5 per cent had errors less than 25 cm. Potential sources of these errors are discussed, but one of them is likely to be the difference between the two methods for obtaining elevation data.
- As a result of data analysis. In this study the interpolation procedures are a potential source of error. Ten different methods were used to generate DEMs using four interpolation techniques (see Table 3-10 in Chapter 3). Each method produced a different RMSE.

Apart from the uncertainty in the DEM, there is also uncertainty about the SLR resulting from climate change. There are three main sources of uncertainty in the SLR prediction, which are: model, scenario and internal variability (Lafaysse et al., 2014). The first source is model uncertainty. As the temperature of the ocean increases, melt-back of ice sheets and continental ice occurs, leading to a rise in sea level (Hu & Deser, 2013). Sea level rise is a complex event to predict because climate change affects many factors, such as thermal expansion of water, inputs from ice sheets, changes in land water storage and coastal erosion (Rahmstorf, 2007). It also affects all the

dynamical and thermo-dynamical processes over the full ocean column, making SLR a complex event to predict (Church et al., 2013). Hence, different climate models predict different SLRs. Scenario uncertainty is the second source and is related to the uncertainty of the future GHG emissions. These are specified in SLR projections known as RCP scenarios (as described in detail in previous chapters). These scenarios can result from a diverse range of socio-economic and technological development pathways (IPCC, 2007). Uncertainties tied to the scenarios have a wide range of impacts on the projections of the SLR. The final factor is internal variability. This usually relates to the accuracy of climate models for predicting the temperature and precipitations at national scales (e.g. within Qatar) and constitutes a significant source of uncertainty (Hawkins & Sutton, 2011). In terms of SLR, this may be less of an issue in Qatar as it is a relatively small country.

5.2. Review of the literature

There are several methods through which uncertainty can be assessed. However, often inundation mapping is presented without quantifying the uncertainty information and accuracy assessment, which are essential (Gesch et al., 2009). Therefore, the uncertainty assessment is a key element for the policy development and decision making process. Not including uncertainty in the analysis may lead to policy recommendations which do not capture all the risks and benefits. Consequently, the policy will be ambiguous (Pizer, 1999). The amount of climate change that may happen and its potential impacts are exceptionally large, including changes in precipitation, frequency and intensity and SLR, however the uncertainty about these impacts remains very large (Webster,2000).

There are many ways to quantify uncertainty in inundation mapping with various degrees of complexity. For example, Titus and Richman (2001) used a simple method based on a DEM to predict future shorelines in the United States. They accounted for uncertainty by stating that flooding would be between the 1.5 and 3.5 m contour. In Australia, the government mapped future inundations due to climate change, but they did not quantify the uncertainty level. Instead they provided a statement to explain that uncertainty existed in the DEM and that this might affect their estimations (OZCoasts, 2012).

The most common method reported in the literature is where the interpolated DEM is considered as only one possible representation of the true elevation surface. Multiple simulations of the DEM can be generated using MCS to quantify DEM uncertainty. In this study the MCS was selected because it is a robust technique in mapping SLR uncertainty by generating random errors to simulate uncertainty and generate the probabilities of various scenarios in the simulation (Schmid, 2014). Monte Carlo simulations can represent the DEM of the study area as a set of probability distributions of possible outcomes (Srivastava, 1996).

The MCS creates many DEMs by introducing simulated errors into the DEM in five four steps:

1- Generating a random error map using statistical representation selected for DEM error.
2- The random error map is added to the interpolated DEM.
3- Steps 1 and 2 will be repeated for a number of times to include the distribution of possible elevations.
4- The process of interest, in the case SLRs, will be run a number of times.
5- All the possible outputs are added together to produce a probability map which quantifies uncertainty.

Monte Carlo simulations have been used by many researchers to address DEM uncertainty, but not necessarily associated with SLR. Hunter and Goodchild (1997) studied the influence of simulated changes in elevation at different levels of spatial autocorrelation on slope and aspect calculations. They developed a new method to understand the slope and aspect maps with differing levels of spatial autocorrelation. They demonstrated that uncertainty in slope and aspect depends on the structure of spatial dependence of errors and are inherent in the use of DEMs. They concluded that the uncertainty model helped to understand the quality of the slope and aspect information derived by using GIS.

Liu et al. (2007) used an MCS to assess the effects of vertical error in LIDAR data and uncertainty in the tidal datum on the position of the shoreline. They developed a new method to determine the shoreline based on processing LIDAR images. They then assessed uncertainty in the shoreline positions using MCSs. The shoreline was derived, and the MCS indicated that the high-water mark was horizontally accurate within 4.5 m at a 95 per cent confidence level.

Several studies have also used MCS to focus on SLR. For example, Leon et al. (2014) investigated DEM uncertainty in coastal inundation mapping. They simulated DEM errors using MCS by adding one thousand error simulations to the interpolated DEM. The results of their analysis indicated, as an example, that when a one per cent probability of flooding was considered, the land area was around 11 per cent greater than an analysis which did not consider elevation uncertainty. They found that the MCS is an effective approach for uncertainty assessment and modelling complex and dynamic phenomena, such as inundation due to SLR.

The second source of uncertainty is associated with the SLR. Ruckert et al. (2017) studied the impacts of SLR uncertainty on future flood risks. They used a simple bathtub method and projected a 100-year flood height (tide and SLR) for San Francisco Bay. They demonstrated that SLR uncertainty has a large impact on areas under the risk of inundation. Their case study demonstrated that uncertainty increases the 100 years return level by 0.5 m, and the areas at risk of flooding were doubled.

Schmid et al. (2014) examined different methods of mapping the SLR based on single-surface-type models. They also developed a new method, Z-score-type, to map uncertainty based on elevation. The Z-score technique uses the RMSE of the data and assumes it is normally distributed. The researchers then assigned each cell in a DEM a Z-score according to its height above sea level. The Z-score is calculated in the same way as a standard score (value – mean / standard deviation), but RMSE is used instead of standard deviation (sea level – elevation / RMSE). In order to integrate the uncertainty of the SLR into the equation, the RMSE was replaced by a maximum cumulative uncertainty of inundation, which is the root-sum-of-squares of standard deviation of elevation and sea level. They also concluded that an MCS provides vital information about uncertainty in mapping future SLR inundation because of its ability to include various scenarios in the simulations.

5.3. Aims and study area

In the literature, most of the inundation mapping studies were focused on the uncertainties associated with DEM or SLRs. Schmid et al. (2014) developed a Z-score methodology to investigate the combination effect of DEM and SLR uncertainty. However, their proposed

methodology was limited in addressing other factors, such as hydrologic connectivity, probabilities of DEM and SLR representations. Therefore, in this chapter uncertainty from both DEM and SLR will be quantified based on probability distribution.

The aim of this chapter is to:

- Quantify the impact that uncertainty within the DEM has on inundation
- Quantify the impact that uncertainty within the amount of SLR has on inundation
- Compare uncertainty and error from the DEM with uncertainty and error within SLR.

Monte Carlo simulations were implemented using IDRISI Selva version 17. This was used to quantify the uncertainty in both DEM and RCP. The IDRISI software was used instead of ArcGIS because it has a better functionality, especially the random generation procedures to support MCS. The Al Thakhira area (93.78 km^2) was selected as a case study because it has a reasonable area (not too large, like Doha, and not too small, like Al Khor 1 and 2), which is important for having a practical processing time. Furthermore, RCP 8.5 was selected because it represents the worst-case scenario of climate change. The MCS uses the DEM generated in a previous chapter from a spline interpolation method as this had the lowest RMSE.

For the DEM we have generated two estimates of uncertainty. The first is the uncertainty associated with the spatial interpolation and the second was generated from the ground truth data sampling undertaken in 2016. For this chapter we focus upon the uncertainty associated with the spatial interpolation only. This decision was taken because, for Al Thakhira, only four ground truth points were produced, making it difficult to produce an accurate estimate of uncertainty. In addition, there were differences in time between the original sampling and the ground truth measures, producing further uncertainty on the accuracy measures produced by the ground truth sampling.

5.4. Assessing uncertainty in digital elevation model

5.4.1. Monte Carlo simulation with random errors and no spatial correlation

The simulations were conducted in four steps:

5.4.1.1. Step 1. Simulating digital elevation model with errors

As a first step, 100 new real binary images (RAND) were created using a RANDOM model in IDRISI, based on normal distribution with a mean of zero and a standard deviation equal to the RMSE (0.10). This was the RMSE of the interpolated DEM from Chapter 3. These binary images represent known errors to be added to the interpolated DEM. The reason for having 100 simulations is to be able to determine the probability of flooding. The 100 times simulation was chosen as a balance between the time of data processing and the quality of the outputs. A higher number of simulations may produce better outcomes but they have a longer processing time. On the contrary, lowering the number of simulations may reduce the processing time but will not capture the entire probability distribution, and it is computationally practical for most data sets (Pattengale et al., 2010).

The error maps were then added to the interpolated DEM, creating 100 DEMs with errors (RAND_DEM) by using the OVERLAY function in IDRISI (Figure 5-1).

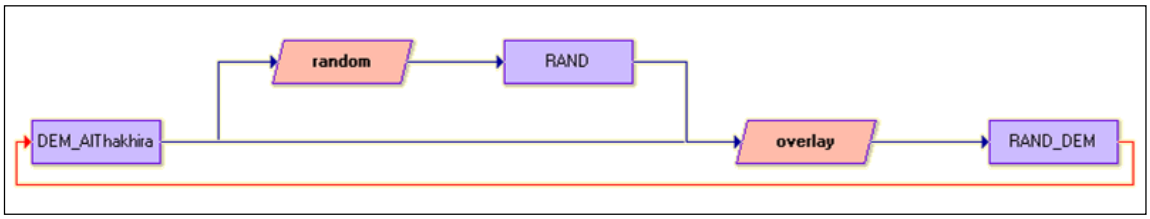

Figure 5-1: Step 1 from MCS: Creating 100 random errors and adding it to the interpolated DEMs using Random and OVERLAY functions.

5.4.1.2. Step 2. Bathtub method

In this step, the 100 DEMs were reclassified to identify the flooded areas based on the SLR from RCP and tidal events (2.06 m). The RECLASS function in IDRISI (Figure 5-2) was used to perform the classification of the bathtub for all of the 100 DEMs. The outcome of this step is 100 images with two classes. Areas above future sea level (unflooded cells) have a zero value, while flooded areas have a value of one.

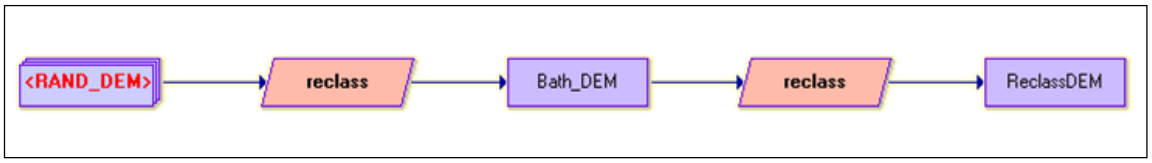

Figure 5-2: Step 2 from MCS: classifying area based on the bathtub method using RECLASS function.

5.4.1.3. Step 3. Hydrologic connectivity

In a previous chapter (Chapter 4), the 8-side rule (using ArcGIS) was used to determine the connectivity of flooded cells to the sea in order to eliminate the flooded areas without hydrologic connectivity. However, in this chapter a different method was used to assess the hydrologic connectivity because of the different functionality of the IDRISI software. This is because in ArcGIS an overlay of vector (coastline) and raster layer (flooded area) were used to determine the connectivity of flooded areas to the sea. In IDRISI there is no option to overlay vector and raster data. However, the two methods achieve the same result.

- To determine the connectivity of each flooded cell the COST function in IDRISI was used (Figure 5-3) to calculate the connectivity of the cells to the sea. The COST function measures the distance/proximity surface (also referred to as a cost surface), where distance is measured as the least cost (in terms of effort, expense, etc.) in moving over a friction surface. The COST function measures the distance by "grid-cell equivalents". Distances are measured in eight directions from any cell, which is equivalent to the 8-side rule used in the previous chapter.
- The output from the previous step (bathtub method) and a raster layer representing the sea in the study area were used as inputs for the COST function.
- Before running the COST function, the inputs from Step 2 were reclassified to give unflooded areas a very high value (cell value = 10,000) while flooded cells remain the same (cell value = 1). This high value ensured that any flooded areas identified by the bathtub method, which is only connected to the sea by unflooded area, obtained a remarkably high value (i.e. > = 10,000) on the cost surface. The cost surface was run to calculate the cost distance of each cell from the coastline.

- Then the outputs from the COST model were reclassified to determine areas connected to the sea (with cell value = 1) and not connected to the sea (with cell value = 0) (Figure 5-4). This was achieved by reclassifying every cell less than 10,000 as flooded and all cells greater than or equal to 10,000 as unflooded.

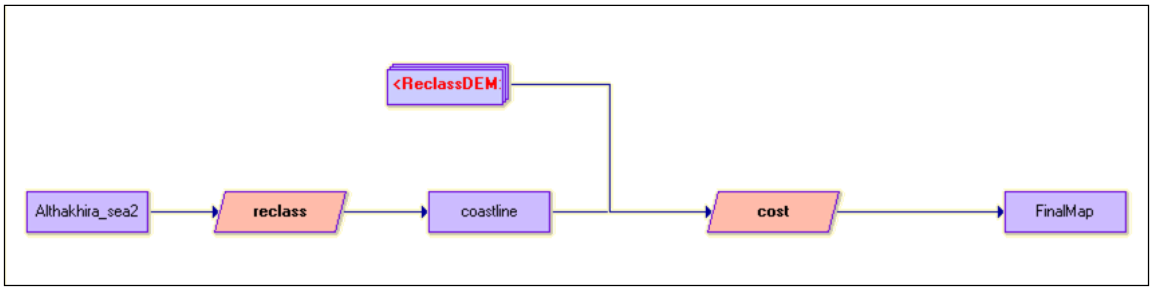

Figure 5-3: Step 3 from MCS: Determine the areas connected to the sea using COST function.

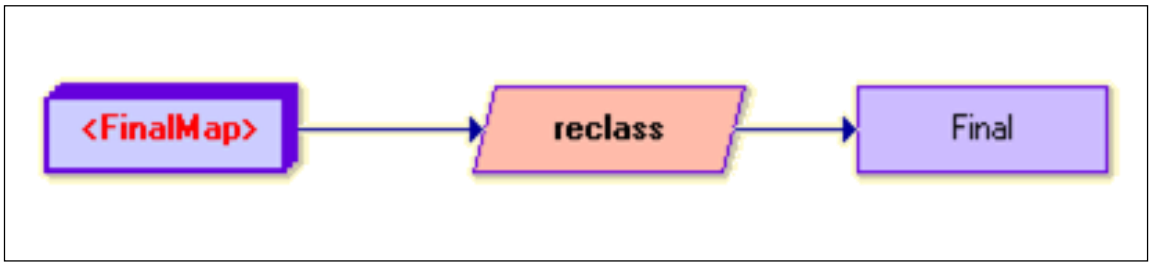

Figure 5-4: Step 3 from MCS: Reclassify the outputs from COST model based on 10,000 value to determine connectivity to the sea.

5.4.1.4. Step 4. Probability map

Adding all the final 100 images from Step 3 helped to create a probability map, indicating the probability of flooding in each cell (Figure 5-5). Then three scenarios were created to compare the error and uncertainty in the interpolated DEM and its impact on flooding. Cells with a flooding probability greater than ten per cent, 50 per cent and 100 per cent were identified.

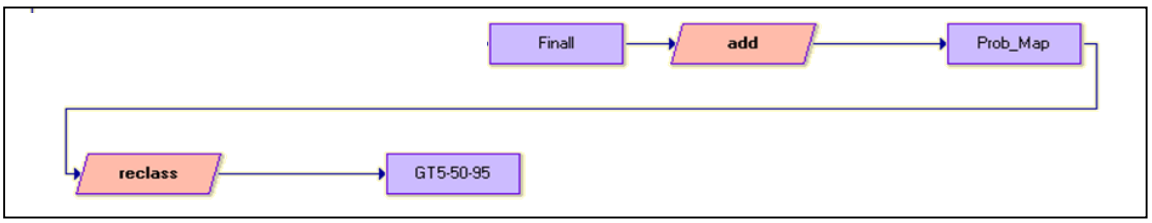

Figure 5-5: Step 4 from MCS: creating a probability map.

The MCS for Al Thakhira was conducted and the probability map was produced (Figure 5-6). In panel (a) the probability is aggregated into ten classes and in panel (b) the probability is aggregated to four classes. In panel (b) the first class includes all the cells with the probability of 0-5 per cent, which represent cells with a "very unlikely" occurrence of flooding. Then, 6-50 per cent represent "unlikely" to flood, 51-94 per cent represent "likely" to flood and 95-100 per cent "very likely" to flood. This classification was based on the statistical confidence intervals.

The probability map (Figure 5-6b) shows that a large part of the study area would be very unlikely to become flooded (0-5 per cent). These areas are mainly higher grounds, which will remain above future sea level or are disconnected from the coast and are located in the central part of the study area. Most of the area with unlikely (6-50 per cent) flooding is located far away from the coastline and in the central part of the study area. The areas likely (51-94 per cent) or very likely (95-100 per cent) to flood are located near the coast and these areas are particularly large in the north and south-east of the study area.

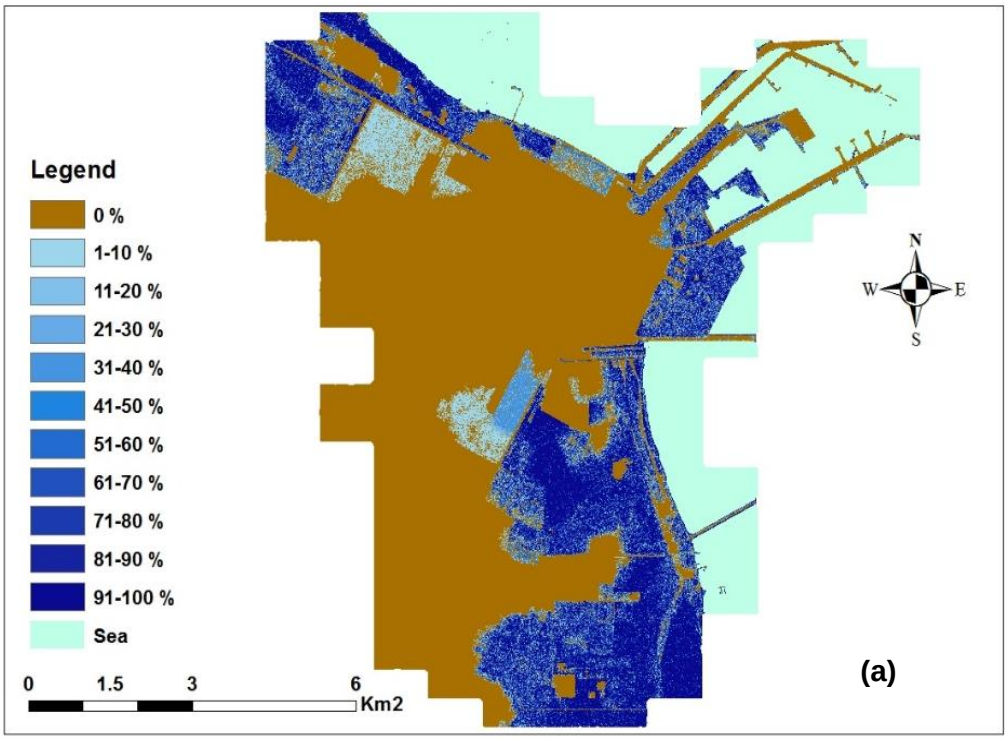

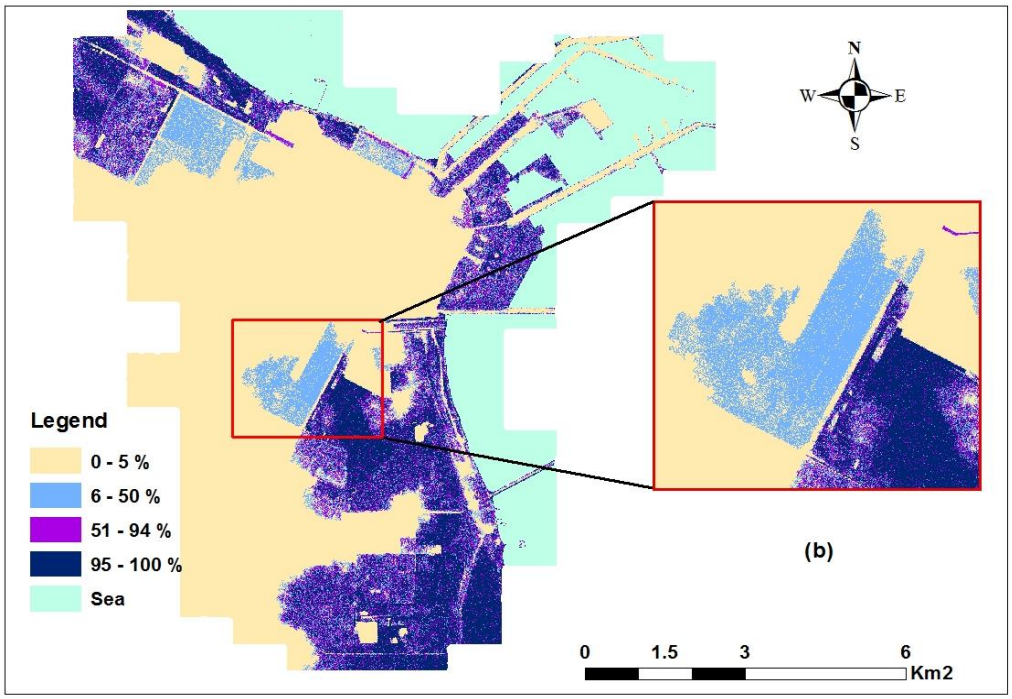

Figure 5-6: Probability map of DEM uncertainty in Al Thakhira area for average RCP 8.5 scenario and HOT based on MCS. (a) The probability is aggregated into ten classes (b) The probability is aggregated into four classes.

5.4.2. Monte Carlo simulation with spatially correlated random error

5.4.2.1. Assessing uncertainty in sea level rise

As described in the previous chapter, RCP 8.5 modelling is based on high GHG concentration levels, Riahi et al. (2011). The projected RCP 8.5 SLR with a five to 95 per cent range of projections from process-based models will be 0.52 to 0.98 m with an average (mean) of 0.74 m. This mean was chosen as it was a better representation of likely future conditions. The SLRs were added to the HOT in the Al Thakhira area (1.32 m). The total SLR used for minimum scenario was 1.84 m, 2.06 m for average and 2.3 m for maximum to assess uncertainty (Figure 4-4).

5.4.2.2. Representative concentration pathways - Monte Carlo simulation

The no-flood areas were determined as those with a height above the future SLR. Those areas are in the central part of the study area. The areas with a likelihood of flooding are located in the eastern and south-eastern part under minimum and average scenarios, while the maximum extends to a deeper part of the central study area. The minimum scenario represents the likelihood of SLR

occurring alongside the coastline, while the maximum (less likely) scenario covers wide areas, including minimum and average scenarios.

A different method to assess uncertainty in MCS was used to simulate a likely SLR. One challenge in doing this was to determine the probability distribution of SLR. One solution was to assume that the difference between maximum and minimum RCP 8.5 SLR scenarios represents the 95 per cent confidence interval around the average RCP. Random numbers were generated using this assumption and added to the sea level. This gave a mean rise of 2.06 m with a standard deviation of 0.10. The simulations were conducted following the same steps described in the previous section (section 5.4). However, instead of generating 100 DEMs to simulate flooding, 100 SLRs were generated. The height was generated based on 95 per cent confidence intervals around the average of RCP 8.5. The heights were created using the Normal Inverse Formula (NORMINV) in Microsoft Excel. This formula uses the Random function (RAND) to select a random set of numbers uniformly distributed between 0 and 1 and forces it to create a normally distributed set of numbers based on a mean and standard deviation (NORMINV (RAND, Mean, Standard Deviation)).

Then the results from the 100 sea levels were stacked together to create a probability map for RCP (Figure 5-7a), where a zero value represents unflooded areas. The probability of flooding changes depending on how many times each pixel was flooded under 100 SLRs. Most of the areas around the coastal line have a high probability of flooding, while areas far away from the coast are less likely to flood. The non-flood areas also cover most of the central part of the study area. In order to make the comparison between the two probability maps, DEM and SLR, the probability map was reclassified into four categories based on the likelihood of flooding (Figure 5-7b).

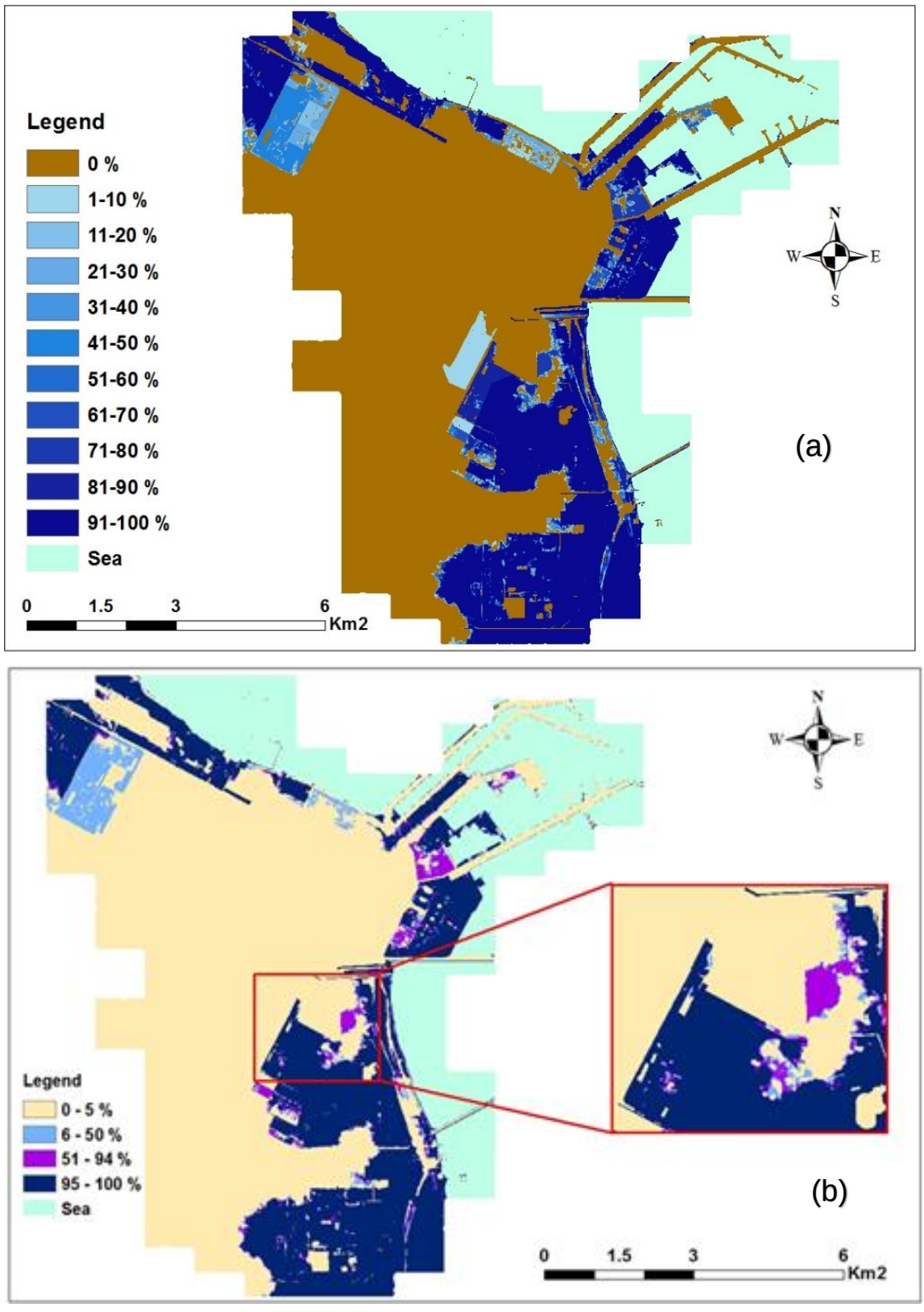

Figure 5-7: (a) Probability map of RCP uncertainty in Al Thakhira area based on MCS (b) Reclassified probability map into four classes.

5.4.2.3. Comparing uncertainty of digital elevation model to representative concentration pathways Monte Carlo simulations

The comparison of the results between DEM and RCP uncertainty using MCSs is presented in Figure 5-8. The RCP simulation predicted two areas (circled in black) with a probability of 6-50 per cent flooding, while this was not predicted using DEM as flooded areas.

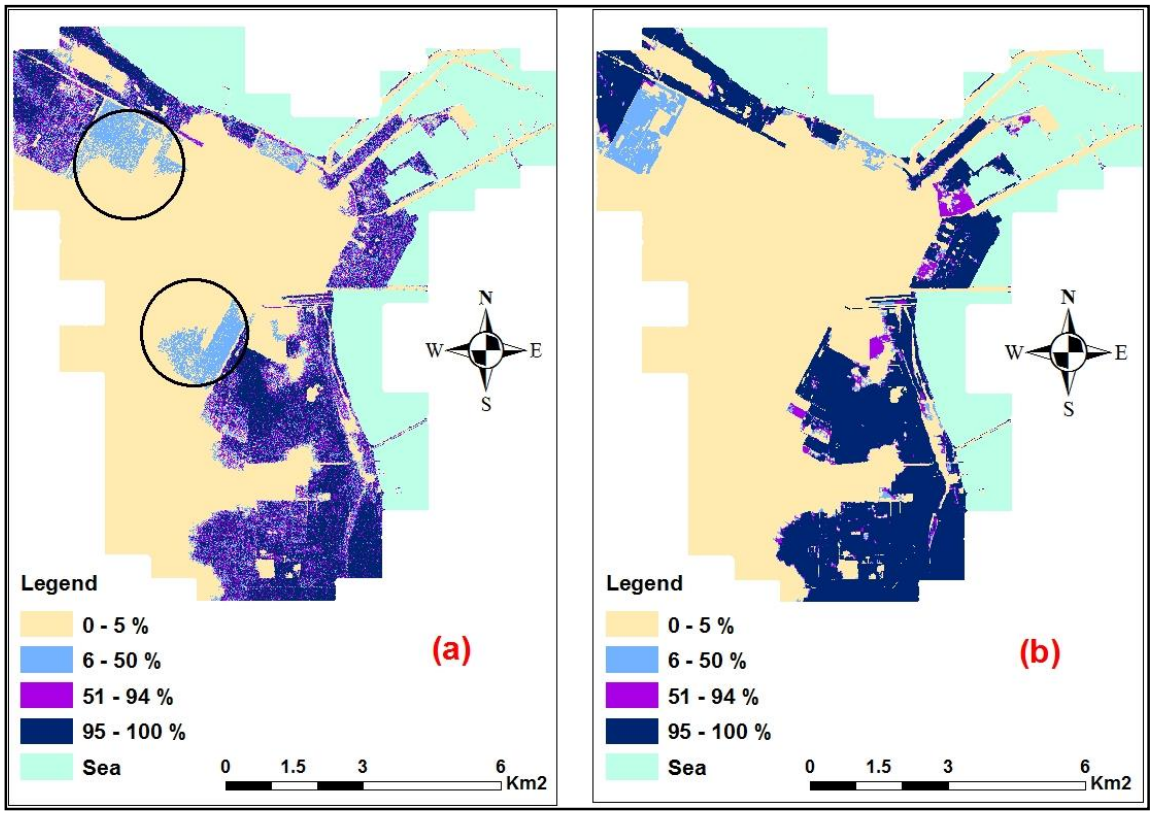

Figure 5-8: Comparing reclassified probability map of (a) DEM uncertainty and (b) RCP uncertainty in Al Thakhira area based on MCS.

The probability maps for both DEM and RCP were divided into four groups: 0-5 per cent to represent areas with very unlikely flooding, 6-50 per cent for unlikely flooding, 51-94 per cent for likely flooding and 95-100 per cent for very likely flooding. The DEM simulation predicted fewer areas as “very unlikely” (0-5 per cent) and “very likely” to flood (95-100 per cent) than the RCP simulation. Yet the RCP simulation predicted fewer areas with flood probabilities of 6-50 per cent and 51-94 per cent than the DEM simulation (Table 5-1).

Table 5-1: Comparison of flooded areas with four probabilities between simulated DEM and simulated RCP.

Probability of flooding (%) based on simulation of RCP	Area (km^2)	Probability of flooding (%) based on simulation of DEM	Area (km^2)
0-5%	48.30	0-5%	47.78
6-50%	2.98	6-50%	4.85
51-94%	1.59	51-94%	4.49
95-100%	19.77	95-100%	15.53
Total	72.64	Total	72.64

5.4.2.4. Combining probability surfaces

The second method consists of combining the probability maps of elevation (Figure 5-8a) with the probability maps of SLR (Figure 5-8b). Both of these were based on MCSs and the probability maps were combined using Equation 5-1.

$$\text{Overall flooding probability} = [\text{Elevflood}_{\text{prob.}} \times (1 - \text{Slrflood}_{\text{prob.}}) + (\text{Slrflood}_{\text{prob}}) \times (1 - \text{Elevflood}_{\text{prob}}) + (\text{Elevflood}_{\text{prob.}} \times \text{Slrflood}_{\text{prob.}}) \quad \text{(Equation 5-1)}$$

The result (Figure 5-9) shows the area with a probability of flooding based on SLR and elevation. There are very few areas with a probability of 51 – 94 per cent. All the other probability categories were shown with clearer zones. The specking effect in this map is lower than on the combining error map because the two surface probability maps were combined (elevation and SLR). The SLR probability map had a perfect spatial correlation because all the cells were provided with the same rate of SLR. The elevation probability map was generated with no spatial correlation. Hence, combining these two maps reduces speckling.

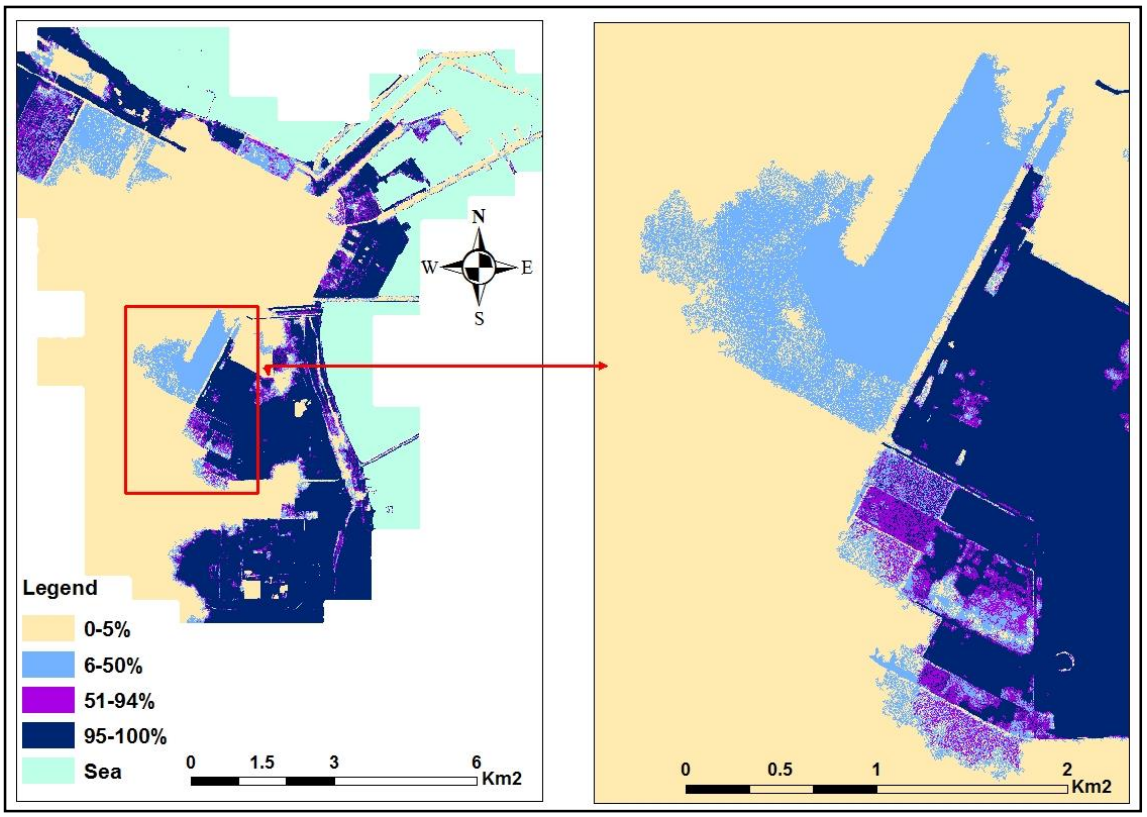

Figure 5-9: Probabiity of flooding from a combination of elevation and SLR uncertainties based on the results of MCSs.

5.4.2.5. Comparison of two methods

The two methods were compared to show the similarities and differences, which was done in several ways. The first was a visual comparison of the two maps (Figure 5-10). This shows a much higher probability (95-100 per cent) of the flooding area in the combined probability surface compared to the combined error map. A greater speckling on the combining error map is also apparent. Finally, the areas at risk of flooding are remarkably similar between the two methods.

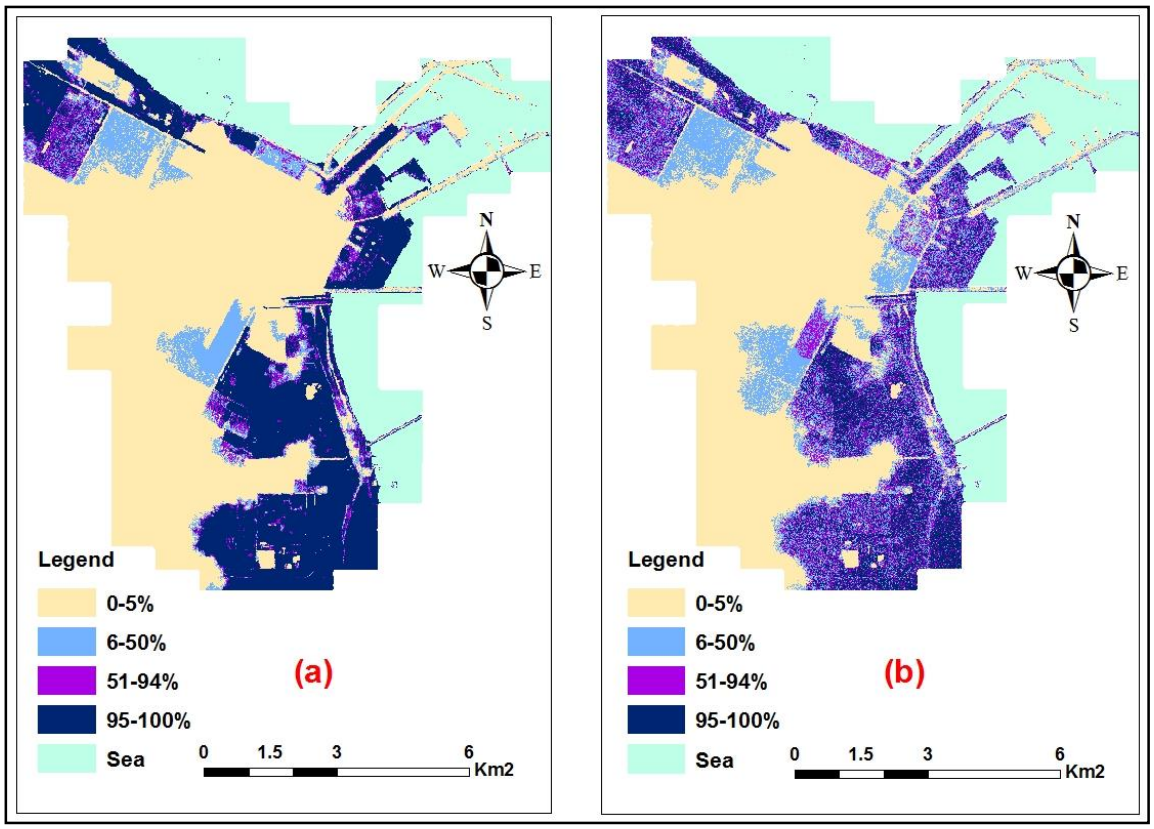

Figure 5-10: Visual comparison between combined probability surface map (a) with combined error map (b) for Al Thakhira area.

For the second method, the areas falling in different bands of flooding probability were combined (Table 5-2). When the probability surfaces were combined, a smaller area was found to be at risk of flooding (i.e. a greater area in the 0 – 5 per cent band). The combined error method produced greater areas with a flooding probability between 6 and 94 per cent.

Table 5-2: Comparison of flooded areas between combining probability surfaces and combining errors in the Al Thakhira area.

Overall probability of flooding (%) (combining probability surfaces)	Area (km^2)	Overall probability of flooding (%) (combining errors)	Area (km^2)
0-5	41.20	0-5	38.01
6-50	7.10	6-50	15.01
51-94	3.47	51-94	9.21
95-100	20.87	95-100	10.41
Total	72.64	Total	72.64

The final method was to perform a cross tabulation of the two probability maps (Table 5-3). Overall, most cells were assigned the same flooding classification. Most differences occur in the yellow cells where the probabilities are only one class different. Another observation from the tabulation of the two probability maps is that the areas with significant probability of non-flooding (0-5 per cent) and flooding (95-100 per cent) when comparing the two methods was small (0.00 and 0.06 km^2). This is an important finding as the two methods are not producing vastly different results.

Table 5-3: Tabulation of the combined probability surface and combined error methods for the Al Thakhira area.

		Overall probability of flooding (%) (combining errors)			
		(0-5%)	**(6-50%)**	**(51-94%)**	**(95-100%)**
Overall probability of flooding (%) (combining probability surfaces)	**(0-5%)**	36.35	4.43	0.42	0.00
	(6-50%)	1.35	4.33	1.30	0.12
	(51-94%)	0.25	1.48	1.27	0.47
	(95-100%)	0.06	4.77	6.22	9.82
Total area (km^2)		38.01	15.01	9.21	10.41

5.5. Comparing spatially independent to dependent error

One reason why the produced map has a speckled effect might be because the errors were introduced into the interpolated DEM (in the MCS) randomly. This means that the error was spatially independent. To understand the importance of spatial autocorrelation in errors and its effect on the probability of flooding, the error introduced in the DEM at three levels of spatial autocorrelation was examined (Moran's I of 0, 0.33 and 0.66).

The objective of this section is to:

- Include spatial correlated errors in the DEM.
- Compare the probability of flooding between models with different levels of spatially correlated error and to understand the impact of the error's spatial dependency on the results.

5.5.1. Methods

Three steps were taken to produce a spatial autocorrelation of errors and compare it to random errors in the DEM. A spatially correlated error was generated using the gstat spatial model in R.

The first step was to obtain the semi-variogram of the interpolated DEM. The interpolated DEM was created by using elevation data points and a spline interpolation method in ArcGIS, as described in Chapter 3. This DEM has a Moran's I of 0.66 (Sill = 2.026 and range = 3399.19 m) (Table 3-5). The high level of spatial autocorrelation in the Al Thakhira DEM, with RSME of 0.10 m (Chapter 4) may be due to the nature of the topographic condition in Qatar. It is a very flat area, hence high spatial autocorrelation. In the next step, an error was generated using these parameters, but the sill was fixed at 2.026 and the range was varied to produce errors with different levels of spatial autocorrelation (Moran's I 0.66, 0.33 and 0). This was done for the area of Al Thakhira.

Finally, the third step compared the outcome of the flood probability mapping using the three levels of spatially correlated error.

5.5.2. Results

Changing the range value affects the level of spatial autocorrelation. The larger the value, the higher the level of spatial autocorrelation in the error. The smaller the value, the lower is the spatial autocorrelation. The impacts of altering the range for Al Thakhira are presented in Table 5-4. A sill of 2.026 m and range of 658.2 m gave the spatial autocorrelation of 0.33, half of the interpolated DEM. When the sill was kept at 2.026 m and the range increased to 1516.19 m, the Moran's I increased from 0.33 to 0.66. This means that the spatial autocorrelation in the error increased. Finally, the range was lowered to 1 m to get a Moran's I of zero (no autocorrelation).

Table 5-4: Simulating spatially autocorrelated errors to achieve a Moran's I of 0.66 and 0.33.

Sill (constant)	Range (altered)	Autocorrelation (Moran's I)
2.026	2000	0.87
2.026	1660	0.72
2.026	1560	0.70
2.026	1525	0.68
2.026	1515	0.60
2.026	1516.19	0.63
2.026	1516.20	0.66
2.026	1516.20	0.66
2.026	1500	0.50
2.026	758.10	0.43
2.026	658.20	0.33

For each value of Moran's I (0, 0.33 and 0.66), 100 simulations of error were produced in the R programme. Then each error was combined with the DEM to create a flood probability map for three levels of spatially autocorrelated errors (Moran's I of 0, 0.33 and 0.66) (Figure 5-11).

In the case of Moran's I of 0.33 and 0.66, the results show a large reduction in areas with a 95-100 per cent probability of flooding. Increases were seen in areas with a probability of flooding ranging from 51 to 94 per cent and 6 to 50 per cent. However, the areas with 0 to 5 per cent probability decreased more under Moran's I of 0.33 than Moran's I of 0.66. This data is shown in Table 5-5. The areas with 0 to 5 per cent flood probability varied between three levels of Moran's I: 47.78 km^2, 28.16 km^2 and 33.43 km^2. These were predicted by Moran's I at zero, 0.66 and 0.33, respectively. The variation in the flooding predictions was slightly greater for 6 – 50 per cent and 51 – 94 per cent. For flooding with a probability of 95-100 per cent, the area under a Moran's I of zero was much greater than Moran's I of 0.33 and 0.66.

Table 5-5: Comparison of flooded areas between flooding probability with different levels of spatial autocorrelation (Sill 2.026) (Range 658.20 and 1516.20).

Probability of flooding (%)	Spatial Correlation 0 Area (km^2)	Spatial Correlation 0.33 Area (km^2)	Spatial Correlation 0.66 Area (km^2)
0-5	47.78	28.16	33.43
6-50	4.85	25.77	19.09
51-94	4.49	18.23	18.73
95-100	15.53	0.49	1.39
Total	72.64	72.64	72.64

The spatial variation of flood probabilities from the three Moran's I scenarios indicates that the effect of the random errors are exhibited in the form of a sprinkle effect (Figure 5-14).

(a)

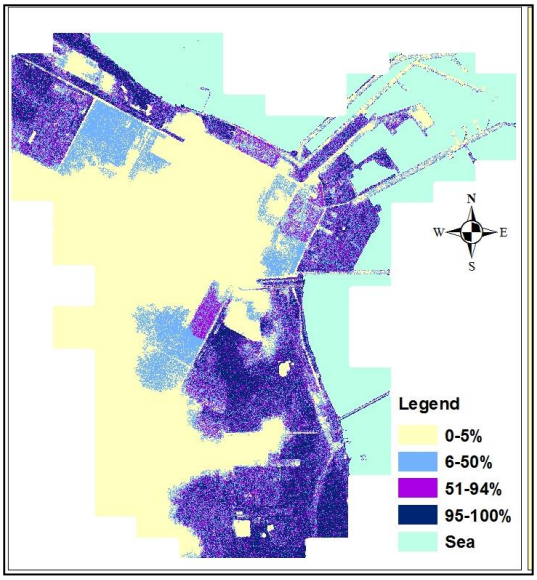

(b)

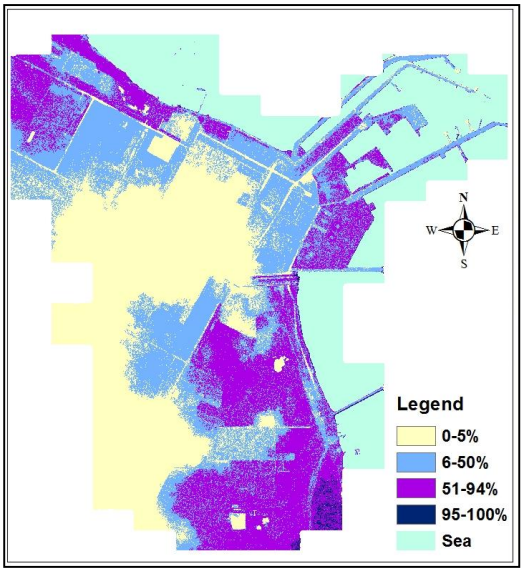

(c)

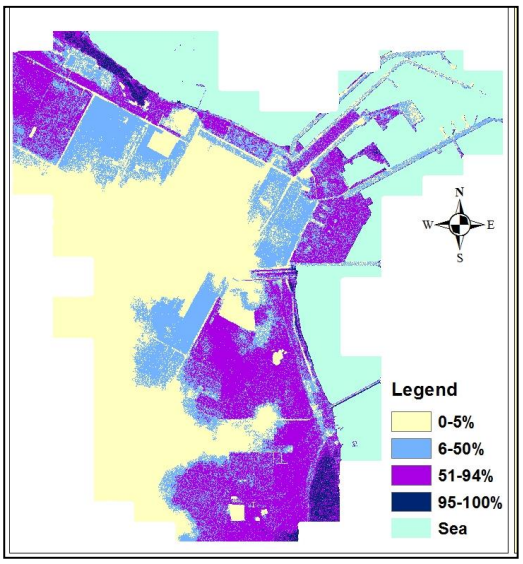

Figure 5-11: (a) Probability of flooding (%) based on spatial correlation of 0 (b) Probability of flooding (%) based on spatial correlation of 0.33 (c) Probability of flooding (%) based on spatial correlation of 0.66.

In order to understand the difference between the flood probability maps (Moran I 0.33 and 0.66), the two results were subtracted from the results with zero spatial autocorrelation. Figure 5-12 shows the difference between the probability of flooding in the case of DEM and errors with zero spatial autocorrelation and in the case of DEM and errors with 0.33 spatial autocorrelation. The areas with zero mean there was no difference between the probability values. Positive areas mean that the probability of flooding under a spatial autocorrelation of zero was greater than when spatial autocorrelation was 0.33. Negative values mean that the probability of flooding under a spatial autocorrelation of zero was lower than when spatial autocorrelation was 0.33.

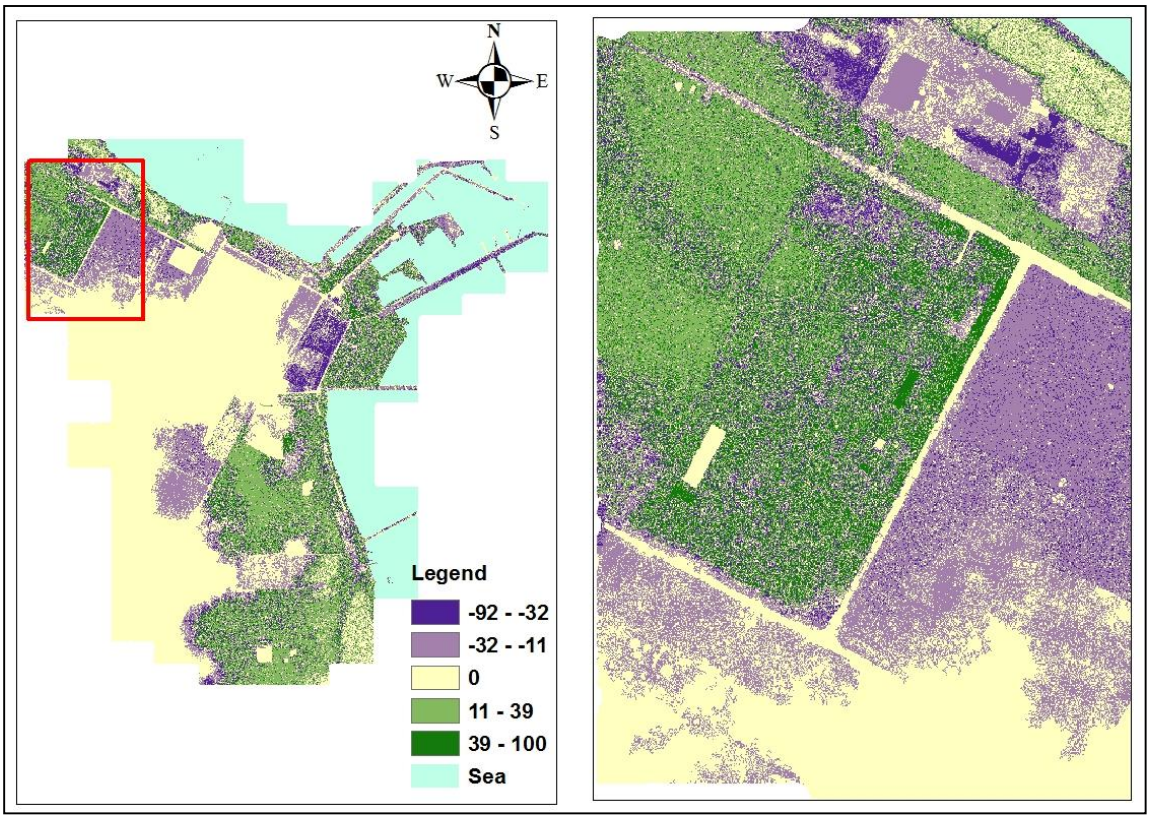

Figure 5-12: The difference in flood probability between zero autocorrelation and Moran's I = 0.33 Sill 2.026, Range 658.20.

Furthermore, a map was produced to show the differences in the flood probabilities between spatially-dependent errors (Moran's I = 0.66) and independent errors (Moran's I = zero, random error). The results in Figure 5-13 show the difference between the probability of flooding in cases of zero spatial autocorrelation and in cases of 0.66 spatial autocorrelation. Most of the study area showed insignificant differences in the flood probability, however, there were some areas with a significant difference.

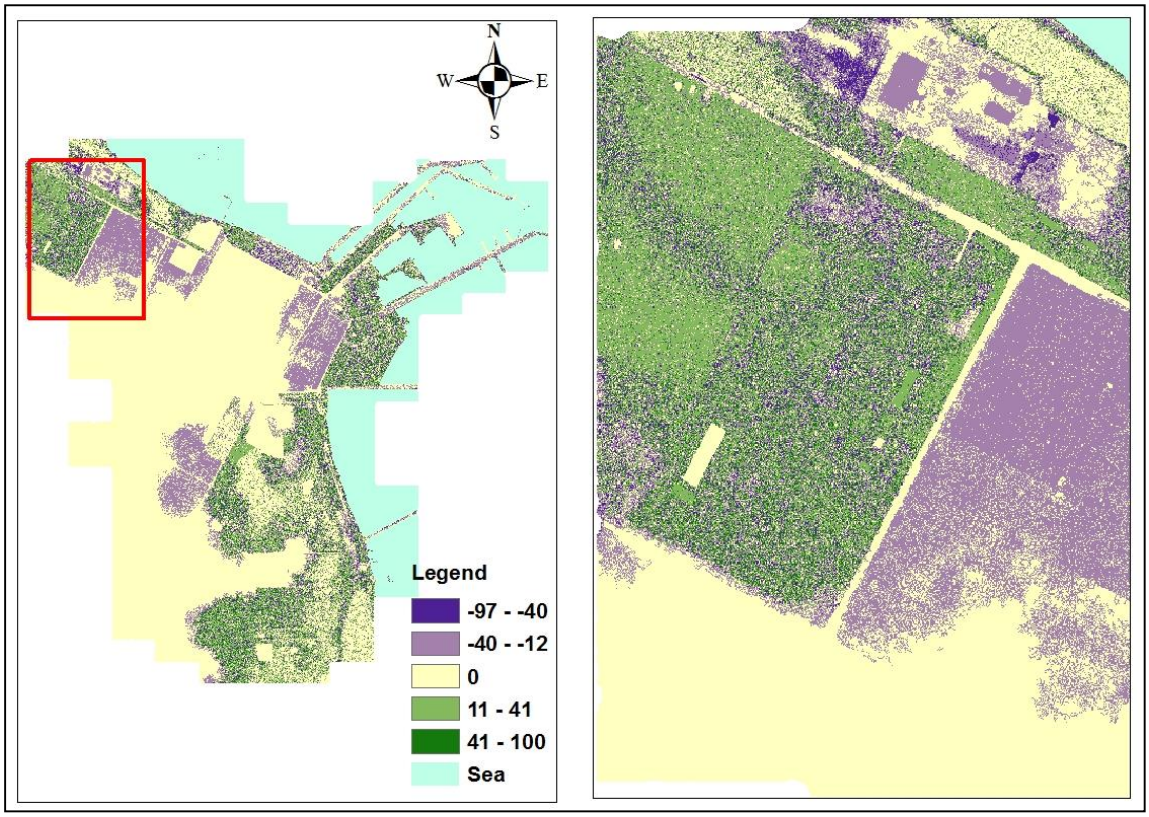

Figure 5-13: The difference in flood probability between zero Moran's I and Moran's I = 0.66. Sill 2.026, Range 1516.20.

5.5.3. Step 2. Varying the value of sill with fixed range values

In the next step of the methodology the sill value was reduced in order to determine its impact on the spatially-correlated error surfaces and on the flooding probability maps. Therefore, this time the sill was reduced to 0.5 with the same ranges of 1, 658.2 and 1516.20. This produced errors with Moran's I of 0, 0.33 and 0.66. Example maps of this spatially autocorrelated error are shown in Figure 5-14.

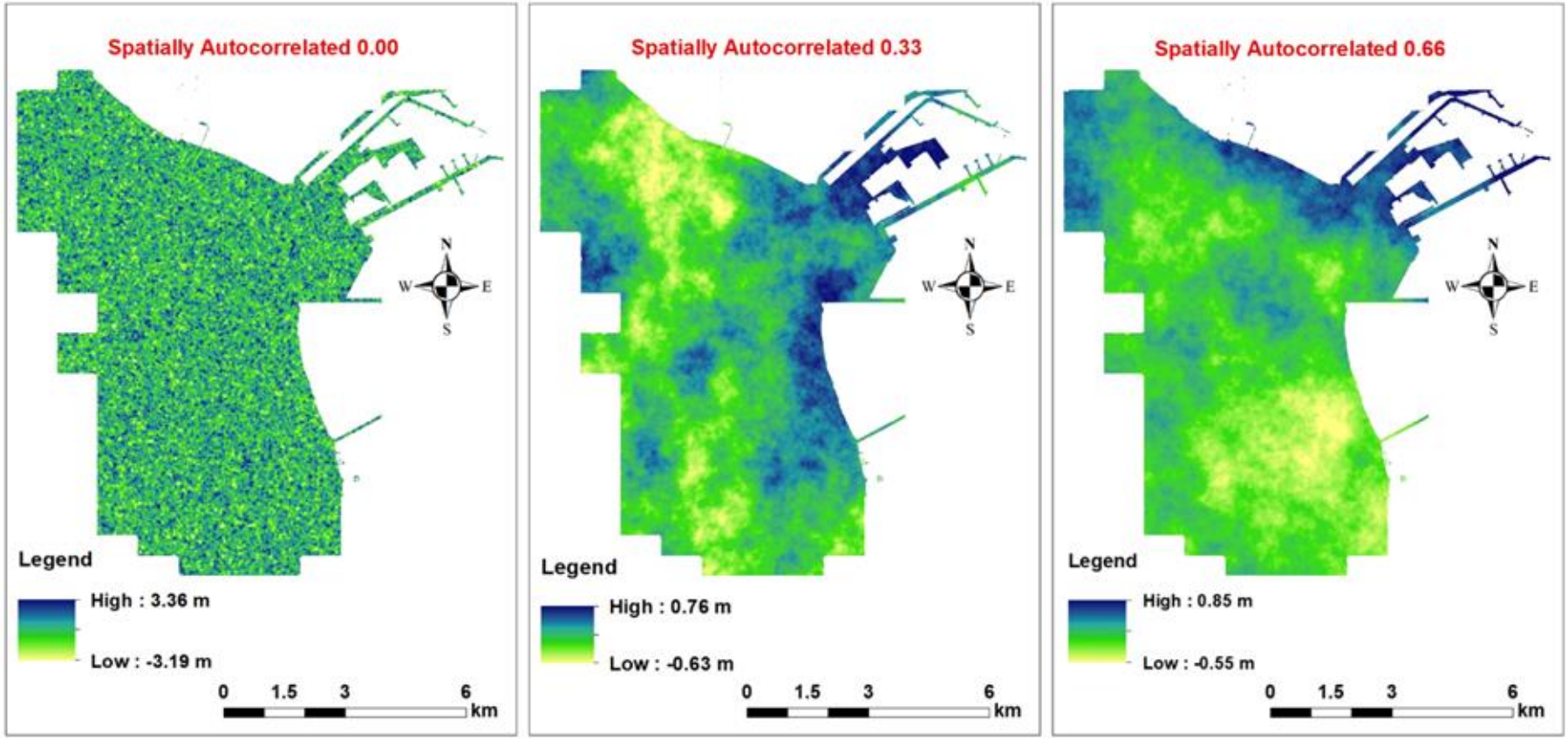

Figure 5-14: Example map of spatially autocorrelated error from R programme with Moran I = zero, 0.33 and 0.66 (Sill 0.50, Range 1, 658.20 and 1516.20).

Monte Carlo simulations were produced and the spatial autocorrelation (0.33 and 0.66) significantly reduced the areas with 95 – 100 per cent probability, while increasing the areas with a probability ranging from 51 to 94 per cent and 6 to 50 per cent. In contrast, the areas of 0 – 5 per cent probability decreased more under the 0.33 autocorrelation than 0.66. The difference in the value of flood probability between a Moran's I of 0 and 0.33 was less than ten per cent for more than 70 per cent of all the pixels, while between a Moran's I of 0 and 0.66 it was less than ten per cent for more than 66 per cent of the pixels (Table 5-6). These results are similar to those seen in Table 5-5.

Table 5-6: Comparison of flooded areas between flooding probability with different levels of spatial autocorrelation.

Probability of flooding (%)	Spatial Correlation 0 Area (km^2)	Spatial Correlation 0.33 Area (km^2)	Spatial Correlation 0.66 Area (km^2)
0-5	39.70	42.51	45.40
6-50	11.04	8.70	5.53
51-94	15.17	16.20	15.14
95-100	6.73	5.23	6.57
Total	72.64	72.64	72.64

The results were then explored in more detail. The first comparison was between the probability of flooding based on the random errors (Moran's I of zero) included in the DEM and based on errors with Moran's I of 0.33 (Figure 5-15). When a difference map was produced, the areas with zero were indicative of no difference between the two. Positive values mean that the flood probability of simulation with random error (Moran's I of zero) was greater than simulated flood probability with errors with Moran's I of 0.33, and the negative values represent the opposite.

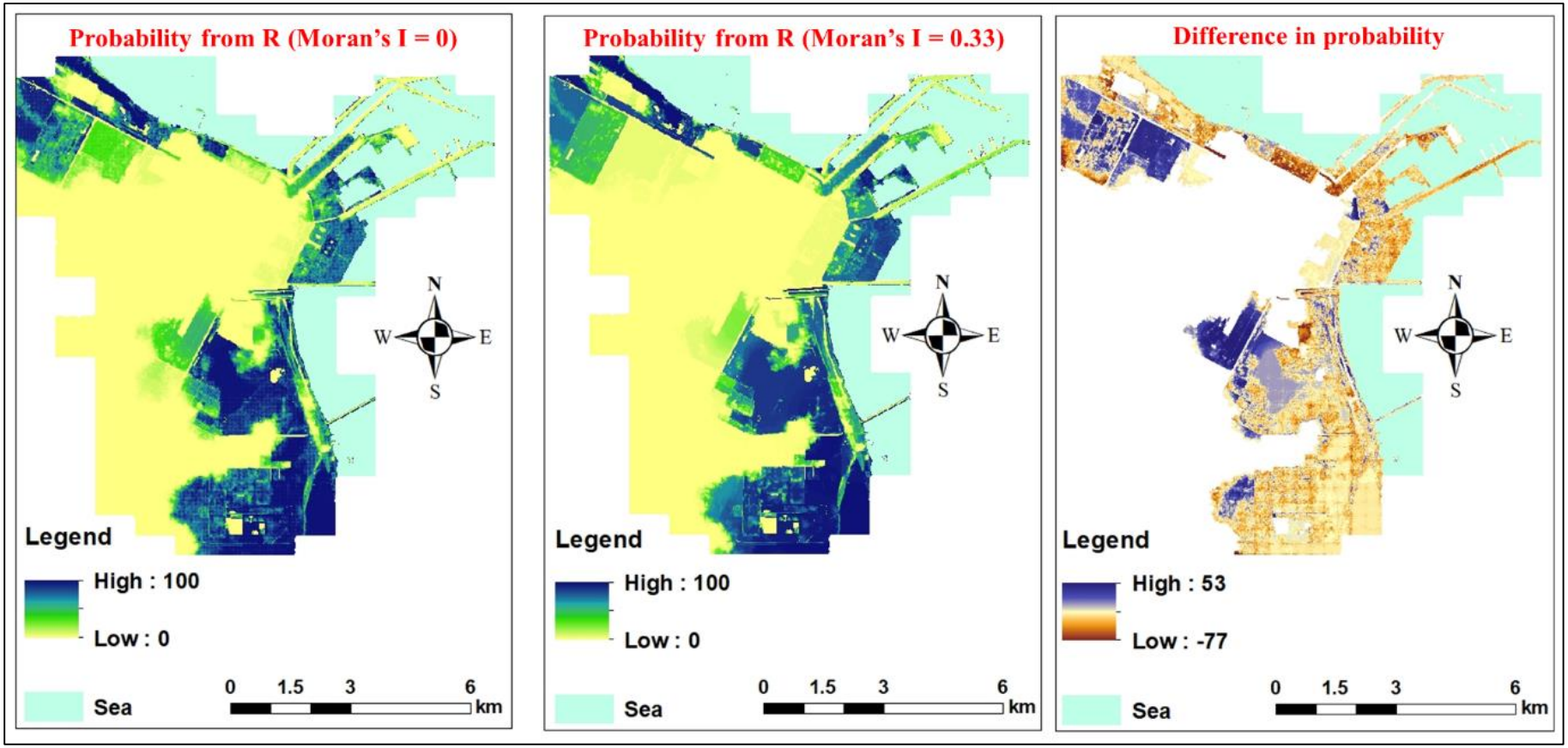

Figure 5-15:The difference in flood probability from R between simulating spatially autocorrelated errors (Moran's I = 0 Sill 0.50, Range 1.00 and Moran's I = 0.33 Sill 0.50, Range 658.20).

To explore these differences further, a histogram of differences was produced (Figure 5-16). The data showed that most of the areas (more than 70 per cent) have a difference of less than ten per cent in the probability of flooding. In only three per cent of the pixels there was a difference of more than 30 per cent. However, the distribution of the differences was not normal. To identify the factors causing the long tail and spike effect in the histogram, areas were investigated on the histogram: *a*_1,2,3 for the long tail and *b* and *c* for the high spike effects.

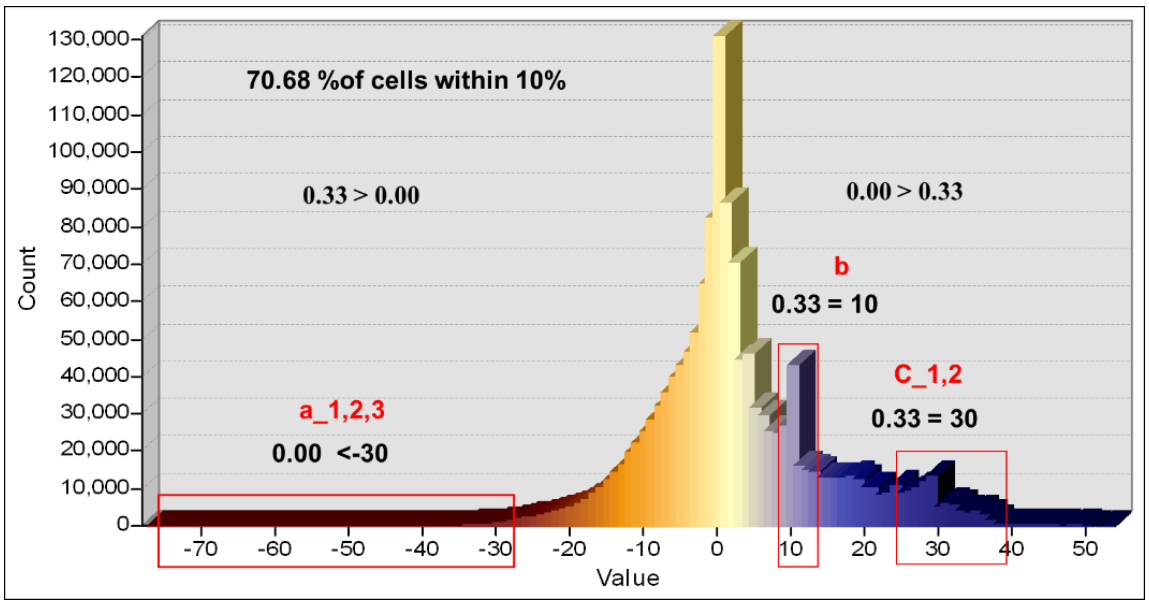

Figure 5-16: Histogram of difference in flood probability from R between (Moran's I = 0 Sill 0.50, Range 1.00 and Moran's I = 0.33 Sill 0.50, Range 658.20).

First, those areas were identified and detailed satellite imagery was obtained. The satellite images and DEM (Figure 5-17, Figure 5-18 and Figure 5-19) show the location of a1, a2 and a3. These appear to be industrial areas and the DEM shows that the area has varying altitude. This is why there were large differences in the probability values depending upon spatial autocorrelation. When there is spatial autocorrelation, the flooding probability increases. But when the area has frequent high and low elevation, the high areas stop the flooding. This is why the probability of flooding is lower when Moran's I is zero compared to Moran's I of 0.33. This creates a long tail in the graph.

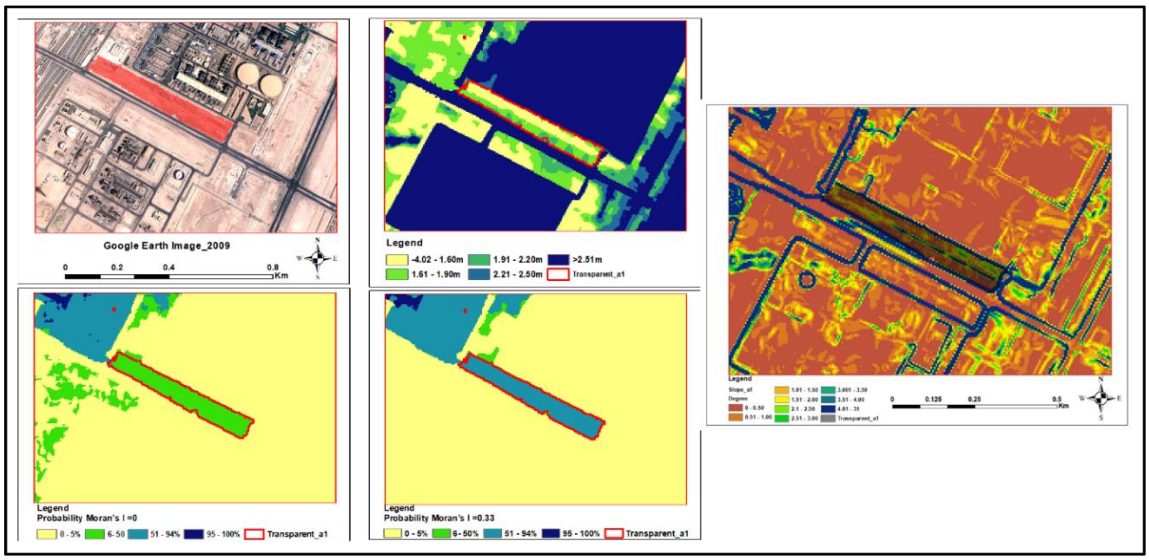

Figure 5-17: Satellite images showing the location of an area (a1) representing a road within an industrial setting, with lower altitude compared to the surrounding areas, as shown in the DEM map.

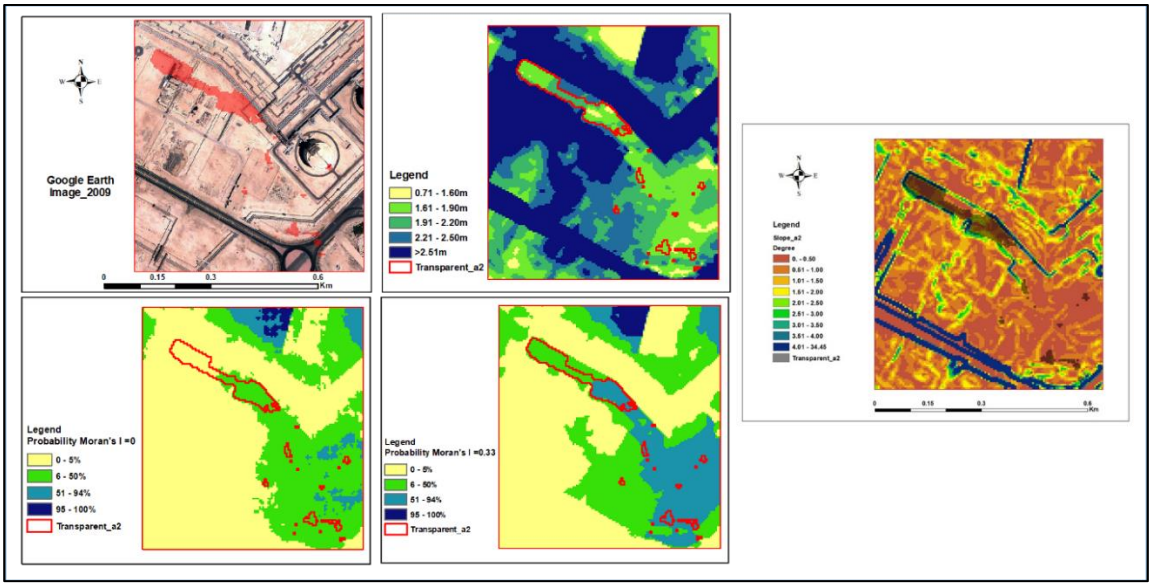

Figure 5-18: Satellite images showing the location of an area (a2) representing a road pipeline, with lower altitude compared to the surrounding areas, as shown in the DEM map.

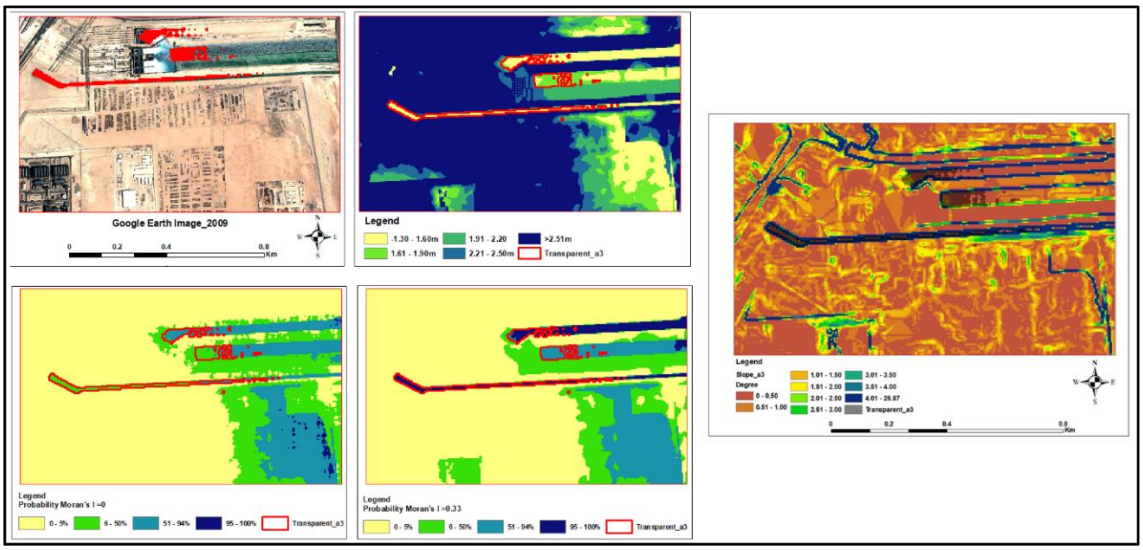

Figure 5-19: Satellite images showing the location of an area (a3) representing a cooling station for a factory, with lower altitude compared to the surrounding areas, as shown in the DEM map.

The satellite images and DEM (Figure 5-20, Figure 5-21 and Figure 5-22) were obtained for the areas indicated on the histogram as spikes b, c1 and c2. The data shows that b, c1 and c2 are marshlands, and the DEM shows low-elevation area (marsh) surrounded by higher-elevated areas. In these areas, the greater spatial correlation reduces the probability of flooding.

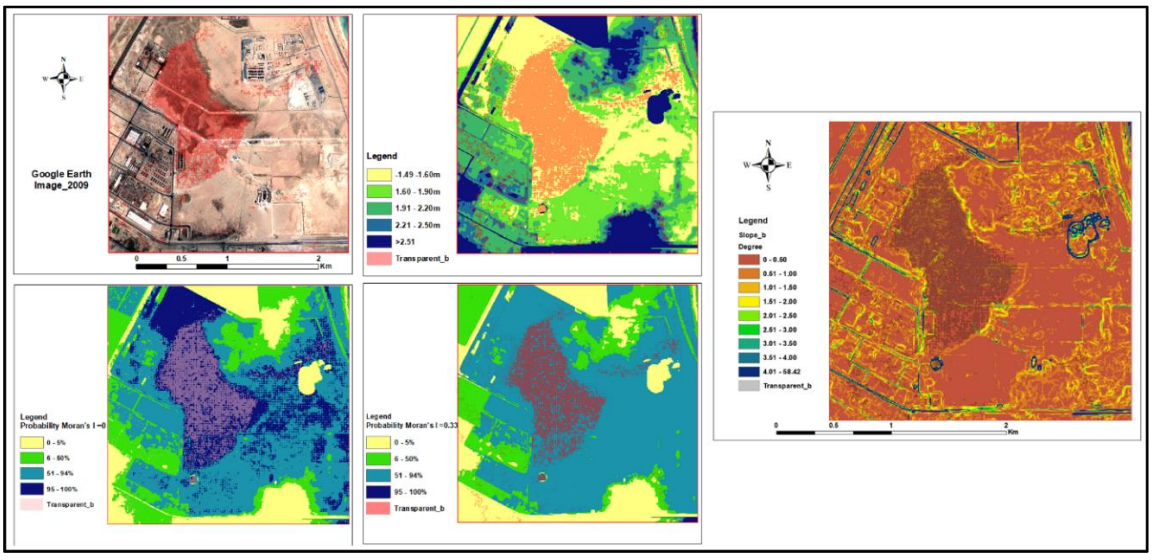

Figure 5-20: Satellite images showing the location of area b, representing low ground marshes, located between relatively higher altitude surroundings, as shown in the DEM map.

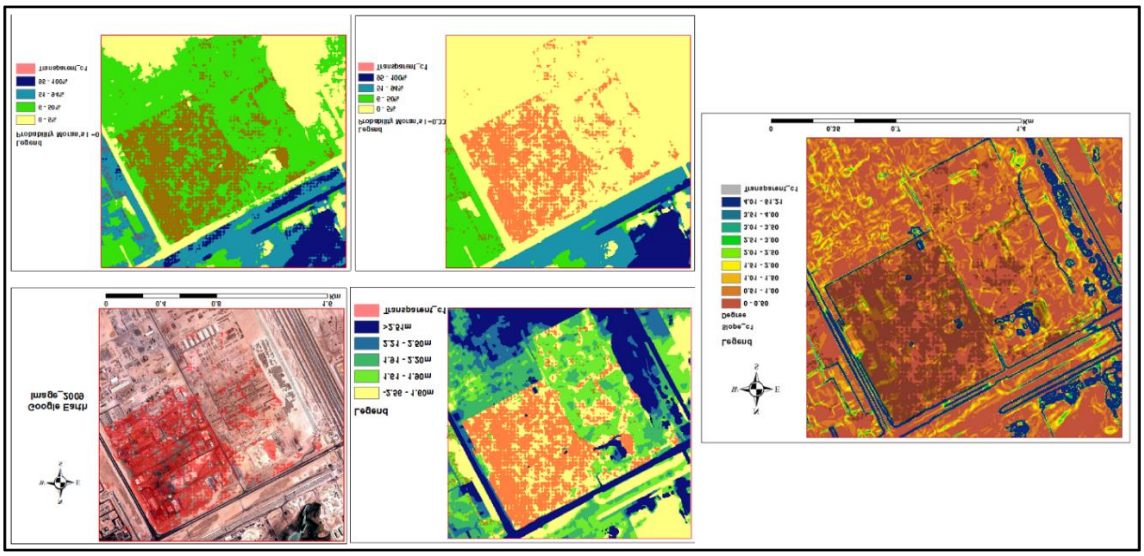

Figure 5-21: Satellite images showing the location of area c1, representing low ground marshes, located between relatively higher altitude surroundings, as shown in the DEM map.

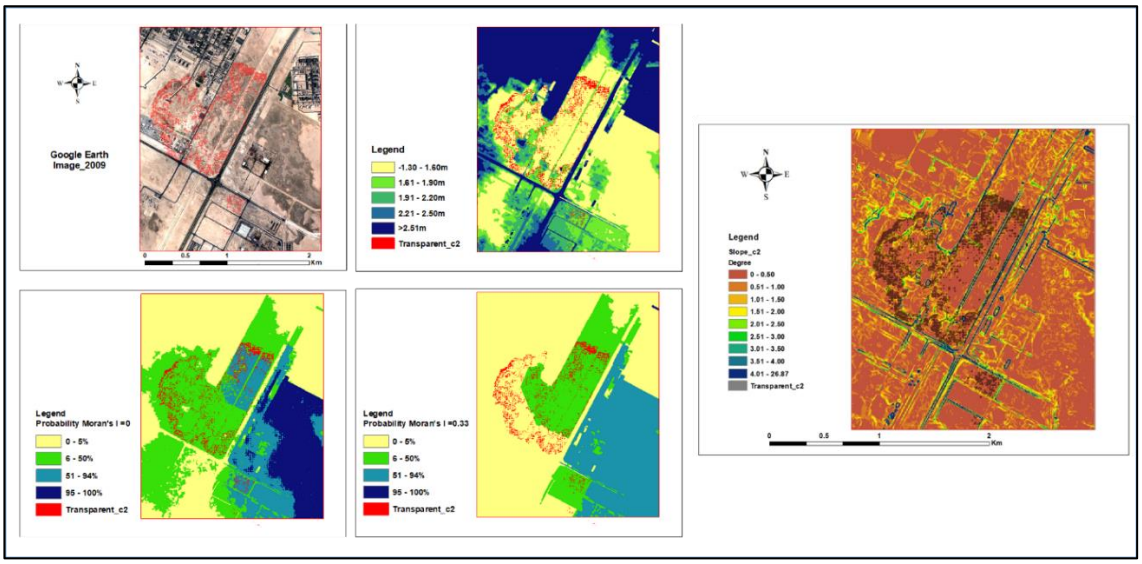

Figure 5-19: Satellite images showing the location of area c2, representing low ground marshes, located between relatively higher altitude surroundings, as shown in the DEM map.

The probability map with random errors (Moran's I = 0) was also compared to the same map using spatial correlation error (Moran's I = 0.66). The results show few major differences between the probability of flooding based on DEM with random errors and errors with Moran's I of 0.66 (Figure 5-23).

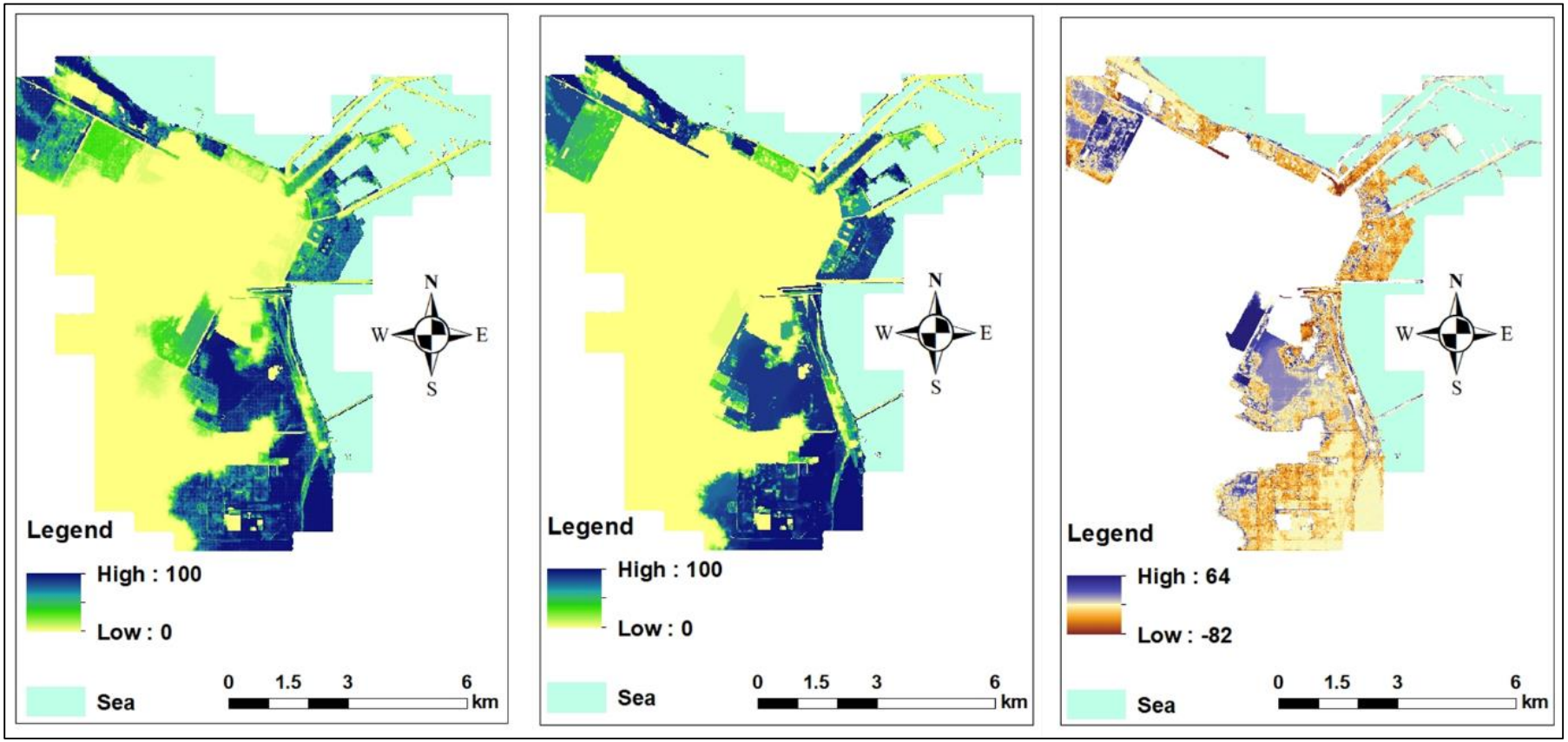

Figure 5-20: The difference in flood probability from R between simulating spatially autocorrelated error (Moran's I = 0 Sill 0.50, Range 1.00 and Moran's I = 0.66 Sill 0.50, Range 1516.20).

The histogram of the difference map between the flood probability with Moran's I equal to zero and Moran's I equal to 0.66 is shown in Figure 5-24. Almost 90 per cent of the area has a difference in flood probability with less than ten per cent. However, the difference in the probability histogram was not normally distributed. There were a long tail and spikes in the shape of the histogram. To understand the cause, three areas (a, d and e) were identified on the histogram for detailed analysis.

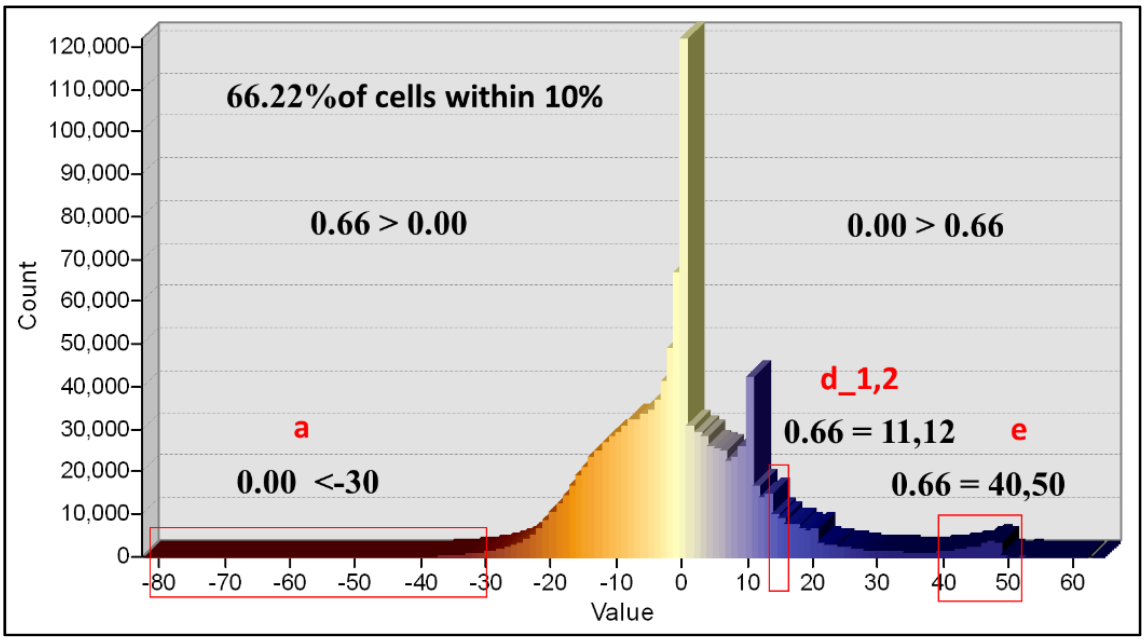

Figure 5-21: Histogram of difference in flood probability from R between (Moran's I = 0 Sill 0.50, Range 1.00 and Moran's I = 0.66 Sill 0.50, Range 1516.20).

Satellite images and DEM (Figure 5-25, Figure 5-26 and Figure 5-27) for these areas were obtained. The satellite images show that the tail in location *a* is similar to those identified in the previous comparison. The spikes in location *d1*, *d2* and *e* represent marshlands, which generally have a low elevation (as indicated in the DEM) and are surrounded by high elevated areas.

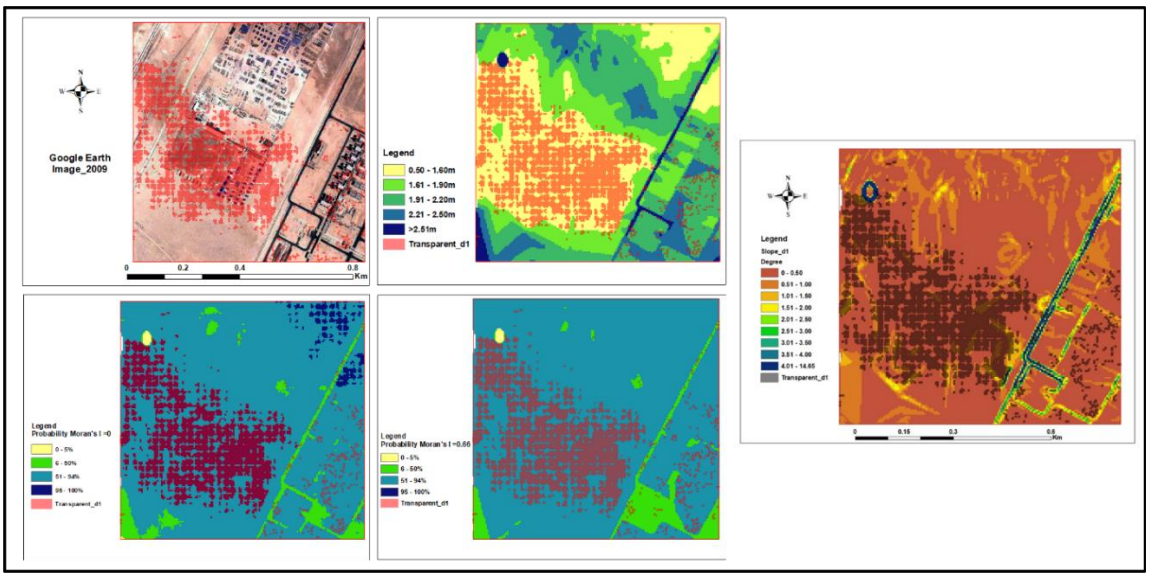

Figure 5-22: Satellite images showing the location of area d1, representing low ground marshes, located between relatively higher altitude surroundings, as shown in the DEM map.

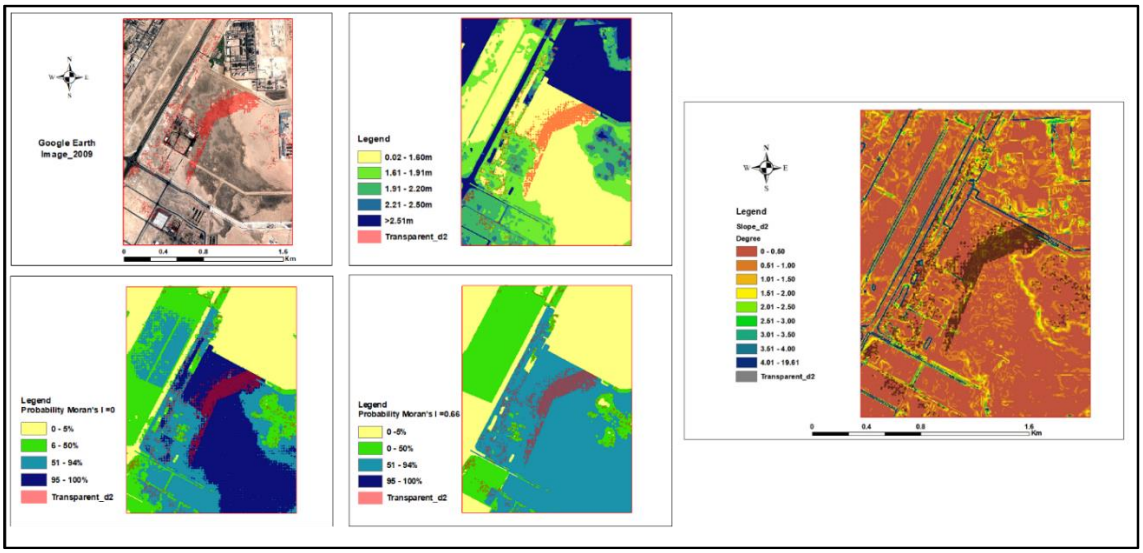

Figure 5-23: Satellite images showing the location of area d2, representing low ground marshes, located between relatively higher altitude surroundings, as shown in the DEM map.

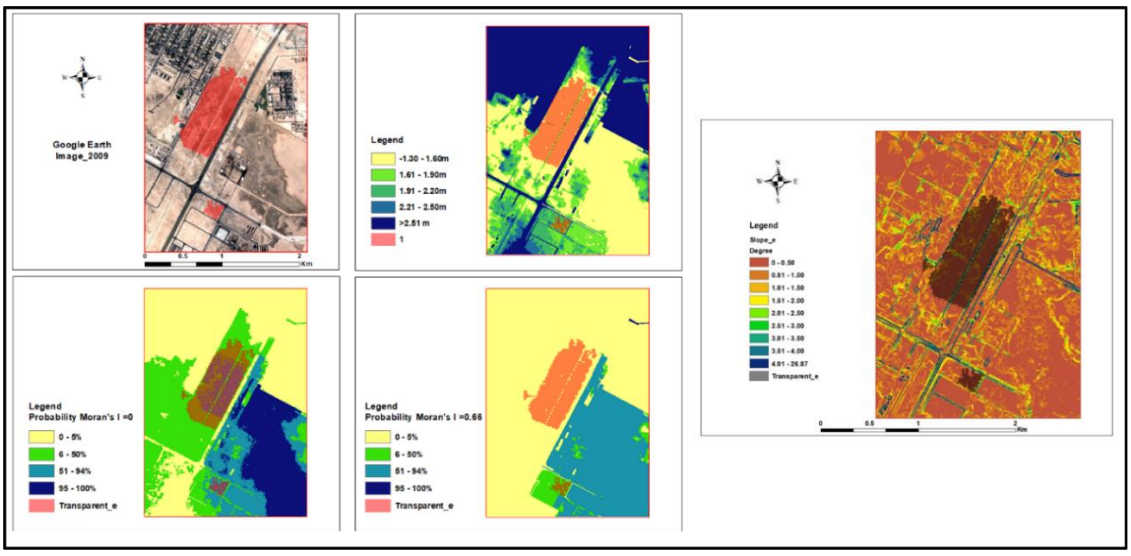

Figure 5-24: Satellite images showing the location of area e, representing roads and low ground marshes, located between relatively higher altitude surroundings, as shown in the DEM map.

5.6. Discussion

Assessing uncertainty is crucial for supporting decision-making processes, especially on future SLR and climate change. The uncertainties in both DEM and SLR (RCP) scenarios have an impact on the outcome of flood probability. Therefore, it is important to study this in more detail.

Table 5-7 summarises the main results from the different assessments of uncertainty. The RCP simulation showed that there are 48.3 km^2 of area with 0-5 per cent probability of flooding (100-95 per cent probability of not flooding), this means that 66.7 per cent of the area will not be flooded as the result of the RCP scenarios. Only 27.2 per cent of the areas had a 95-100 per cent probability of flooding. Therefore, only six per cent of the areas have uncertainty over whether flooding or not flooding will happened in the future.

The simulation of DEM uncertainty provided very similar outcomes, with 65.7 per cent of the areas having a probability of flooding of 0-5 per cent. However, there are lower proportions of the area identified with a high probability of flooding, only 21.4 per cent with the 95-100 per cent. The areas with higher uncertainties increased to 12.9 per cent of the total area.

When the RCP and DEM uncertainties were combined, the proportion of the areas with low probability of flooding (0-5 per cent) reduced to 56.7 per cent, but the areas with a high probability of flooding (95-100 per cent) increased to 28.7 per cent of the total area. However, the areas with uncertainties increased to 14.6 per cent.

Table 5-7: Results from different scenarios to assess the uncertainties associated with DEM and RCP.

Probability of flooding (%)	Simulation of RCP Area (km^2)	Simulation of DEM Area (km^2)	Combining probability surfaces Area (km^2)	Combining errors Area (km^2)	Spatial Correlation 0.00 Area (km^2)	Spatial Correlation 0.33 Area (km^2)	Spatial Correlation 0.66 Area (km^2)
0-5%	48.3	47.78	41.2	38.01	39.7	42.51	45.4
6-50%	2.98	4.85	7.1	15.01	11.04	8.7	5.53
51-94%	1.59	4.49	3.47	9.21	15.17	16.2	15.14
95-100%	19.77	15.53	20.87	10.41	6.73	5.23	6.57
Total	72.64	72.64	72.64	72.64	72.64	72.64	72.64

The DEM created using elevation points in Chapter 3 is one representation of reality. By introducing error into the simulations, 100 representations of reality for the DEM were generated. Future SLR is also uncertain, and this was additionally simulated by creating 100 representations of SLR.

The two methods for assessing the overall impact of these two sources of uncertainty were (1) combining probability surfaces, and (2) combining errors, with both producing similar results. They predicted large proportions of areas with no flooding (with probability of 0-5 per cent) (Table 5-3). The probability of flooding for the areas with more than five per cent and less than 95 per cent flooding were overestimated when errors were combined, in comparison to combining probability surfaces. However, the areas with the highest probability of flooding (96-100 per cent) were underestimated by the combining errors.

The previous chapter did not take spatial autocorrelation of error into account. This was included in this chapter, which allows consideration of its impact on flooding probability. Introducing spatial autocorrelation avoided having an immediate neighbour with extreme peaks

and troughs. There are two situations in which spatial autocorrelation had a large influence on the flooded areas. First, where there were areas with sudden changes in elevation in the built-up areas, for example, long and narrow areas with low elevation (less than 2.2 m) surrounded by large and higher blocks of man-made structures with steeper slopes between these structures and the surrounding areas. Secondly, large and flat areas with very low elevation (less than 1.60 m), surrounded by higher topography, such as mainly marshland areas surrounded by natural elevated features. The probability of flooding when errors were random (Moran's I = 0) was higher than the spatially autocorrelated probability map, but there were many small places dotted around the study area.

The key reason for these differences in the flood probability (when created based on random versus spatial autocorrelation) might be due to the changes in elevation and slope. When the changes in elevation were man-made, meaning less spatially autocorrelated, the probability of flooding was greater as the errors will reduce these random changes. However, when the changes in elevations were natural (spatially autocorrelated), the probability of flooding was lower.

However, in overall terms, the impact of spatial autocorrelation on the flooding probability maps was fairly small. As Table 5-7 showed, the differences between the areas with high flood probability (95-100 per cent) were not significant, with 6.73 km^2 for zero autocorrelation and 5.67 km^2 for 0.66 spatial autocorrelation. The 0.33 spatial autocorrelation has a smaller area (5.23 km^2) under high flooding probability. However, for the non-flooded areas (0-5 per cent probability) the high spatial autocorrelation for the area was greater. The spatial autocorrelation of 0.66 overestimated the non-flood area by 14 per cent but this was not a consistent trend in other flood probability categories.

In the literature, spatial dependence was used as a grid-cell uncertainty model. This model was developed by Hunter and Goodchild (1995) to integrate spatial autocorrelation. The grid-cell uncertainty model is a highly complex technique and takes more time to set up and implement. However, it has been used in numerous studies, such as Hunter et al. (1995), Hunter and Goodchild (1997), Murillo and Hunter (1997), Zerger et al. (2002) and Darnell et al. (2010).

Systematic error assessment is a complex process. It requires time (Wechsler, 2006), which cannot be achieved in this study due to some constraints, lack of resources and lack of expertise. Furthermore, there is evidence in the literature that, even in cases of doing systematic error assessment, there is a possibility that the quality of the outcomes may not improve significantly (Darnell et al., 2010). This was the case in this chapter.

Elevation data can be used to determine areas susceptible to floods. Introducing error in the DEM to assess the uncertainty in the accuracy of DEM for representing the actual elevation has an impact on the resulting boundaries of the flooded area. However, it is important to recognise that the true nature and extent of these errors is unknown. Therefore, the impact of errors added to the DEM for assessing uncertainty remains unexplained. “Even with an understanding of the size and texture of spatial data uncertainty, it is not possible to determine what is actually ‘out there’ as long as there is any amount of uncertainty. All that can be achieved is the generation of representations of what may potentially be there, and the use of these potential realisations to develop a stochastic understanding of how spatial data uncertainty affects a geographic information application of any complexity” (Ehlschlaeger, 1998, p. 6; as cited by Wechsler, 2006).

Chapter 6: Critical Area for Barrier Construction

6.1. Introduction

In previous chapters, the key parameters to identify the areas under high risk of flooding as the result of SLR were studied. In Chapter 3, the DEM of the coastal area was produced using a variety of interpolation techniques. This was used to assess the likelihood of flooding based on different climate change scenarios in Chapter 4 and the accuracy of the DEM was considered in those assessments. Furthermore, the interdependency and spatial autocorrelation of DEM errors and their impact on flooding probability were assessed and reported in Chapter 5. This helped to ensure that the resultant flood probability map is the best possible representation of the potential impact of climate change on SLR.

The objective of this chapter is to identify critical areas for building a barrier to prevent inundation as the result of future SLR. Geographic information system tools and multi-criteria evaluation (MCE) were used to identify and select the most cost-effective locations to build barriers that can prevent land inundation from SLR as the result of climate change. The rationale for this chapter is that, in the literature there are many studies using GIS to assess the impact of flooding. These frequently overlap flooding extent with land use/land cover data or other measures of impact. However, there are fewer studies assessing the most suitable location for dam placements in river systems and virtually no studies using GIS as a decision-making tool to assess the most suitable location for dams to prevent coastal inundation. Hence this chapter develops a relatively new methodology for adapting to the potential impacts of climate change. Through discussions with academics in Qatar there was felt to be a real need for research such as this.

6.2. Literature review

6.2.1. Overview

This literature review will have two sections. The first will provide an introduction to MCE, while the other presents a review of studies that have assessed suitable locations for barrier/dam siting.

6.2.2. Multi-criteria evaluation

Multi-criteria evaluation is a technique used to make better decisions. It is often used for assessing environmental factors (Jiang & Eastman, 2000). Eisenfuhr (2011, page 2) defined decision making as a "process of making a choice from a number of alternatives to achieve a desired result". Decision making in relation to site selection (spatial decision) is based on several criteria related to the geographic information. Geographic information systems are a particularly useful tool for undertaking MCE (Chakhar & Mousseau, 2008). A simple overlay of flooding with land use is useful in terms of assessing flood risk but does not consider the relative importance of different land-use types. It also makes it challenging to evaluate the relative merits of impacts measured on different scales, e.g. area vs flood depth. The advantage of MCE is to provide a tool for decision making in selecting the right place to build barriers to prevent flooding in this case. The tool can include multiple points of view from different stakeholders when it comes to flood prevention.

Geographic information systems are widely used in making decisions on spatial resource allocation based on multiple factors and criteria. This is known as MCE in various disciplines and environmental planning is one of the main areas. For example, Tiryaki and Karaca (2018) used GIS and MCE to produce a flood susceptibility map based on numerous factors, specifically slope, aspect, elevation, geology, land use and proximity to the river. Many other examples of MCE exist, including in transportation (Jha et al., 2001), urban and regional planning (Ward et al., 2003), waste management (Leao et al., 2004), hydrology and water resource (Martin et al., 1999), agriculture (Morari et al., 2004), forestry (Kwaku, 2004), natural hazard management (Ayalew et al., 2004), recreation and tourism management (Feick & Hall, 2004), housing and real estate (Johnson, 2001), geology and geomorphology (Burton & Rosenbaum, 2003), industrial facility management (Vlachopoulou et al., 2001) and cartography (Armstrong et al., 2003).

In the past three decades GIS has been widely used in the MCE process and is mainly used in two ways (Jiang & Eastman, 2000). The first consists of converting the criteria into Boolean maps, meaning that the criteria evaluated is based on a specific threshold of suitability. This is a simple binary classification of the criteria as either included or excluded. Therefore, these Boolean maps can be seen as constraints because they exclude areas that are not suitable for consideration. The constraints can be analysed in GIS by using functions, such as intersection (logical AND), union (logical OR) or a combination of both.

The second way consists of standardising the criteria. This approach is where other criteria, which are called factors, are given degrees of suitability for the decision under consideration. For example, in assessing flooding because of SLR, areas closer to the sea have a higher probability of flooding than the areas further away from the coastal line. These areas will be given higher values to indicate a higher probability of flooding. These criteria are not binary in their suitability, they are continuous and can be expressed as a range, 0 to 100, for example. These approaches can be combined, for example, to create a suitability map. All the factors are weighted and then multiplied by each other. They may then be multiplied by any Boolean constraints. Eastman et al. (1995) suggested following a general formula for measuring the suitability:

$$Suitability\ (S) = \sum (wi\ Xi) * II\ C_j \qquad \text{(Equation 6-1)}$$

where wi = weight assigned to factor i

Xi = criterion score of factor i

C_j = constraint j

II= The product

However, Eastman (1995) highlighted several issues with these traditional uses of MCE in GIS:

- The choice of Boolean operator is critical. For example, some areas might be excluded if a single criterion did not pass the threshold when the intersection (AND) procedure is used. However, when the union function (OR) is used, an area might be included for consideration in the decision even if only a single criterion meets its threshold.

- Also, in a Boolean system, in the final suitability map one area with low suitability can be compensated by another area with high suitability.
- In the standardisation approach, the weights increase linearly using a simple linear conversion, which might not be the case for all factors. For example, the risk of flooding from the SLR does not increase proportionally as the factor of proximity to the sea increases. The areas closer to the sea have a greater risk than areas further away. There are other factors too, such as elevation.
- Whenever weights are given to some factors by professionals, there is subjectivity. One group might give a higher weight to a factor while others might not.
- Both approaches have a simple way to manage errors in the decision. There is no consideration of the uncertainties associated with those factors; they, therefore, do not consider a decision as a probability risk of getting it wrong.

Rikalovic et al. (2014) highlights the advantages of using two stages in MCE to select locations. This consists of screening and evaluation stages. In the screening stage, a relatively large number of potential sites are selected based on several criteria. In the second stage these sites will be narrowed down using more detailed criteria to select the most suitable locations.

The MCE was selected as a method for site selection to build barriers to prevent flooding from SLR as it can integrate many factors in the calculation and can be used in ArcGIS environments.

6.2.3. Suitable locations for barrier/dam siting

Most of the research reviewed focused on the suitability of a limited number of sites to protect urban areas from flooding due to high rainfall events. Abushandi (2016) studied the possibility of building a dam at a single wadi as a flood prevention measure. He used several factors, such as land cover type, catchment characteristics and hydrology factors (rainfall and DEM (slope)) to select a suitable site for building a dam. The MCE methodology was found to be effective for selecting a site in a single wadi to prevent flash flooding.

Jozaghi et al. (2018) comment that determining the best location for a dam construction is an extremely complex decision. They used MCE and GIS to improve their decision-making process

for a dam site selection in Iran. They used an analytic hierarchy process (AHP), a graphical representation of the problem, to help understand and solve the problem. They also used the Technique for Order of Preference by Similarity to Ideal Solutions (TOPSIS), a method of giving priority in MCE. This technique is widely used in MCE for water resource management. Their method was based on two main criteria, the elevation and the shape of the valley. They argue that this is because the best site for dam construction is where the valley is narrow and the collected volume of water for irrigation and domestic water supply is adequate. They also considered factors that include geology, land use, sediment, erosion, ground water, volumetric flow rate and other hydrological situations. They found that the integration of MCE and GIS improved the dam site selection by reducing cost and providing a holistic approach in the process.

Moiz et al. (2018) similarly used GIS and MCE for a hydropower site selection in Pakistan. In the study they used a wide range of geographic criteria, including DEM, soil type and land use. These were integrated with other data sets, such as meteorological data, to develop a tool for a preliminary hydropower site selection. The tool calculates discharge and dam height, which, they argue, reduces the time for investigations and evaluates sites using a more systematic approach. However, they recognise that other factors, such as social factors, need to be incorporated into their analysis.

Romanelli et al. (2018) used a similar method to classify areas of priority for hydropower construction in Brazil. However, this study used as its starting point several proposed dam sites and then evaluated each based on environmental conservation priority, geomorphology and socio-environmental use. Larentis et al. (2010) also studied the application of MCE and GIS technologies for selecting a hydropower site in Brazil. However, this analysis was based on evaluating potential sites along a pre-existing stream network. Potential dam height and discharge were calculated, but there were no estimates of potential upstream impacts. The authors suggest that the method provided an effective way to select hydropower sites and a reasonable prediction of the main parameters for planning purposes.

Capilla et al. (2016) also used MCE and GIS to optimise the site selection process for building a reservoir. In this scheme, water is pumped upstream during a period of surplus power but released

during high power demand using a normal hydroelectric plant. A two-step MCE was used. First, a broad site selection was undertaken based on topography (land flatness), distance between the two reservoirs, water availability and storage capacity. Once a potential suitable site had been found, the second step was a more detailed screening process using other factors, such as economic, environmental and social criteria. Similarly, Fedorov et al. (2016) used DEM, flow direction, river network and hydrological data to create multilayers of geo-information. These were then applied to a site selection model. The model was based on catchments and sub-catchments generated for their study area. They assessed suitability based on the relationship between basin storage capacity and the amount of runoff generated in the drainage basin. The method they used was based on self-regulated flood dam parameters, which included the height of the dam, the geographic location along the river and the potential impact of the dam on the surrounding environment.

The previous section was focused on dam creation in relation to river flooding. However, the coastal area is also at risk of flooding from the sea. This makes these areas vulnerable. Nonetheless, there exists limited literature on coastal barrier selection. Li et al. (2017), for example, studied the risk of sea flooding in China by using GIS and spatial analysis and modelling multiple typhoon scenarios, flood depth, the extent of areas at risk of flooding and type of land use. The study helped to identify the effectiveness of current flood barriers and the likelihood of flooding in most residential areas. This work contributed to the development of long-term strategies to reduce the impact of typhoon flooding. The selection of new barrier sites was yet to be considered. Having an effective barrier will provide significant benefits to the people and businesses living and operating near the coastal line and at risk of flooding (Davlasheridze et al., 2019). Natural England (Risk and Policy Analysis Limited, 2006) provided generic guidance for selecting sites to prevent coastal flooding. These include:

- description of conservation designation and citations,
- key features, habitats and species,
- flood history of the site,
- site objectives and conservation objectives for the area,
- description of flood risk management (past and present),

- future changes to the site (e.g. climate change),
- impacts of doing nothing (no active intervention),
- impacts associated with different standards of protection.

De Serio et al. (2018) suggested that the criteria used in site selection to build barriers to prevent flooding from the sea are driven by those factors contributing to coastal vulnerability. They list the main criteria as below:

1- Physical criteria:

- Slope
- Coastline features
- Wave height
- Shoreline change rate
- Sea level rise
- Tidal data
- Elevation

2- Socio-economic:

- Population
- Road network
- Land use

Maanan et al. (2018) used coastal erosion as the key indicator of coastal vulnerability in Morocco. This study used MCE and GIS, including layers such as population, erosion and SLR as the result of climate change. Tonmoy and El-Zeinb (2018) used an indicator-based assessment of vulnerability on eight beaches in Australia. This research took a more local approach and engaged the local authorities to weight the criteria based on the well-being of beach residents, the well-being of the residents and the functionality of the infrastructure at the beaches.

Boateng et al. (2017) studied coastal vulnerability based on a wide range of factors, including geomorphology, coastal elevation, geology, local subsidence, SLR, shoreline change rates, mean tidal range, mean wave height and the population density of the coastal areas. These factors were used in GIS to develop a coastal vulnerability index (CVI) for Ghana's coastal areas. Other

researchers used the CVI based on a wide range of indicators (Cutter et al., 2000; Yohe & Tol, 2002; Abuodha & Woodroffe, 2010) to analyse the vulnerability of coastal areas. The CVI was required to define the vulnerability of the coastal area and the future aspect of the vulnerability (Hinkel, 2011).

In any siting study, it is important to identify the critical factors that affect the vulnerability of the area to flooding. Several studies highlight the importance of area topography (Abushandi,, 2016; Jozaghi et al., 2018; Moiz et al., 2018; Capilla et al., 2016; De Serio et al., 2018; Boateng et al., 2017). Elevation is also an important factor, but it is much more dependent on the magnitude of the SLR (Mannan et al., 2018; Boateng et al., 2017). Elevation and SLR determine the flood depth, which is an important factor for deciding on the location of barriers (Li et al., 2017). When considering the impact of any flooding, this is dependent on how long the water will stay in that area, the depth of the flooding and the functionality of the area where the flooding happened. For example, the impact of flood depth on a residential area is much greater than flooding in an undeveloped area. Therefore, land use is another key factor when assessing impact (Li et al., 2017; De Serio et al., 2018; Moiz et al., 2018; Abushandi, 2016). This will influence the site selection.

One limitation of previous studies is that they do not take DEM uncertainty into account. This is surprising as many studies have demonstrated the impact this uncertainty can have.

In addition to a location that minimises impacts, the best place to build a barrier is where the catchment boundaries and the shape of the valley is narrow (Jozaghi et al., 2018). This will result in a relatively small barrier to protect a large area from flooding. This produces a more cost-effective solution.

In summary, this review has highlighted that determining the best location for barrier construction is complex. However, it has shown the benefits of combining MCE and GIS for site selection where the focus of the study is on a large scale. The literature has shown that the choice of DEM is one of the key criteria in site selection for building barriers to prevent flooding, depending on the elevation of the area and the likelihood of water level rise. In terms of assessing potential barrier sites, the review highlights the importance of identifying narrow locations to minimise costs. In terms of assessment criteria, land use is a common aspect but other studies

consider factors such as depth of flooding and how long the area will be inundated. However, most of the literature does not consider DEM uncertainty when identifying suitable barrier sites. In spite of this, the previous chapter has presented this as an important factor to consider. The proposed methodology will identify suitable sites by using a DEM and considering uncertainty within it. It will also consider land use, depth of flooding and depth of pooling. A questionnaire will be used to weigh these factors within an MCE. Following this screening stage, a more detailed evaluation stage will be conducted.

The main reason for the questionnaire is to provide information on the weights that should be provided to different factors. Without this it would be difficult to know how different factors should be weighed against each other. The questionnaire provides a more objective approach in assigning weight for these factors. In this study weights were based on the views of coastal professionals working in the academic and policy environment.

6.3. Methodology

6.3.1. Selection of study area

A small part of the Al Thakhira study area was selected to develop a methodology for identifying the critical area to build a barrier to prevent sea inundations. This area was selected based on several criteria. It was an individual, potentially flooded basin, not part of any other basin and connected to the sea. It was also relatively small to speed processing during this methodology development and contained a variety of land uses, including industrial activities, and was therefore of economic importance. This study area is presented in Figure 6-1.

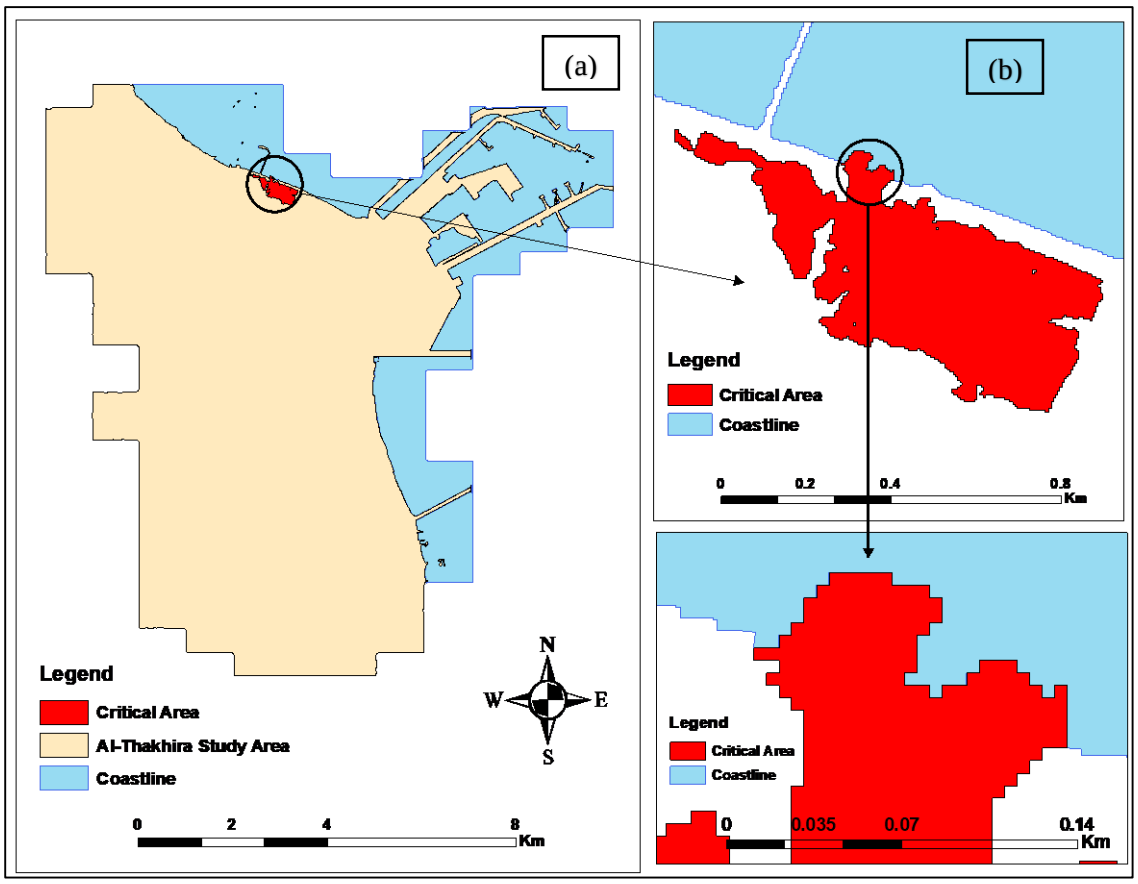

Figure 6- 1: Study area (a) Al Thakhira (b) Small part of Al Thakhira was selected.

There are three main uses of land in the selected study area: industrial sites, roads and undeveloped land, with a total area of 256,000 m^2. The study area has direct contact to the sea on the northern side.

6.3.2. Factors that may influence flood impact

The area of flooded land upstream from any cell, as measured by flow accumulation, is a key factor to consider when assessing impact. Once this has been identified, potential barrier sites can be determined. In a GIS, the flow accumulation function calculates the accumulated flow for each cell based on the direction of the flow from the surrounding cells. There is equal weighting for each cell (a weight of one is applied to each cell). However, there are other factors that are important to consider: (1) the importance of land use within the flooded area, (2) the depth of the flooding, (3) the depth of pooling and the depth of remaining water bodies after the flooding.

6.3.2.1. Land use

Land use is important because it helps determine the economic, environmental and social costs of flooding. The six main types of land use in the entire study area of Al Thakhira were residential buildings, roads, industrial sites, commercial sites, agriculture and farms and undeveloped land. A land-use map was produced by digitising the one from OpenStreetMap (OpenStreetMap, 2018). The vector file was converted into a raster format to be used for further analysis.

6.3.2.2. Depth of Flooding

The depth of flooding is also another important factor because if the flood depth is only a few centimetres the impact will potentially be less than if it is a few metres. The depth of flooding was calculated as a difference between the highest SLR scenario, which is 2.06 m under the average RCP 8.5 scenario in 2100, and the elevation of the ground using the digital elevation model (2.06 m – DEM). The areas with low elevation will have a high depth of flooding while the areas with high elevation will have a lower depth of flooding. Areas with an elevation higher than 2.06 m will not be flooded.

6.3.2.3. Depth of pooling

Water pooling is a small area of still water, typically one formed naturally (Oxford Dictionary, 2019). It occurs when an area of land is lower than its surroundings. In other words, when the sea retreats the water will remain. This implies that the damage may be more severe as there will be longer contact with seawater. This will be a particular problem if, for example, this occurs on an industrial site.

6.3.2.4. Weighting the factors that may affect flood impact

The relative importance of the three factors and how each can be weighed is crucial to produce measures of impact that can be used to identify potential barrier sites. To assess relative importance, a survey/questionnaire was conducted in Qatar to produce an importance weighting for the three main factors. as well as the six types of land use.

The questionnaire was designed to capture the response of participants with a knowledge of coastal systems by asking them to indicate the importance of the three main factors. The survey focused on the views of experts and professionals working in the area, mainly those inland and from water-related professions in Qatar. The questionnaire and an English translation is presented in Appendix 1. The key objectives of the questionnaire were to get an independent and unbiased view from coastal experts on how to weight the three factors. It is assumed that each stakeholder might have a different view on the importance of each land use. The average importance was used in the analysis.

In the first three questions of the questionnaire, the participants were asked to weigh the three main factors in pairs and score them between one and seven, where one is least important and seven is most important. Although a five-point scale is commonly used in such surveys, this study chose a seven-point scale. This is believed to differentiate participants' feelings and responses more adequately (Krosnick & Presser, 2010). The participants were asked to score two factors at a time against each other (in pairs) to account for the recency effect and help them think about both factors at the same time. The recency effect happens when selecting different options; respondents tend to select the option they find towards the top of the list (Harrison, 2017).

Furthermore, there was another question on the importance of the six different types of land use. This was to be able to rank the most important land use in case of sea inundations. In this question the six categories of land use were listed all together, not in pairs. This method was preferred, as a paired approach would have led to a large number of questions. In addition, it made it easier for the participants to make a comparison between all the items. The survey participants were selected from the Qatar University database of staff, depending on relevant experience and interest in climate change, flooding, urban planning and environmental management. The questionnaire was sent electronically in both Arabic and English to eliminate any misunderstanding and confusion about the questions.

The last four questions asked the age, sex and occupation of the participants. This was to assess whether the survey was able to obtain information from a range of participants covering a wide range of expertise in this area.

6.3.2.5. Calculating factor weightings

Once the questionnaire responses were obtained, they were converted to a weighting for each factor. The proportion of responses for each weighting categories was determined, for example, if only three participants selected category two, ten participants selected category five and seventeen participants selected category seven. The weighting was calculated by multiplying the proportion of participants by the value of that category. So, the weighting for category two would be the number of participants (three), divided by the total participants (30), then multiplied by two. Therefore, the weighting would be 0.2 for category two, 1.67 for category five and 3.96 for category seven. By adding up all these weightings for this factor, a total weighting of 5.83 was obtained.

As the factors were scored in pairs, each of them obtained two weighting values. The average was taken as a final weighting for each of them, then the weighting was calculated proportionally between the three factors; for example, if the land use scored a final weighing of nine, depth of flooding eight and depth of pooling seven, then each of these weightings was divided by 24 (total weighting of the three factors) and multiplied by ten. This would result in the weighting being 3.75 for land use, 3.33 for depth of flooding and 2.91 for depth of pooling. The same approach was used to calculate the weighting for each type of land use.

To calculate flow accumulation with a weighting for all the three factors and the six land uses, one raster file needed to be used in the ArcGIS with a weighting for each cell. To create this collective weighting, the map for each factor was multiplied by the final weighting from the survey in ArcGIS. The results were then normalised (from zero to ten) by dividing the value of each pixel by the maximum value then multiplied by ten. Finally, the three maps were added together to create a collective weighting for the flow accumulation calculation.

6.3.3. Cost benefit of flood protection options

6.3.3.1. Calculating flood protection benefits (weighted flow accumulation)

To calculate the weighted flow accumulation there are two key components. The first is the flow accumulation, which is based on the DEM and the subsequent flow direction between different cells. One key element mentioned in Chapter 2 was the role of uncertainty and errors associated with the DEM. In this chapter these will be incorporated into the assessment. However, we have chosen to only consider DEM uncertainty as opposed to SLR uncertainty. This is because the purpose of this chapter is to develop a methodology and it was decided that including both would add unnecessary complexity in this development stage. Once the method has been determined it would be relatively straightforward to include SLR uncertainty.

The second component is the weighting of factors affecting the flow accumulation. The flow accumulation function in ArcGIS was used to calculate the flow in the study area. This enabled the calculation of accumulated flow from the surrounding area (pixels) into each downslope cell in the output raster. The flow accumulation provides information on the number of flooded cells. To assess flood protection benefits, it is important to consider the three factors (land use, depth of flooding and depth of pooling), which provide a measure of flood impact. These can be used to weight each cell in the flow accumulation calculation. The steps to calculate weighted flow accumulation are now considered.

6.3.3.2. Flow direction

Flow accumulation is generated from a DEM by first generating the flow direction. This is one of the hydrological factors of a surface which determines the direction of flow from the surrounding area (cell in the raster map). The flow direction value for each cell is calculated based on the elevation value of the surrounding cells (Jenson & Domingue, 1988). In this process, uncertainty in the DEM will be incorporated. This implies that there will also be uncertainty associated with the flow direction as a result of DEM. To account for the uncertainty in the DEM in calculating flow direction, I used the same MCS method used in the previous chapter (DEM uncertainty only).

One hundred DEMs were created with random errors (Figure 6-2, (2)), using the same parameters as in Chapter 2. Briefly, 100 new real binary images were created using the RANDOM model in IDRISI, based on normal distribution with a mean of zero and a standard deviation equal to the RMSE (0.10) of the original DEM. The binary images represent the known errors to be added to the original DEM. These were then filled to remove sinks (Figure 6-2, (3)) and create 100 flow direction grids (Figure 6-2, (4)). Sinks are filled as opposed to previous chapters as flow accumulation is being determined.

However, not all parts of the study area will be flooded. Only areas with an elevation lower than 2.06 m (the maximum SLR scenario) are concerned. Therefore, the 100 DEMs created in the MCS were used to identify areas below 2.06 m and these were combined to provide 100 simulations of the areas' flow direction (Figure 6-2).

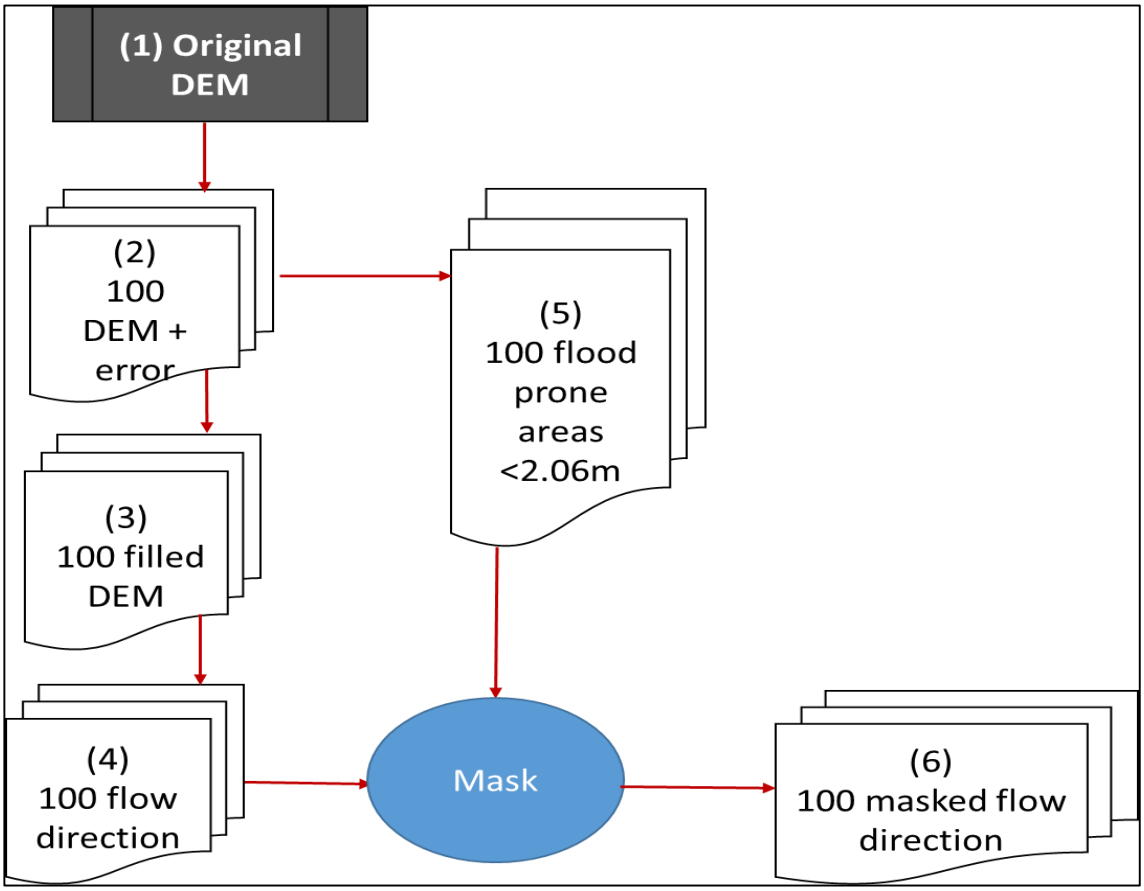

Figure 6- 2: Monte Carlo simulation to create 100 flow direction.

6.3.3.3. Weighted flow accumulation

The previous section indicated how the three main factors (land use, depth of flooding and depth of pooling), as well as each individual type of land use, were provided with weightings. These were input as weightings into the flow accumulation calculation in order to make the calculation consistent and take uncertainty into account. These were generated separately for each of the 100 simulations and combined with the land use map to create 100 collective weightings (Figure 6-3).

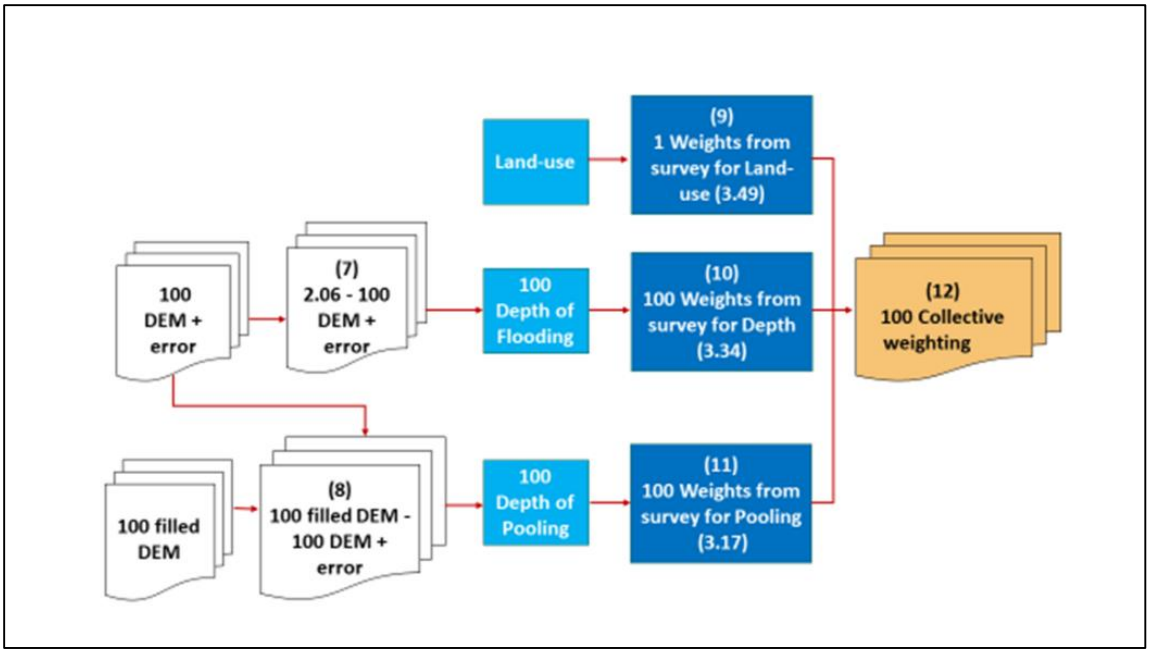

Figure 6- 3: Monte Carlo simulation to create collective weighting from three main factors influencing flow accumulation.

Finally, both simulated outcomes from the direction flow and collective weightings were brought together to calculate the weighted flow accumulation (100 times) for the study area. From this, an average weighted flow accumulation grid was calculated (Figure 6-4).

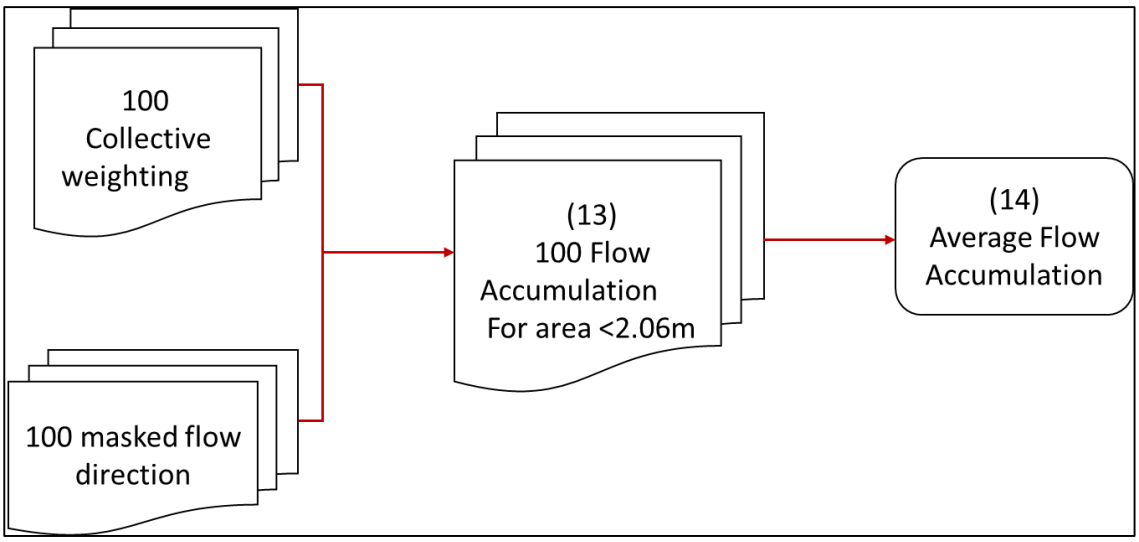

Figure 6- 4: Monte Carlo simulation to create average flow accumulation.

6.3.3.4. Generating barrier size

The previous section should calculate, for every cell in the study area, the benefits of preventing upstream flooding. This section produces, also for every cell in the study area, the likely size and costs of flooding barriers at these locations. To achieve this, the boundary of the potentially flooded area (catchment) was determined by using a flood probability map as produced in Chapter 3. The flood probability map was calculated using the results from the 100 simulations and reclassified into two categories: flooded and unflooded areas. Flooded areas were defined as those with more than a zero per cent flood probability. This was converted into lines indicating the boundary of the catchment.

The next step was to convert the boundary line into ten smaller segment lines. This was to make sure that the distance calculated from every point (cell) in the study area is correctly measured from one edge of the catchment to the other. The number of lines (polylines in ArcGIS) required will depend on the size of the catchment area. The bigger the size, the larger is the number of polylines required for selecting the distance between the nearest two polylines. The distance between each cell in the study area and the nearest two segment lines was calculated using the Proximal Generate Near Table function in ArcGIS. This helped to determine the distance between the flow accumulation point and the nearest two segment lines. This is illustrated in Figure 6-5. In panel (a), the catchment is divided into two lines and the distance from the one calculated from the

red point is determined. In this example the distance is incorrect. In panel (b), the catchment is divided into ten segments and the correct distance (i.e. length of barrier) is calculated. The subdivision of the catchment boundary ensures that the narrowest distance for each flow accumulation point was selected as a potential area to build a barrier. The sum of these two distances provides an estimate of a likely barrier length for each point. An estimated barrier height was calculated using the flooding depth value at this point. Then the volume of the barrier for each point was calculated, assuming that each barrier was a cuboid with a 1 m width (length x height x 1 m).

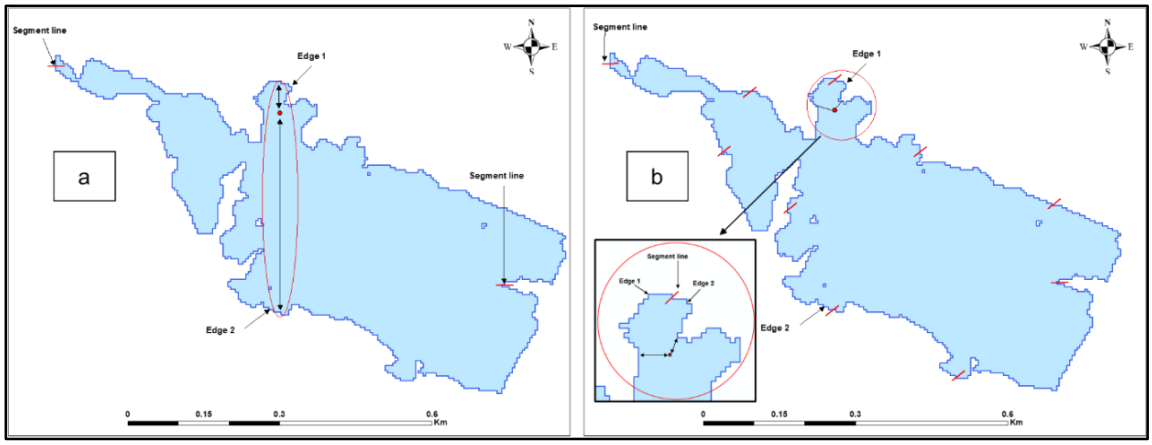

Figure 6- 5: Calculating the distance between the two edges of the catchment to determine the length of a possible barrier.

6.3.4. Identifying suitable barrier sites

6.3.4.1. Barrier size and its relationship to weighted flow accumulation

For every point in the study area, the relationship between the weighted flow accumulation and the barrier size is an indicator to determine suitable barrier locations. Suitable sites are likely to be those where weighted flow accumulations are high (i.e. large benefits of protection) but with relatively low barrier sizes (i.e. less costly to construct).

For every point in the study area, the weighted flow accumulation value was plotted against the volume of the barrier to determine potential sites (containing several sites in each area) for building the barrier. Potential barrier sites were visually selected based on Figure 6-8. Potential sites were then examined in a second-stage process to determine their potential suitability in more detail. This second stage is now described.

6.3.4.2. Cost-benefits of the site selection

Potentially suitable sites were selected. To decide on the final site for building the barrier in the study area, further analysis was undertaken on a limited number of sites. A more accurate barrier volume was generated along with the average flow accumulation (based on the MCS) by determining a height profile and the length of each barrier using the profile tools in ArcGIS. The flow accumulation at every point along this barrier was obtained by calculating the maximum flow accumulation for each simulation and by averaging all the maximum flow accumulations. This will allow us to identify the maximum flow that the barrier can prevent in each scenario. Finally, the cost of each barrier was divided by the weighted flow accumulation to estimate a cost-to-benefit ratio.

6.4. Results

The questionnaire was distributed to 50 people from various professions and 42 responses (17 males and 25 females) were received. Thirteen participants work at Qatar University, 12 work at the Ministry of Municipality and Environment-Urban Planning, eight participants work at the Ministry of Transport and Communication (land transport), five at Planning and Statistics Authority-Information Systems, two at Sultan Qaboos University (geography department) and two at the Arabian Gulf University (geo-informatics).

The age of participants ranged from 20 to over 51 years old, with ten participants from 20 to 30 years old, 15 participants from 31 to 40 years old, nine participants from 41 to 50 years old and eight participants over 51 years old.

As part of the questionnaire the respondents weighed the three factors (land use, depth of flooding and depth of pooling) influencing the flow accumulation. This was done in pairs in the first three questions. The results (Table 6-1) shows that the majority (over 75 per cent) thought that the three factors are important by giving scores of five or more.

Table 6- 1: Results from the questionnaire for the first three questions (number of responses).

Question-1:	How important do you rate the following factors to protect Qatar coastal area from flooding?						
Weighting	**1**	**2**	**3**	**4**	**5**	**6**	**7**
1. Land use (Residential building, commercial, roads, industrial sites and undeveloped land)	1	1	1	1	3	9	26
2. Depth of flooding (Depth of water in flooded area during the flooding)	0	2	2	5	6	6	21
Question-2:	How important do you rate the following factors to protect Qatar coastal area from flooding?						
Weighting	**1**	**2**	**3**	**4**	**5**	**6**	**7**
1. Land use (Residential building, commercial, roads, industrial sites and undeveloped land)	1	0	2	1	6	9	23
2. Depth of pooling (Depth of water that remains inland after flooding)	2	2	1	5	7	7	18
Question-3:	How important do you rate the following factors to protect Qatar coastal area from flooding?						
Weighting	**1**	**2**	**3**	**4**	**5**	**6**	**7**
1. Depth of flooding (Depth of water in flooded area during the flooding)	0	2	1	3	5	9	22
2. Depth of pooling (Depth of water that remains inland after flooding)	1	2	3	4	5	5	22

The responses were surprisingly similar in terms of the importance of these factors, with most of the participants agreeing that almost all the factors were important, with little differentiation in the weighting they gave to each factor. This may have been avoided if the questionnaire was designed in a way that could force the participants to choose between one of two factors. For example, if they said one factor is scored highly (e.g. six out of seven) by default the weight for the other factor would be low (e.g. one out of seven).

In the fourth question the participants assessed the importance of the six land-use categories in case of flooding. Residential buildings and roads were the most important land use, with more than 50 per cent of respondents giving them the highest score (seven). This was followed by

industrial sites, commercial and agriculture and farms, with more than 50 per cent of the participants giving a score of five or more. Undeveloped land was the least important, with more than 75 per cent of participants giving a score of five or lower (Table 6-2). It was somewhat surprising that such similar results were produced for each land use.

Table 6- 2: Result of the land-use weighting for all six categories (number of responses).

Question-4:	How important do you rate the following land uses to protect Qatar coastal areas from flooding?						
Weighting	1	2	3	4	5	6	7
1. Residential building	0	2	0	1	4	6	29
2. Roads	1	1	1	1	4	12	22
3. Industrial sites	0	0	4	1	8	9	20
4. Commercial	0	1	2	6	7	10	16
5. Agriculture & Farms	2	1	5	9	8	7	10
6. Undeveloped land	7	5	7	8	10	2	3

Based on the participants' responses, the total weighting for each factor was determined out of ten, with the land-use factor scoring highest (8.79 out of ten), followed by depth of flooding (8.42 out of ten) and depth of pooling (8.01 out of ten). These weightings were normalised (Table 6-3) and the final weightings were used when the three factors were combined to create a collective weighting.

Table 6- 3: The final weighting for the main factors influencing flow accumulations.

Factor	Average Weight	Final Weight (out of 10)
Land use	8.80/25.23 *10	3.49
Depth of flooding	8.42/25.23 *10	3.34
Depth of pooling	8.01/25.23 *10	3.17

A similar approach was used to calculate the weighting for each land-use category, giving the highest weighting to the residential building (9.1 out of ten), followed by road (8.7 out of ten), industrial sites (8.4 out of ten), commercial sites (8.1 out of ten), agriculture and farms (seven out of ten) and undeveloped land (5.3 out of ten). In the study area, only three land-use categories

existed; these were industrial sites, roads and undeveloped land. All those weightings were used to create a collective weighting map. An example is shown in Figure 6-6.

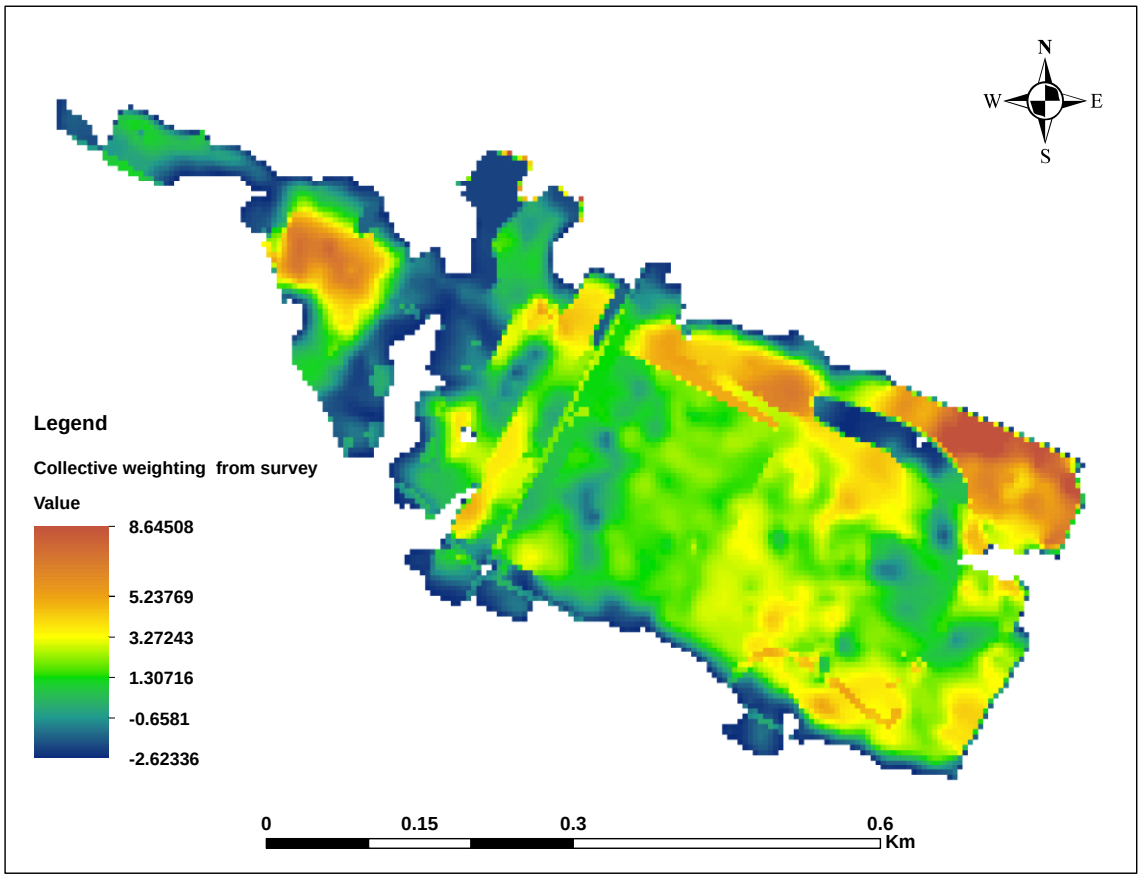

Figure 6- 6: Collective weighting for all three factors influencing flow accumulation.

The average weighted flow accumulation produced for the selected study area using 100 MCSs with collective weightings is shown in Figure 6-7. The value of the flow accumulation ranged from zero to over 14,000. The pixel value in the weighted flow accumulation map represents the total number of cells that flow into each cell and are weighted by their land use, depth of flooding and depth of pooling.

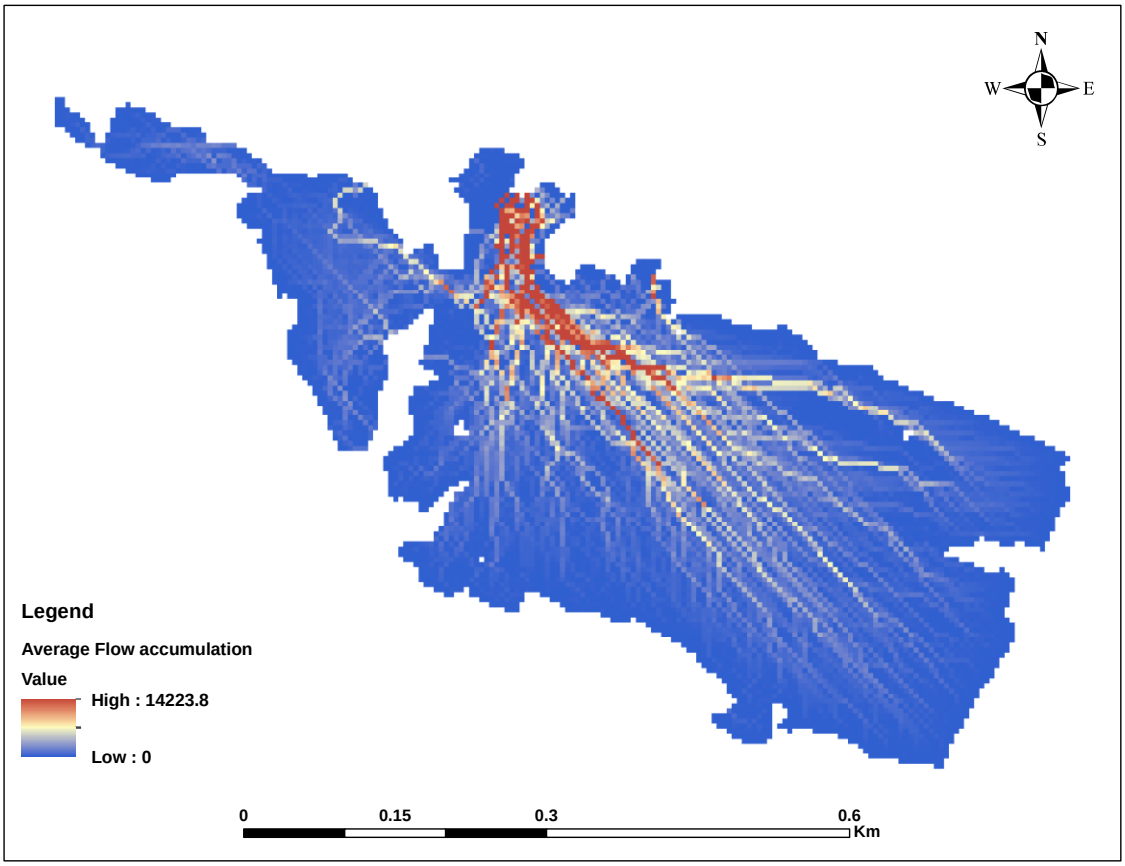

Figure 6- 7: Average flow accumulation based on the MCS.

For each pixel in the average weighted flow accumulation map, the potential barrier volume (likely costs) was calculated and plotted against the weighted flow accumulation value (flood protection benefits) (Figure 6-8). The flow accumulation map shows that the study area represents a flat topography, therefore a small change in elevation will make noticeable changes in the flow accumulation. The flow accumulation increases towards the coastal line from the surrounding area.

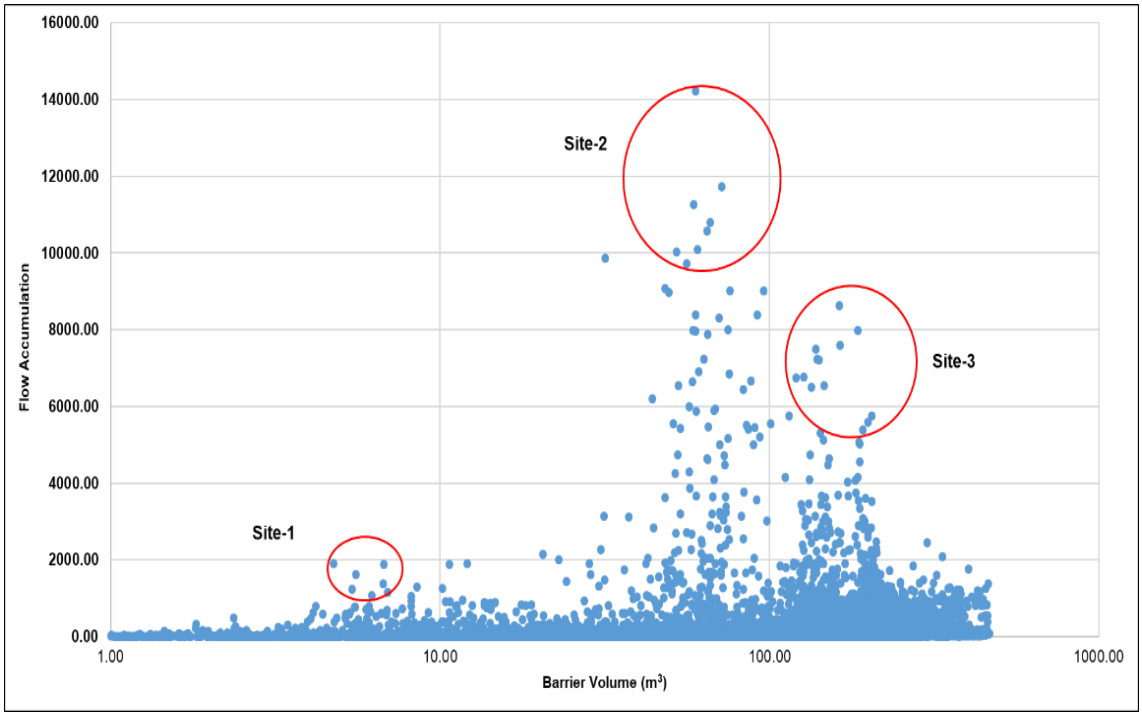

Figure 6- 8: Relationship between flow accumulation and distance between two edges of the catchment.

The results show that a plot of barrier volume (cost) and weighted flow accumulation (benefits) is potentially an effective visual method to select sites for building barriers. Sites with high weighted flow accumulations in comparison to their barrier volumes are clear to see. Based on that principle, three groups of points were selected at three different distances with the highest flow accumulation. These were site-1, site-2 and site-3 (Figure 6-9). In each site, one point with the highest flow accumulations was selected. In site-1, the weighted flow accumulation was 1894 and the barrier volume was 4.76 m^3. In site-2, the flow accumulation was 14,223 and the barrier volume was 59.71 m^3. In site-3, the flow accumulation was 7977 and the barrier volume was 185.47 m^3. The reasons for selecting the three sites was to explore the costs and also the benefits at each site in more detail.

Initially, a fourth site was selected close to site-2, but this site was removed from the analysis. This was because, although it had a high flow accumulation in some simulations, these were very variable as changes in the DEM led to water leaving the study area and entering the coastline in different locations.

Once the three potential sites were identified, further details on each of them were obtained. In each site, a straight line connecting the two edges of the catchment were selected as the location for the barrier. A cross-section profile of the barrier based on the maximum SLR (2.06 m) was determined to calculate the volume of the barrier (assuming a width of 1 m).

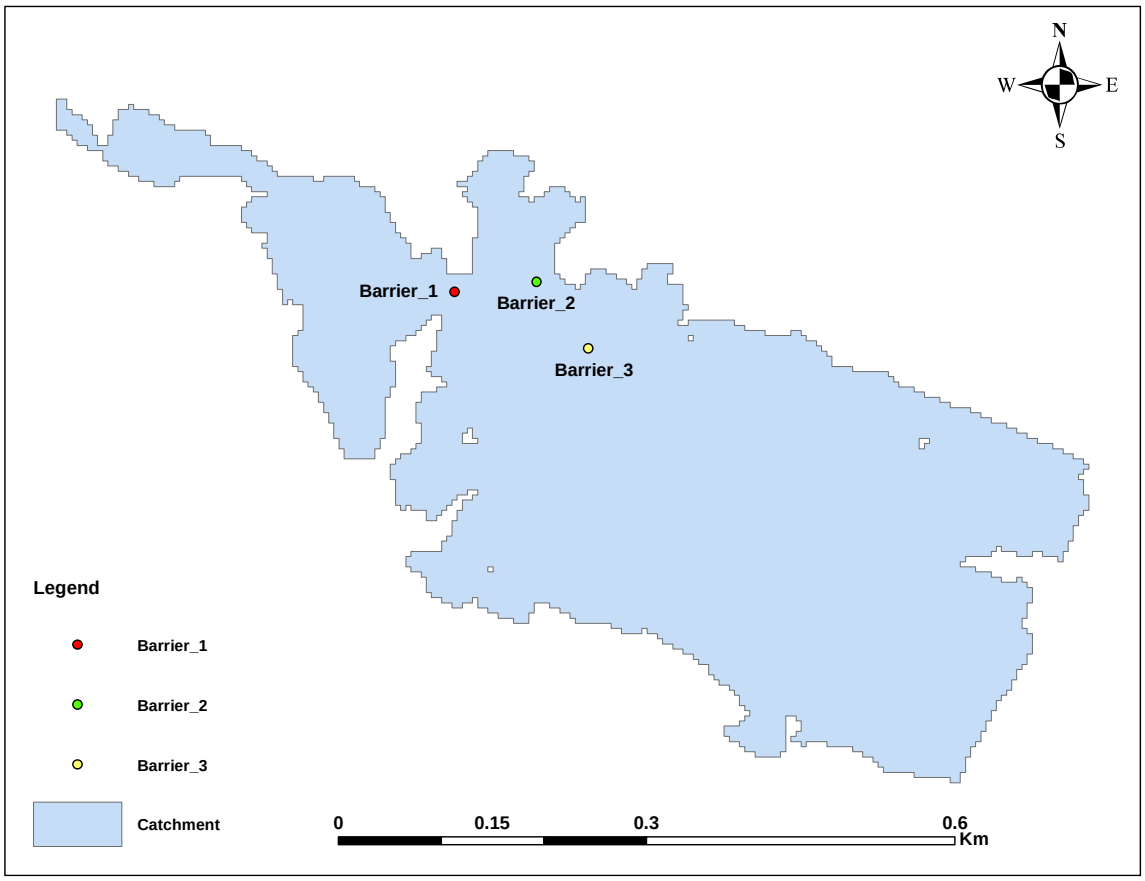

Figure 6- 9: The location for the three selected sites.

The volume of the barrier in site-1 (blue line) was the smallest, with 11.90 m^3. The barrier in site-2 (orange line) was 244.13 m^3, and the third barrier (black line) had the largest volume of 2561,87 m^3 (Figure 6-10).

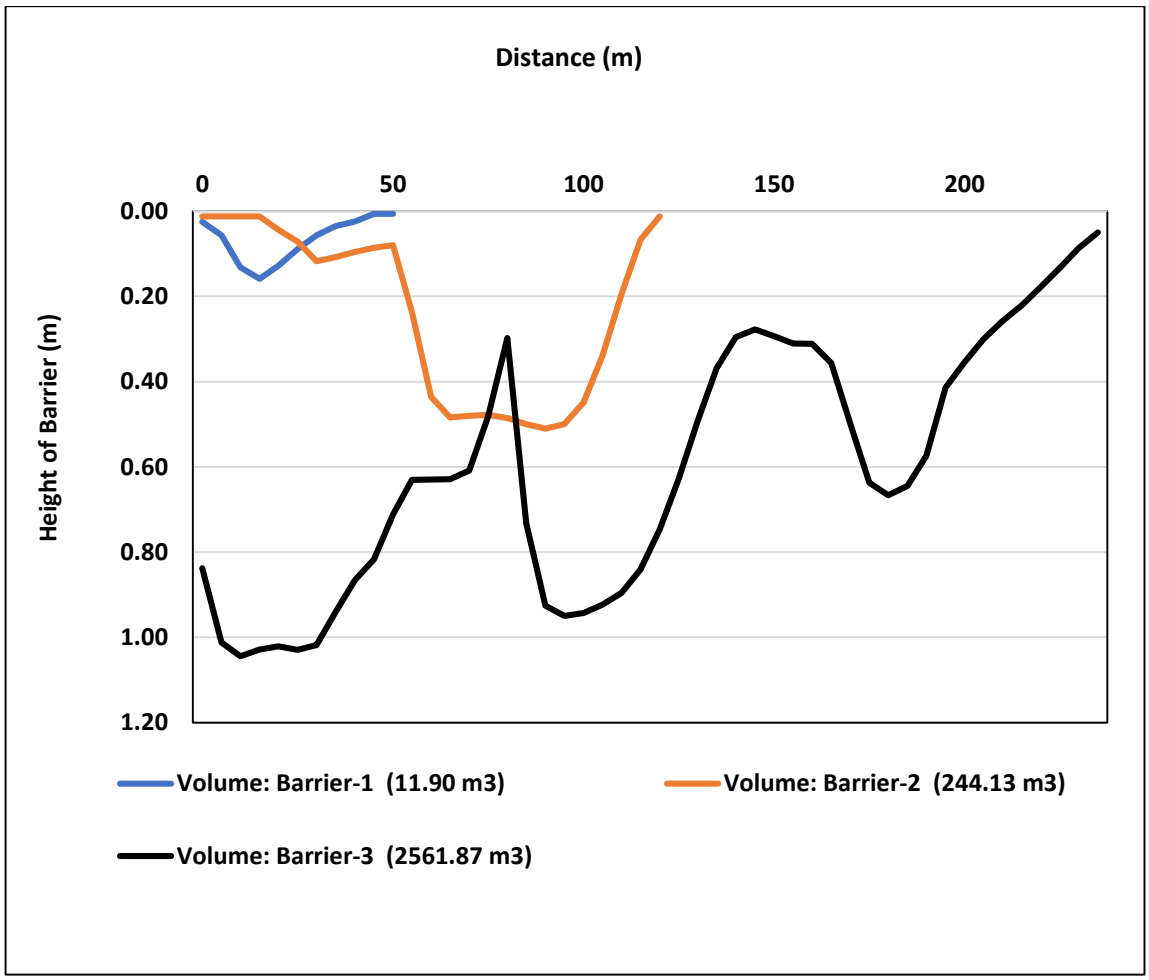

Figure 6- 10: The profile of the barriers in three sites.

Similarly, the summed average flow across each barrier was calculated to obtain a better estimate of the flood protection benefits (Figure 6-4).

The protected area by each barrier was identified (Figure 6-11). Barrier one protected only 15 per cent of the study area, while barrier two provided a maximum protection of 96 per cent. The barrier in the third site only protected 74 per cent of the area.

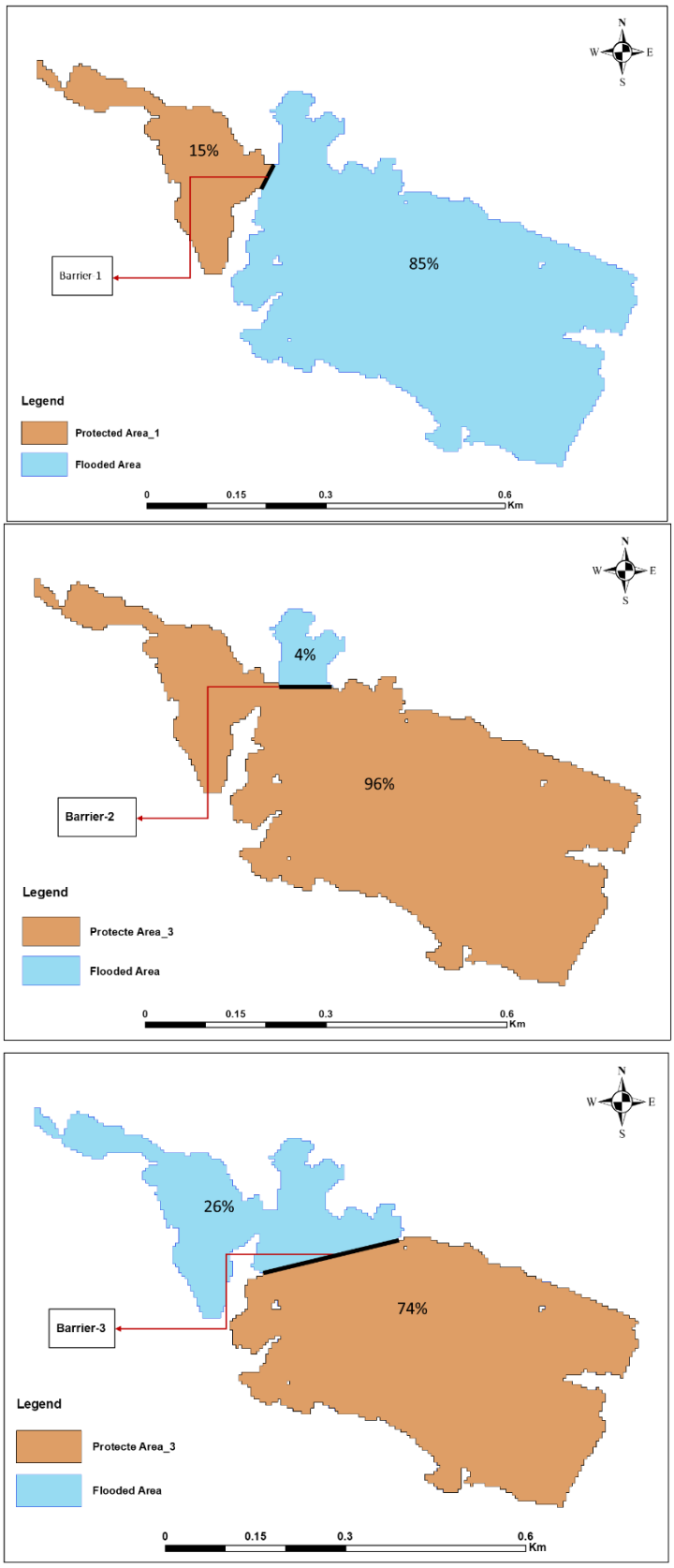

Figure 6- 11: Protected area from flooding in three selected sites.

The benefits for each site were calculated based on the weighted flow accumulation and the cost based on the volume of the barrier. The weighted flow accumulation was divided by the volume of the barrier to provide a benefit-cost ratio (Table 6-4). Site-3 was revealed as the lowest (6.35) because it has the longest barrier and does not protect the whole study area. This was followed by site-1, with a ratio of 30.76. It has the smallest barrier volume and protects a small area from flooding. The site with the best benefit-cost ratio was site-2. The ratio of flow accumulation to the volume of the barrier for this site was reasonable and protects 96 per cent of the study area (Table 6-4). For each barrier, the areas and percentages of different land uses protected is also presented in this table.

If the cost of the barrier (volume) was the only important factor (not the protected area), the barrier at site-1 would be the best option.

Table 6- 4: Protected areas and the cost-benefit ratio for the three barrier sites.

Name	Volume of the barrier (m^3) from profile	Total average Flow Accumulation	Protected area (m^2)				Benefit: Cost Ratio (flow accumulation/ volume of barrier)
			Roads	Industrial sites	Total protected area	Proportion of protected areas to the total flooded area	
Barrier 1	11.90	2,440.02	996.00	1,104.00	38,667.00	15%	2440.02/11.90 = 205.04*0.15= 30.76
Barrier 2	244.13	32,656.42	4,513.00	4,686.00	245,243.00	96%	32656.42/244.13= 133.77*0.96= 128.42
Barrier 3	2,561.87	21,999.19	3,510.00	3,323.00	189,169.00	74%	21999.19/2561.87= 8.5*0.74= 6.35

6.5. Discussion and conclusions

Providing a robust method to estimate future flooding as the result of climate change is crucial for minimising the impact on coastal areas. The main challenge in developing a method is the uncertainties associated with many parameters included in the calculations. Taking uncertainties into consideration will help policy makers to make better decisions on future planning. This is important to justify investment.

The reviewed literature showed that there are many methodologies developed for site selection. However, most of those studies focused on flooding from rivers. A few of them investigated the SLR inundation, however, the uncertainties associated with the factors included in the calculation were not considered.

This study has developed a new methodology for identifying critical areas to build barriers for protecting coastal areas from sea level inundation. These methods can be used to address the challenges of current coastal flooding caused by climate change. There are several areas where this study made a contribution by improving the methodology, most notably by including uncertainties. Key among these was where the study took DEM uncertainties into account. This study used 100 simulated DEMs instead of one representation of the ground elevation. This allowed the creation of 100 flow directions as inputs to the average flow accumulation. In addition, uncertainty was also included in the calculation of impact measures. Measures of impact by depth of flooding and depth of pooling also varied according to DEM simulation. Including uncertainties in the site selection is a new approach, as previous researchers used one DEM to estimate the potential flood risks (Mannan et al, 2018; Boateng et al, 2016 and Li et al, 2017). Only DEM uncertainty was taken into account, but future research could incorporate uncertainty in SLR.

Another advancement of this study is the use of a questionnaire approach to give weightings to factors that were used to develop measures of impact. This reduced the subjectivity in weighting the factors in case values were derived from one person and was used for weighting each of the individual land uses and for weighting land use against depth of flooding and depth of pooling. Surprisingly, the participant weighted all three factors very similarly. This might be due to unfamiliarity with a weighting approach, and one solution might be to rank factors forcing the participant to select the most important one. However, this method could be improved. It is important to understand which views should be considered in site selection studies. One development would be to target participants from a wider range of backgrounds and interests rather than just academics. This would provide a more representative weighting for each factor. It could also have been possible to conduct a survey of key decision makers and stakeholders in the study area. Other studies reviewed, as part of this study, did not use questionnaire approaches to develop measures of impact accumulation, e.g. Fedorov et al. (2016). Another problem potentially identified was that all factors were provided with high impacts by questionnaire respondents. This was surprising, as one would expect that much higher values would be given to the protection of roads as opposed to unused land, as an example. The reasons for this are unclear but will mean that

the methods produced to identify suitable barrier sites will not differentiate hugely between areas with different land uses. Future work could use qualitative surveys to understand more fully the weightings produced. In addition, it would be useful to repeat such an analysis in different country settings.

Measures of impact based on weighted flow accumulation are key aspects of this study. When selecting a site, the costs of barrier construction are important as well. In this study, the cost was estimated based upon the shortest distance between the two sides of the catchment. This process was automated in the ArcGIS, allowing us to identify the narrow valley-shaped areas. One limitation of this methodology was the time involved in manually splitting the catchment. Automating the catchment splitting process would be an important area for further development.

In addition, when estimating the volume of the barrier the scoping method simply assumed that the barrier was a cuboid shape. Further development using the profiling tools in ArcGIS might provide an automatic way of generating a more accurate barrier volume and cost.

As part of the methodology, barrier volume was plotted against the weighted flow accumulation (measures of impact). This visual method of cost-benefit comparison was found to be useful for identifying sites for further analysis. This is an important step when the scope of the study covers large geographic areas, minimising the cost and the time of investigation in the site selection process.

This method has the potential to provide decisions globally, with tools for prioritising decisions on where to build barriers to prevent future flooding from SLR. Taking uncertainties at all stages of modelling and flood forecasting into account will help decision makers to minimise the risk in their planning and investment decision-making process.

The method proposed in this study will provide a tool for allocating resources to prevent the environmental consequence of climate change and improve future coastal environment.

In Qatar, most industrial activities, especially in the oil and gas industry, are concentrated in the coastal areas. This study will provide a tool for those companies to plan and manage the risk of climate change and mitigate consequences of SLR in the future. The economic benefit of protecting those areas from flooding is important for the wider economy of the country. Therefore,

prioritising the areas based on the risk of flooding and the identification of the right areas to build barriers will help decisions on future investments by companies operating in those areas.

The method developed in this study has a wider implication for other countries like Qatar that are under the threat of SLR and climate change. The key contributions from the method in managing the risk of SLR are:

- Accounting for DEM uncertainty to provide a better understanding of events, such as SLR caused by climate change.
- The inclusion of stakeholders' views for weighting the factors in the multi-criteria evolution is important. It provides a comprehensive and balanced approach to MCE.

6.5.1. Limitations and future research

Several limitations were identified during this study; the key limitations were:

- Due to time and resource constraints, this method was only validated in a small part of Qatar. Future studies need to look at other areas with different topographical characteristics in comparison to Qatar, which has a very flat topography. Also, future work could look at areas with a wider range of land use and stakeholders. It might also be possible to explore the best sites for barrier construction for different stakeholders. Different stakeholders may have different views.
- This study assumed that all barriers have the same shape (rectangular cuboid) to calculate the volume; this might not be the case for all the sites. Future work to provide more details on the exact shape of the barrier is done in the second stage of site selection. It may provide a better understanding of the cost of the barrier at the first stage.
- In order to compare the benefits of building each barrier, the volume of the barrier was compared to stated preferences of impacts. Future work could include a full cost benefit assessment to provide a more realistic value for building the barrier. Davlasheridze (2019) used various economic models to estimate the cost-benefit ratio of the coastal barrier in the USA. This study used many economic factors, including the cost of

flooding to residential areas and production losses in manufacturing activities due to flood disruption. Such an approach could be developed into this study.

- Most of the analysis depends on the original elevation point data sets and their accuracy. A higher accuracy of elevations for this type of analysis might improve the analysis, especially for areas closer to the sea. The RMSE of the DEM in this study was 0.10 m. However, in this study a MCS was shown to be an effective way of accounting for the uncertainty in the DEM calculation. Therefore, a higher accuracy DEM might not improve the site selection greatly but would certainly need much larger processing power and time if it led to smaller cell sizes.

Chapter 7: Conclusion and Recommendations

7.1. Overview

Among the many consequences of climate change, SLR ranks as the most critical. This is because more than 20 per cent of the world's population lives within 100 km of the coast and less than 100 m above sea level (Nicholls et al., 2007). This means that even a relatively small SLR can pose a significant threat to human society. By comprehending the severe impacts of SLR, the scientific community has devoted significant efforts to building mathematical models to simulate and project climate change based on SLR. These studies, reported in the literature, have projected future SLR and indicate that it is not spatially uniform (Barron, 2012; Beatley, 2012; McGuire, 2017). Building upon these studies, the aims of this thesis were:

- To apply and evaluate various spatial interpolation methods and techniques to generate high resolution DEMs in complex urban areas.
- To assess the SLR inundation in a coastal area.
- To quantify the impact of uncertainty in the DEM and in SLR estimates upon flooding projections.
- To evaluate the importance of taking spatial autocorrelation into account when modelling the impacts of uncertainty.
- To explore methods to identify critical areas for barrier construction to prevent sea level inundation.

This chapter will now reconsider each of these research objectives, summarise the main findings and consider the wider implications for the scientific literature.

7.2. Data limitations

There are several data limitations of the analysis undertaken in this study. First, accessing good quality data is limited in Qatar, for example, the elevation data was particularly good in terms of spatial distribution, but it was not up to date. The other data sets, such as land use, detailed storm

and coastal erosion data sets, were not readily available. Likewise, there were many limitations in accessing data in Qatar:

- The government departments and agencies have long procedures to access data for academic purposes.
- Most of the data sets were hard copy, especially tidal data sets.
- Most of the data sets were not up to date.

The other limitation is that, due to time and resource constraints, this research was conducted only in parts of Qatar. Future studies need to look at other areas with different topographical characteristics in Qatar, and also other areas globally to see whether the techniques developed and the results obtained are the same in different settings.

7.3. Summary of the research findings

Objective 1: To apply and evaluate various spatial interpolation methods and techniques to generate high resolution DEMs in complex urban areas.

As highlighted in Chapter 1, one key challenge in the flooding literature is the generation of DEMs in complex urban areas of a sufficient spatial resolution (Wang et al., 2018). High accuracy DEM has been proved to be an important input in modelling future SLR (Gesch, 2018). This is addressed in Chapter 3. In this chapter I applied and evaluated a number of different interpolation techniques to produce a grid with a spatial resolution of 5 m. This was generated from points with an original horizontal resolution of 10 m. In addition, the original points were a bare-earth model, with buildings and other features removed to leave "gaps" in the elevation data. Yet these areas are important to consider in an evaluation of areas subject to flooding. Hence, we explored a number of techniques to account for these data "gaps".

Four interpolation techniques were investigated to generate an accurate DEM, namely IDW, spline, kriging (with four different semi-variogram models) and TIN. The DEM was created for the five locations (Doha, Mesaieed, Al Khor 1, Al Khor 2 and Al Thakhira) and the performance of each interpolation technique was evaluated using RMSE. In this study, the performance of IDW, spline, kriging and TIN were assessed in order to generate the most accurate DEM for the studied

area. This is justified by the flat nature of the study area. As there is very little evidence in the literature on the performance of TIN to generate DEM, it has also been incorporated in Chapter 3.

Initially, three different data interpolation methods were used to create the DEM from elevation points spaced at 10 m to produce a DEM at 5 m horizontal resolution. These were IDW, kriging and TIN.

The stated accuracy of the elevation points was ± 10 mm vertical. At the outset of the chapter, the stated accuracy of these points was further validated by visiting a number of sites in the study area. The result of the survey showed that all 33 visited points had an error of less than a metre, with an average error of 33 cm. This meant that 78.8 per cent of the points had errors of less than half a metre and 51.5 per cent had less than 25 cm of error. This was lower than the stated vertical accuracy of the elevation data and in most cases the recoded elevation in the DEM was lower. However, only 33 points were compared, making robust comparison difficult. Also, the validation occurred several years after the elevation data was produced and the landscapes may have changed in the intervening period. Future research should have many more validation points closer in time to when the original survey was taken. Should this occur, then it would be more straightforward to validate the accuracy of the original points and incorporate this into analyses.

When the main interpolation was undertaken the overall results showed that IDW performed better (with lower RMSE value) than kriging, while TIN was the least accurate interpolation method (highest RMSE values) in predicting the elevation values. This is not unexpected as most of the interpolations were from regularly spaced points (Li & Heap, 2014; Burrough, McDonnell & Lloyd, 2015). Overall, the difference between kriging and IDW was not large, but IDW showed slightly better results. The average RMSE difference between the best kriging procedure and IDW was 5 cm.

The DEMs then had to be enhanced by exploring various options to include break lines. Breaklines delineated areas within the study area where the elevation changed rapidly, and within which there were no elevation data. These commonly occurred in built-up areas, e.g. road embankments. The chapter explored incorporating breaklines as a series of points (with their elevations attached) or as barriers to interpolation. Breaklines contribute to an increase in the

terrain model accuracy in data reduction (Liu et al., 2011). The incorporation of breaklines decreases the data density and thus the DEMs produced are adequately accurate. However, in our study, due to ArcGIS limitations, it was only possible to incorporate breaklines as barriers using IDW or spline methods of interpolation (spline was not used in earlier simulations due to large computational times). The results indicated that using a spline technique, incorporating breaklines as barriers, provided a better DEM (with a lower RMSE) in comparison to IDW.

One limitation of using barriers in any interpolation is that it leaves "gaps" in the DEM where data is not interpolated. In this study we provide data for these "gaps" by replacing the values from neighbouring cell values. This is an important step to remove gaps resulting from using breaklines as barriers in generating DEM before assessing the accuracy using RMSE. The final DEM had an average RMSE in all areas of 0.10 m. The methods used in this section are not reported in the literature and may be a guide for future researchers generating DEMs in urban areas. However, because the RMSE calculations can only be performed from areas where there is elevation data, the true value of these techniques is unknown, i.e. it is difficult to know the true accuracy as we have calculated elevation in areas where there are no elevations on the data set. Future work could obtain real elevation data from these "gaps" and compare these to the values generated. Filling the gaps was required, even when creating DEMs for uniform water surfaces, by using conditional statements and functions of focal statistics (Gonçalves & Oliviera, 2004), indicating that this could be a better technique to create DEMs for different study areas. A comparison between the DEMs created without any smoothing to that extracted by including the gaps showed that the edited DEMs were found to have more accuracy in relation to a control DEM obtained from aerial photographs. It was recommended that editing based on the knowledge of the terrain can be adopted to increase the accuracy of the derived DEMs.

Our research demonstrates that different interpolation techniques produce different results and that, even within our study areas, no one interpolation technique was superior in all areas. Therefore, we encourage future research to explore different methods of interpolation to determine the best one for their study area (Li & Heap, 2014; Burrough, McDonnell & Lloyd, 2015). Inverse distance weighting, kriging and splines all worked reasonably well, producing similar RMSEs.

Triangulated irregular networks performed less well. It was also concluded by Polat et al. (2015) that any one interpolation technique cannot be underscored as a superior method of rasterization. They also found that applying TIN algorithms for the filtering process produced agreeable results for extracting DEMs, and the Natural Neighbour interpolation technique was more efficient in analysing terrain features. It was, however, suggested that the filtering parameters defined by the user will affect the results attained. Our research was conducted in relatively flat coastal areas and different results may be produced in areas with different elevations; future research needs to be expanded to other settings. A comparative evaluation of interpolation techniques has been carried out over terrains which are not uniform and it was concluded that different interpolation techniques are required for generating DEMs of different terrains (Binh & Thuy, 2008; Arun, 2013; Tan & Xu, 2014; El-Quilish et al., 2018).

Objective 2: To assess the SLR inundation in a coastal area.

The focal point of Chapter 4 was to develop methods to assess SLR in coastal areas. The literature review for Chapter 4 showed a large number of papers that assess SLR using a bathtub method, which simply reclassifies all cells below an elevation threshold as "at risk of flooding" (studies reviewed in Schmid et al., (2014)). In this chapter, to determine flooded areas, three methods were used. Firstly, the bathtub method, and then two further methods to ensure that the potentially flooded methods were connected to the sea. These were the four-side connectivity rule and eight-side connectivity rule (Poulter & Halpin, 2008) and the "eight-sided" rule was chosen by a recent study (Fu et al., 2017) as it was intended that overestimation could be more acceptable for planning purposes. The eight-side approach considers wider possibilities for hydrological connectivity and so is likely to produce a larger inundated area than the four-sided rule. Each of these was evaluated to select the most appropriate method to produce the final inundation map for all areas. It was somewhat surprising that the different methods did not produce hugely different results, except in Doha where the eight-sided rule produced a 0.86 per cent larger inundated area than the bathtub simulation. This was assessed and concluded to be due to the nature of the study area. Bathtub simulations usually present overestimations of inundated areas (Webster et al., 2004). The

literature review has shown that in many studies bathtub modelling is used for predicting the risk areas affected by SLR. This method is simple and can be used to obtain several SLR possibilities, identifying and assessing the associated risk of inundation. Models developed by the bathtub approach can be user friendly too. However, this chapter has shown that it is easy to calculate connectivity to the sea using the four or eight-sided connectivity rule, potentially producing a more accurate result in terms of flooding extent. Therefore, we recommend it for all future studies of SLR. The four and eight-sided connectivity rules produce marginally different results, but it is not possible to know which presents a more accurate assessment of flooding risk without ground truthing of results.

Many previous studies consider flooding as the level above the mean sea level (e.g. Mimura, 2013; Farinotti et al., 2019; Kirezci et al., 2020). This ignores the fact that flooding occurs on top of tidal extremes. This was incorporated in this study by calculating the SLR for three tidal states (HOT, Mean Sea Level and MHHW). A similar dynamic modelling approach integrated the factors of SLR and tides to model flood-hazard ensued by climate change (Barnard et al., 2019). It was predicted that the magnitude of flooding could increase the coastal water levels significantly, which could amplify the threat to the population and infrastructure along the coast. In terms of climate change there is additional future uncertainty as to the level of SLR, so this was calculated for both RCP 4.5 and RCP 8.5 scenarios and for the minimum, average and maximum simulations of those RCPs. We demonstrate how such uncertainty is relatively straightforward to incorporate into assessments of future flooding. We recommend such approaches for future studies.

The total SLR (RCP + Tide) was calculated for both RCP 4.5 and RCP 8.5 scenarios (maximum, average and minimum RCP scenarios) and three tidal states (HOT, Mean Sea Level and MHHW) as mentioned earlier. This chapter demonstrates how uncertainty can simply be calculated and presented. The results indicate that, for both RCPs in Al Thakhira, the inundated areas will increase as the SLR increases. The large area of flooding would be mainly due to the elevations in Al Thakhira being low. The effect of SLR in both Al Khor 1 and 2 would not be large as the elevations in both areas are higher in comparison to Al Thakhira. In Doha, the SLR would only create flooding in less than two per cent of the area under the maximum RCP 8.5 with HOT.

One challenge in producing such estimates of flooding is that it is not possible to know if they are correct. They are simulations. Future research could compare current flood extents from high tides to those predicted for high tides from our models. This would provide some data on whether the results that are produced are accurate or not. Chapter 4 also demonstrates comprehensively how uncertainty associated with RCP prediction can be quantified and displayed to enable the reader to make an informed assessment on the potential impact of flooding or to compare different RCP scenarios (Stammer et al., 2013). However, ensuring that decision makers implement and utilise uncertainty information is a challenge for future research (Deitrick-Hirsch et al., 2010). The concept of uncertainty inherent in GIS-based modelling, however, is new to decision makers or risk managers (Zerger, 2002). There is an urgent need to make uncertainty explicit to these professionals by simulating error in deriving spatial models that can be evaluated by decision makers with relative ease for risk management. Geographic information systems and spatial modelling provide a spatial context in predicting risk, and this is an emerging science that has the potential to be applied for diminishing natural hazard risk. Thus, GIS techniques can evolve to apply minimum data, with less complexity, and improve the level of risk modelling that integrates uncertainty if the inputs by decision makers are considered early in the process. Improved decision making can be achieved when the risk mapping is tailor-made to policy goals. All the possible interpretations of our flood prediction maps by policy makers in Qatar can be another topic for furthering this research. This transformation of GIS into a tool critical to decision making can be a new challenge. The map outputs, from both computer and manual sources, can be powerful in visualising risk assessment that can aid in decision making (Zerger, 2002). Future studies can focus on cartographic representation of analogue maps by including cartographic elements like colour, shade, hue, generalisation, symbols and other cognitive variables. This is to improve the human interaction aspect that seems to be lacking in GIS, as a GIS researcher is more conscientious about the software, spatial data and spatial modelling issues but not on human sensitivity. Future research can also consider non-technical issues like assessing the utility of models and applicability of spatial data for decision making, which are usually barriers in the successful implementation of GIS models regardless of the natural hazard under study.

There are limitations to the work undertaken in this thesis. One such constraint faced is that the drainage systems (e.g. draining pipes under roads) within the study area and other infrastructures that effect the hydrological connectivity, such as current and planned barriers, were not considered. Also, there is no data currently available for such mitigation structures in Qatar. These will affect the inundation mapping due to SLR and including future drainage infrastructures, such as canals, ditches and culverts, may remain a challenge in future flood mapping (Gesch, 2013). Also, the tidal flows are different in various locations due to varying coastal configurations, and these were not accounted for. It also does not include the impact of wind and wave patterns and, as such, it is not fully capable of forecasting floods from events like storm surge. All these can be potential topics for future research on inundation risk due to SLR in Qatar. Ground truthing existing floods (explore the impact of existing floods) would be one method of assessing the potential importance of these. Flood predictions were assessed against ground-truth using social media, remote sensing and map data (Rosser et al., 2017) for mapping rapid flood scenarios and simple procedures. Social media surveys were found to be critical in flood risk assessment.

Future research is also needed to more fully capture SLR. Global SLR scenarios were used in this study, but local conditions may lead to different values in the Gulf (El Raey, 2010). A related point is that a more detailed consideration of potential storm surges, for example, by looking at a much longer sea level data set, would also have been helpful. For future inundation assessment studies, the potential change of land topography during SLR and the inundation process should be considered to better capture the potential impacts, especially at a local scale. For example, maps of land use, elevation and spatial attributes were overlaid to obtain damage units (Jonge et al., 1996). Depending on the types of land use, four different categories are prone to damage, such as public entities, private ownerships, industry and agriculture were derived. First, the possibility of flooding of the damage unit was checked by the damage assessment model, based on the flooding level exceeding a certain threshold. If there is a possibility of flooding, a function of damage, along with the land use type, were applied to estimate the damage. However, a major limitation of many studies on SLR-related inundation mapping is that they consider the coastal topography and inundation as static entities, which are greatly dynamic in reality (Leon et al., 2014). They also

assume that SLR is a gradual phenomenon and the coastal zone is not impacted much by it, but this is apparently incorrect as the coastal zone changes with storm surges or SLR. However, it is practically impossible to estimate the future topography. Nevertheless, future research can attempt to combine the storm surge modelling and flood mapping with SLR.

Another actual change that could be included is the change in population, which cannot be known. Future research can also evolve analyses where urban and population growth scenarios are included, though this might increase the complexity of the analyses (Mondal et al., 2012; Kim et al., 2019). In this study property and/or infrastructure values are not accounted for and the potential losses of the same due to coastal inundation have not been estimated. This analysis can be pursued in further research endeavours, which can be utilised in deciding local adaptive measures and other cost-benefit analysis. Future research on adaptive measures for mitigating coastal inundation due to SLR and decision making on investments in coastal management can be built on the current findings. They can also address the gaps described above (e.g. Hinkel et al., 2013; Refaat et al., 2016; Barnard et al., 2019).

Coastal erosion, especially under rising sea levels, can change the current DEM and it is another phenomenon that was not considered in this study. This could affect the area at risk of flooding and its hydrological connectivity (Coveney and Fotheringham, 2011). Further research can be focussed on developing models that can overcome all these critical challenges.

Objective 3: To quantify the impact of uncertainty in the DEM and in SLR estimates upon flooding projections.

In Chapter 5, MCS were used to predict inundation, exploring the uncertainty in the DEM alongside uncertainty in the SLR scenario. As well as being scientifically justified, MCS have the additional advantage of presenting one probabilistic output (map) as opposed to multiple maps (e.g. minimum, maximum, average SLR). To fully assess the potential impact of climate change on SLR and consequent flooding, it is paramount to consider uncertainty, providing decision makers with a more complete picture of future SLR.

The previous chapter has demonstrated how the methods used to generate DEMs introduce additional uncertainties, as highlighted by the different RMSEs. Chapter 2 has outlined sources of uncertainty in SLR scenarios.

Digital elevation model uncertainty was explored using MCS with random errors (based upon the RMSE calculated in Chapter 1). The error was assumed to have no spatial correlation. There are several papers in the literature that use such a method (e.g. Openshaw et al., 1991; Fisher,1991; Lanter & Veregin, 1992; Holmes et al., 2000; Schmid et al., 2014; Cooper & Chen, 2013; Leon et al., 2014). We aimed for 100 simulations to determine the probability of flooding to provide a balance between the time of data processing and the quality of the outputs, with a higher number of simulations expected to produce better outcomes despite the longer processing time. This was followed by the bathtub method, which generated 100 grids of flooded and unflooded areas.

Flooded areas connected to the sea were identified. Finally, a probability map was created, adding the final 100 images that indicated the probability of flooding in each cell. To compare the error and uncertainty in the original DEM and its impact on predicting flooding, three reclassifications were produced. The MCS for Al Thakhira was conducted and the probability map was produced. In Al Thakhira, an area probability map of DEM uncertainty was created for average RCP 8.5 scenario and highest observed tide based on MCS.

Monte Carlo simulations were also applied to assess the uncertainty in SLR to produce a probability map for the RCP. Although there is much research on DEM uncertainty, there is less research on how uncertainties in climate model projections may influence flooding extent (Collet et al., 2018), exceptions include Amante (2019). The uncertainty bounds in SLR scenarios (RMSE) were based upon the minimum, average and maximum stated SLR for each RCP scenario.

In order to make the comparison between the two probability maps, DEM and SLR, the probability map was reclassified into four categories based on the likelihood of flooding. The uncertainties in both DEM and SLR (RCP) scenarios were shown to have an impact on the outcome of flood probability. Most importantly, the probability of flooding for each pixel in both methods was compared and found to be reasonably similar. One very visible effect of DEM uncertainty was

the specking effect on the flooding probability maps, indicating adjacent cells with very different probabilities of flooding. This effect was less visible on the MCS of SLR, as the level of flooding rather than the elevation of the land was changed in each simulation.

To provide an overall assessment of the impact of uncertainty on flooding associated with SLR, we combined the two probability surfaces from SLR and elevation into one surface. There are few examples, if any, of this in the literature and we argue this provides a more complete picture of the likely impacts of flooding and we suggest for future research. One visual advantage of this approach is that the speckling effect seen on the MCS of the DEM is less apparent as the MCS from the SLR is a relatively smooth probability surface. It can be emphasised that using two probability maps was an important strategy as this method identified the flooded and non-flooded areas.

The outputs of multiple simulations produced a surface indicating the probability of flooding. This was performed on the Al Thakhira area and the probability map showed that a large part of the study area was very unlikely to be susceptible to flooding, with a probability of 0-5 per cent. These areas are mainly higher grounds, which will either remain above future sea level or are disconnected from the coast. Most of the areas with unlikely flooding (6-50 per cent) are located far away from the coastline and in the central part of the study area. The areas likely (51-94 per cent) or very likely (95-100 per cent) to flood are located near the coast, and these areas are particularly large in the north and south-east of the study area. The probability maps of both RCP simulations show that 27.2 per cent of the area has 95-100 per cent flooding and those created by simulation with DEM uncertainty show that 21.4 per cent of the studied area has 95-100 per cent of flooding. The combined output of RCP and DEM shows that the areas with significant probability of non-flooding (0-5 per cent) and flooding (95-100 per cent) when comparing the two methods was small (0.00 and 0.06 km^2). This is an important finding as the two methods are not producing vastly different results.

This study has shown that MCS have certain limitations. It took a long time and involved using multiple packages. It was not an integral part of ArcGIS, a commercial GIS package, and this is a

recognised problem. Although the assessment of error is still an important issue on the GIS research agenda, few commercial GIS packages incorporate the tools to permit this to occur in an easy manner (Duckham & McCreadie, 2002). This is argued to be because there is limited agreement on what constitutes "error" and the methods to collect and report it. Another relevant research topic could be the prevalence of error in GIS modelling and several methods that were described for the estimation of errors propagated. However, not all the methods are applicable to all types of processes. None of them are ideal as they involve approximations and some of them are time consuming (Heuvelink, 1999), but there is always the possibility of evolving a method appropriate for a research problem under study. Unfortunately, clear information about the errors related to different attributes studied in GIS is lacking, and if the values for these errors are not realistic the error propagation analysis cannot yield sensible results. Hence, performing error propagation analyses is not yet the norm in GIS practice and is mostly an exception. It is essential that the function of error propagation is added to the products by GIS manufacturers and map makers should produce accurate maps routinely, even when accuracy is mandatory. Computing output error may not be more significant than error analysis as the partitioning characteristic of error analysis lets one calculate how much output error is contributed by each individual input. Thus, users can explore how to reduce input error to improve the output quality and can weigh the cost benefit of stepping up the sampling. The impacts of input and model error can also be compared by using the partitioning property. Geographic information systems come with many free computational models, which can be employed by ignorant users who can easily disturb the balance between input and the model error, who may apply models to wrong scales or for improper purposes or add highly uncertain data to them. This can be avoided when error propagation analysis becomes the rule of GIS communities and the users are aware of maintaining spatial data quality, as well as the cursory nature of most metadata, the highly specialised nature of error assessment techniques such as MCS, and the negative image of the word "error" that usually falls outside of research.

Objective 4: To evaluate the importance of taking spatial autocorrelation into account when modelling the impacts of uncertainty.

When simulating uncertainty in Objective 3, the models assumed that the error was not spatially correlated. This is unlikely and neighbouring cells are unlikely to be extremely different in terms of error. One impact of this was the specking of adjacent higher and lower probability cells observed in the previous chapter. Another highlight of this research is Objective 4, where the potential impact of spatial autocorrelation in error is explored. This is a relatively novel approach for flood modelling, particularly in coastal flood modelling, and there are very few similar studies using spatial autocorrelation, as per the review of literature.

Error was introduced into the original DEM (in the MCS) at three levels of spatial autocorrelations (Moran's I of 0, 0.33 and 0.66). Accounting for uncertainty was a large part of this objective and the thesis in general. This often involved using multiple GIS packages, such as ArcGIS, IDRISI and R (to simulate spatially correlated error). This again suggests that GIS manufacturers should enhance their efforts to add the function of error propagation (Heuvelink, 1999). More automatic methods of producing such uncertainty assessment, such as error simulation tools built into ArcGIS, would have greatly aided this research. This again highlights the challenges of incorporating error simulations in commercial GIS packages (Duckham & McCreadie, 2002). Three flood probability maps were produced with Moran's I of 0, 0.33 and 0.66.

The results of Chapter 5 clearly show that the land areas flooded, and locations of these flooded areas were not hugely different between the three levels of autocorrelated error. However, the overall impact of spatial autocorrelation on the flooding probability maps appears to be fairly small, as explained in detail in Chapter 5, based on the tabulated results. For example, when the spatial autocorrelation in the error was set to zero, 6.73 km^2 of the area was susceptible to a high flood probability (95-100 per cent). When spatial autocorrelation in the error was set to 0.66, 5.67 km^2 of the study area was classified as susceptible to a high flood probability.

Where there were differences between the simulations it was possible to explain these based upon the nature of the study terrain. Incorporating spatial autocorrelation of error is supported in the scientific literature (Darnell et al., 2010), and although relatively complex to incorporate, it did produce meaningful results. However, it was not possible to know what the "correct" level of spatial autocorrelation of error was in reality. Hence, although different results were produced it was not possible to know which provided better representation of the DEM. The research therefore reaches no clear results as to whether future research should simulate spatially autocorrelated error. Future research could use ground truthing to overcome these issues, as well as find more efficient methods for incorporating spatially autocorrelated error into MCS.

Objective 5: To explore methods to identify critical areas for barrier construction to prevent sea level inundation.

As outlined in the introduction, there are many studies using GIS to assess the impact of flooding and also some studies assessing the most suitable location for freshwater dam location. However, there are virtually no studies using GIS as a decision-making tool to assess the most suitable location for dams to prevent coastal inundation. This is Objective 5. Geographic information systems were combined with MCE to identify and select optimal locations to build barriers that can prevent land inundation from SLR ensuing from climate change. This piece of work was particularly novel as MCS was used to take account of DEM uncertainty. Previous studies have not included this step (e.g. Al-Ruzouq et al., 2019; Adham et al., 2018).

The key steps of the methodology to select barrier locations were to identify a flow accumulation for every point in the study area, with each cell weighted using land use, depth of flooding and depth of pooling as a weighting factor affecting the value of the flow accumulation. For every point, the cost of building a barrier was then estimated based upon the distance from one side of the catchment to the other. The two values were then compared to produce an assessment of the cost/benefit ratio of building a barrier at any point in the study area. This study recommends that even a moderate investment could have major benefits in terms of protecting areas/people.

This methodology could be crucial for decision makers in Qatar and elsewhere to develop strategies to prioritise areas on which to build barriers for preventing future flooding from SLR. The methods developed in this study can be applied for flood mapping in other countries like Qatar that are under the threat of climate change and SLR. We argue that the methodology has potentially wide usage, but as it was developed in a relatively small area in a relatively flat coastal area of Qatar, different results may be produced in areas with different elevations. Future research needs to be expanded to other settings as has been done in various earlier studies, which showed that different terrains require different interpolation techniques (Binh & Thuy, 2008; Arun, 2013; Tan & Xu, 2014; Rishikeshan et al., 2014; El-Quilish et al., 2018). In the chapter, MCS were applied based upon DEM uncertainty and future work could incorporate additional elements of uncertainty explored in this thesis (e.g. SLR uncertainty, spatial autocorrelated error).

In this study, MCE was applied to weight the influence of different factors that affect flooding impacts. A novel strategy was adopted of questionnaire distribution to people from various professions to assess the relative importance of land use, depth of flooding and depth of pooling in influencing the flow accumulation. Earlier it was found that translating and adapting English language questionnaires for Arabic-speaking people can be challenging (Siddiqui et al., 2017). Testing the reliability and validity of English language questionnaires by translation is of great value, so an expert committee was constituted to smoothly translate and adapt the questionnaires in foreign languages, and it took several months to get an appropriate translation. Our plan to present the survey questions in two languages resulted in greater reliability with no cost expenditure. The results showed that the majority of respondents gave land-use factors the highest score, followed by depth of flooding and depth of pooling. However, it was surprising that many factors were similarly rated, with respondents not providing a big difference between land uses, such as developed and undeveloped land. There are a number of ways that this could be explored further. Examples include follow-up questions to obtain views on the survey or more detailed face-to-face interviews. Most importantly, face-to-face interviews could be part of the piloting process. It may be that a survey based upon western examples is less feasible and culturally appropriate in Qatar and surveys could explore this issue in further detail. Papadimitropoulos et al. (2015) discuss

the challenges of obtaining an individual's stated preferences in a nearly Arab country. Some of the issues uncovered include a dislike of choice making, the challenges of translation and a high level of dissatisfaction with standard interview approaches. These are issues that may be explained in future research that can also evolve certain standard questionnaire values that can be set which are applicable for Qatar and Middle East regions.

Another limitation is that this study considers only coastal inundation associated with SLR. One important additional component of flooding not considered is the overwhelming drainage systems caused by excessive rainfall from extreme storms. Such flooding could occur concurrently with storm surges. In low relief areas, such as the study area, the backup of storm/sewage systems has caused major short-term flooding. The reason for this omission is the difficulty of accounting for the range of factors, such as impervious surfaces and drainage networks that promote surface flooding.

The interaction of SLR with a river system was also investigated by developing a hydrodynamic river model, as flood mapping by tying up hydrodynamic models with GIS is common practice (Mah, 2011). The model not only calculates water levels in the river network but also interpolates the levels at points away from the network, taking into consideration the existing natural barriers and available flow paths. The flood depths and the possible levels of flooding were obtained by subtracting the ground elevation in these points. The effect of SLR could also be estimated and a management strategy developed by using this model. It was, however, concluded that a river model has more credibility in site-specific hydrological analysis, which includes increase of sea levels. The concept of "failure probability" was used to assess coastal flood risk arising from different future SLR scenarios (Moftakhari et al., 2017). Sea level rise attributed to anthropogenic global warming is a global threat to coastal populations and assets. One driver at a time, such as fluvial flooding only or ocean flooding only, is considered for assessing flood hazard commonly, whereas in reality coastal cities are at risk of flooding from multiple drivers, such as high coastal tide, flood level and flow of river water. Coastal populations and properties can be damaged by both oceanic and fluvial surges. A unique bivariate flood risk assessment that takes into consideration the potential compounding impacts of the interplay of primary oceanic

inundation hazard, water level on the coast and fluvial inundation hazards are presented here instead of one flood driver at a time. The findings of this research show that future SLR ensuing from warming temperatures increases the failure probability and also intensifies the combining effects of different flood drivers mentioned earlier. As Qatar has a porous limestone ground structure water rises rapidly when rains occur, inundating the urban areas in the coastal zone. Future research could be conducted by taking all these dynamics of coastal regions into consideration for obtaining better realistic results.

The other limitation of this research was the time involved in manually splitting the catchment to calculate barrier length. Automating the catchment splitting process would be an important aspect for further research on building barriers. Automatic profile extraction would also produce a more meaningful cost estimate at the outset.

Another interesting and relevant direction for future research work could be the engineering aspects, like analysing the strength required for flood barriers and the factors that might dent these structures, including tide gates, culverts, sewage outflows and narrow sea walls, which is beyond the scope of this study. Developing hydrodynamic models could also be considered a future research exercise that could take into account vital but smaller topographic features related to flood mitigation. The MCE is an effective tool for site selection, however, developing an objective method to weigh each factor is crucial. The novel approach of questionnaire distribution can include more extensive representations from all the stakeholders who can be affected by flooding and this can also be crucial in evolving effective strategies that can be adapted to mitigate the adverse effects of coastal inundation induced by SLR.

7.4. Research contributions of this study

This study provided a methodology based on spatial technology, such as GIS, to provide stakeholders with a decision-making tool for a better understanding of uncertainties in climate change study and future flood defence planning. A comprehensive literature review on the importance of the DEM and the associated uncertainties that can impact the outcome of the climate change projections is also presented here. The granularity of the method used in this research

provides a tool for local decision making. The high horizontal and vertical resolution DEM plays an important role in this approach and the method also integrated the hydrological connectivity to the sea as the source of the inundation.

Identifying the critical area in studying SLR inundation is crucially important for the decision makers to plan to prevent future flooding by building barriers. This study developed a method to include factors affecting the site selection by integrating MCE with GIS tools for site selection. The factors developed and the weighting assigned are based on experts' views to take into consideration various opinions.

Qatar is a small peninsular state which is particularly vulnerable to coastal flooding as several urban areas are coastal. This includes the capital city of Doha, which itself is located on the coast with a land area of over 100 km^2. Doha city and other areas of interest to the present study are all adjacent to the shoreline and are economically and politically significant. Furthermore, recent developments and megaprojects, like the Lusail neighbourhood, run along the coast. The potential impact of climate change is already recognised in Qatar, and the Interim Coastal Development Guidelines highlights that at least one main coastal zone is "likely to be inundated due to rises in sea level consequent upon global warming" (Ministry of Municipality and Urban Planning, *Interim Coastal Development Guidelines* (2013)). With 18.2 per cent of Qatar's land area already prone to inland flooding, this makes it especially prone to inundation due to SLR. Our research (Chapter 5) shows that the areas of likely (51-94 per cent) or very likely (95-100 per cent) flooding are located near the coast, and these areas are particularly large in the north and south-east of the study area. The report by the Ministry of Municipality and Urban Planning emphasises that most of the regions will be highly impacted by 2100 due to SLR related to climate change (Ministry of Municipality and Urban Planning, *Interim Coastal Development Guidelines* (2013)). Any SLR will adversely affect approximately 90 per cent of Qatar's population inhabiting the coastal cities (Ministry of Environment, *Intended Nationally Determined Contributions Report* (November 19, 2015)). Thus, the probability of SLR has been identified as an obvious risk in Qatar, and this influenced the development of the Qatar National Master Plan and the more recent Climate Change Strategy for

the Urban Planning and Urban Development Sector (www.mme.gov.qa/ Qatar Master Plan /default .aspx).

In summary, this thesis has applied various spatial interpolation methods and techniques to generate high resolution DEMs in complex urban areas from coarser resolution point data. These methods are applicable to other study sites. These DEMs have been used to assess the potential for SLR inundation. We have explored numerous methods for quantifying the impact of uncertainty in the DEM and SLR estimates on the flooding projections, which are relatively novel, and can be applied in other coastal locations. The thesis has also explored the importance of taking spatial autocorrelation into account when modelling the impacts of uncertainty but has not come to any firm conclusions on its usefulness. Finally, the thesis develops novel methods to identify critical areas for barrier construction to prevent sea level inundation. It is key for future research to attempt to ground truth the results produced, as well as explore their benefits in other countries and landscape settings.

References

Aarup, T., Church, J., Wilson, W.S. and Woodworth, P.L., (2010) *Sea level rise and variability: a summary for policy makers*. UNESCO/IOC, 12pp.

Abulfatih, H.A., (2001) *Vegetation of Qatar*. Scientific and Applied Research Center (SARC), University of Qatar.

Abuodha, P. A. & Woodroffe, C. D. (2010) 12 Vulnerability assessment. In *Coastal zone management.* Thomas Telford Ltd, pp. 262-290.

Abushandi, E. (2016) 'Flood prevention dams for arid regions at a micro-scale sub-catchment, case study: Tabuk, Saudi Arabia', *Water Science and Technology*, 74(11), pp.2523-2533.

Adham, A., Sayl, K. N., Abed, R., Abdeladhim, M. A., Wesseling, J. G., Riksen, M., Fleskens, L., Karim, U., & Ritsema, C. J. (2018) 'A GIS-based approach for identifying potential sites for harvesting rainwater in the Western Desert of Iraq', *International Soil and Water Conservation Research*, 6(4), pp.297-304.

Al-Buloshi, A., Al-Hatrushi, S., & Charabi, Y. (2014) 'A GIS-based framework for the simulation of the impacts of sea level rise and coastal flooding on Oman', *Journal of Earth Science & Climatic Change*, 5(10), p.1.

Al-Jeneid, S., Bahnassy, M., Nasr, S., & El Raey, M. (2008) 'Vulnerability assessment and adaptation to the impacts of sea level rise on the Kingdom of Bahrain', *Mitigation and Adaptation Strategies for Global Change*, 13(1), p.87.

Alley, R. B., Clark, P. U., Huybrechts, P., & Joughin, I. (2005) 'Ice-sheet and sea-level changes', *Science*, 310(5747), pp.456-460.

Al-Ruzouq, R., Shanableh, A., Yilmaz, A. G., Idris, A., Mukherjee, S., Khalil, M. A., & Gibril, M. B. A. (2019) 'Dam site suitability mapping and analysis using an integrated GIS and machine learning approach', *Water*, 11(9), p.1880.

Alsahli, M. M. & AlHasem, A. M. (2016) 'Vulnerability of Kuwait coast to sea level rise', *Geografisk Tidsskrift-Danish Journal of Geography*, 116(1), pp.56-70.

Amante, C. J. (2019) 'Uncertain seas: probabilistic modelling of future coastal flood zones', *International Journal of Geographical Information Science*, 33(11), pp.2188-2217.

Antunes, C., Rocha, C., & Catita, C. (2019) 'Coastal flood assessment due to sea level rise and extreme storm events: A case study of the Atlantic Coast of Portugal's mainland', *Geosciences*, 9(5), p.239.

Armstrong, M. P., Xiao, N., & Bennett, D. A. (2003) 'Using genetic algorithms to create multicriteria class intervals for choropleth maps', *Annals of the Association of American Geographers*, 93(3), pp.595-623.

Arnell, N. W., Cannell, M. G., Hulme, M., Kovats, R. S., Mitchell, J. F., Nicholls, R. J., Parry, M. L., Livermore, M. T., & White, A. (2002) 'The consequences of CO_2 stabilization for the impacts of climate change', *Climatic Change*, 53(4), pp.413-446.

Arun, P. V. (2013) 'A comparative analysis of different DEM interpolation methods', *The Egyptian Journal of Remote Sensing and Space Science*, 16(2), pp.133-139.

Ashghal, (2012) *Shallow Groundwater Monitoring in Greater Doha, Wakrah and Khor Project-CP761*. Initial Hydrogeological Report (M5). Public Works Authority, D.Q.

Ayalew, L., Yamagishi, H., & Ugawa, N. (2004) 'Landslide susceptibility mapping using GIS-based weighted linear combination, the case in Tsugawa area of Agano River, Niigata Prefecture, Japan', *Landslides*, 1(1), pp.73-81.

Ayhan, M.E. and Alothman, A., (2009) 'Sea level rise within the west of Arabian Gulf using tide gauge and continuous GPS measurements', In *Geophysical Research Abstracts* (Vol. 11). EGU General Assembly 2009, held 19-24 April 2009 in Vienna, Austria http://meetings.copernicus.org/egu2009, p.6006

Babar, Z. (2015) 'Population, power, and distributional politics in Qatar', *Journal of Arabian Studies*, 5(2), pp.138-155.

Babu, D. S., Sivalingam, S., & Machado, T. (2012) 'Need for adaptation strategy against global sea level rise: an example from Saudi coast of Arabian gulf', *Mitigation and adaptation strategies for global change*, 17(7), pp.821-836.

Barnard, P.L., Erikson, L.H., Foxgrover, A.C., Hart, J.A.F., Limber, P., O'Neill, A.C., van Ormondt, M., Vitousek, S., Wood, N., Hayden, M.K. and Jones, J.M., (2019). Dynamic flood modeling essential to assess the coastal impacts of climate change. *Scientific reports*, 9(1), pp.1-13.

Barnett, J. & O'Neill, S. (2010) 'Maladaptation', *Global environmental change*, 2(20), pp.211-213.

Barron, S., Canete, G., Carmichael, J., Flanders, D., Pond, E., Sheppard, S. and Tatebe, K. (2012) 'A climate change adaptation planning process for low-lying, communities vulnerable to sea level rise', *Sustainability*, 4(9), pp.2176-2208.

Batanouny, K. H. (1981) *Ecology and Flora of Qatar.* Oxford: Alden Press

Beatley, T. (2012). *Planning for coastal resilience: Best practices for calamitous times*. Island Press.

Binh, T. Q. & Thuy, N. T. (2008) 'Assessment of the influence of interpolation techniques on the accuracy of digital elevation model', *VNU Journal of Science: Earth and Environmental Sciences*, 24(4), pp. 176-183.

Boateng, I., Wiafe, G., & Jayson-Quashigah, P. N. (2017) 'Mapping vulnerability and risk of Ghana's coastline to sea level rise', *Marine Geodesy*, 40(1), pp.23-39.

Booker, J. M. & Ross, T. J. (2011) 'An evolution of uncertainty assessment and quantification', *Scientia Iranica*, 18(3), pp.669-676.

Broadus, J., Milliman, J., Edwards, S., Aubrey, D. G., & Gable, F. (1986) 'Rising sea level and damming of rivers: possible effects in Egypt and Bangladesh', *Effects of changes in stratospheric ozone and global climate*, 4, pp.165-189.

Burrough, P. A. & McDonnell, R. A. (1998) *Principles of Geographic Information Systems.* 3rd edition. Oxford: Oxford University Press.

Burrough, P. A. (1986) *Principles of geographical information systems for land resource assessment.* Oxford: Oxford University Press.

Burrough, P. A., McDonnell, R. A., & Lloyd, C. D. (2015) *Principles of Geographic Information Systems.* 3rd edition. Oxford: Oxford University Press.

Burton, C. & Rosenbaum, M. (2003) 'Decision support to assist environmental sedimentology modelling', *Environmental Geology*, 43(4), pp.457-465.

Bush, D. M., Richmond, B. M., & Neal, W. J. (2001) 'Coastal-zone hazard maps and recommendations: eastern Puerto Rico', *Environmental Geosciences*, 8(1), pp.38-60.

Capilla, J. J., Carrión, J. A., & Alameda-Hernandez, E. (2016) 'Optimal site selection for upper reservoirs in pump-back systems, using geographical information systems and multicriteria analysis', *Renewable Energy*, 86, pp.429-440.

Cardona, O.D., van Aalst, M. K. , Birkmann, J., Fordham, M., McGregor, G., Perez, R., Pulwarty, R. S., Schipper, E. L. F. and Sinh, B. T, (2012) 'Determinants of risk: exposure and vulnerability',

In: [Field, C.B., V. Barros, T.F. Stocker, D. Qin, D.J. Dokken, K.L. Ebi, M.D. Mastrandrea, K.J. Mach, G.-K. Plattner, S.K. Allen, M. Tignor, and P.M. Midgley (eds.)]. *Managing the Risks of Extreme Events and Disasters to Advance Climate Change Adaptation*. A Special Report of Working Groups I and II of the Intergovernmental Panel on Climate Change (IPCC). Cambridge University Press, Cambridge, UK, and New York, NY, USA, pp. 65-108.

Carter, R. (2006) 'Boat remains and maritime trade in the Persian Gulf during the sixth and fifth millennia BC', *Antiquity*, 80(307), pp.52-63.

Cazenave, A., Henry, O., Munier, S., Delcroix, T., Gordon, A. L., Meyssignac, B., Llovel, W., Palanizamy, H., & Becker, M. (2012) 'Estimating ENSO influence on the global mean sea level, 1993–2010', *Marine Geodesy*, 35(sup1), pp.82-97.

Chai, T. & Draxler, R. R. (2014) 'Root mean square error (RMSE) or mean absolute error (MAE)? – Arguments against avoiding RMSE in the literature', *Geoscientific model development*, 7(3), pp.1247-1250.

Chakhar, S. & Mousseau, V. (2008) 'Spatial multicriteria decision making', *Encyclopedia of GIS*, 10, pp.978-0.

Chaplot, V., Darboux, F., Bourennane, H., Leguédois, S., Silvera, N., & Phachomphon, K. (2006) 'Accuracy of interpolation techniques for the derivation of digital elevation models in relation to landform types and data density', *Geomorphology*, 77(1-2), pp.126-141.

Church, J. A. & White, N. J. (2011) 'Sea-level rise from the late 19th to the early 21st century', *Surveys in geophysics*, 32(4), pp.585-602.

Church, J. A., Clark, P. U., Cazenave, A., Gregory, J. M., Jevrejeva, S., Levermann, A., Merrifield, M. A., Milne, G. A., Nerem, R. S., Nunn, P. D., & Payne, A. J. (2013) 'Sea-level rise by 2100', *Science*, 342(6165), pp.1445-1445.

Church, J. A., Clark, P. U., Cazenave, A., Gregory, J. M., Jevrejeva, S., Levermann, A., Merrifield, M. A., Milne, G. A., Nerem, R. S., Nunn, P. D., & Payne, A. J. (2013) Sea *level change*. PM Cambridge University Press.

Chust, G., Caballero, A., Marcos, M., Liria, P., Hernández, C., & Borja, Á. (2010) 'Regional scenarios of sea level rise and impacts on Basque (Bay of Biscay) coastal habitats, throughout the 21st century', *Estuarine, Coastal and Shelf Science*, 87(1), pp.113-124.

Ciscar, J. C., Iglesias, A., Feyen, L., Szabó, L., Van Regemorter, D., Amelung, B., Nicholls, R., Watkiss, P., Christensen, O. B., Dankers, R., & Garrote, L. (2011) 'Physical and economic consequences of climate change in Europe', *Proceedings of the National Academy of Sciences*, 108(7), pp.2678-2683.

Clarke, L., Edmonds, J., Jacoby, H., Pitcher, H., Reilly, J., & Richels, R. (2007) Scenarios of greenhouse gas emissions and atmospheric concentrations. *Sub-Report 2.1a of Synthesis and Assessment Product 2.1 by the U.S. Climate Change Science Program and the Subcommittee on Global Change Research*, Department of Energy, Office of Biological & Environmental Research, Washington DC.

Collet, L., Beevers, L., & Stewart, M. D. (2018) 'Decision-making and flood risk uncertainty: Statistical data set analysis for flood risk assessment', *Water Resources Research*, 54(10), pp.7291-7308.

Cooper, H. M., Chen, Q., Fletcher, C. H., & Barbee, M. M. (2013) 'Assessing vulnerability due to sea-level rise in Maui, Hawaii, using LiDAR remote sensing and GIS', *Climatic Change*, 116(3-4), pp.547-563.

Cooper, H.M. & Chen, Q. (2013) 'Incorporating uncertainty of future sea-level rise estimates into vulnerability assessment: A case study in Kahului, Maui', *Climatic Change, 121*(4), pp.635-647.

Couclelis, H. (2003) 'The certainty of uncertainty: GIS and the limits of geographic knowledge', *Transactions in GIS*, 7(2), pp.165-175.

Coveney, S. & Fotheringham, A. S. (2011) 'The impact of DEM data source on prediction of flooding and erosion risk due to sea-level rise', *International Journal of Geographical Information Science*, 25(7), pp.1191-1211.

COWI (2008) *Qatar national aerial mapping.* Available at: http://www.cowi.com/menu/project/GeographicalInformationandIT/3Dvisualizationandmodelling/3Dmodelling/Pages/QatarNationalAerialMapping2008.aspx (Accessed: 20 December 2015).

CSIRO (2014) *Past sea level change.* Available at https://research.csiro.au/slrwavescoast/sea-level/sea-level-changes/ (Accessed: 15 March 2020).

Cutter, S. L., Mitchell, J. T., & Scott, M. S. (2000) 'Revealing the vulnerability of people and places: A case study of Georgetown County, South Carolina', *Annals of the association of American Geographers*, 90(4), pp.713-737.

Darboux, F. & Huang, C. H. (2003) 'An instantaneous-profile laser scanner to measure soil surface microtopography', *Soil Science Society of America Journal*, 67(1), pp.92-99.

Darnell, A. R., Lovett, A. A., Barclay, J., & Herd, R. A. (2010) 'An application-driven approach to terrain model construction', *International Journal of Geographical Information Science*, 24(8), pp.1171-1191.

Darnell, A. R., Tate, N. J., & Brunsdon, C. (2008) 'Improving user assessment of error implications in digital elevation models', *Computers, Environment and Urban Systems*, 32, 268–277.

Darwish, M. A. (2015) *Desalination engineering.* Balaban Desalination Publication.

Dasgupta, S., Laplante, B., Meisner, C., Wheeler, D., & Yan, J. (2007) 'The impact of sea level rise on developing countries: a comparative analysis', *Climatic Change* 93, 379-388

Davlasheridze, M., Atoba, K. O., Brody, S., Highfield, W., Merrell, W., Ebersole, B., Purdue, A., & Gilmer, R. W. (2019) 'Economic impacts of storm surge and the cost-benefit analysis of a coastal spine as the surge mitigation strategy in Houston-Galveston area in the USA', *Mitigation and adaptation strategies for global change*, 24(3), pp.329-354.

De Bel-Air, F. (2014) Demography, *migration, and labour market in Qatar*.

De Serio, F., Armenio, E., Mossa, M., & Petrillo, A. F. (2018) 'How to Define Priorities in Coastal Vulnerability Assessment', *Geosciences*, 8(11), p.415.

De Sherbinin, A., Schiller, A., & Pulsipher, A. (2007) 'The vulnerability of global cities to climate hazards', *Environment and urbanization*, 19(1), pp.39-64.

DeConto, R. M. & Pollard, D. (2016) 'Contribution of Antarctica to past and future sea-level rise', *Nature*, 531(7596), p.591.

Deitrick-Hirsch, S., Wentz, E. A., White, D., Larson, K. L., & Howard, J. (2010) 'The Role of GIS to Enable Public-Sector Decision Making Under Conditions of Uncertainty', *GeoDa Center Working Papers*, pp.1181-1187.

Dronkers, J.J., Misdorp, R. and Spradley, J.R. (1990) Strategies *for adaptation to sea level rise*. Report of the IPCC Coastal Zone Management Subgroup: Intergovernmental Panel on Climate Change. Geneva: Intergovernmental Panel on Climate Change.

Duckham, M. and McCreadie, J.E., (2002) 'Error-aware GIS Development', in Wenzhong Shi, Peter Fisher, Michael F. Goodchild (Eds.) *Spatial Data Quality*, p.64. CRC Press.

Duke, G. D., Kienzle, S. W., Johnson, D. L., & Byrne, J. M. (2003) 'Improving overland flow routing by incorporating ancillary road data into digital elevation models', *Journal of Spatial Hydrology*, 3(2).

Duke, G. D., Kienzle, S. W., Johnson, D. L., & Byrne, J. M. (2006) 'Incorporating ancillary data to refine anthropogenically modified overland flow paths', *Hydrological Processes: An International Journal*, 20(8), pp.1827-1843.

Dumitru, P. D., Plopeanu, M. A. R. I. N., & Badea, D. R. A. G. O. S. (2013) 'Comparative study regarding the methods of interpolation', *Recent advances in geodesy and Geomatics engineering*, 1, p.45.

Eastman, J. R., Jin, W., Kyem, P. A., & Toledano, J. (1995) 'Raster procedures for multi-criteria/multi-objective decisions', *Photogrammetric Engineering and Remote Sensing*, 61(5), pp.539-547.

Eccleston, B. L. & Ḥarḥash, I. A. S. (1982) The *hydrogeology of Qatar*. Doha, Qatar.

Economides, M. J. & Wood, D. A. (2009) 'The state of natural gas', *Journal of Natural Gas Science and Engineering*, 1(1-2), pp.1-13.

Ehlschlaeger, C. (1998) The *Stochastic Simulation Approach: Tools for Representing Spatial Application.* Ph.D Dissertation Uncertainty, University of California.

Eisenfuhr, F. (2011) *Decision making*. New York, NY: springer.

El Quilish, M., El-Ashquer, M., Dawod, G., & El Fiky, G. (2018) 'Development and Accuracy Assessment of High-Resolution Digital Elevation Model Using GIS Approaches for the Nile Delta Region, Egypt'. *American Journal of Geographic Information System*, 7(4), pp.107-117.

El Raey, M. (2009) 'Impact of climate change: Vulnerability and Adaptation', in Tolba, M. K. and Saab, N. W. (eds.) *Coastal Areas*. Pp.47-52.

El Raey, M. (2010) 'Impact of sea level rise on the Arab Region', *University of Alexandria. Arab Academy of Science, Technology, and Maritime*, pp.1-89.

Environment Public Authority (2012) *Kuwait's Initial National Communications under the United Nations Framework Convention on Climate Change, State of Kuwait*. Available at: http://unfccc.int/resource/docs/natc/kwtnc1.pdf (Accessed: 15 October 2015).

ESRI (2015) *ArcGIS Resources* Available at: https://resources.arcgis.com/ en/help (Accessed: 17 December 2015).

ESRI (2016) *Breaklines in surface modelling- ArcGIS Desktop Help 9.3.* Available at: http://webhelp.esri.com/arcgisdesktop/9.3/index.cfm?TopicName=Breaklines%20in%20surface%20modeling (Accessed: 24 Jun 2016).

ESRI (2017) *An overview of the Interpolation toolset - How Spline works.* Available at: https://pro.arcgis.com/en/pro-app/tool-reference/spatial-analyst/how-spline-works.htm (Accessed: 17 Jan 2017).

Eyring, V., Isaksen, I. S., Berntsen, T., Collins, W. J., Corbett, J. J., Endresen, O., Grainger, R. G., Moldanova, J., Schlager, H., & Stevenson, D. S. (2010) 'Transport impacts on atmosphere and climate: Shipping', *Atmospheric Environment*, 44(37), pp.4735-4771.

Fang, T., Chen, Y., Tan, H., Cao, J., Liao, J., & Huang, L. (2019) 'Flood risk evaluation in the middle reaches of the Yangtze River based on eigenvector spatial filtering poisson regression. *Water*, 11(10), p.1969.

Faour, G., Fayad, A., & Mhawej, M. (2013) 'GIS-based approach to the assessment of coastal vulnerability to sea level rise: Case study on the eastern Mediterranean', *Journal of Surveying and Mapping Engineering*, 1(3), pp.41-48.

Farinotti, D., Huss, M., Fürst, J. J., Landmann, J., Machguth, H., Maussion, F., & Pandit, A. (2019) 'A consensus estimate for the ice thickness distribution of all glaciers on Earth'. *Nature Geoscience*, *12*(3), pp.168-173.

Fedorov, M., Badenko, V., Maslikov, V., & Chusov, A. (2016) 'Site selection for flood detention basins with minimum environmental impact', *Procedia engineering*, 165, pp.1629-1636.

Feick, R. & Hall, B. (2004) 'A method for examining the spatial dimension of multi-criteria weight sensitivity', *International Journal of Geographical Information Science*, 18(8), pp.815-840.

Fisher, P. F. & Tate, N. J. (2006) 'Causes and consequences of error in digital elevation models', *Progress in physical Geography*, 30(4), pp.467-489.

Fisher, P. F. (1991) 'First experiments in viewshed uncertainty: the accuracy of the viewshed area', *Photogrammetric engineering and remote sensing*, 57(10), pp.1321-1327.

FitzGerald, D. M., Fenster, M. S., Argow, B. A., & Buynevich, I. V. (2008) 'Coastal impacts due to sea-level rise', *Annual Review of Earth and Planetary Sciences*, 36, pp.601-647.

Fowler, R. J. & Little, J. J. (1979) 'Automatic extraction of irregular network digital terrain models', *ACM SIGGRAPH Computer Graphics*, 13(2), pp.199-207.

Fu, X. & Song, J. (2017) 'Assessing the Economic Costs of Sea Level Rise and Benefits of Coastal Protection: A Spatiotemporal Approach', *Sustainability*. 9. 1495. 10.3390/su9081495.

Fujino, J., Nair, R., Kainuma, M., Masui, T., & Matsuoka, Y. (2006) 'Multi-gas mitigation analysis on stabilization scenarios using AIM global model', *The Energy Journal*, (Special Issue# 3), pp.343-353.

Gesch, D. B. (2009) 'Analysis of lidar elevation data for improved identification and delineation of lands vulnerable to sea-level rise', *Journal of Coastal Research*, (53), pp.49-58.

Gesch, D. B. (2013) ‘Consideration of vertical uncertainty in elevation-based sea-level rise assessments: Mobile Bay, Alabama case study’, *Journal of Coastal Research*, (63), pp.197-210.

Gesch, D. B. (2018) ‘Best practices for elevation-based assessments of sea-level rise and coastal flooding exposure’, *Frontiers in Earth Science*, 6, p.230.

Getis, A., (2007) ‘Reflections on spatial autocorrelation’, *Regional Science and Urban Economics*, *37*(4), pp.491-496.

GonÇalves, J. A. & Oliveira, A. M. (2004) ‘Accuracy analysis of DEMs derived from ASTER imagery’, *International Archives of Photogrammetry and Remote Sensing*, 35, pp.168–172.

Griggs, G., Árvai, J., Cayan, D., DeConto, R., Fox, J., Fricker, H. A., Kopp, R. E., Tebaldi, C., & Whiteman, E. A. (2017) Rising Seas in California: An Update on Sea-Level Rise Science. California Ocean Science Trust.

Guo-an, T. A. N. G., Strobl, J., Jian-ya, G. O. N. G., Mu-dan, Z. H. A. O., & Zhen-Jiang, C. (2001) ‘Evaluation on the accuracy of digital elevation models’, *Journal of Geographical Sciences*, 11(2), pp.209-216.

Hamza, W. & Munawar, M. (2009) ‘Protecting and managing the Arabian Gulf: past, present and future’, *Aquatic Ecosystem Health & Management*, 12(4), pp.429-439.

Hanson, S., Nicholls, R., Ranger, N., Hallegatte, S., Corfee-Morlot, J., Herweijer, C., & Chateau, J. (2011) ‘A global ranking of port cities with high exposure to climate extremes’, *Climatic change*, 104(1), pp.89-111.

Harrison, C. (2017) *Harvard University Program on Survey Research: Tip Sheet on Question Wording*. Available at: http://psr. iq. harvard. edu/files/psr/files/PSRQuestionnaireTipSheet_0. pdf. (Accessed: 26 Jun 2019).

Hawkins, E. & Sutton, R. (2011) ‘The potential to narrow uncertainty in projections of regional precipitation change’, *Climate Dynamics*, 37(1-2), pp.407-418.

Hay, C. C., Morrow, E., Kopp, R. E., & Mitrovica, J. X. (2015) ‘Probabilistic reanalysis of twentieth-century sea-level rise’, *Nature*, 517(7535), p.481.

Heuvelink, G. B. (1998) Error *propagation in environmental modelling with GIS*. CRC press.

Heuvelink, G. B. M. (1999) ‘Propagation of error in spatial modelling with GIS’, In: Longley, P. et al. (eds), Geographical information systems. Wiley, pp. 207–217.

Hijioka, Y., Matsuoka, Y., Nishimoto, H., Masui, M., & Kainuma, M. (2008) 'Global GHG emission scenarios under GHG concentration stabilization targets', *Journal of global environment engineering*, 13, pp.97-108.

Hinkel, J. (2011) '"Indicators of vulnerability and adaptive capacity": towards a clarification of the science–policy interface', *Global environmental change*, 21(1), pp.198-208.

Hinkel, J., van Vuuren, D.P., Nicholls, R.J. and Klein, R.J. (2013). 'The effects of adaptation and mitigation on coastal flood impacts during the 21st century. An application of the DIVA and IMAGE models', *Climatic Change*, *117*(4), pp.783-794.

Holmes, K. W., Chadwick, O. A., & Kyriakidis, P. C. (2000) 'Error in a USGS 30-meter digital elevation model and its impact on terrain modelling', *Journal of Hydrology*, 233(1-4), pp.154-173.

Hoozemans, F. M. J., Marchand, M., & Pennekamp, H. A. (1993) A global vulnerability analysis: vulnerability assessment for population, coastal wetlands and rice production on a global scale. *Delft Hydraulics and Rijkswaterstaat, Delft and The Hague, The Netherlands*.

Hoozemans, F. M. J., Marchand, M., Pennekamp, H. A., Stive, M., Misdorp, R., & Bijlsma, L. (1992) 'The impacts of sea-level rise on coastal areas: Some global results', *Proceedings 'The Rising Challenge of the Sea*, pp.9-13.

Hu, A. & Deser, C. (2013) 'Uncertainty in future regional sea level rise due to internal climate variability', *Geophysical Research Letters*, 40(11), pp.2768-2772.

Hunter, G. J. & Goodchild, M. F. (1997) 'Modelling the uncertainty of slope and aspect estimates derived from spatial databases', *Geographical Analysis*, 29(1), pp.35-49.

Hunter, G. J., Caetano, M., & Goodchild, M. F. (1995) 'A methodology for reporting uncertainty in spatial database products', *URISA-WASHINGTON DC-*, 7, pp.11-21.

Huq, S., Ali, S. I., & Rahman, A. A. (1995) 'Sea-level rise and Bangladesh: A preliminary analysis', *Journal of Coastal Research*, pp.44-53.

Integrated Coastal Zone Management Plan for the State of Qatar, Climate Change and Sea Level Rise Study (ICZMP-CCSLR, 2014). Ministry of Municipality and Urban Planning (MMUP).

IPCC (2000) *IPCC Special Report – Emission Scenarios*. Available at: https://www.ipcc.ch/site/assets/uploads/2018/03/sres-en.pdf (Accessed: 5 May 2017).

IPCC (2007) *The physical science basis. Contribution of working group I to the fourth assessment report of the Intergovernmental Panel on Climate Change*. Cambridge University Press, Cambridge, United Kingdom and New York, NY, USA, 996, p.2007.

IPCC (2014) ‘Summary for policymakers’, in Field, C. B., Barros, V. R., Dokken, D. J., Mach, K. J., Mastrandrea, M. D., Bilir, T. E., Chatterjee, M., Ebi, K. L., Estrada, Y. O., Genova, R. C., Girma, B., Kissel, E. S., Levy, A. N., MacCracken, S., Mastrandrea, R. R., and White, L. L., (eds.), *Climate Change 2014: Impacts, Adaptation, and Vulnerability. Contribution of Working Group II to the Fifth Assessment Report of the Intergovernmental Panel on Climate Change*. Cambridge University Press, Cambridge, UK and New York, NY, USA.

IPCC (2018) *Intergovernmental Panel on Climate Change.* Available at: http://www.ipcc.ch (Accessed: 5 January 2020).

IPCC CZMS (1992) *Global climate change and the rising challenge of the sea.* Report of the Coastal Zone Management Subgroup. IPCC Response Strategies Working Group, Rijkswaterstaat, The Hague.

Jenson, S. K. & Domingue, J. O. (1988) ‘Extracting topographic structure from digital elevation data for geographic information system analysis’, *Photogrammetric engineering and remote sensing*, 54(11), pp.1593-1600.

Jevrejeva, S., Grinsted, A., & Moore, J. C. (2014) ‘Upper limit for sea level projections by 2100’, *Environmental Research Letters*, 9(10), p.104008.

Jha, M. K., McCall, C., & Schonfeld, P. (2001) ‘Using GIS, genetic algorithms, and visualization in highway development’, *Computer-Aided Civil and Infrastructure Engineering*, 16(6), pp.399-414.

Jiang, H. & Eastman, J. R. (2000) ‘Application of fuzzy measures in multi-criteria evaluation in GIS’, *International Journal of Geographical Information Science*, 14(2), pp.173-184.

Johnson, M. P. (2001) ‘Decision support for family relocation decisions under the section 8 housing assistance program using geographic information systems and the analytic hierarchy process’, *Journal of Housing Research*, pp.277-306.

Jonge, T. de, Kok, M. and Hogeweg, M. (1996) ‘Modelling floods and damage assessment using GIS’, in HydroGIS 96: Application of Geographical Information Systems in Hydrology and Water Res. Management and Planning (Proceedings of the Vienna Conference, 4-1996, IAHSPubl. no. 235, pp.299-306.

Jozaghi, A., Alizadeh, B., Hatami, M., Flood, I., Khorrami, M., Khodaei, N. and Ghasemi Tousi, E. (2018) ‘A comparative study of the AHP and TOPSIS techniques for dam site selection using GIS: A case study of Sistan and Baluchestan Province, Iran’, *Geosciences*, 8(12), p.494.

Kane, H. H., Fletcher, C. H., Frazer, L. N., Anderson, T. R., & Barbee, M. M. (2015) 'Modelling sea-level rise vulnerability of coastal environments using ranked management concerns', *Climatic change*, 131(2), pp.349-361.

Khan, N. Y., Munawar, M., & Price, A. R. (2002) The *gulf ecosystem: Health and sustainability*. Leiden, The Netherlands: Backhuys.

Kim, Y. & Newman, G. (2019) 'Climate change preparedness: Comparing future urban growth and flood risk in Amsterdam and Houston', *Sustainability*, *11*(4), p.1048. https://doi.org/10.3390/su11041048

Kim, Y. D., Tak, Y. H., Park, M. H., & Kang, B. (2020) 'Improvement of urban flood damage estimation using a high-resolution digital terrain', *Journal of Flood Risk Management*, 13, p.e12575.

Kirezci, E., Young, I. R., Ranasinghe, R., Muis, S., Nicholls, R. J., Lincke, D., & Hinkel, J. (2020) 'Projections of global-scale extreme sea levels and resulting episodic coastal flooding over the 21st Century', *Scientific reports*, *10*(1), pp.1-12.

Kopp, R. E., Mitrovica, J. X., Griffies, S. M., Yin, J., Hay, C. C., & Stouffer, R. J. (2010) 'The impact of Greenland melt on local sea levels: a partially coupled analysis of dynamic and static equilibrium effects in idealized water-hosing experiments', *Climatic Change*, 103(3-4), pp.619-625.

Krosnick, J. A. & Presser, S. (2010) 'Question and questionnaire design', in Marsden P. V. and Wright J. D. (eds.) *Handbook of Survey Research* 2nd edition. San Diego, CA: Elsevier.

Ksiksi, T. S., Youssef, T., & Abdelmawla, E. (2012) 'Sea level rise and Abu Dhabi coastlines: an initial assessment of the impact on land and mangrove areas', *J Ecosyst Ecogr*, 2(115), p.2.

Kwaku Kyem, P.A. (2004) 'Of intractable conflicts and participatory GIS applications: The search for consensus amidst competing claims and institutional demands', *Annals of the Association of American Geographers*, 94(1), pp.37-57.

Lafaysse, M., Hingray, B., Mezghani, A., Gailhard, J., & Terray, L. (2014) 'Internal variability and model uncertainty components in future hydrometeorological projections: The Alpine Durance basin', *Water Resources Research*, 50(4), pp.3317-3341.

Lanter, D. P. & Veregin, H. (1992) 'A research paradigm for propagating error in layer-based GIS', *Photogrammetric Engineering and Remote Sensing*, 58(6), pp.825-833.

Larentis, D. G., Collischonn, W., Olivera, F., & Tucci, C. E. (2010) 'Gis-based procedures for hydropower potential spotting,' *Energy*, 35(10), pp.4237-4243.

Leao, S., Bishop, I., & Evans, D. (2004) ‘Spatial–temporal model for demand and allocation of waste landfills in growing urban regions’, *Computers, Environment and Urban Systems*, 28(4), pp.353-385.

Leica Geosystems AG - Part of Hexagon (2019) *Leica Viva GNSS GS08 plus receiver Datasheet.* Available at: http://www.surveyequipment.com/PDFs/leica-viva-gs08-plus-datasheet.pdf (Accessed: 7 July 2019).

Leica Geosystems AG. (2012) *Viva GNSS GS08plus receiver Datasheet.* Available at: http://docs.onepointsurvey.com/pdf/Leica-Viva-GS08-NetRover-Datasheet.pdf (Accessed: 27 July 2020).

Leon, J. X., Heuvelink, G. B., & Phinn, S. R. (2014) ‘Incorporating DEM uncertainty in coastal inundation mapping’, *PLoS one*, 9(9), p.e108727. https://doi.org/10.1371/journal.pone.0108727

Levermann, A., Clark, P. U., Marzeion, B., Milne, G. A., Pollard, D., Radic, V., & Robinson, A. (2013) ‘The multimillennial sea-level commitment of global warming’, *Proceedings of the National Academy of Sciences*, 110(34), pp.13745-13750.

Li, J. and Heap, A.D. (2014) ‘Spatial interpolation methods applied in the environmental sciences: A review’, *Environmental Modelling & Software*, *53*, pp.173-189. 10.1016/j.envsoft.2013.12.008.

Li, X., Liu, J. P., Saito, Y., & Nguyen, V. L. (2017) ‘Recent evolution of the Mekong Delta and the impacts of dams’, *Earth-Science Reviews*, 175, pp.1-17.

Li, Z., Zhu, C., & Gold, C. (2004) *Digital terrain modelling: principles and methodology*. CRC press.

Linyu, G., Xiaopingb, L., Yingcheng, L., Pei, L., Xiaofeng, S. and Huijie, L. (2012) ‘Application of breakline and manual additional points in Tin modelling’, *International Society for Photogrammetry and Remote Sensing (ISPRS)*, pp.346-351.

Liu, H., Sherman, D., & Gu, S. (2007) ‘Automated extraction of shorelines from airborne light detection and ranging data and accuracy assessment based on Monte Carlo simulation’, *Journal of Coastal Research*, pp.1359-1369.

Liu, X. & Zhang, Z (2011) ‘Effects of LiDAR Data Reduction and Breaklines on the Accuracy of Digital Elevation Model’’, *Survey Review*, 43, pp.614-628. 10.1179/003962611X13117748892317.

Maanan, M., Rueff, H., Adouk, N., Zourarah, B., & Rhinane, H. (2018) ‘Assess the human and environmental vulnerability for coastal hazard by using a multi-criteria decision analysis’, *Human and Ecological Risk Assessment: An International Journal*, 24(6), pp.1642-1658.

Mah, D. (2011) 'Modelling of sea level rise and river system', *Disaster Prevention and Management*, 20, pp.108-114. 10.1108/09653561111126058.

Maplecroft, (2009) *Global Risk Portfolio.* Available at: http://www.maplecroft.com and http://www.globalrisks.com/climate_change/ (Accessed: 12 Jan 2020).

Marcy, D., Brooks, W., Draganov, K., Hadley, B., Haynes, C., Herold, N., McCombs, J., Pendleton, M., Ryan, S., Schmid, K., & Sutherland, M. (2011) 'New mapping tool and techniques for visualizing sea level rise and coastal flooding impacts', In *Solutions to Coastal Disasters 2011* (pp. 474-490).

Martin, N. J., St Onge, B., & Waaub, J. P. (1999) 'An integrated decision aid system for the development of Saint Charles River alluvial plain, Quebec, Canada', *International Journal of Environment and Pollution*, 12(2), pp.264-279.

Massoud, M. A., Scrimshaw, M. D., & Lester, J. N. (2003) 'Qualitative assessment of the effectiveness of the Mediterranean action plan: wastewater management in the Mediterranean region', *Ocean & Coastal Management*, 46(9-10), pp.875-899.

Matzke, B. D., Newburn, L. L., Hathaway, J. E., Bramer, L. M., Wilson, J. E., Dowson, S. T., Sego, L. H., & Pulsipher, B. A. (2014) Visual *Sample Plan Version 7.0 User's Guide* (No. PNNL-23211). Pacific Northwest National Lab. (PNNL), Richland, WA (United States).

McCarthy, J. J., Canziani, O. F., Leary, N. A., Dokken, D. J., & White, K. S. (eds) (2001) Climate *change 2001: impacts, adaptation, and vulnerability: contribution of Working Group II to the third assessment report of the Intergovernmental Panel on Climate Change* (Vol. 2). Cambridge University Press.

McGranahan, G., Balk, D., & Anderson, B. (2007) 'The rising tide: assessing the risks of climate change and human settlements in low elevation coastal zones', *Environment and urbanization*, 19(1), pp.17-37.

McGrath, H., Bourgon, J. F., Proulx-Bourque, J. S., Nastev, M., & El Ezz, A. A. (2018) 'A comparison of simplified conceptual models for rapid web-based flood inundation mapping', *Natural Hazards*, 93(2), pp.905-920.

McGuire, C.J. (2017) Adapting to sea level rise in the coastal zone: Law and policy considerations. Routledge.

Mimura, N. (2013) 'Sea-level rise caused by climate change and its implications for society'. *Proceedings of the Japan Academy, Series B*, 89(7), pp.281-301. https://doi.org/10.2183/pjab.89.281.

Ministry of Development Planning and Statistics (2016) *Population Statistics*. Available at: http://www.gsdp.gov.qa/portal/page/portal/gsdp_en (Accessed: 10 October 2017).

Ministry of Development Planning and Statistics (MDPS) (2015) *Environmental statistics in State of Qatar*. Available at: https://www.psa.gov.qa/en/statistics/ /Environmental/EnvironmentalStatistics/Environment_QSA_EN_2015.pdf. (Accessed: 10 October 2017).

Ministry of Municipality & Urban Planning (MMUP) Qatar (2013) *Study of Regional Design Rainfall in Qatar*. Technical Report

Ministry of Municipality and Environment (MME), Qatar (2017) *Qatar Rainfall and Runoff (QRR)*. Technical Report.

Mitas, L. and Mitasova, H. (2005) Spatial Interpolation. In: Longley, P.A., Goodchild, M.F., Maguire, D.J. and Rhind, D.W., Eds., *Geographic Information Systems: Principles, Techniques, Management and Applications*, 2nd Edition, Vol. 1, Part 2, Chapter 34. www.geos.ed.ac.uk/~gisteac/gis_book_abridged/

Moftakhari, H.R., Salvadori, G., AghaKouchak, A., Sanders, B.F. and Matthew, R.A. (2017) 'Compounding effects of sea level rise and fluvial flooding', *Proceedings of the National Academy of Sciences*, 114, 201620325. 10.1073/pnas.1620325114.

Moiz, A., Kawasaki, A., Koike, T., & Shrestha, M. (2018) 'A systematic decision support tool for robust hydropower site selection in poorly gauged basins', *Applied Energy*, 224, pp.309-321.

Mondal, P. & Tatem, A. J. (2012) 'Uncertainties in measuring populations potentially impacted by sea level rise and coastal flooding', *PLoS One, 7*(10), p.e48191.

Moorhead, K. K. & Brinson, M. M. (1995) 'Response of wetlands to rising sea level in the lower coastal plain of North Carolina', *Ecological applications*, 5(1), pp.261-271.

Morari, F., Lugato, E., & Borin, M. (2004) 'An integrated non-point source model-GIS system for selecting criteria of best management practices in the Po Valley, North Italy', *Agriculture, ecosystems & environment*, 102(3), pp.247-262.

Moser, S. C. (2005) 'Impact assessments and policy responses to sea-level rise in three US states: An exploration of human-dimension uncertainties', *Global Environmental Change*, 15(4), pp.353-369.

Murdukhayeva, A., August, P., Bradley, M., LaBash, C., & Shaw, N. (2013) 'Assessment of inundation risk from sea level rise and storm surge in north-eastern coastal national parks', *Journal of Coastal Research*, 29(6a), pp.1-16.

Murillo, M. L. & Hunter, G. J. (1997) 'Assessing uncertainty due to elevation error in a landslide susceptibility model', *Transactions in GIS*, 2(4), pp.289-298.

Netz, B., Davidson, O. R., Bosch, P. R., Dave, R., & Meyer, L. A. (2007) *Climate change 2007: Mitigation. Contribution of Working Group III to the Fourth Assessment Report of the Intergovernmental Panel on Climate Change. Summary for Policymakers.* Cambridge University Press, Cambridge, United Kingdom and New York, NY, USA

Neumann, B., Vafeidis, A. T., Zimmermann, J., & Nicholls, R. J. (2015) 'Future coastal population growth and exposure to sea-level rise and coastal flooding-a global assessment', *PloS one*, 10(3), p. e0118571.

Nicholls, R. J. & Cazenave, A. (2010) 'Sea-level rise and its impact on coastal zones', *Science*, 328(5985), pp.1517-1520.

Nicholls, R. J. & Lowe, J. A. (2004) 'Benefits of mitigation of climate change for coastal areas', *Global environmental change*, 14(3), pp.229-244.

Nicholls, R. J. & Tol, R. S. (2006) 'Impacts and responses to sea-level rise: a global analysis of the SRES scenarios over the twenty-first century', *Philosophical Transactions of the Royal Society A: Mathematical, Physical and Engineering Sciences*, 364(1841), pp.1073-1095.

Nicholls, R. J. (1995) 'Coastal megacities and climate change', *GeoJournal*, 37(3), pp.369-379.

Nicholls, R. J. (2000) 'An analysis of the flood implications of the IPCC Second Assessment global sea-level rise scenarios', *Floods*. London: Routledge, pp.148-162.

Nicholls, R. J. (2004) 'Coastal flooding and wetland loss in the 21st century: changes under the SRES climate and socio-economic scenarios', *Global Environmental Change*, 14(1), pp.69-86.

Nicholls, R. J. (2007) 'The impacts of sea level rise', *Ocean Challenge*, 15(1), pp.13-17.

Nicholls, R. J. (2011) 'Planning for the impacts of sea level rise', *Oceanography*, 24(2), pp.144-157.

Nicholls, R. J., Hoozemans, F. M., & Marchand, M. (1999) 'Increasing flood risk and wetland losses due to global sea-level rise: regional and global analyses', *Global Environmental Change*, 9, pp.S69-S87.

Nicholls, R. J., Wong, P. P., Burkett, V. R., Codignotto, J. O., & Hay, J. E. (2007) 'Coastal systems and low-lying areas', in Parry, M. L., Canziani, O. F., Palutikof, J. P., van der Linden, P. J. and Hanson, C. E. (eds.) *Climate Change 2007: Impacts, Adaptation and Vulnerability*. Cambridge, UK: Cambridge University Press. pp. 315–356.

Nicholls, R. J., Wong, P. P., Burkett, V., Woodroffe, C. D., & Hay, J. (2008) 'Climate change and coastal vulnerability assessment: scenarios for integrated assessment', *Sustainability Science*, 3(1), pp.89-102.

NOAA (2020) *NOAA's Center for Operational Oceanographic Products and Services (CO-OPS), Tidal Datum.* Available at: https://tidesandcurrents.noaa.gov/publication/tidal_datums_and_their_application.pdf (Accessed: 15 January 2020).

Norton, J., Majid, S.A., Allan, D., Al Safran, M., Böer, B. and Richer, R., 2009. *An illustrated checklist of the flora of Qatar*. Gosport: Browndown Publications.

Oliver, M. A. & Webster, R. (1990) 'Kriging: a method of interpolation for geographical information systems', *International Journal of Geographical Information System*, 4(3), pp.313-332.

Openshaw, S., Charlton, M., & Carver, S. (1991) 'Error propagation: a Monte Carlo simulation', *Handling geographical information Methodology & Potential Applications*, pp.78-101. Longman Scientific & Technical: London.

OpenStreetMap (2018) *Open data platform.* Available at: www.openstreetmap.org (Accessed: 11 December 2018).

Oppenheimer M., Bruce G., Jochen H., van Roderik., Alexandre M., Amr A., Cai R., Cifuentes-Jara M., De R., Tuhin G., John H., Marzeion B., Benoit M., Zita S., Smit A. J., Sönke D. and Thomas F (2019). 'Sea Level Rise and Implications for Low Lying Islands, Coasts and Communities', in: Pörtner, H.-O. et al. (eds), *IPCC Special Report on the Ocean and Cryosphere in a Changing Climate*, Cambridge University Press, Cambridge, UK.

Östman, A. (1987) 'Quality control of photogrammetrically sampled digital elevation models', *The Photogrammetric Record*, 12(69), pp.333-341.

Oxford Dictionary (2019) Available at: https://en.oxforddictionaries.com/ (Accessed: 31 March 2019).

OZCoasts. Australian online coastal information (2012) *Sea Level Rise Maps.* Available at: https://ozcoasts.org.au/indicators/coastal-issues/sea_level_rise/ (Accessed: 11 December 2017).

Pachauri, R. K., Allen, M. R., Barros, V. R., Broome, J., Cramer, W., Christ, R., Church, J. A., Clarke, L., Dahe, Q., Dasgupta, P., & Dubash, N. K. (2014) Climate *change 2014: synthesis report. Contribution of Working Groups I, II and III to the fifth assessment report of the Intergovernmental Panel on Climate Change* (p. 151). IPCC.

Pallathu, A. (2015) Interview with *Face to face meeting on elevation data sets in Qatar*. Interview *with* A. Almannai. 12 March, Doha

Papadimitropoulos, E.A., Elbarazi, I., Blair, I., Katsaiti, M.S., Shah, K.K. and Devlin, N.J. (2015) 'An investigation of the feasibility and cultural appropriateness of stated preference methods to generate health state values in the United Arab Emirates', *Value in Health Regional Issues*, *7*, pp.34-41. doi: 10.1016/j.vhri.2015.07.002. Epub 2015 Sep 29. PMID: 29698150.

Parris, A. S., Bromirski, P., Burkett, V., Cayan, D. R., Culver, M. E., Hall, J., Horton, R. M., Knuuti, K., Moss, R. H., Obeysekera, J., & Sallenger, A. H. (2012) Global sea level rise scenarios for the United States National Climate Assessment. NOAA Tech Memo OAR CPO-1. 37 pp.

Parry, M., Arnell, N., McMichael, T., Nicholls, R., Martens, P., Kovats, S., Livermore, M., Rosenzweig, C., Iglesias, A., & Fischer, G. (2001) 'Millions at risk: defining critical climate change threats and targets', *Global environmental change*, 11(3), pp.181-183.

Parry, M., Rosenzweig, C., Iglesias, A., Fischer, G., & Livermore, M. (1999) 'Climate change and world food security: a new assessment', *Global environmental change*, 9, pp. S51-S67

Pattengale, N. D., Alipour, M., Bininda-Emonds, O. R., Moret, B. M., & Stamatakis, A. (2010) 'How many bootstrap replicates are necessary?', *Journal of computational biology*, 17(3), pp.337-354.

Pike, R. J. (2002) 'A bibliography of terrain modelling (geomorphometry), the quantitative representation of topography', *USGS Open file report*, pp.02-465.

Pizer, W. A. (1999) 'The optimal choice of climate change policy in the presence of uncertainty', *Resource and Energy Economics*, 21(3-4), pp.255-287.

Planning and Statistics Authority (2015) *Census 2010* Available at: https://www.psa.gov.qa/en/statistics1/StatisticsSite/Census/Pages/default.aspx (Accessed: 15 December 2015).

Polat, N., Uysal, M. & Toprak, A.S. (2015) 'An investigation of DEM generation process based on LiDAR data filtering, decimation, and interpolation methods for an urban area', *Measurement*, 75, pp.50-56. 10.1016/j.measurement.2015.08.008.

Poulter, B. & Halpin, P. N. (2008) 'Raster modelling of coastal flooding from sea-level rise', *International Journal of Geographical Information Science*, 22(2), pp.167-182.

Qatar Meteorology Department (QMD) (2016) *Climatological Normals,* Available at: http://www.qweather.gov.qa/ClimateNormals.aspx. (Accessed: 20 April 2020).

Rahmstorf, S. (2007) ‘A semi-empirical approach to projecting future sea-level rise’, *Science*, 315(5810), pp.368-370.

Refaat, M.M. and Eldeberky, Y., (2016) ‘Assessment of coastal inundation due to sea-level rise along the Mediterranean Coast of Egypt’, *Marine Geodesy*, *39*(3-4), pp.290-304.

Reid, R. O. & Bodine, B. R. (1968) ‘Numerical model for storm surges in Galveston Bay’, *Journal of the Waterways and harbors Division*, 94(1), pp.33-58.

Riahi, K., Grübler, A., & Nakicenovic, N. (2007) ‘Scenarios of long-term socio-economic and environmental development under climate stabilisation’, *Technological Forecasting and Social Change*, 74(7), pp.887-935.

Riahi, K., Rao, S., Krey, V., Cho, C., Chirkov, V., Fischer, G., Kindermann, G., Nakicenovic, N., & Rafaj, P. (2011) ‘RCP 8.5—A scenario of comparatively high greenhouse gas emissions’, *Climatic change*, 109(1-2), p.33.

Rikalovic, A., Cosic, I., & Lazarevic, D. (2014) ‘GIS based multi-criteria analysis for industrial site selection’, *Procedia Engineering*, 69(12), pp.1054-1063.

Rishikeshan, C.A., Katiyar, S.K. and Mahesh, V.V. (2014) ‘Detailed evaluation of DEM interpolation methods in GIS using DGPS data’, In *2014 International Conference on Computational Intelligence and Communication Networks* (pp. 666-671). doi: 10.1109/CICN.2014.148.

Risk and Policy Analysis Limited (2006) Flood defence standards for designated sites. *English Nature Research Reports, No 629.*

Romanelli, J. P., Silva, L. G., Horta, A., & Picoli, R. A. (2018) ‘Site selection for hydropower development: a GIS-based framework to improve planning in Brazil’, *Journal of Environmental Engineering*, 144(7), p.04018051.

Rosser, J.F., Leibovici, D.G. & Jackson, M.J. (2017) ‘Rapid flood inundation mapping using social media, remote sensing and topographic data’, *Nat Hazards,* 87, pp.103–120. https://doi.org/10.1007/s11069-017-2755-0

Ruckert, K. L., Oddo, P. C., & Keller, K. (2017) ‘Impacts of representing sea-level rise uncertainty on future flood risks: An example from San Francisco Bay’, *PloS one*, 12(3), pp.1-17.

Sahin, O. & Mohamed, S. (2014) ‘Coastal vulnerability to sea-level rise: a spatial–temporal assessment framework’, *Natural hazards*, 70(1), pp.395-414.

Satgé, F., Bonnet, M. P., Timouk, F., Calmant, S., Pillco, R., Molina, J., Lavado-Casimiro, W., Arsen, A., Crétaux, J. F., & Garnier, J. (2015) 'Accuracy assessment of SRTM v4 and ASTER GDEM v2 over the Altiplano watershed using ICESat/GLAS data', *International Journal of Remote Sensing*, 36(2), pp.465-488.

Scheibert, C., Stietiya, M.H., Sommar, J., Abdalla, O.E.S., Schramm, H. and Al Memah, M. (2005) The atlas of soils for the State of Qatar. *Ministry of Municipal Affairs and Agriculture, Doha*.

Schmid, K., Hadley, B., & Waters, K. (2014) 'Mapping and portraying inundation uncertainty of bathtub-type models', *Journal of Coastal Research*, 30(3), pp.548-561.

Sea Level Rise Explorer (2015) *Global Warming Art*, Available at: http://www.globalwarmingart.com/sealevel (Accessed: 8 October 2015).

SEL (1980) *Qatar Geological Map Explanatory Booklet*. Seltrust Engineering Limited, Industrial Development Technical Centre, Doha.

Shen, J., Tan, F., & Zhang, Y. (2018) 'Improved building treatment approach for urban inundation modeling: A case study in Wuhan, China', *Water*, 10(12), p.1760.

Siddiqui, K.S., Abu-Riash, M. and Al-Suliman, A. (2017) 'Translation and Adaptation of English Language Questionnaire into Arabic for Implementation of a Large Survey on Assessing the Symptoms of Bleeding Disorders in Saudi Arabia', *Journal of Applied Hematology*, 8, pp.156-8. 10.4103/joah.joah_70_17.

Simpson, G. & Wu, Y. H. (2014) 'Accuracy and effort of interpolation and sampling: can GIS help lower field costs?', *ISPRS International Journal of Geo-Information*, 3(4), pp.1317-1333.

Small, C. & Nicholls, R. J. (2003) 'A global analysis of human settlement in coastal zones', *Journal of coastal research*, pp.584-599.

Smith, J. B., Schellnhuber, H. J., Mirza, M. M. Q., Fankhauser, S., Leemans, R., Lin, E., Ogallo, L., Pittock, B., Richels, R. G., Rosenzweig, C., & Tol, R. S. J. (2001) 'Vulnerability to climate change and reasons for concern: a synthesis', *Climate change*, pp.913-967.

Snoussi, M., Niazi, S., Khouakhi, A., & Raji, O. (2010) 'Climate change and sea-level rise: Agis-based vulnerability and impact assessment, the case of the Moroccan coast', *Geomatic Solutions for Coastal Environments; Nova Science Publishers Inc.: Hauppauge, NY, USA*, pp.275-310.

Solomon, S., Manning, M., Marquis, M., & Qin, D. (2007) Climate *change 2007-the physical science basis: Working group I contribution to the fourth assessment report of the IPCC* (Vol. 4). Cambridge University Press.

Spirandelli, D. J., Anderson, T. R., Porro, R., & Fletcher, C. H. (2016) 'Improving adaptation planning for future sea-level rise: understanding uncertainty and risks using a probability-based shoreline model', *Journal of Planning Education and Research*, 36(3), pp.290-303.

Srivastava, M. R. (1996) May. An overview of stochastic spatial simulation. In *Spatial accuracy assessment in natural resources and environmental sciences: second international symposium. US Department of Agriculture, Forest Service, Fort Collins, General Technical Report RM-GTR-277* (pp. 13-22).

Stammer, D., Cazenave, A., Ponte, R. M., & Tamisiea, M. E. (2013) 'Causes for contemporary regional sea level changes', *Annual review of marine science*, 5, pp.21-46.

Stefanescu, E. R., Bursik, M., Cordoba, G., Dalbey, K., Jones, M. D., Patra, A. K., Pieri, D. C., Pitman, E. B., & Sheridan, M. F. (2012) 'Digital elevation model uncertainty and hazard analysis using a geophysical flow model', *Proceedings of the Royal Society A: Mathematical, Physical and Engineering Sciences*, 468(2142), pp.1543-1563.

Stocker, T. (2014) Climate *change 2013: the physical science basis: Working Group I contribution to the Fifth assessment report of the Intergovernmental Panel on Climate Change*. Cambridge University Press.

Stocker, T. F., Qin, D., Plattner, G. K., Tignor, M., Allen, S. K., Boschung, J., Nauels, A., Xia, Y., Bex, V., & Midgley, P. M. (2013) Climate change 2013: The physical science basis. Contribution of working group I to the fifth assessment report of the intergovernmental panel on climate change, 1535.

Strauss, B. H., Ziemlinski, R., Weiss, J. L., & Overpeck, J. T. (2012) 'Tidally adjusted estimates of topographic vulnerability to sea level rise and flooding for the contiguous United States', *Environmental Research Letters*, 7(1), p.014033.

Syvitski, J. P., Vörösmarty, C. J., Kettner, A. J., & Green, P. (2005) 'Impact of humans on the flux of terrestrial sediment to the global coastal ocean', *Science*, 308(5720), pp.376-380.

Tan, Q. & Xu, X. (2014) Comparative analysis of spatial interpolation methods: an experimental study. *Sensors & Transducers*, *165*(2), p.155.

The World Bank (2010) Development and Climate Change. *World Development Report 2010.* http://www.worldbank.org/wdr.

Thumerer, T., Jones, A. P., & Brown, D. (2000) 'A GIS based coastal management system for climate change associated flood risk assessment on the east coast of England', *International Journal of Geographical Information Science*, 14(3), pp.265-281.

Tiryaki, M. & Karaca, O. (2018) 'Flood susceptibility mapping using GIS and multicriteria decision analysis: Saricay-Çanakkale (Turkey)', *Arabian Journal of Geosciences*, 11(14), p.364.

Titus, J. G. & Richman, C. (2001) 'Maps of lands vulnerable to sea level rise: modelled elevations along the US Atlantic and Gulf coasts', *Climate Research*, 18(3), pp.205-228.

Titus, J. G. & Wang, J. (2008) 'Maps of lands close to sea level along the middle Atlantic Coast of the United States: an elevation data set to use while waiting for LIDAR', *Background documents supporting climate change science program synthesis and assessment product*, 4, pp.2-44.

Tolba, M. K. & Saab, N. W. (2009) Arab environment: Climate change. In *Beirut, Technical Publications and Environment & Development magazine.*

Tonmoy, F. N. & El-Zein, A. (2018) 'Vulnerability to sea level rise: A novel local-scale indicator-based assessment methodology and application to eight beaches in Shoalhaven, Australia', *Ecological Indicators*, 85, pp.295-307.

Troup, L. & Fannon, D. (2016) 'Morphing climate data to simulate building energy consumption', *Proceedings of SimBuild*, 6(1), pp.439-446.

Tucci, M. & Giordano, A. (2011) 'Positional accuracy, positional uncertainty, and feature change detection in historical maps: Results of an experiment', *Computers, Environment and Urban Systems*, 35(6), pp.452-463.

Turner, J., Orr, A., Gudmundsson, G. H., Jenkins, A., Bingham, R. G., Hillenbrand, C. D., & Bracegirdle, T. J. (2017) 'Atmosphere-ocean-ice interactions in the Amundsen Sea Embayment, West Antarctica', *Reviews of Geophysics*, 55(1), pp.235-276.

United Nations (1997) *Information Provided by the Government of Qatar to the United Nations Commission on Sustainable Development Fifth Session.* Available at: http://www.un.org/esa/earthsummit/qatar-cp.htm. (Accessed: 30 October.2017).

USGS, U.S. (1997) Geological Survey: Standards for Digital Elevation Models, Part 1: General, Part 2: Specifications, Part 3: Quality Control.

Valiela, I. (2009) Global *coastal change*. John Wiley & Sons.

Van De Sande, B., Lansen, J., & Hoyng, C. (2012) 'Sensitivity of coastal flood risk assessments to digital elevation models', *Water*, 4(3), pp.568-579.

Van Vuuren, D. P., Den Elzen, M. G., Lucas, P. L., Eickhout, B., Strengers, B. J., Van Ruijven, B., Wonink, S., & Van Houdt, R. (2007) 'Stabilizing greenhouse gas concentrations at low levels: an assessment of reduction strategies and costs', *Climatic change*, 81(2), pp.119-159.

Van Vuuren, D. P., Edmonds, J., Kainuma, M., Riahi, K., Thomson, A., Hibbard, K., Hurtt, G. C., Kram, T., Krey, V., Lamarque, J. F., & Masui, T. (2011) 'The representative concentration pathways: an overview', *Climatic change*, 109(1-2), p.5.

Vlachopoulou, M., Silleos, G., & Manthou, V. (2001) 'Geographic information systems in warehouse site selection decisions', *International journal of production economics*, 71(1-3), pp.205-212.

Wang, Y., Chen, A. S., Fu, G., Djordjević, S., Zhang, C., & Savić, D. A. (2018) 'An integrated framework for high-resolution urban flood modelling considering multiple information sources and urban features', *Environmental modelling & software*, 107, pp.85-95.

Ward, D. P., Murray, A. T., & Phinn, S. R. (2003) 'Integrating spatial optimization and cellular automata for evaluating urban change', *The Annals of Regional Science*, 37(1), pp.131-148.

Watson, R. T., Zinyowera, M. C., & Moss, R. H. (1996) Climate *change 1995. Impacts, adaptations and mitigation of climate change: scientific-technical analyses Cambridge University Press*, pp. 223-229.

WCC'93, 1994. Preparing to meet the coastal challenges of the 21st century.

Webster, M (2002) 'The curious role of "learning" in climate policy: Should we wait for more data?' *Energy Journal*, vol. 23, no. 2, pp. 97-119.

Webster, T. L., Forbes, D. L., Dickie, S., & Shreenan, R. (2004) 'Using topographic lidar to map flood risk from storm-surge events for Charlottetown, Prince Edward Island, Canada', *Canadian Journal of Remote Sensing*, 30(1), pp.64-76.

Webster, T. L., Forbes, D. L., MacKinnon, E., & Roberts, D. (2006) 'Flood-risk mapping for storm-surge events and sea-level rise using lidar for southeast New Brunswick', *Canadian Journal of Remote Sensing*, 32(2), pp.194-211.

Wechsler, S. P. & Kroll, C. N. (2006) 'Quantifying DEM uncertainty and its effect on topographic parameters', *Photogrammetric Engineering & Remote Sensing*, 72(9), pp.1081-1090.

Weiss, J. L. & Overpeck, J. T. (2003) Climate Change and Sea Level.

Weissenberger, S. & Chouinard, O. (2015) Adaptation *to climate change and sea level rise: The case study of coastal communities in New Brunswick, Canada*. Springer.

West, H., Horswell, M., & Quinn, N. (2018) 'Exploring the sensitivity of coastal inundation modelling to DEM vertical error', *International Journal of Geographical Information Science*, 32(6), pp.1172-1193.

Wilson, J. P. & Gallant, J. C. (eds) (2000) Terrain *analysis: principles and applications*. John Wiley & Sons.

Winslow, F. P. & El Hakim, M. (2009) *Studying and Developing the Natural and Artificial Recharge of the Groundwater Aquifer in the State of Qatar*. Ministry of Environment, State of Qatar.

Wise, M., Calvin, K., Thomson, A., Clarke, L., Bond-Lamberty, B., Sands, R., Smith, S. J., Janetos, A., & Edmonds, J. (2009) 'Implications of limiting CO_2 concentrations for land use and energy', *Science*, 324(5931), pp.1183-1186.

Wise, S. M. (1998) The effect of GIS interpolation errors on the use of digital elevation models in geomorphology. *Landform monitoring, modelling and analysis*.

Woodroffe, C. D., Kennedy, D. M., Brooke, B. P., & Dickson, M. E. (2006) 'Geomorphological evolution of Lord Howe Island and carbonate production at the latitudinal limit to reef growth', *Journal of Coastal Research*, pp.188-201.

Woosnam, K. M. (2017) 'High tide on main street: Rising sea level and the coming coastal crisis', *Community Development*, 48(4), pp.597-598.

Wuebbles, D. J., Fahey, D. W., & Hibbard, K. A. (2017) ''Climate science special report: fourth national climate assessment', volume I., *U.S. Global Change Research Program*, pp. 470

Xuejun, L. I. U. & Lu, B. I. A. N. (2008) 'Accuracy assessment of DEM slope algorithms related to spatial autocorrelation of DEM Errors', In *Advances in Digital Terrain Analysis* (pp. 307-322). Springer, Berlin, Heidelberg.

Yao, X., Fu, B., Lü, Y., Sun, F., Wang, S. and Liu, M., (2013) 'Comparison of four spatial interpolation methods for estimating soil moisture in a complex terrain catchment', *PloS one*, *8*(1), p.e54660.

Yehia, M. A., Harhash, I. E., & El-Harouni, M. (1982) Landsat image investigation of major surface structures, topography, and hydrology in Qatar. *Center Remote Sens. Information and Analysis, Environ. Res. Inst., Mich*

Yin, J., Griffies, S. M., & Stouffer, R. J. (2010) 'Spatial variability of sea level rise in twenty-first century projections', *Journal of Climate*, 23(17), pp.4585-4607.

Yohe, G. & Tol, R. S. (2002) 'Indicators for social and economic coping capacity—moving toward a working definition of adaptive capacity', *Global environmental change*, 12(1), pp.25-40.

Zerger, A. (2002) 'Examining GIS decision utility for natural hazard risk modelling', *Environmental Modelling & Software*, 17, pp.287-294. 10.1016/S1364-8152(01)00071-8.

Zerger, A., Smith, D. I., Hunter, G. J., & Jones, S. D. (2002) 'Riding the storm: a comparison of uncertainty modelling techniques for storm surge risk management', *Applied Geography*, 22(3), pp.307-330.

Appendix-1

Qatar University
College of Arts and Sciences
Geography and Urban Planning

University of East Anglia
United Kingdom
School of Environmental Science

PhD project on Evaluation of sea level rise on the eastern coastal area in the State of Qatar using Geographic Information System

Dear Sir/ Madam

My name Abdulaziz Al-Mannai, I am lecturer at Qatar University and currently a PhD student at University of East Anglia working on a project evaluating the impact of climate change on sea level rise. One of my objective is to identify the appropriate place to build a barrier to minimize the impact of sea flooding. To help identify a suitable location I need to identify which factors are most important in determining which areas to protect from flooding in Qatar. These are:

1- Land-use: This includes residential area, industrial area, undeveloped land and roads
2- Depth of flooding: This is representing the depth of the water after sea inundation
3- Depth of pooling: The depth of the water remaining after the sea returns to the original phase

Your views are important to me in finding out the importance of these 3 factors. The collected data from this questionnaire is an essential to conduct this study as your knowledge and practical experience plays an important part to determine the weighting for these factors.

I am kindly asking for a few minutes of your valuable time to participate in this survey and answer a few simple questions. Your response is very much appreciated as your knowledge and experience will help me with my studies. Thank you in advance for your participation and your input to this study. I also would like to let you know that all of the information will remain confidential and will only be use for the purpose of this study.

AbdulAziz Almanai

Lecturer at Qatar University and

PhD Student at University of East Anglia

Part 1: How important do you rate the following factors to protect Qatar coastal area from flooding?

Factors	1	2	3	4	5	6	7
	Low			Importance			High
Land-use (Residential building, roads, industrial sites and undeveloped land)							
Depth of flooding (Depth of water in flooded area during the flooding)							

Part 2: How important do you rate the following factors to protect Qatar coastal area from flooding?

Factors	1	2	3	4	5	6	7
	Low			Importance			High
Land-use (Residential building, roads, industrial sites and undeveloped land)							
Depth of pooling (Depth of water that remains in-land after flooding)							

Part 3: How important do you rate the following factors to protect Qatar coastal area from flooding?

Factors	1	2	3	4	5	6	7
	Low			Importance			High
Depth of flooding (Depth of water in flooded area during the flooding)							
Depth of pooling (Depth of water that remains in-land after flooding)							

Part 4: How important do you rate the following land-uses to protect Qatar coastal area from flooding?

Different Land-use	1	2	3	4	5	6	7
	Low			Importance			High
Residential building							
Roads							
Industrial sites							
Commercial							
Agriculture & Farms							
Undeveloped land							

Part 5: To help me understand the results would you let me know some details about yourself

1- **Sex**: ☐ Male ☐ Female

2- **Occupation and where**:

Department:

3- **Age:**

20-30 years old	31-40 years old	41-50 years old	Over 50 years old

Thank you for helping me with my study,

جامعة قطر
كلية الآداب والعلوم
برنامج جغرافيا تخطيط عمراني

جامعة ايست انجليا
مدرسة العلوم البيئية
المملكة المتحدة

بحث دكتوراة في تقييم آثار ارتفاع مستوى مياه البحر على المناطق الساحلية الشرقية
لدولة قطر باستخدام نظم المعلومات الجغرافية

السيدات والسادة المحترمين

السلام عليكم ورحمة الله وبركاته

أنا عبد العزيز علي المناعي، محاضر في جامعة قطر كلية الآداب والعلوم قسم العلوم الإنسانية برنامج تخطيط عمراني، حاليا طالب دكتوراه في جامعة إيست أنجليا بالمملكة المتحدة، أعمل على بحث دكتوراه في تقييم آثار ارتفاع مستوى سطح البحر على المناطق الساحلية الشرقية لدولة قطر باستخدام نظم المعلومات الجغرافية. من أحد أهداف هذا البحث تحديد العوامل الأكثر أهمية لتحديد المناطق التي يجب حمايتها من تأثير ارتفاع مستوى سطح البحر على المناطق الساحلية، وهي كمايلي:

1. **استخدامات الأراضي**: وتشمل في هذه الدراسة المناطق الساحلية السكنية والصناعية والطرق.
2. **المناطق المنخفضة**: وهي تلك المناطق التي سوف يتم غمرها بالمياه أثناء ارتفاع منسوب سطح البحر في المستقبل.
3. **المناطق المنخفضة العميقة**: وهي المناطق التي تتجمع بها مياه البحر لفترة طويلة بعد انحسار الماء.

إن البيانات المجمعة عن طريق هذا الاستبيان تمثل أحد العناصر الأساسية للبحث، لذا فإن استجابتكم، بالإجابة على الاستبيان المرفق مهمة جدا لإنجاز هذا البحث ونحن نثق بسعة صدوركم وخبرتكم العلمية والعملية في هذا التجاوب.

نشكركم مقدماً على حسن تعاونكم وصادق اهتمامكم وتشجيعكم للبحث العلمي، علماً أن جميع الإجابات ستعامل بسرية تامة، ولن تستخدم إلا لأغراض البحث. مع مراعاة أن إجابتك على هذا الاستبيان بدقة وموضوعية ستثري هذه الدراسة.

عبد العزيز علي المناعي
محاضر في جامعة قطر
طالب دكتوراه في جامعة إيست أنجليا

الجزء الأول: ما مدي اهميه تقييم العوامل التالية لمنع الفيضانات المستقبلية على المناطق الساحلية الشرقية لدولة قطر؟

	العوامل	1	2	3	4	5	6	7
		أقل أهمية						أكثر أهمية
1	**استخدام الأراضي**: وتشمل في هذه الدراسة المناطق الساحلية السكنية والصناعية والطرق							
2	**المناطق المنخفضة**: وهي تلك المناطق التي سوف يتم غمرها بالمياه أثناء ارتفاع منسوب سطح البحر في المستقبل.							

الجزء الثاني: ما مدي اهميه تقييم العوامل التالية لمنع الفيضانات المستقبلية على المناطق الساحلية الشرقية لدولة قطر؟

	العوامل	1	2	3	4	5	6	7
		أقل أهمية						أكثر أهمية
1	**استخدام الأراضي**: وتشمل في هذه الدراسة المناطق الساحلية السكنية والصناعية والطرق							
2	**المناطق المنخفضة العميقة**: وهي المناطق التي تتجمع بها مياه البحر لفترة طويلة بعد انحسار الماء							

الجزء الثالث: ما مدي اهميه تقييم العوامل التالية لمنع الفيضانات المستقبلية على المناطق الساحلية الشرقية لدولة قطر؟

	العوامل	1	2	3	4	5	6	7
		أقل أهمية						أكثر أهمية
1	**المناطق المنخفضة**: وهي تلك المناطق التي سوف يتم غمرها بالمياه أثناء ارتفاع منسوب سطح البحر في المستقبل.							
2	**المناطق المنخفضة العميقة**: وهي المناطق التي تتجمع بها مياه البحر لفترة طويلة بعد انحسار الماء							

الجزء الرابع: ما مدي أهمية نوع استخدامات الأراضي التالية لحمايتها من الفيضانات المستقبلية على دولة قطر؟

	استخدام الأراضي المختلفة	1	2	3	4	5	6	7
		أقل أهمية						أكثر أهمية
1	**المباني السكنية**							
2	**الطرق**							
3	**المواقع الصناعية**							
4	**التجارية**							
5	**المناطق الخضراء والمزارع**							
6	**الأراضي غير المطورة**							

الجزء الخامس: لمساعدتي على فهم النتائج أرجو تزويدي بالبيانات الشخصية التالية:

✓ **الجنس:** ذكر ☐ أنثى ☐

✓ **المهنة:**

✓ **مكان العمل:**

✓ **القسم:**

✓ **العمر:**

☐ من 20 الى 30 سنة

☐ من 31 الى 40 سنة

☐ من 41 الى 50 سنة

☐ فوق 51 سنة